ALMA MATER STUDIORUM
UNIVERSITÀ DI BOLOGNA
Dipartimento di Scienze della Terra
e Geologico-Ambientali

DOTTORATO IN SCIENZE DELLA TERRA
Settore scientifico-disciplinare: GEO/01 Paleontologia e paleoecologia
XIX CICLO
Coordinatore: Prof. William Cavazza

Stratigrafia ad alta risoluzione dei depositi quaternari in Adriatico centrale e meridionale: impatto di cambiamenti climatici a scala sub-Milankoviana sulla circolazione in Mediterraneo

High-resolution stratigraphy of Central and Southern Adriatic Quaternary deposits: impact of sub-Milankovian climate change on Mediterranean circulation

Dottorando	Relatore
Dr. Andrea Piva	Prof. Gian Battista Vai
	Co-relatori
	Dr. Alessandra Asioli
	Dr. Fabio Trincardi
	Prof. Ralph R. Schneider

Bologna, 15 marzo 2007

INDEX

Asioli and Piva, *Informatore Botanico* Italiano, in press

Trincardi et al., *Marine* Geology, in press

Riassunto

Questa tesi racchiude il lavoro di tre anni di Dottorato di ricerca, durante i quali sono stati analizzati sedimenti marini dell'Adriatico centrale e meridionale, ottenuti mediante la perforazione di pozzi e carote, grazie ad una ottima conoscenza sismo-stratigrafica dell'area indagata. Il lavoro è stato svolto nell'ambito dei progetti EC-EURODELTA (coord. Fabio Trincardi, ISMAR-CNR), EC-EUROSTRATAFORM (coord. Phil P. E. Weaver, NOC, UK) e EC-PROMESS1 (coord. Serge Bernè, IFREMER, Francia). Le successioni sedimentarie analizzate presentano intervalli stratigrafici espansi, in particolare per gli ultimi 400, 60, e 6 kyr BP. I tre intervalli di tempo indagati sono riflessi in una tripartizione della tesi stessa. Lo studio è consistito nell'analisi quantitativa delle associazioni a foraminiferi planctonici e bentonici, per oltre 560 campioni analizzati, nella preparazione del materiale per l'analisi degli isotopi stabili di ossigeno e carbonio e nella interpretazione e discussione del dato ottenuto.

Si è provveduto all'inquadramento cronologico per gli ultimi 400 kyr del pozzo PRAD1-2, perforato in Adriatico centrale alla profondità di 186.5 m (ciò ricadeva nell'unità operativa WP6 del progetto PROMESS1). La cronologia proposta è il frutto di un approccio multidisciplinare, dato dall'integrazione di parametri diversi ed indipendenti, alcuni dei quali forniti dagli altri specialisti coinvolti nel progetto. La cronologia del pozzo è basata su: micropaleontologia (bioeventi a foraminiferi e nannoplancton calcareo), ciclicità climatica (associazioni a foraminiferi), geochimica (isotopi stabili dell'ossigeno su record planctonico e bentonico), paleomagnetismo, datazioni radiometriche (^{14}C AMS), tephrocronologia, riconoscimento di livelli sapropel-equivalenti (Se). Va notato anche come il record isotopico dell'ossigeno del pozzo PRAD1-2 mostri un'ottima correlabilità con record più profondi del Mediterraneo. I parametri indagati hanno consentito di riconoscere nel pozzo PRAD1-2 la presenza di tutti gli stadi isotopici dal MIS1 al MIS10, mentre la base del pozzo è stata ascritta alla parte terminale del MIS11.

Gli stadi interglaciali e glaciali incontrati in PRAD1-2 sono stati analizzati in dettaglio anche dal punto di vista del paleoambiente. Ad esempio, gli intervalli glaciali (in particolare MIS6, MIS8 e MIS10) presentano associazioni a foraminiferi peculiari, dominate da specie bentoniche tipiche di regioni polari, non più presenti attualmente nell'Adriatico Centrale. Si evidenzia inoltre un trend di approfondimento nella paleoprofondità durante i glaciali dal MIS10 (ambiente di piattaforma interna) al MIS4 (ambiente di piattaforma media).

Dieci livelli sapropel-equivalenti sono stati riconosciuti nel record centro-adriatico del pozzo PRAD1-2. Essi mostrano differenti associazioni a foraminiferi planctonici, che hanno permesso di distinguere in prima istanza eventi sviluppatisi in condizioni climatiche calde (Se5, Se7), fredde (Se4, Se6 e Se8), ed intermedie-temperate (Se1, Se3, Se9, Se', Se10), in accordo con la letteratura. Dal punto di vista della colonna d'acqua, i livelli depositatisi in condizioni climatiche fredde, sembrano essere privi della fase oligotrofica, mentre quelli formatisi in condizioni climatiche temperato-calde presentano sia la fase oligotrofica sia quella eutrofia (eccetto Se1). Considerando anche l'associazione a foraminiferi bentonici questi sapropel-equivalenti indicano condizioni del fondo variabili, da relativamente ossigenate (Se1, Se3), a disossiche (Se9, Se' e Se10), a fortemente disossiche (Se4, Se6 e Se8), fino a casi in cui i foraminiferi bentonici sono assenti (Se5 e Se7). In questi due ultimi livelli il sedimento si presenta laminato, condizione finora mai registrata in ambienti così poco profondi. In sintesi, considerata la forte stratificazione della colonna d'acqua durante gli eventi Se8, Se7, Se6, Se5 e Se4, nonché la concomitante notevole diluizione dell'acqua superficiale testimoniata dal record isotopico, si avanza l'ipotesi secondo cui la piovosità dovesse essere molto intensa nell'area centro-adriatica durante questi eventi e che quindi il monsone africano dovesse aver raggiunto latitudini più elevate rispetto al suo posizionamento durante gli altri intervalli sapropel-equivalenti. Infine, il confronto di dettaglio dell'espressione del Sapropel Se5 nel record centro-adriatico di PRAD1-2 con quelle di altre aree del Mediterraneo orientale, indica una sostanziale somiglianza nella sequenza dei bioeventi a foraminiferi planctonici, testimoniando una simile evoluzione della colonna d'acqua per tutto il Mediterraneo orientale, anche se un sincronismo non può essere dimostrato.

E' stata condotta un'analisi ad alta risoluzione delle oscillazioni climatiche degli ultimi 6000 anni, riconosciute nell'area adriatica mediante bioeventi a foraminiferi planctonici e bentonici. In particolare, i picchi del foraminifero planctonico *Globigerinoides sacculifer* (quattro negli ultimi 5500 anni BP nella carota a più alto tasso di sedimentazione) sono stati interpretati, sulla base delle esigenze ecologiche di questa specie, come intervalli a clima caldo e poco piovoso, ascrivibili a momenti di relativo ottimo climatico, quali, ad esempio, il Periodo Caldo Medievale, l'Età Romana, la Tarda Età del Bronzo e l'Età del Rame. Di conseguenza, i minimi di abbondanza di questo bioindicatore corrisponderebbero ad intervalli relativamente più freddi e piovosi. Queste conclusioni trovano buon riscontro nel dato isotopico e pollinico. La Last Occurrence (LO) di *G. sacculifer* è stata datata in questo lavoro a circa 550 anni BP, e risulta il bioevento a foraminiferi che meglio approssima la base della Piccola Età del Ghiaccio in Adriatico. Dalla letteratura risulta che lo

stesso bioevento è occorso con età confrontabili anche nel Bacino Levantino. Potenzialmente, quindi, la LO di *G. sacculifer* è estendibile a tutto il Mediterraneo Orientale. All'interno della Piccola Età del Ghiaccio il foraminifero bentonico *Valvulineria complanata* mostra due picchi distinti nelle carote prossimali adriatiche analizzate, prelevate a centinaia di chilometri di distanza nell'ambiente di facia dei limi. Sulla base delle caratteristiche ecologiche di questa forma, i due picchi sono stati interpretati come le oscillazioni (fredde e piovose) più intense della Piccola Età del Ghiaccio. L'inquadramento cronologico delle carote analizzate è robusto, in quanto si fonda su numerose datazioni ^{14}C AMS, su stime derivanti dalla curva secolare di variazione del campo magnetico, su stime geochimiche della profondità di attivazione del radionuclide ^{210}Pb, e trova un buon riscontro nel dato tephrocronologico, pollinico e micropaleontologico. Le oscillazioni climatiche intraoloceniche individuate in Adriatico sono state confrontate con quelle segnalate in letteratura in altri record dell'emisfero Nord, e il riscontro cronologico appare molto buono.

Infine, le successioni sedimentarie analizzate hanno permesso una revisione ed un aggiornamento della ecobiostratigrafia a foraminiferi disponibile in letteratura per l'Adriatico, grazie all'ottenimento di 16 ecobiozone per gli ultimi 60 kyr BP. Alcuni bioeventi sono validi limitatamente all'Adriatico centrale (ad esempio la LO del foraminifero bentonico *Hyalinea balthica*, che approssima il limite MIS3/MIS2), mentre altri sembrano validi per tutto il bacino adriatico (ad esempio la LO del planctonico *Globorotalia inflata* nel MIS3, che individua il ciclo di Dansgaard-Oeschger 8 (Denekamp)).

Parole chiave: Adriatico, foraminiferi, isotopi, sapropel, paleoceanografia, paleoclima, paleoambiente.

Abstract

This volume is a collection of the work done in a three years-lasting PhD, focused in the analysis of Central and Southern Adriatic marine sediments, deriving from the collection of a borehole and many cores, achieved thanks to the good seismic-stratigraphic knowledge of the study area.

The work was made out within European projects EC-EURODELTA (coordinated by Fabio Trincardi, ISMAR-CNR), EC-EUROSTRATAFORM (coordinated by Phil P. E. Weaver, NOC, UK), and PROMESS1 (coordinated by Serge Bernè, IFREMER, France). The analysed sedimentary successions presented highly expanded stratigraphic intervals, particularly for the last 400 kyr, 60 kyr and 6 kyr BP. These three different time-intervals resulted in a tri-partition of the PhD thesis. The study consisted of the analysis of planktic and benthic foraminifers' assemblages (more than 560 samples analysed), as well as in preparing the material for oxygen and carbon stable isotope analyses, and interpreting and discussing the obtained dataset.

The chronologic framework of the last 400 kyr was achieved for borehole PRAD1-2 (within the work-package WP6 of PROMESS1 project), collected in 186.5 m water depth. The proposed chronology derives from a multi-disciplinary approach, consisting of the integration of numerous and independent proxies, some of which analysed by other specialists within the project. The final framework based on: micropaleontology (calcareous nannofossils and foraminifers' bioevents), climatic cyclicity (foraminifers' assemblages), geochemistry (oxygen stable isotope, made out on planktic and benthic records), paleomagnetism, radiometric ages (^{14}C AMS), teprhochronology, identification of sapropel-equivalent levels (Se). It's worth to note the good consistency between the oxygen stable isotope curve obtained for borehole PRAD1-2 and other deeper Mediterranean records. The studied proxies allowed the recognition of all the isotopic intervals from MIS10 to MIS1 in PRAD1-2 record, and the base of the borehole has been ascribed to the early MIS11.

Glacial and interglacial intervals identified in the Central Adriatic record have been analysed in detail for the paleo-environmental reconstruction, as well. For instance, glacial stages MIS6, MIS8 and MIS10 present peculiar foraminifers' assemblages, composed by benthic species typical of polar regions and no longer living in the Central Adriatic nowadays. Moreover, a deepening trend in the paleo-bathymetry during glacial intervals was observed, from MIS10 (inner-shelf environment) to MIS4 (mid-shelf environment).

Ten sapropel-equivalent levels have been recognised in PRAD1-2 Central Adriatic record. They showed different planktic foraminifers' assemblages, which allowed the first distinction of events occurred during warm-climate (Se5, Se7), cold-climate (Se4, Se6 and Se8) and temperate-intermediate-climate (Se1, Se3, Se9, Se', Se10) conditions, consistently with literature. Cold-climate sapropel equivalents are characterised by the absence of an oligotrophic phase, whereas warm-temeprate-climate sapropel equivalents present both the oligotrophic and the eutrophic phases (except for Se1). Sea floor conditions vary, according to benthic foraminifers' assemblages, from relatively well oxygenated (Se1, Se3), to dysoxic (Se9, Se', Se10), to highly dysoxic (Se4, Se6, Se8) to events during which benthic foraminifers are absent (Se5, Se7). These two latter levels are also characterised by the lamination of the sediment, feature never observed in literature in such shallow records. The enhanced stratification of the water column during the events Se8, Se7, Se6, Se5, Se4, and the concurring strong dilution of shallow water, pointed out by the isotope record, lead to the hypothesis of a period of intense precipitation in the Central Adriatic region, possibly due to a northward shift of the African Monsoon. Finally, the expression of Central Adriatic PRAD1-2 Se5 equivalent was compared with the same event, as registered in other Eastern Mediterranean areas. The sequence of substantially the same planktic foraminifers' bioevents has been consistently recognised, indicating a similar evolution of the water column all over the Eastern Mediterranean; yet, the synchronism of these events cannot be demonstrated.

A high resolution analysis of late Holocene (last 6000 years BP) climate change was carried out for the Adriatic area, through the recognition of planktic and benthic foraminifers' bioevents. In particular, peaks of planktic *Globigerinoides sacculifer* (four during the last 5500 years BP in the most expanded core) have been interpreted, based on the ecological requirements of this species, as warm-climate, arid intervals, correspondent to periods of relative climatic optimum, such as, for instance, the Medieval Warm Period, the Roman Age, the Late Bronze Age and the Copper Age. Consequently, the minima in the abundance of this biomarker could correspond to relatively cooler and more rainy periods. These conclusions are in good agreement with the isotopic and the pollen data. The Last Occurrence (LO) of *G. sacculifer* has been dated in this work at an average age of 550 years BP, and it is the best bioevent approximating the base of the Little Ice Age in the Adriatic. Recent literature reports the same bioevent in the Levantine Basin, showing a rather consistent age. Therefore, the LO of *G. sacculifer* has the potential to be extended to all the Eastern Mediterranean. Within the Little Ice Age, benthic foraminifer *V. complanata* shows two distinct peaks in the shallower Adriatic cores analysed, collected hundred kilometres apart, inside

the mud belt environment. Based on the ecological requirements of this species, these two peaks have been interpreted as the more intense (cold and rainy) oscillations inside the LIA. The chronologic framework of the analysed cores is robust, being based on several range-finding ^{14}C AMS ages, on estimates of the secular variation of the magnetic field, on geochemical estimates of the activity depth of ^{210}Pb short-lived radionuclide (for the core-top ages), and is in good agreement with tephrochronologic, pollen and foraminiferal data. The intra-holocenic climate oscillations find out in the Adriatic have been compared with those pointed out in literature from other records of the Northern Hemisphere, and the chronologic constraint seems quite good.

Finally, the sedimentary successions analysed allowed the review and the update of the foraminifers' ecobiostratigraphy available from literature for the Adriatic region, thanks to the achievement of 16 ecobiozones for the last 60 kyr BP. Some bioevents are restricted to the Central Adriatic (for instance the LO of benthic *Hyalinea balthica*, approximating the MIS3/MIS2 boundary), others occur all over the Adriatic basin (for instance the LO of planktic *Globorotalia inflata* during MIS3, individuating Dansgaard-Oeschger cycle 8 (Denekamp)).

Keywords: Adriatic, foraminifera, O and C stable isotopes, paleoceanography, paleoclimate, paleoenvironment.

PREFACE

Paleoceanographic research has become of increasing interest in the late decades, and produced a huge amount of literature. Many studies have been devoted to Quaternary marine and continental sequences, since this time interval shows a very high climatic complexity. Rapid climatic changes at millennial, secular or decadal scale characterise the Quaternary, in particular during the last 90-100kyrs (for instance Dansgaard-Oeschger cycles, Heinrich events, Little Ice Age) (Dansgaard et al., 1993; Bond et al., 1993; Maslin et al., 2001 and references therein). This variability, including the rapid changes from different circulation regimes, occurs in a very short (even decadal) time interval, comparable to the human life duration (Alley and Clark, 1999).

The Mediterranean Sea is a very good area for paleoclimatic studies, being a land-locked marginal sea, located in an intermediate position between high latitude climate, obliquity (41ka)-driven and lower latitude climate, dominated by north African climate, and strictly linked to the precession (22ka). Moreover, the Mediterranean area shows depositional environments very suitable to high resolution paleoceanographic studies, such as wide and well developed shelves (for instance North-Central Adriatic, Gulf of Lyon) that allow the accumulation of very expanded sedimentary sequences for the last 500ka. This is a key time interval, because it contains the climatic oscillations used for the construction of models, predicting climatic variations, and it overlaps to the time interval spanned by the ice core records of Greenland and Antarctica (Dansgaard et al., 1993; Petit et al., 1999; EPICA Community members, 2004). Central Adriatic and the Gulf of Lyon are the sites selected by the EC-PROMESS project (PROfiles across MEditerranean Sedimentary Systems; coordinator Dr. Serge Bernè, IFREMER, France; Contract n. EVK1-CT-2002-40024).

This PhD thesis is mainly focused on this EC project, and it must contribute, for the Adriatic area, to the goals of the Work Package 6 (Chronostratigraphy, paleoclimate and paleoceanography). In particular this PhD thesis is in charge to:

- develop/propose an integrated stratigraphy for borehole PRAD1-2, using and interpreting not only the proxies (planktic and benthic foraminifera) here analysed, but all the available proxies (such as ^{14}C AMS datings, O and C stable isotope, nannoplancton bioevents, tephrochronology, magnetostratigraphy), produced by the PROMESS community
- to reconstruct the paleoenvironment for the last 400kyrs in the Central Adriatic based on variation of foraminifera assemblages and O and C stable isotope records, with particular

attention to the intervals characterised by low bottom ventilation and their relationship with the sapropels deposited in the Eastern Mediterranean

Moreover, an additional research opportunity for this PhD was the availability of cores suitable to reconstruct a high resolution (centennial) paleoenvironmental history of the late Holocene (last 6000 years BP). As this time interval is very condensed in PRAD1-2 borehole, the study has been carried out within the CA-EURODELTA (coordinator: Dr. Fabio Trincardi, ISMAR, Italy, Contract n. EVK3-CT2001-20001) and the EC-EUROSTRATAFORM projects (coordinator: Prof. Phil P. E. Weaver, NOC, U.K., Contract n. EVK3-CT-2002-00079). In summary, these two projects are focused on, respectively:

- the formation of the prodelta systems in Mediterranean and Black Sea during the last 5500 years, their evolution and long-term stability
- the interdisciplinary study of the sediment dynamic on continental margins from the source to the accumulation sites (shelf, slope and deep basin) in four key study areas (Adriatic, Western Mediterranean, Western Atlantic Iberian margin and Northern Norwegian margin) for the last climatic cycle (125000 years).

The study of the cores belonging to these two projects, along with the data obtained in PRAD1-2 borehole, allow to refine and update the foraminifera ecobiostratigraphy of the Central Adriatic and to compare it with the Southern Adriatic one. This opportunity represents the third main goal of this PhD thesis.

Therefore, the frame of this thesis reflects someway the above reported goals. Indeed, the thesis is composed of three parts:

- Part I is focused on the results of borehole PRAD1-2, and it is divided in three chapters, presenting the chronological framework (Chapter I), the paleoenvironmental reconstruction (Chapter II) and a detailed discussion on sapropel-equivalent levels (Chapter III)
- Part II is dedicated to Late Holocene ecobiostratigraphy and paleoenvironmental reconstruction of sequences of the Central and Southern Adriatic in different settings (mid shelf and slope)
- Part III presents the updated foraminifera ecobiostratigraphy for the last 60 kyr

Each part contains a list of the cited references, whereas the geological and oceanographic setting is presented before the Part I.

At the end of the PhD thesis, two publications, already accepted and in press, at which the author co-worked, are attached. They are:

- Asioli, A., and A. Piva. Il ruolo dei foraminiferi nelle ricostruzioni paleoceanografiche e paleoclimatiche: esempi dal Mediterraneo Centrale (Adriatico) per il tardo Olocene attraverso un approccio multidisciplinare. Atti del Convegno Interdisciplinare La ricerca paleobotanica/paleopalinologica in Italia: stato dell'arte e spunti di interesse (Modena, 20-21 novembre 2003). *Informatore Botanico Italiano*, in press.
- Trincardi, F. F. Foglini, G. Verdicchio, A. Asioli, A. Correggiari, D. Minisini, A. Piva, A. Remia, D. Ridente, M. Taviani. The Bari Canyon System: interaction between mass-transport and along-slope processes on the SW-Adriatic Margin (Central Mediterranean). *Marine Geology Special Publication on "Submarine Canyons"*, T. Van Weering and S. Heussner editors, in press.

This thesis presents the results of an original research, undertaken by the author, and none of the results, illustrations or text are based on the published or unpublished work of others, except where specified and acknowledged.

References

Alley, R. B., and P. U. Clark (1999). The deglaciation of the northern hemisphere: a global perspective. *Ann. Rev. Earth Planet. Sci.*, 27, 149-182.

Bond G., W. Broecker, S. Johnsen, J. McManus, L. Labeyrie, J. Jouzel, and G. Bonani (1993). Correlations between climate records from North Atlantic sediments and Greenland ice. *Nature*, 365, 143-147.

Dansgaard W., S. J. Johnsen, H. B. Clausen, D. Dahl-Jensen, N. S. Gundenstrup, C. U. Hammer, G. S. Hviderg, J. P. Steffensen, A. E. Sveinbjornsdottir, J. Jouzel, and G. Bond (1993). Evidence for general instability of past climate from a 250-kyr ice-core record. *Nature*, 364, 218-220.

EPICA Community Members (2004). Eight glacial cycles from an Antarctic ice core. *Nature*, 429, 623–628.

Maslin M., D. Seidov, and J. J. Lowe (2001). Synthesis of the Nature and Causes of Rapid Climate Transitions During the Quaternary (A Review). In: *Seidov, Haupt e Maslin (ed.), The Oceans and Rapid Climate Change: Past, Present and Future, Geophysical Monograph*, 126, 9-52.

Petit J.R., J. Jouzel, D. Raynaud, N. I. Barkov, J. –M. Barnola, I. Basile, M. Bender, J. Chappellaz, M. Davisk, G. Delaygue, M. Delmotte, V. M. Kotlyakov, M. Legrand, V. Y. Lipenkov, C. Lorius, L. Pe´ pin, C. Ritz, E. Saltzmank, and M. Stievenard (1999). Climate and atmospheric history of the last 420,000 years from the Vostok ice core. *Nature*, 399, 429-436.

GEOLOGICAL AND OCEANOGRAPHIC SETTING

The modern Adriatic Sea is a narrow epicontinental basin (ca. 200 x 800 km) with a low axial topographic gradient (ca. 0.02°) in the north, and a steeper shelf farther south. The Adriatic shelf surrounds the Mid Adriatic Deep (MAD), a small slope basin about 250 m deep, where a continuous section of marine mud deposited during the Quaternary including the eustatic minima of the Last Glacial Maximum (LGM) and previous glacial intervals (Trincardi et al., 1996).

GEOLOGICAL EVOLUTION AND PLIO-QUATERNARY STRATIGRAPHY

Geodynamic and sedimentary reconstructions of the geohistory of the Adriatic basin document its evolution from a Mesozoic passive margin to the Cenozoic foreland of the Apennine and Dinaric thrust belts (D'Argenio and Horvath, 1984; Royden, Patacca and Scandone, 1987), that record the collision of the African and European plates (Geiss, 1987). The growth of structural highs of tectonic origin, east of the Gargano Promontory (i. e. the NW-SE oriented Gallignani and Pelagosa ridges, and the SW-NE oriented Tremiti Structural high), took place since the late Pliocene and resulted in the segmentation of the foredeep into two distinct basins: the Adriatic foredeep basin, north of the Gargano, and the Bradano foredeep basin to the south (Casnedi, 1978, 1988; Capuano et al., 1996).

The seismic-stratigraphic study of the Plio-Quaternary basin-fill of the Adriatic evidences repeated variations in sediment flux, depositional styles and prograding directions during the displacement of the Apennine chain (Ori et al. 1986; Ciabatti et al. 1987; Vai and Martini, 2001).

Seismic reflection studies based on Industry data (characterised by deep penetration but limited vertical resolution) showed that the sediments filling the Adriatic basin during the late Quaternary mainly came from the northwest, in an axial direction (Ori et al., 1986; Ciabatti et al., 1987). In particular, the combined supplies of the Po Plain (the major drainage area feeding the basin) and of several smaller coalescing drainage basins dissecting the Apennine chain fed the major progradational units during the LGM (Milliman & Syvitski 1992; Trincardi et al. 1994a). During this time interval, and in the early portion of the following sea-level rise, a shallow sill, less than 50 m deep, connected the Adriatic basin to the rest of the Mediterranean Sea, probably not allowing full exchange of intermediate and deep water masses, as testified by regional bathymetric contours, and by the scarcity or even the absence of planktic foraminifera in LGM sediments (Jorissen et al., 1993; Asioli, 1996). Paleobathymetric reconstructions estimated that, at the onset of the relative sea-level rise following the LGM, only 1/7th of the modern basin was under water, while most of it was subaerially exposed (Trincardi et al., 1994a, b; Correggiari et al., 1996; Vai and Cantelli, 2004). Between about 17000 and 5500 years BP (Fairbanks, 1989), during the late Pleistocene-Holocene relative sea level rise, a wide portion of the northern and central Adriatic alluvial plain, deposited during the glacial time, was progressively drowned, and the Adriatic shelf became eight-fold wider (Trincardi et al., 1994a, b; Correggiari et al., 1996a, b; Cattaneo and Trincardi, 1999). Deposition was condensed on the outer shelf, but expanded both in the deeper basin (Colantoni et al., 1989; Asioli et al., 1996), and in the inner shelf (Trincardi et al., 1996).

LATE HOLOCENE DEPOSITION AND ADRIATIC MORPHOLOGY

The late Holocene clinoform on the Adriatic shelf reaches up to 35 m in thickness with a volume of 180 km^3 (that correspond to 450 10^9 tons of sediment at an average density of 2.5 g cm^{-3}) and rests above a regional downlap surface, the maximum flooding surface (mfs), dated ca. 5.5 cal kyr BP (Asioli, 1996; Correggiari et al., 2001; Cattaneo et al., 2003; Cattaneo et al., 2007). On seismic profiles, the Adriatic shelf clinoform is composed of elementary sigmoid units and shows foresets dipping typically 0.5° to 1.2°. The maximum foreset steepness is consistently observed on sections perpendicular to the coast and reaches the absolute maximum on the E-W stretch North of Gargano Promontory which acts as an obstacle for the Western Adriatic Coastal Current (WACC) sediment dispersal system. High-resolution seismic-stratigraphic and tephra correlation indicate that a thin basal unit represents condensed deposition between 5.5 and 3.7 cal. kyr BP over much of the basin (Correggiari et al., 2001; Oldfield et al., 2003; Lowe et al., 2007). Above this unit, sediment accumulation rates increased to high values (up to 1.5 cm yr^{-1}) due to the forcing from high frequency climatic or anthropogenic changes (Correggiari et al., 2005a).

A coast-parallel, laterally extensive sediment prism, formed in the western side of the Adriatic epicontinental shelf, during the last 5500 years, after the attainment of the present sea level highstand, (Correggiari et al., 1996a, b, Trincardi et al., 1996, Correggiari et al., 2001), and articulated in three distinct but genetically related depocentres, i. e. the Po river prodelta, the Central Adriatic mud wedge, fed by coalescing Apennine rivers, and the Gargano subaqueous delta. This latter depocentre, located far from any direct river input, is entirely composed of marine mud, and is fed by sediment supply derived from multiple, but exclusively northern, sources, transported to the southeast by shore parallel currents; within this prism, the most recent sigmoid developed during a phase of substantial outbuilding of the modern Po delta, corresponding to the Little Ice Age (Cattaneo et al., 2003; Correggiari et al., 2005a, b).

Then, late-Holocene deltas and mud wedges clearly record both short-term climatic changes and/or human impacts through pulses in sediment supply and autocyclic advances, retreats and lateral shifts of deltaic lobes (Cattaneo et al., 2003; Correggiari et al., 2005b). Moreover, the land-locked nature of the Adriatic basin strongly influenced its paleoclimatic history, making climate fluctuations more intense.

Boasting the deposition of a stratigraphically expanded muddy succession during the late-Quaternary, rather continuous and undisturbed, as a result of a weak wavy regime, the Central Adriatic basin offers a great potential for paleoenvironmental studies (Trincardi et al., 1996).

Several volcanoclastic tephra layers deposited in the Adriatic basin, because of the intense volcanic activity of the Italian region in recent and past times. These deposits are strongly useful for stratigraphic purposes, since they provide precious time-lines for correlation and, in many cases, can be reliably dated on land (Lowe et al, 2007). The extensive geophysical database allows definition of an extremely refined seismic stratigraphic framework, which showed how the stratigraphic impact of glacioeustatic fluctuations, variability of sediment influx (in space and time) and high frequency climate oscillate before and during increasing human impact.

Beside the eustatic signal, dominant particularly over the last 800 kyr, other factors concurred to the definition of Adriatic sea-level cycles during the late-Quaternary; these factors include:

1) short-term changes in supply regime (Trincardi et al. 1996)

2) changes in size and shape of the basin and consequently its oceanographic regime (Correggiari et al. 1996a; Cattaneo and Trincardi, 1999)

3) changes in the degree of connection to the rest of the Mediterranean (Asioli et al. 1996).

Repeated depositional cycles, occurring in the Adriatic under the control of Quaternary, high-frequency (fourth order) eustatic cycles, are recorded in four depositional sequences, mainly composed of forced-regressive deposits (Trincardi and Correggiari 2000; Ridente and Trincardi, 2002), varying greatly in thickness and internal geometry along the margin.

OCEANOGRAPHIC SETTING

The Adriatic basin has a microtidal regime and is dominated by a cyclonic circulation driven by thermohaline currents (Poulain, 2001). The North Adriatic Sea receives the highest river runoff of the entire Mediterranean Sea. The basin is highly sensitive to variations in river runoff and atmospheric conditions because of its shallowness (the Adriatic area North of the Po delta is less than 35 m deep). River runoff affects the circulation through buoyancy input, which is one of the major driving forces of the Western Adriatic Coastal Current (WACC; Orlic et al., 1992), and impacts the entire basin by introducing high loads of sediment and related organic matter, nutrients and pollutants (Miserocchi et al., 2007).

The Po River, with an average annual discharge of 1500 m^3s^{-1}, accounts for about 50% of the total northern Adriatic river runoff (Syvitski and Kettner, 2007). A cyclonic circulation gyre is enhanced by the Po River plume and results in trapping fresh waters along the west side of the basin. In this shallow part of the basin, hypoxic events occur, typically, between September and November and reflect: low current velocities at the gyre centre, enhanced water stratification which reduces vertical mixing, and high turbidity which prevents light penetration. Currents are stronger away from the gyre centre, resulting in a prevailing flow to the SE along the Italian coast, a flow that appears consistent with the overall shore-parallel thickness distribution of the late-Holocene clinoform (Cattaneo et al., 2003). Sediment transport is enhanced in the northern Adriatic by the northeasterly Bora wind that enhances waves and currents especially in winter, with an average southward transport along the shelf and reduced across-shelf transport (Lee et al., 2005).

Moreover, the cyclonic Northern Adriatic circulation registers seasonal variations in its strength, and modifications by the occurrence of intensified jets along the Adriatic western coast (Artegiani et al., 1997). Shallow Modified Atlantic Waters (MAW) mix with the fresh, nutrient-rich waters of the Po river runoff and flow parallel to the Italian coast, resulting in enhanced primary productivity in the upper part of the water column (Revelante and Gilmartin, 1977; Boldrin et al., 2005).

The Northern Adriatic plays also a major paleoceanographic role, being one of the sites of dense water formation, which concur in ventilating the Eastern Mediterranean. During the winter season, in fact, outbreaks of the cold and dry north-easterly Bora wind make Northern Adriatic surface waters colder and denser, making them sink (Zore-Armanda, 1963; Artegiani et al, 1989, 1997) and move towards the deeper regions of the Ionian and Eastern Mediterranean (Eastern Mediterranean Deep Waters, EMDW) (Bignami et al., 1990).

The Northern-Central Adriatic basin is connected to the Southern Adriatic via the Pelagosa sill, presently about 160 m deep, and the connection of this semi-enclosed basin with the Eastern Mediterranean is granted by the Otranto Strait, which allows shallower Modified Atlantic Waters and Levantine Intermediate Waters to reach the Adriatic basin (Orlic et al., 1992). The presence of sills and structural highs played a major role in the paleoceanographic evolution of the Adriatic during the past sea-level oscillations, sometimes seriously hampering deeper water masses to pass and ventilate the Adriatic sea floor, isolating the Northern-Central basin and making its history slightly different from that of the Eastern Mediterranean.

The Southern Adriatic is a much deeper basin which connects the Northern-Central Adriatic to the rest of the Eastern Mediterranean, being the site of convergence of two distinct water masses, the North Adriatic Dense Water and the Levantine Intermediate Water, and concurring in the dense water production, as well (Civitarese et al., 2005). Winter convection and dense water formation, in fact, take place in the centre of the Southern Adriatic Pit (SAP), 1200 m deep, as a result of outbreaks of cold continental air from the Balkan Peninsula, which takes heat from the sea surface layer through cooling and evaporation, and causes movement through the water column in the centre of a gyre that rotates counter-clockwise. This winter convection, seldom reaching the basin floor, is significantly variable, strongly depending on local climatic conditions (i. e. number, duration and intensity of the outbreaks). Nevertheless, the deriving winter vertical mixing regularly erodes the deeper nutrient-rich layer and brings nutrient into the photic zone, triggering a spring phytoplankton bloom after the mixing ends. Therefore, the winter convective mixing determines the functioning and the efficiency of the biological pump in the SAP (Gacic et al., 2002).

SUPPLY REGIME

Fluvial sediment sources are located almost exclusively along the north and western side of the Adriatic basin, with a combined modern delivery of 51.7 10^6 t yr^{-1} of mean suspended load with contributions of 3 10^6 t y^{-1} from eastern Alpine rivers, 15 10^6 t y^{-1} from the Po river, 32.2 10^6 t y^{-1} from the eastern Apennine rivers and 1.5 10^6 t y^{-1} from rivers south of the Gargano promontory (Frignani et al., 1992; Milliman and Syvitski, 1992; Sorgente, 1999; Cattaneo et al., 2003). In spite of a smaller drainage area, the Apennine rivers have a sediment yield double of that of the Po river, mainly in response of the muddy lithologies of their catchment basins. Frignani et al. (2005) calculated the balance between mass accumulation rates throughout the mud wedge of the North and Central Adriatic (41.95 10^6 t yr^{-1} of sediment accumulating along the Italian coast) and riverine sediment supply (46.72 10^6 t yr^{-1}) and suggested an annual export of 4.77 10^6 t (6-10% of the river supply) from the continental shelf to the South Adriatic basin.

As already discussed, the Adriatic sediment supply, mainly deriving from the Po and Apennine river runoff, did not accumulate in front of the river mouth but migrated southward, parallel to the coastline and to the clinoform strike (Cattaneo et al., 2003; 2004). The interaction of the marine currents, ventilating the Adriatic basin, with the asymmetric location of the sediment entry points, almost exclusively on the western side of the basin, played an important role in the shaping of sedimentary sequences. Recent studies (Nittrouer et al., 2004) quantified and documented, by means of tripods and moorings, a huge southward sediment advection along the Adriatic shelf to the South Adriatic basin, estimated around four million tons, stocked in the area south of Ancona, demonstrating that advection controls (and controlled) the sedimentation in the basin. However, the strength of the water circulation and the intensity of the wave regime changed repeatedly, and likely on diverse time scales, in response to paleoclimatic, paleophisiographic and paleoenvironmental forcing.

References

Artegiani, A., R. Azzolini, and E. Salusti (1989). On dense water in the Adriatic Sea. *Oceanologica Acta*, 12, (2), 151–160.

Artegiani, A., D. Bregant, E. Paschini, N. Pinardi, F. Raicich, A. Russo (1997). The Adriatic Sea general circulation, Part I. Air–sea interactions and water mass structure. *Journal of Physical Oceanography*, 27, 1492–1514.

Asioli, A., F. Trincardi, A. Correggiari, L. Langone, L. Vigliotti, S. Van Der Kaars, and J. Lowe (1996). The late-Quaternary deglaciation in the Central Adriatic basin. In: Late-Glacial and Early Holocene climatic and environmental changes in Italy. *Il Quaternario, Italian Journal of Quaternary Sciences*, 9, (2), 627-642

Asioli, A. (1996). High resolution foraminifera biostratigraphy in the central Adriatic basin during the last deglaciation: a contribution to the PALICLAS Project. In: Guilizzoni, P. & F. Oldfield (Eds), *Palaeoenvironmental Analysis of Italian Crater Lake and Adriatic Sediments (PALICLAS). Memorie dell' Istituto italiano di Idrobiologia*, 55, 197-217.

Bally, A. W., L. Burbi, C. Cooper, R. Ghelardoni (1986). Balanced sections and seismic reflection proxles across the central Apennines. *Memorie della Società Geologica Italiana*, 35, 257-310.

Bignami, F., E. Salusti, and S. Schiarini (1990). Observations on a bottom vein of dense water in the Southern Adriatic and Ionian Seas. *Journal of Geophysical Research*, 95 (C5), 7249-7259.

Boldrin, A. L. Langone, S. Miserocchi, M. Turchetto, F. Acri (2005). Po River plume on the Adriatic continental shelf: Dispersion and sedimentation of dissolved and suspended matter during different river discharge rates. *Marine Geology*, 222-223, 135-158.

Capuano, N., G. Pappafico, G. Augelli (1996). Ricostruzione dei sistemi deposizionali Plio-Pleistocenici del margine settentrionale dell'avanfossa pugliese. *Memorie della Società Geologica Italiana*, 51, 273-292.

Casnedi, R. (1978). Sedimentazione e tettonica pliocenica nel sottosuolo della bassa valle del Fortore (Foggia). *Memorie della Società Geologica Italiana*, 19, 605-612.

Casnedi, R., (1988). La Fossa bradanica: origine, sedimentazione e migrazione. *Memorie della Società Geologica Italiana*, 41, 439-448.

Cattaneo, A., and F. Trincardi (1999). The late-Quaternary transgressive record in the Adriatic epicontinental Sea: basin widening and facies partitioning. In: Bergman, K., J. Snedden (Eds.), *Isolated Shallow Marine Sand Bodies: Sequence Stratigraphic Analysis and Sedimentologic Interpretation. SEPM Special Publication*, 64, 127-146.

Cattaneo, A., A. Correggiari, L. Langone, and F. Trincardi (2003). The late-Holocene Gargano subaqueous delta, Adriatic shelf: Sediment pathways and supply fluctuations. *Marine Geology*, 193, 61-91.

Cattaneo, A., F. Trincardi, L. Langone, A. Asioli, P. Puig (2004). Clinoformation Generation on Mediterranean Margins. *Oceanography*, 17, 104-117.

Cattaneo A., F. Trincardi., A. Asioli, A. Correggiari (2007). Clinoform formation in the Adriatic Sea: energy-limited bottomset. *Continental Shelf Research*, special issue on Sediment Dynamics in the Western Adriatic (Tim G. Milligan and Antonio Cattaneo guest editors, 27 (3-4), 506-525.

Ciabatti, M., P. V. Curzi, and F. Ricci Lucchi (1987). Quaternary sedimentation in the Central Adriatic Sea. *Giornale di Geologia*, 49, 113-125.

Civitarese, G., M. Gacic, V. Cardin, and V. Ibello (2005). Winter Convection continues in the Warming Southern Adriatic. *Eos*, 45, (8), 445-451.

Colantoni, P., A. Asioli, A. M. Borsetti, L. Capatondi, and C. Vergnaud-Grazzini (1989). Subsidenza tardo-pleistocenica ed olocenica nel medio Adriatico evidenziata dalla geofisica e da ricostruzioni paleoambientali. *Memorie della Società Geologica Italiana*, 42, 209-220.

Correggiari, A., M. E. Field, F. Trincardi (1996)a. Late Quaternari transgressive large dunes on the sediment-starved Adriatic shelf. In: De Batist, M., Jacobs, P. (Eds.), *Geology of Siliciclastic Shelf Seas. Geological Society Special Publication*, 117, 155-169.

Correggiari, A., M. Roveri, and F. Trincardi (1996)b. Late-Pleistocene and Holocene evolution of the North Adriatic Sea. In: *Late-Glacial and Early Holocene Climatic and Environmental Changes in Italy. Il Quaternario, Italian Journal of Quaternary Science*, 9, 697-704.

Correggiari, A., F. Trincardi, L. Langone, and M. Roveri (2001). Styles of failure in heavily-sedimented highstand prodelta wedges on the Adriatic shelf. *Journal of Sedimentary Research*, 71, 218-236.

Correggiari, A., A. Cattaneo, F. Trincardi (2005)a. Depositional patterns in the Late-Holocene Po delta system. In Bhattacharya, J.P., Giosan, L. (Eds.), River Deltas: Concepts, Models and Examples. *SEPM Special Publication*, 83, 365-392.

Correggiari, A., A. Cattaneo, and F. Trincardi (2005)b. The modern Po Delta system: lobe switching and asymmetric prodelta growth. *Marine Geology*, 222-223, 49-74.

D'Argenio, B., and F. Horvath (1984). Some remarks on the deformation history of Adria, from the Mesozoic to the Tertiary. *Ann. Geophys.* 2, 143-146.

Fairbanks, R. G. (1989). A 17,000 year glacio-eustatic sea level record: Influence of glacial melting rates on the Younger Dryas event and deep-ocean circulation. *Nature*, 342, 637-642.

Frignani, M., L. Langone, M. Pacelli, M. Ravaioli (1992). Input, distribution and accumulation of dolomite in sediments of the Middle Adriatic Sea. *Rapp. Comm. int. Mer Medit.* 33, p. 324.

Frignani, M., L. Langone, M. Ravaioli, D. Sorgente, F. Alvisi, S. Albertazzi (2005). Fine sediment mass balance in the western Adriatic continental shelf over a century time scale. *Marine Geology*, 222-223, 113-133.

Gačić, M., G. Civitarese, S. Miserocchi, V. Cardin, A. Crise, and E. Mauri (2002). The open-ocean convection in the southern Adriatic: A controlling mechanism of the spring phytoplankton bloom, *Continental Shelf Research*, 22, 1897–1908.

Geiss, E. (1987). A new compilation of crustal thickness data for the Mediterranean area. *Ann. Geoph.* 5B, 623-630.

Jorissen, F. J., A. Asioli, A. M. Borsetti, L. Capotondi, J. P. de Visser, F. J. Hilgen, E. J. Rohling, K. van der Borg, C. Vergnaud Grazzini, and W. J. Zachariasse (1993). Late Quaternary central Mediterranean biochronology. *Marine Micropaleontology,* 21, 169-189.

Lee, C. M., F. Askari, J. Book, S. Carniel, B. Cushman-Roisin, C. Dorman, J. Doyle, P. Flament, C. K. Harris, B. H. Jones, M. Kuzmic, P. Martin, A. S. Ogston, M. Orlic, H. Perkins, P. –M. Poulain, J. Pullen, A. Russo, C. Sherwood, R. P. Signell, D. Thaler Detweiler (2005). Northern Adriatic Response to a Wintertime Bora Wind Event. *Eos Transactions*, *86/16*, 157-168.

Lowe, J. J., S. Blockley, F. Trincardi, A. Asioli, A. Cattaneo, I. P. Matthews, A. M. Pollard, S. Wulf (2007). Age modelling of late Quaternary marine sequences in the Adriatic: towards improved precision and accuracy using volcanic event stratigraphy. *Continental Shelf Research*, 27 (3-4), 560-582.

Milliman, J., and J. Syvitski (1992). Geomorphic/tectonic control of sediment discharge to the ocean: the importance of small mountainous rivers. *Journal of Geology*, 100, 525-544.

Miserocchi, S., L. Langone, and T. Tesi (2007). Concentration and isotopic composition of organic carbon within a flood layer in the Po River prodelta (Adriatic Sea). *Continental Shelf Research*, 27 (3-4), 338-358.

Nittrouer, C. A., S. Miserocchi, and F. Trincardi (2004). The PASTA Project: Investigation of Po and Apennine Sediment Transport and Accumulation. *Oceanography*, 17, 46-57.

Ori, G. G., M. Roveri, and F. Vannoni (1986). Plio-Pleistocene sedimentation in the Apenninic-Adriatic foredeep (Central Adriatic sea, Italy). In: Allen, P. A., P. Homewood (Eds.), *Foreland Basins. IAS Special Publication*, 8, 183-198.

Orlic, M., M. Gacic, and P. E. La Violette (1992). The currents and circulation of the Adriatic Sea. *Oceanologica Acta*, 15,(2), 109-122.

Pieri, M., and G. Groppi (1981). Subsurface geological structure of the Po Plain, Italy. In: *Progetto Finalizzato Geodinamica. CNR Publ.* 414, 13 pp.

Poulain, P.-M., (2001). Adriatic Sea surface circulation as derived from drifter data between 1990 and 1999. *Journal of Marine Systems*, 29, 3-32.

Revelante, N., and M. Gilmartin (1977). The effects of northern Italian rivers and eastern Mediterranean ingressions on the phytoplankton of the Adriatic sea. *Hydrobiologia*, 56, 229-240.

Ridente, D., and F. Trincardi (2002). Eustatic and tectonic control on deposition and lateral variability of Quaternary regressive sequences in the Adriatic basin. *Marine Geology*, 184, 273-293.

Royden, L., E. Patacca, and P. Scandone (1987). Segmentation and configuration of subducted lithosphere in Italy; an important control on thrust-belt and foredeep-basin evolution. *Geology*, 15, 714-717.

Sorgente, D. (1999). Studio della sedimentazione attuale e recente nel medio Adriatico attraverso l'uso di traccianti radioattivi. *PhD Thesis*, University of Bologna, 178 pp.

Syvitski, J. P. M., and A. J. Kettner (2007). On the Flux of Water and Sediment into the Northern Adriatic. *Continental Shelf Research*, 27 (3-4), 296-308.

Trincardi, F., A. Correggiati, and M. Roveri (1994)a. Late-Qaternary transgressive erosion and deposition in a morden epicontinental shelf the Adriatic semienclosed basin. *Geo-Marine Letters*, 14, 41-51.

Trincardi, F., A. Correggiari, A. Asioli, and M. Roveri (1994)b. Diachronous low-stand wedges filling the Quaternary Adriatic foreland basin. 15th IAS Regional Meeting, Ischia, Italy; 13th-15th April 1994.

Trincardi, F., Asioli, A., Cattaneo, A., Correggiari, A., Langone, L., (1996). Stratigraphy of the late-Quaternary deposits in the Central Adriatic basin and the record of short-term climatic events. *Mem. Ist. Ital. Idrobiol.* 55, 39-70.

Vai, G. B. and I. P. Martini (Eds), (2001). *Anatomy of an Orogen. The Apennines and Adjacent Mediterranean Basins*. Kluver Academic Publishers, 632 pp.

Vai G. B. and L. Cantelli (Eds), (2004). *Litho-paleoenvironmental maps of Itlay during the last two climatic extremes*; explanatory notes by Antonioli and Vai. 32nd IGC, Florence, Italy.

Zore-Armanda, M. (1963). Les masses d'eau de la mer Adriatique. *Acta Adriatica*, 10, (3), 1-94.

Trincardi, F., and A. Correggiari (2000). Quaternary forced-regression deposits in the Adriatic basin and the record of composite sea-level cycles. In: Hunt, D., Gawthorpe, R. (Eds.), Depositional Response to Forced Regression. *Geological Society Special Publication*, 172, 245-269.

PART I

PRAD1-2 borehole

CHAPTER 1: PRAD1-2 STRATIGRAPHY

1.1 INTRODUCTION

The EC funded project PROMESS 1 (PROfiles across MEditerranean Sedimentary Systems) is the first attempt to realise scientific drilling in the Mediterranean Sea, with the aim of deciphering past climate change at century to decadal-scale resolution over the last ca. 500 kyr. The general objective of PROMESS 1 is to obtain comprehensive transects across two Deltaic Margins in the NW Mediterranean (the Rhone and Catalan-Languedocian river system) and in the Adriatic (the Po and Apennine river system). These two areas have high sedimentation rates, good sequence preservation but contrasting regional tectonic settings. The huge data base and background scientific knowledge already available in the two study areas, as well as the unique preservation of thick sedimentary sequences, offer the opportunity to interpret the borehole stratigraphies in light of a detailed knowledge of the sedimentary architecture of both continental margins. Indeed, the two areas, in contrast with other Mediterranean margins, have a sufficiently broad continental shelf to permit an interpretation of seismic units and discontinuities in terms of changes of relative sea-level, accommodation space, sediment supply and oceanographic regime (sediment dispersal). The possibility of physical correlation between shelf and slope domains provides the opportunity to exploit the rather thick shelf successions for paleoenvironmental reconstructions during distinctive intervals whose understanding requires extremely high stratigraphic resolution.

PROMESS 1 focuses on the past ca 500 kyr because this period (a) encompassed several orders of cyclicity that are characteristic of past Quaternary climate change (100, 40, 20 kyr) and millennial-scale episodes of abrupt climatic change, and (b) overlaps with studies based on Greenland, North Atlantic and Antarctic ice cores.

More specific objectives of this project are:

1. to determine the stratigraphic response to glacio-eustatic and climatic changes during the last 500 kyr.
2. to study the impact of changing oceanographic regime and sediment supply on continental slope stability.
3. to quantify slope processes by *in situ* measurements of physical parameters in zones prone to failure, or where slides already occurred.

4. to reconstruct the stratigraphic impact of oceanographic and climatic change in the Mediterranean area, within complementary intervals over the last 500 kyr, including (a) the Milankovitch scales, and (b) the sub-Milankovitch (Dansgaard-Oeschger) scale, in particular for intervals that can be precisely constrained geochronologically such as during the last deglacial period.

5. to investigate depositional processes, architecture and preservation potential of sand bodies within shelf, slope and deep-sea environments.

6. to define criteria for disentangling the signature of eustatic changes from that of tectonic deformation at short time scales.

This paper aims at satisfying the first and the fourth objective of the project for the Adriatic area, providing the chrono-stratigraphic framework for borehole PRAD1-2, by integrating different proxies, among which the detection in a shelf environment of bottom water low-oxygenation episodes, to be linked to the (deep-water) sapropels deposition in the Eastern Mediterranean. The paleodepth oscillations throughout the glacial-interglacial cycles along with the paleoenvironmental reconstruction constitute additional goals.

Several papers in the recent literature provide stratigraphic and paleoceanographic reconstructions for the Adriatic Sea, but high resolution records have been obtained only for the last deglaciation and Holocene intervals (Asioli et al., 1999, 2001). The longest continuous record published for the Adriatic region is borehole VE1 (Massari et al., 2004), drilled in the Venice lagoon and reaching upper Pliocene sediments, where glacial-interglacial cycles of the last 400 kyr are represented by repeated oscillations from continental to inner shelf environment. In addition, Amorosi et al. (1999, 2004) published a detailed stratigraphy of several boreholes reaching MIS7c on the coastal plain near Ravenna where they identified the base of MIS5e at 126.7m below sea level. Therefore, PRAD1-2 borehole represents a unique opportunity to study a continuous marine record for understanding this area, particularly interesting for its geological and oceanographic setting.

1.2 MATERIALS AND METHODS

PRAD1-2 borehole was collected in the Mid-Adriatic Deep, (LAT 42°40'34.7826"N LONG 14°46'13.5565"E) in a water depth of 185.5 m (Fig. 1.1). The multi-corer device on board Bavenit geotechnical ship provided a sediment core of 71.2 m, with a recovery of 99.96%. This is the longest

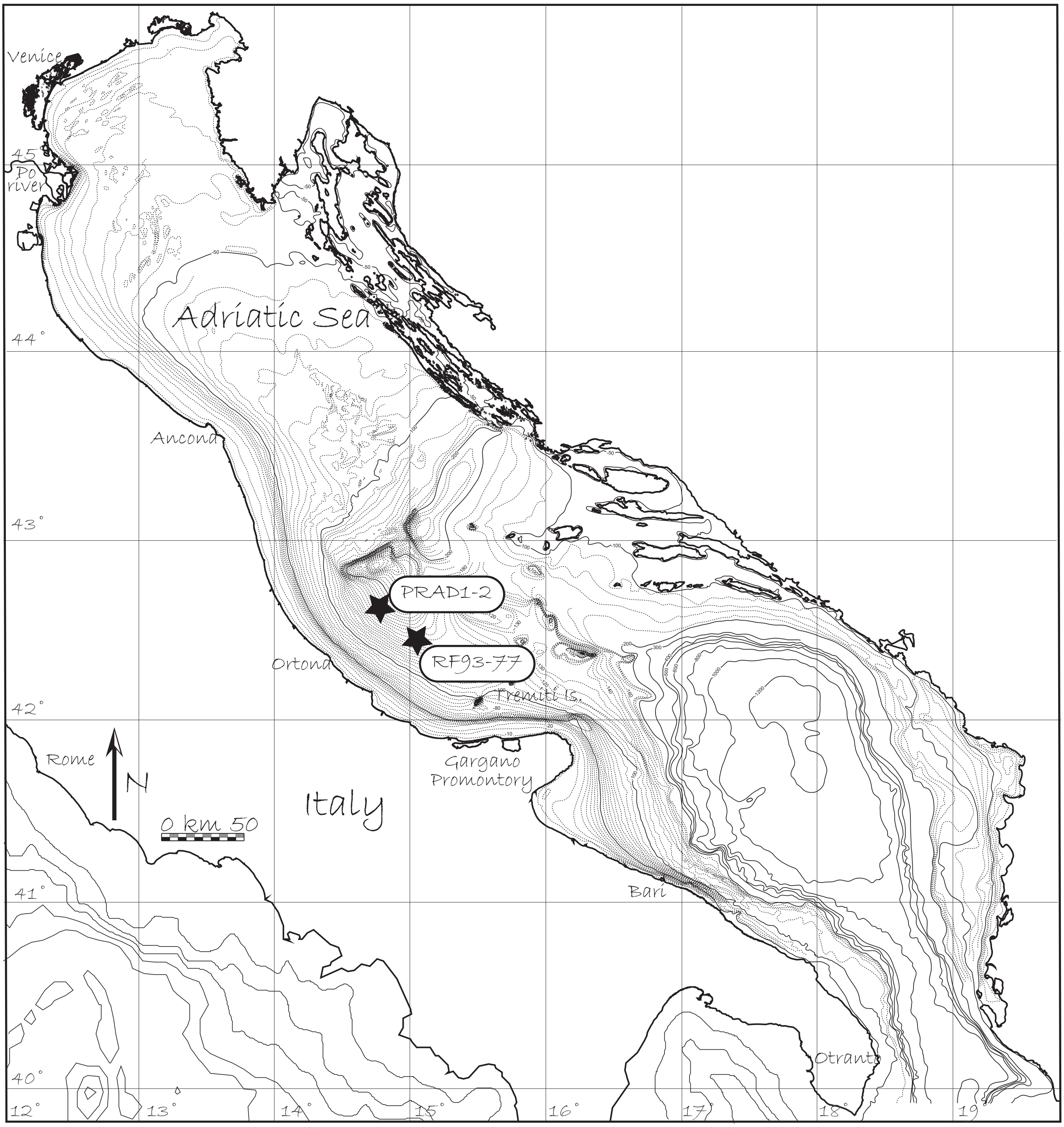

Fig. 1.1 Location of borehole PRAD1-2 and of the reference core RF93-77.

record of continuous and almost undisturbed sediment available up to now for the Adriatic basin. The borehole consists of 89 sections, each of which is about 75-80 cm long on average and 6cm in diameter. After splitting, one half core has been stored as archive, whereas the working half has been sampled for multiple analyses (micro- and macropaleontology, sedimentology, magnetostratigraphy, geochemistry and sediment properties). Materials and methods used for the chronostratigraphic framework and for the paleoenvironmental studies include:

- Foraminifera. The samples were taken in slices 2 cm thick (about 28-30 cc), with an average sampling interval of 10 cm; in correspondence of lithologic variations, the sampling gap was reduced. Additional samples were collected wherever significant micropaleontologic variations occurred and a higher resolution record was required. All the 784 subsamples were dried in the oven at 50°C, weighed, then washed and sieved through a 63 μm mesh and dried again at 50°C. The samples were finally split into aliquots using a Jones microsplitter, and a number of aliquots was counted to reach at least 300 planktic and 300 benthic foraminifers' specimens. The counting of the foraminifers' content of each aliquot provided an estimate of the total number of specimens of each species for each sample. The counting was performed on the fraction >106 μm, to avoid juvenile specimens and, especially during glacial periods or in tephra layers, the finest terrigenous material. However, the fraction <106 μm was always checked, in order not to miss those specimens which can pass the mesh because of an elongated shape of their shell (such as *Fursenkoina*), or of a small size also in their adult stage of life (such as *Epistominella*). Taxa are quantified as percentages of the total number of planktic and benthic foraminifera, while the concentration is reported as number of specimens per gram of dry sediment. The study of foraminifers' assemblage was arranged in two steps: firstly, the semi-quantitative analysis of all the samples of the borehole allowed defining a preliminary general stratigraphic trend, along with some evidence about the depositional environment. Secondly, based on the indications suggested by this preliminary survey, selected samples have been analysed quantitatively (in total 307 samples). The intervals corresponding to MIS1-3 and to MIS 10 were analysed at lower resolution than the rest of the hole, because a) MIS1-4 had already been analysed in detail in core RF93-77, collected in the same area of hole PRAD1-2 and studied with a multi-proxy approach (Guillizzoni and Oldfield, 1996), and b) MIS10 foraminifers' assemblage shows several homogeneous intervals, without significant variations within. Some planktic species or morphotypes are lumped together according to the following scheme: *Globigerinoides* ex gr. *ruber* includes *Globigerinoides ruber* and *Globigerinoides elongatus*; *Orbulina* includes both *Orbulina universa* and *Orbulina suturalis*; *Globigerinoides sacculifer* comprehends *Globigerinoides trilobus, Globigerinoides sacculifer* and *Globigerinoides quadrilobatus* (sensu Hemleben *et al.* 1989).

•Oxygen and Carbon stable isotopes. The analyses were made out on the same samples used for the micropaleontological study, on the $CaCO_3$ of the shells of selected monospecific foraminifers' specimens. In particular, twenty specimens (on average) of *Globigerina bulloides* (planktic) and *Bulimina marginata* (benthic) were picked up from the size fraction >180 µm; these two species were chosen because they grant the widest continuity along the borehole. The analysis were performed at the Leibniz Laboratory for Radiometric Dating and Stable Isotope Research, CAU Kiel, Germany (Dr. Nils Andersen), by means of a device, developed in Kiel labs, connected to a MAT 251 mass spectrometer. In the Kiel device, CO_2 is liberated from the carbonate samples by adding several drops of 100% phosphoric acid individually to each sample. The reaction with phosphoric acid in evacuated sample vials takes place at a constant temperature of 75°C. The reaction time is about 4 minutes. The liberated CO_2 and the H_2O, which is also produced during the reaction, are afterwards quantitatively frozen in a so called multi-loop with the help of liquid nitrogen (about -196°C), and subsequently heated to a temperature of about -55°C; at this temperature H_2O is still frozen in the multi-loop, but all CO_2 is liberated again. Each sample is measured ten times (in a succession of reference gas, sample gas, reference gas, sample gas etc.). The external error of each measure is better than 0.04‰ (^{13}C) and 0.06‰ (^{18}O).

•^{14}C AMS datings were performed on benthic monospecific samples (*Elphidium crispum* or *Hyalinea balthica*) at the Poznan Radiocarbon Laboratory, Poland, (Dr. Tomasz Gozlar), from the size fraction >250 µm. Ages were calibrated using two calibration programs: Calib 5.0.2 Radiocarbon Calibration Program on line (Stuiver & Raimer, 1993) for Radiocarbon ages BP younger than 20000 years (marine sample= 100%, Calibration data set: Marine04 ^{14}C according to Hughen et al. 2004) and the recently published online calibration program by Fairbanks et al. (2005) (http://radiocarbon.LDEO.columbia.edu) for ages between 0 and 55,000 years.

Calibration with Calib 5.0.2. In order to calculate the ΔR (reservoir), two sites on the western side of the Adriatic were selected from the Calib 5.0.2 database, from Northern Adriatic (Rimini) and Southern Adriatic (Barletta), neglecting data from Dalmatia and Croatia (Rovigne). The calculated weighted mean ΔR value is 135.8 with a standard deviation of 40.8. The calibrated age ranges are reported in years BP and referred to 2σ (Table 1.1).

Lab. N.	Sample	Material	^{14}C age	Calibrated age (yr BP)
Poz-16129	PRAD1-2 S8 cm 40-42	E. crispum	14930 ± 90 BP	16760 - 17776
Poz-16130	PRAD1-2 S10 cm 60-62	E. crispum	16530 ± 100 BP	18968 - 19411

Table 1.1. Calibrated ages according to Calib5.0.2 ^{14}C dating program.

Calibration with Fairbanks et al. (2005). The same two sites from the Adriatic were selected from Fairbanks et al. (2005), Butzin et al., (2005) and Cao et al., (2007) for the reservoir output. The calculated reservoir is 262 and 254 years for Rimini and Barletta sites, respectively. Then, a mean age of 258 years has been used for the calibration (^{14}C age minus 258=^{14}C age to be calibrated). The calibrated ages are reported in years BP and referred to 2σ (Table 1.2). In comparison with the ages obtained with Calib 5.0.2, the calibrated ages are slightly older (the mean age corresponds to the older limit calculated by Calib 5.0.2).

Lab. N.	Sample	Material	^{14}C age (BP)	Calibrated version mean (yr BP)	Standard deviation
Poz-16129	PRAD1-2 S8 cm 40-42	E. crispum	14930 ± 90	17894	168
Poz-16130	PRAD1-2 S10 cm 60-62	E. crispum	16530 ± 100	19423	83
Poz-16131	PRAD1-2 S17 cm 60-62	E. crispum	24130 ± 15	28435	178
Poz-16132	PRAD1-2 S17 cm 60-62	H. balthica	23390 ± 150	27654	181
Poz-17321	PRAD1-2 S19 cm 40-42	E. crispum	28960 ± 270	33450	482
Poz-17320	PRAD1-2 S21 cm 40-42	H. balthica	36700 ± 600	41626	376

Table 1.2. Calibrated ages according to Fairbanks et al. (2005) ^{14}C dating program.

Finally, as comparison for the calibration of ages older than 20,000 years the CalPal (Cologne Radiocarbon Calibration and Paleoclimate Research Package) online program (B. Weninger & O. Jöris & U. Danzeglocke 2005) has been run. This software in fact allows the calibration up to 50 kyr. Nevertheless, it must be taken into account that CalPal Online is designed to support explorative research mainly on hominid behavioural response to Pleistocene climate change, and the procedures implemented may not in all cases be identical to the procedures officially recommended by the ^{14}C-community. Before running the program ca. 580 years have been subtracted to the ^{14}C age of each sample, that is the average of the ^{14}C ages reported for the shells collected in 1906 and 1911 from Northern Adriatic (Rimini) and Southern Adriatic (Barletta). The results obtained are reported in the Table marked with a star. Note that the resulting age ranges are referred to 1σ (Table 1.3).

Lab. N.	Sample	Material	^{14}C age	Calibrated age (yr BP)
Poz-16131	PRAD1-2 S17 cm 60-62	E. crispum	24130 ± 150 BP	28513 - 29229*
Poz-16132	PRAD1-2 S17 cm 60-62	H. balthica	23390 ± 150 BP	27455 -28033*
Poz-17321	PRAD1-2 S19 cm 40-42	E. crispum	28960 ± 270 BP	32222 - 33754*
Poz-17320	PRAD1-2 S21 cm 40-42	H. balthica	36700 ± 600 BP	41093 - 42106*

Table 1.3. Calibrated ages according to CalPal ^{14}C dating program.

Substantially, the ages obtained with CalPal do not show a great variation in comparison with the calibration program by Fairbanks et al. (2005).

• Magnetic properties (measurements by Dr. Luigi Vigliotti, ISMAR, CNR, Italy). U-channels were extracted from the working half of the 89 sections of PRAD1-2 borehole. A full paleomagnetic study of the U-channel has been carried out at the University of California Laboratory in Davis, using an automated 2G Enterprises cryogenic magnetometer. Paleomagnetic and rock-magnetic investigations were carried out at 1cm spacing, following this strategy (L. Vigliotti in: "EC-PROMESS1 final report", 2006):

- First the NRM was measured and investigated by stepwise AF demagnetisation in 5 steps up to 50-60 mT, depending on the coercivity of the sediment. These peak-fields were identified by preliminary tests as sufficient to reduce the NRM at about 10% of the initial value and to remove secondary overprints.

- Subsequently an ARM (90 mT AF+ 0.1 mT DC field) was imparted to the sediments and demagnetized in 3 steps (20-30-40 mT) representing most of the magnetic coercivity spectrum.

- An isothermal remnant magnetization (IRM) at 1T was applyed to the sediments. The U-channels were demagnetized in 6 steps up to 60 mT.

- A back-field IRM (BIRM) was imparted to U-channel from sections 16-89.

• Calcareous nannoplancton (analysis by Dr. Elena Colmenero-Hidalgo, Univeristy of Salamanca, Spain). Details on this analysis are reported in Colmenero-Hidalgo and Flores (2005). Here are highlighted the main information on this method. Samples of about 1 cc of sediment were extracted from the bottoms of all the sections immediately after the core arrived on board. This material was taken from the centre of the transversal bottom section in order to avoid contamination by sediment from other depths, drilling muds or by external material that could have been accumulated near the PVC border.

The smear slides were examined on a light microscope at around x1000 magnification under both cross-polarized and transmitted light. Observations over more than 100 visual fields were performed, searching for age marker taxa in critical stratigraphic intervals. A variable number of coccoliths was identified and counted in each slide, depending on the general abundance of all coccoliths and on the abundance of specific taxa. The abundance of the different species was estimated in a semi-quantitative fashion (relative abundances).

During the counting, several taxonomic classifications have been followed. Regarding *Emiliania huxleyi*, forms larger and smaller than 4 μm were counted separately following the criteria given on Colmenero-Hidalgo et al. (2002). For the genus *Gephyrocapsa*, the proposal of Flores et al. (1999) has been followed, although *Gephyrocapsa caribbeanica* has not been divided into size groups.

•Colour reflectance (measurements made out by Dr. Bernard Dennielou, IFREMER, Brest, France). Spectral reflectance has been measured at IFREMER (Brest) by means of a Spectrophotometer Minolta CM-508. Data from 400 to 700 nm wave length (measured with a wave length interval of 10 nm) were obtained every two centimetres and are expressed as percentage.

1.3 CHRONOSTRATIGRAPHIC FRAMEWORK

The chronostratigraphic framework is based on the following integrated proxies:

- Oxygen and Carbon stable isotope stratigraphy
- Biostratigraphy (calcareous nannoplancton, planktic and benthic foraminifera)
- Magnetostratigraphy
- ^{14}C AMS datings
- Tephrochronology
- Foraminifera climate cyclicity
- Sapropel stratigraphy

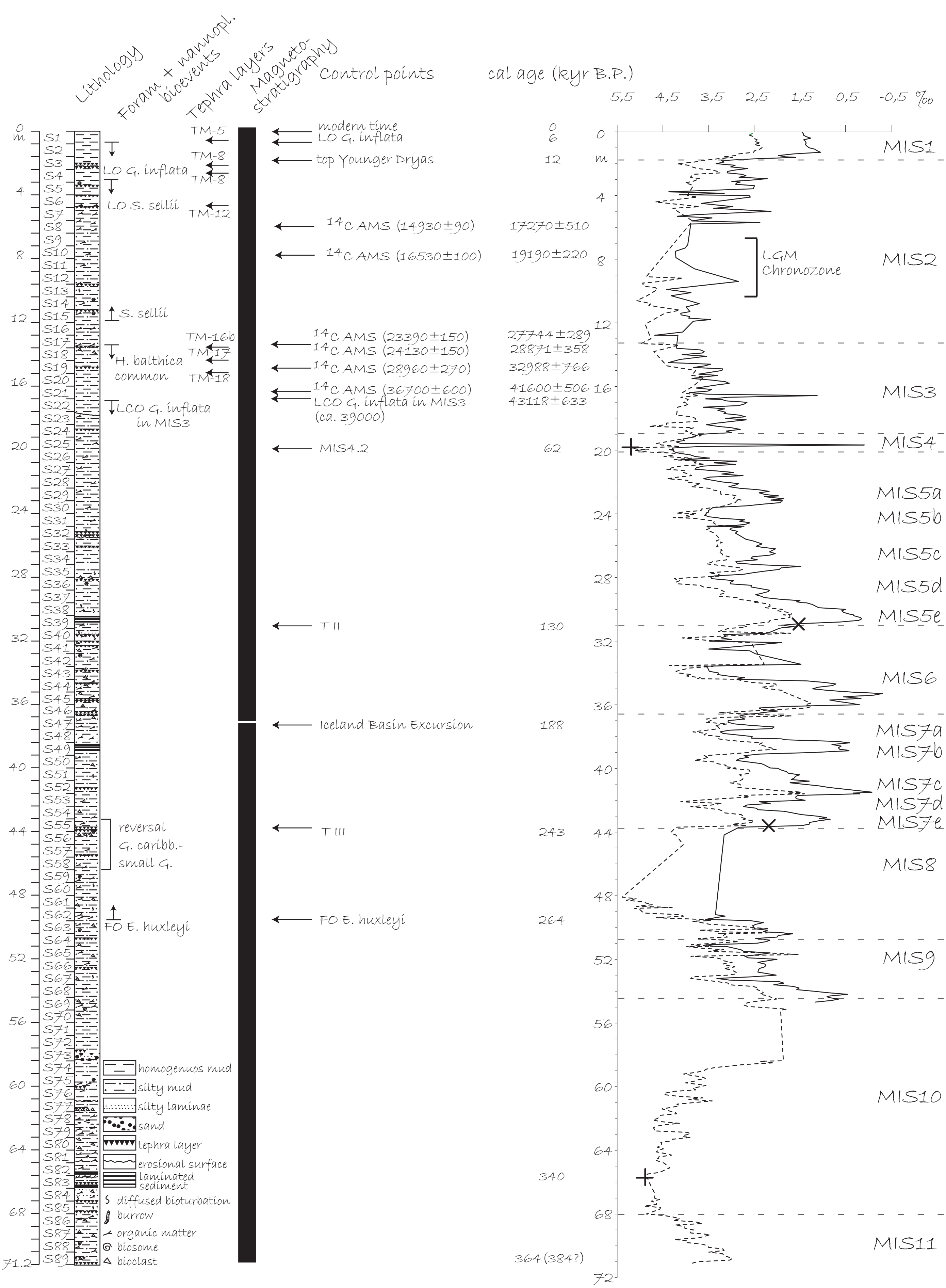

Fig. 1.2a. PRAD1-2 stratigraphic scheme based on isotope stratigraphy, magnetostratigraphy, radiocarbon datings, tephrochronology and bioevents. X correspond to the control points at the Terminations mid-points (Lisiecki and Raymo, 2005); + correspond to control points at glacial maxima values (Bassinot et al., 2004). Lithologic description according to D. Ridente and M. Bassetti

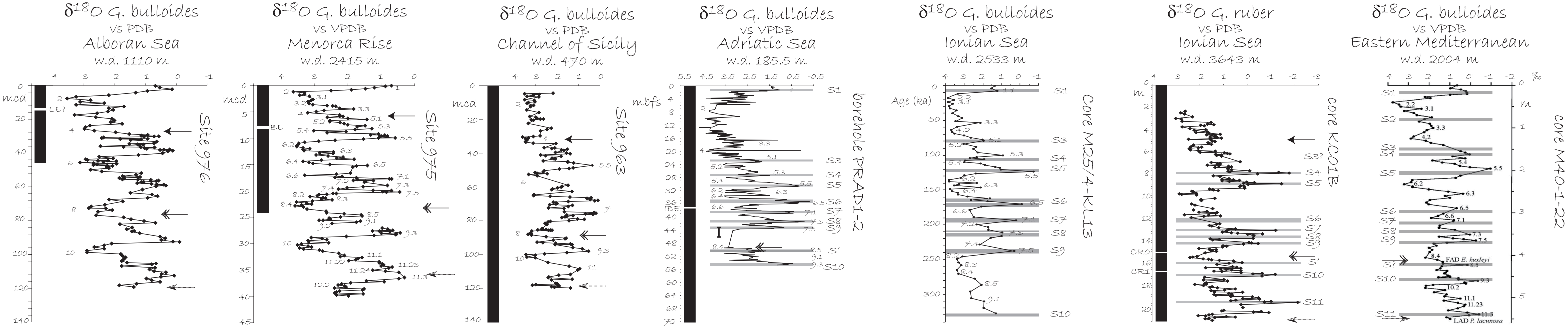

Von Grafenstein et al. (1999) Pierre et al. (1999) Howell et al. (1998) Schmiedl et al. (1998) Lourens (2004) Löwemark et al. (2006)

←	F Eh>Geph l	Bottom acme E. huxleyi = FO E. huxleyi > Gephyrocapsa spp. (MNN 21a- 21b)
↞	F Eh	FO E. huxleyi (MNN 20-21a)
⇠	L Pl	LO P. lacunosa (MNN 19f- 20)
I		reversal G. caribbeanica - small Gephyrocapsa

Nannofossil bioevents	age (kyr B.P.)	
FO E. huxleyi > Gephyrocapsa spp.	0.070*	0.052#
FO E. huxleyi (MNN 20-21a)	0.270*	264#
LO P. lacunosa (MNN 19f- 20)	0.406*	465#

* according to de Kaenel (1999)
\# according to Lourens (2004)

Hole	Geomagnetic event		Age (kyr B.P.)	Reference
KC01B	CR0	Calabrian Ridge	260	Langereis et al. (1997), Lourens (2004)
	CR1	Calabrian Ridge	319	Lourens (2004)
PRAD1-2	IBE	Island Basin Excursion	188	
ODP 975	BE	Blake Event	117-123	Capotondi and Vigliotti (1999)
	LE?	Lashamp Excursion	32-50	Capotondi and Vigliotti (1999)
ODP 963				Richter et al. (1998)

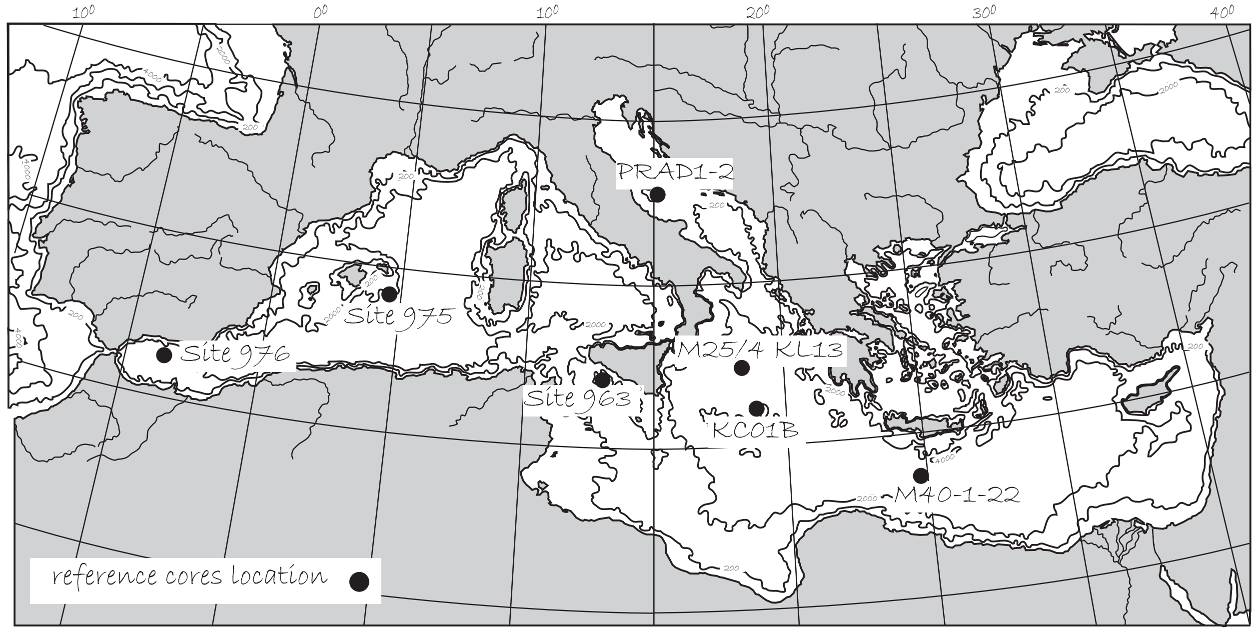

Fig. 1.2b.
Above: Mediterranean planktic oxygen records transect from West to East. Calcareous nannoplankton events as well as magnetic stratigraphy are reported where available.

These proxies are discussed separately. The chronological framework is obtained in two steps: the first is based on "traditional" proxies, such as isotope stratigraphy, magnetostratigraphy, radiocarbon datings, the main microfaunistic bioevents and tephrochronology (Fig. 1.2a). The second step, that allows refining the chronological frame of the borehole, is based on the climatic cyclicity (Fig. 1.3) and on the sapropel stratigraphy (Fig. 1.4). This second step needs the paleoenvironmental interpretation of the foraminiferal record and of the other proxies. The final chronology is summarized in the age model reported at the end of this chapter (Fig. 1.5).

Isotope stratigraphy

Although not continuous, especially in some glacial periods, during which plankton becomes rare (very scarce in MIS2) or near-absent (MIS8 and MIS10), the $\delta^{18}O$ record of *G. bulloides* allows a characterization of all the most significant stratigraphic events (MIS) from MIS1 down to MIS9, identified for comparison with many time equivalent $\delta^{18}O$ (*G. bulloides*) curves, obtained from Mediterranean records (see Fig. 1.2b and the discussion below). The $\delta^{18}O$ record is available also for the benthic foraminifer *B. marginata,* since this species is present in intervals where plankton is poorer (e.g. early MIS8, MIS10 and late MIS11). The benthic $\delta^{18}O$ curve was obtained on an infaunal species (*B. marginata*) and parallels the *G. bulloides* one although with heavier values: this evidence suggests that, in general, oceanographic changes occurring in the area involved the whole water column and that the benthic $\delta^{18}O$ curve somehow may integrate or complement the planktic one. Both the planktic and the benthic records allow also the recognition of minor climatic oscillations, such as the cold isotopic substages inside interglacial MIS5, MIS7 and MIS9 (Fig. 1.2a).

The interpretation of the lowermost part of the hole, below 55 mbsf, that is below the base of MIS9, is more problematic. For this interval, only the benthic record is available, because the environment was too shallow to allow a rich planktic foraminifers' assemblage. The benthic record presents the most positive values (ca. +4.7‰) between 65.5 and 68 mbsf, interval that here is tentatively equated to MIS10.2. Above 65.5 mbsf the oxygen composition moves gradually and with small fluctuations towards lighter values (ca. +3.7‰), culminating with a strong shift around +1.7‰ at 58.2 mbsf, comparable to the ones of MIS9. Below 68 mbsf the benthic $\delta^{18}O$ reaches ca. +3‰, value comparable with, or even lighter than, the ones typical of warm intervals, such as MIS9, MIS5c, MIS5a and MIS3. Therefore, the bottom of the borehole is tentatively ascribed to MIS11.1 (or MIS 11.2.3).

In Fig. 1.2b Mediterranean planktic oxygen records are reported for comparison with PRAD1-2, in a transect from West to East. Even though the land-locked Central Adriatic basin was heavily influenced by variations in salinity, induced by the unsteady run off from the Alps and Apennines, the oxygen record is consistent with those available not only for the Adriatic basin (Vergnaud-Grazzini and Pierre, 1992, Ariztegui et al., 2000, Siani et al., 2000), but also for other Mediterranean deep basins (e.g. Schmiedl et al., 1998, Negri et al., 1999, Lourens 2004 for the Ionian Sea, Howell et al., 1998, Kroon et al., 1998, Löwemark et al., 2006 for the Eastern Mediterranean, von Grafenstein et al., 1999, Pierre et al., 1999 for the Western Mediterranean). This remarkable coherency with other Mediterranean isotopic records, confers to the shallow PRAD1-2 borehole a regional significance and a great potential for correlation outside the Mediterranean. A strong local signal, caused by high freshwater discharge, could in fact be expected, in particular during glacial intervals, because riverine sources were even closer to the location of PRAD1-2 hole. Nevertheless, the record does not appear to be heavily affected by dilution, since water dominant basin-scale circulation likely confined fluvial runoff along the coastline.

Both the planktic and benthic records allow the recognition of the major Glacial Terminations (TI, TII and TIII), whose mid-points have been taken as time-lines (referring to Lisiecki and Raymo, 2005) for the age model. These mid points are marked by “x” in Fig. 1.2a.

An additional control point (“+” in Fig. 1.2a), refers to MIS4.2 cold oscillation dated by Bassinot et al., (2004).

Biostratigraphy

- The preliminary semiquantitative analysis of the calcareous nannoplancton biostratigraphy was carried out onboard R/V Bavenit during the PROMESS1 cruise, by means of smear slides (Colmenero-Hidalgo and Flores, 2005). The preservation of coccoliths is moderate to good, dissolution is not high and specimens are generally abundant. Species belonging to genus *Gephyrocapsa* and the species *Emiliania huxleyi* dominate the nannoplancton assemblage. Anyway, the amount of reworked nannofossils in PRAD1-2 samples shows several peaks reaching up to 80% in respect to the total of counted coccoliths, especially at 5-10 mbsf (MIS2), 33 mbsf (MIS6), 46mbsf (MIS8) and 60 mbsf (MIS10) (Colmenero-Hidalgo and Flores, 2005). Nevertheless, some biostratigraphic event has been determined and the following selected bioevents were considered for the stratigraphy of the borehole:

a) Although few specimens of *Pseudoemiliania lacunosa* were identified at the very bottom of the borehole, the extensive reworking in these samples makes their origin uncertain (Colmenero-Hidalgo and Flores, 2005). Therefore, according to these authors, the age of the base of the borehole is younger than the Last Occurrence of *P. lacunosa* (sensu Rio et al., 1990, end of Nannofossil Zone NN19 of Martini, 1971) which is usually established around 460 kyr.

b) The first occurrence of *E. huxleyi* (Rio et al., 1990) was identified at around 49,5 mbsf, (bottom of section 62). Thierstein et al. (1977), established an age of 268 kyr (top of MIS8) for this event (Colmenero-Hidalgo and Flores, 2005). In this work the astronomically calibrated age of 264 kyrs according to Lourens (2004) has been used.

c) A reversal in the dominance of the assemblage from *G. caribbeanica* to the group of small *Gephyrocapsa* is recorded between 46.33 and 43.17 mbsf (bottoms of sections 58 to 54). According to its position on the borehole, near the FO of *E. huxleyi* (dated at 268 kyr by Thierstein *et al.*, 1977), this reversal can be identified as the equivalent to the one commonly observed in Atlantic records during MIS 8 (Hine and Weaver, 1994) and that has been dated by Villanueva *et al.* (2002) to occur between 260 and 245 kyr (top of MIS 8) in a core north of the Azores Islands) (Colmenero-Hidalgo and Flores, 2005).

- In addiction, some foraminifera-based bioevents constrain the Late Glacial-Holocene interval, based on the well constrained biostratigraphy established for the Central Adriatic (Jorissen et al., 1993, Ariztegui et al., 2000, Asioli et al., 1999 and 2001). These bioevents are:

a) LO *Globorotalia inflata* at 6 kyrs BP approximating the mid-Holocene

b) LO *Globorotalia truncatulinoides* at 9.5 kyr B.P. during the pre-Boreal (this age origins from the re-calibration according to Fairbanks et al 2005 of the age proposed by Asioli et al. 1999)

Magnetostratigraphy and magnetic properties

After AF cleaning the NRM directions exhibit a constant normal polarity for all the sections, so that the borehole can be completely ascribed to Brunhes Normal-polarity Magnetozone (L. Vigliotti in: "EC-PROMESS1 final report", 2006). Two intervals with reverse polarity have been observed at around 37 and 58 mbsf. The former spans about 12 cm (37.28-37.40 mbsf.) and is well supported by changes in both magnetic declination and inclination. According to oxygen stable isotope stratigraphy, this excursion is close to the boundary between MIS7 and MIS6. On this basis, it can be correlated with the Iceland Basin Excursion (IBE) corresponding to an age of about 188kyrs BP (L. Vigliotti in: "EC-PROMESS1 final report", 2006). Another reverse interval observed at around 58.45 mbsf is quite suspicious because it is constrained only by negative inclinations. There is the chance that this level could only have a stronger overprint; further investigations are therefore necessary to check if it could be really representative of a true excursion (L. Vigliotti in: "EC-PROMESS1 final report", 2006).

Radiometric dating

The ^{14}C ages obtained allowed refine the chronology in the uppermost part of the borehole. These ages, along with the control points available for core RF93-77, (Trincardi et al., 1996, Asioli, 1996) collected very close to PRAD1-2, allowed to approximate the following foraminiferal bioevents:

- the Last Glacial Maximum Chronozone, according to Mix et al. (2001), can be defined between 19000 and 23000 cal. yrs BP (i.e. 16100-19500 ^{14}C-yr BP). Interpolating the radiocarbon datings available in PRAD1-2, the LGM Chronozone should range between 7.7 and 10.3mbsf. This chronozone seems to be positioned just above the heaviest ^{18}O values in MIS2.
- the temporary disappearance of the benthic foraminifer *H. balthica* (ca. 28ka cal. age BP), before its reoccurrence at the base of the GI-1, approximates the boundary MIS3/MIS2 (ca. 29ka cal. age in Voelker et al. 2002).
- the last common occurrence of *G. inflata* during MIS3 in core RF93-77 (Asioli, 1996) shows a ^{14}C age of 39040 ± 800 yrs B. (43118±633 yrs BP calibrated with CalPal as described previously). This bioevent approximates (pre-dates) the occurrence of the Campanian Ignimbrite (TM-18) tephra. This age seems to be coherent with the position of the LCO of *G. inflata* in PRAD1-2 during MIS3 (Section 22 cm 10-12).

Tephrochronology

Bourne (2006) identified the main volcanic layers in the uppermost part of PRAD1-2 record. The results are reported in Table 1.4 and in Fig. 1.2a.

Tephra level (cm)	Origin	Volcanic event	Monticchio Varve age (yr BP)
55-60	Phlegrean Fields	Agnano Monte Spina (TM-5)	4620
215-220/265-270	Phlegrean Fields	Neapolitan Yellow Tuff (TM-8)	14120
470-475	Vesuvius	Greenish (Verdoline) (TM-12)	17560
1355-1360	Vesuvius	Codola (Base) (TM-16b)	26790
1430-1435	Alban Hills	Peperino Albano (TM-17)	29700 ±400*
1510-1515	Phlegrean Fields	Campanian Ignimbrite (TM-18)	32970

Table 1.4. Identification of the main tephra layers in the uppermost part of borehole PRAD1-2 and their correspondent ages.(*^{14}C yr BP).

Foraminifera climate cyclicity (Fig. 1.3)

The variation in the composition of planktic foraminifers' assemblages delineates a climatic cyclicity in the hole, that mimics the oxygen stratigraphy. Indeed, a succession of warm and cold intervals, corresponding to the period from MIS10 till the present interglacial, is clearly observed. Interglacial periods are characterised by abundant planktic foraminifera, typical of warm climate conditions (*Globigerinoides* ex gr. *ruber*, *Orbulina*, *Zeaglobigerina rubescens, Globigerinoides sacculifer*, *Globigerinella* spp), whereas glacial intervals show scarce (*Globigerina bulloides*, *Globigerina quinqueloba* and in some case *Neogloboquadrina pachyderma*) or absent cold water planktic foraminifera assemblages. In the lowermost part of the borehole, from 72 to 69 mbsf, the foraminiferal assemblage indicates relatively warm conditions and a slight deepening, compared to the overlaying sections; this is in agreement with the benthic oxygen isotope curve, and corroborates the hypothesis that the base of the borehole may have reached late MIS11.

Planktic foraminifera are scarce or absent during glacial intervals, since the thickness of the water column was strongly reduced because of the sea level fall. The glacial signal is therefore better described by the benthic assemblage, which points out oscillations in the paleodepth: interglacial intervals are characterised by an outer shelf to upper slope foraminiferal assemblage (*Uvigerina peregrina*, *Uvigerina mediterranea*, *Gyroidinoides* spp, *Cibicidoides pachyderma*, *Bulimina ex gr. marginata*, *Brizalina spathulata-catanensis*, *Trifarina angulosa*, *Hyalinea balthica*, *Cassidulina laevigata carinata*), whereas glacials show a marked shift towards middle to inner shelf paleo-bathymetries (assemblages dominated by *Elphidium* spp, *Ammonia perlucida*, *Nonion* spp, *Bulimina* ex gr. *marginata*, *Cassidulina laevigata carinata*, *Islandiella islandica*). These oscillations in the paleodepth are represented in Fig 1.3 by the *Elphidium + Ammonia* curve (inner shelf assemblage).

Sapropel stratigraphy

Sapropels appear as dark, often laminated layers, rich in organic matter. Their deposition has been proven to be related to orbitally driven oscillations in the Northern Hemisphere insolation (Rossignol-Strick et al., 1988, Hilgen, 1991) and it has been correlated to minima in the orbital precession, as well as to Northern Hemisphere insolation maxima (Lourens et al., 1996). When they are observed, or recognizable by means of geochemical/biological indicators, sapropel layers are considered a very useful tool to infer the chronometry of a sedimentary sequence.

Sapropel layers have been mainly defined based on their content in organic matter (>2% according to DSDP Leg 42A definition, 0.5-2% according to Kidd et al., 1978). As summarized by

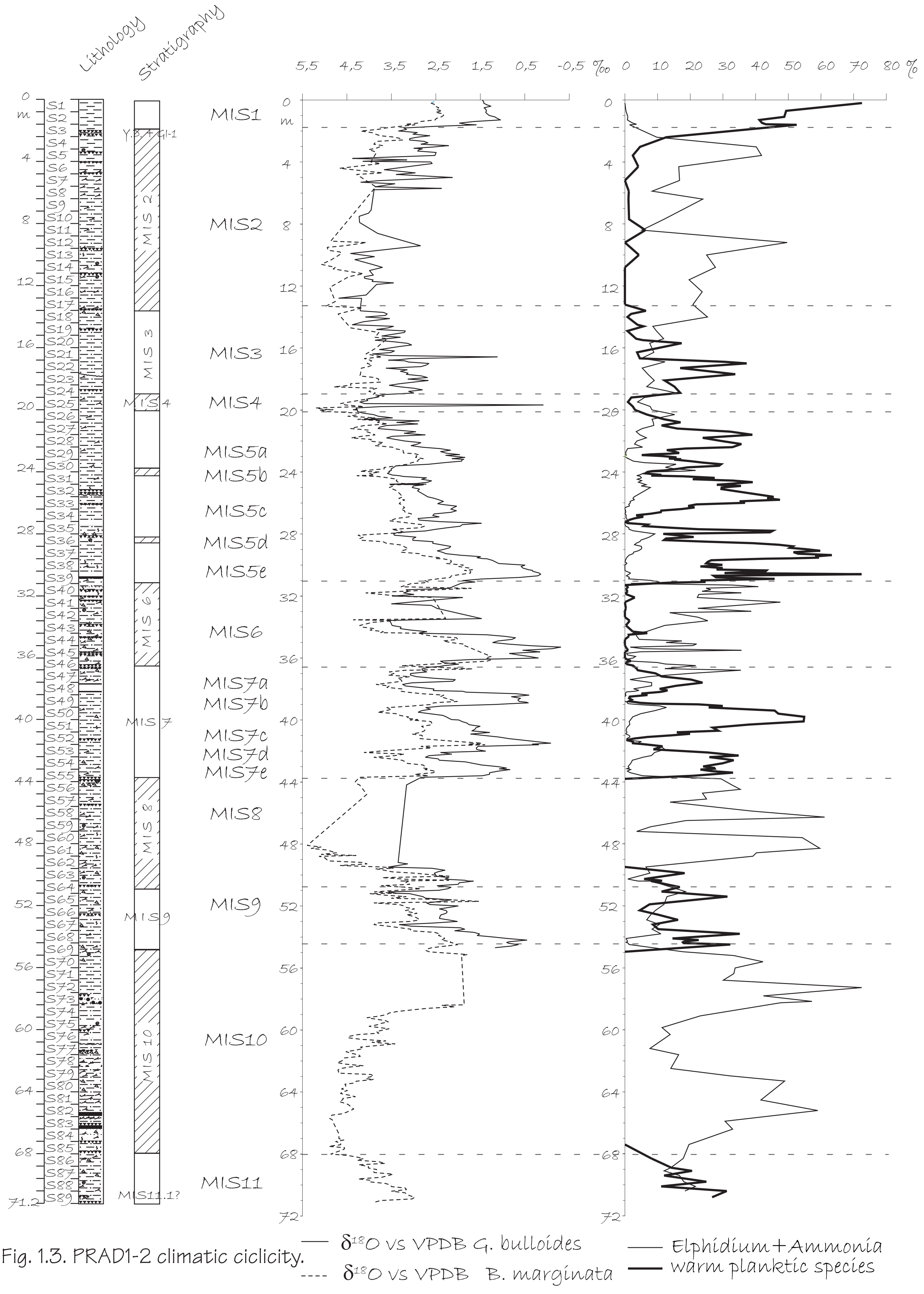

Fig. 1.3. PRAD1-2 climatic ciclicity.

Cramp and O'Sullivan (1999), these restrictive definitions became of limited use as they did not take into account post depositional processes that may significantly reduce/increase the amount of buried organic Carbon. Also the less restrictive definition by Hilgen (1991) ("brownish, often laminated interbeds") can not be easily applied, since the lamination is not always observed. Even though only in few cases PRAD1-2 lithology records laminated and/or dark sediments, and Total Organic Carbon analysis is not available; nevertheless, thanks to distinctive features in the micropaleontological, physical, lithologic, geochemical and paleomagnetic records, it has been possible to recognize ten peculiar intervals, which have been equated to the deposition of correlative sapropels in the Eastern Mediterranean.

These intervals are in fact characterised by outstandingly low values of $\delta^{18}O$ and $\delta^{13}C$, by minima in concentration-related magnetic parameters (e.g. ARM), by dark and in some case laminated sediments, by a decrease in the colour reflectance, as well as by a peculiar foraminifers' microfauna. The benthic assemblage is mostly represented by (deep-) infaunal benthic taxa, and in some intervals the sediment is even devoid of benthic fauna. The planktic assemblage is largely dominated by Neogloboquadrinids and/or *Globigerinoides ruber* (pink). For this reason it was decided to name these Central Adriatic layers sapropel equivalents (Se 1, Se 3 and so on) (Fig. 1.4).

The age ascribed to PRAD1-2 sapropel equivalents refers to Lourens (2004), who provided a new sapropel-based astronomical time scale for the Eastern Mediterranean during the last 1.1 Myr, in the reference core KC01B, collected in the Ionian Sea. Lourens (2004) based the age calibration points on sapropel midpoints (m), recognized mainly by the visual colour change, by geochemical analysis (Langereis et al. 1997) for the "ghost" levels and by the decrease in percentage of the colour reflectance and of the oxygen isotope signal. The ages are referred to their correlative 3kyr lagged insolation maxima. As regards PRAD1-2 borehole, the selection of the sapropel equivalents' age control points has been based on the lightest $\delta^{18}O$ value present in each sapropelic interval, delimited by the colour reflectance signal, by the micropaleontological content and by $\delta^{18}O$, $\delta^{13}C$ and magnetic properties anomalies. The control points are marked with a black "X" in Fig. 1.4. This choice imposes the synchronism of the $\delta^{18}O$ signal between borehole PRAD1-2, located in the Central Adriatic and very close to the land, and the more oceanic Ionian core KC01B. As highlighted by Emeis et al. (2003), the use of sapropels mid-points as age markers with a constant time lag of 3 kyr (between the insolation peak and the sapropel deposition) is a simple and effective method, but it may be too coarse if applied to studies needing the exact timing of sapropels. However, referring to the presently available literature, the problem of the exact timing of the upper Quaternary sapropels in the Eastern Mediterranean, crucial for paleoceanographic and paleoclimatic reconstructions, seems to be very difficult to solve at the moment, since only the age of Sapropel 1 deposition can be assessed by radiocarbon datings (see for instance Strohle and Krom 1997). Different choices about the reference level to employ were made: for instance, the base of each sapropel layer (Emeis et al., 2003), method that imposes their synchronism with insolation maxima, or unambiguous bioevents, such as last or first zero abundance levels, along with O and C stable isotope signals on shallow and deep-living species (Cane et al., 2002, Capotondi et al. 2006); this choice can be applied only to basins of rather limited dimensions (for instance, open Eastern Mediterranean in Cane et al. 2002). Moreover, Strohl and Krom (1997) demonstrated a time transgressive migration of the anoxia from shallow (900 m ca. water depth at 8900 yr BP) to deep water (3500 m w.d. at 8200 yr BP) during Sapropel 1 deposition. Hole PRAD1-2 has been retrieved at 180 m w.d. in a peculiar basin (Central Adriatic), then it can not be ruled out that the onset of the sapropel-equivalent intervals can be relatively dichronous in respect to deep water sapropels in more (Southern Adriatic) or less (Ionian Sea, Eastern Mediterranean) adjacent basins. At this stage, the choice as tie points of the lightest $\delta^{18}O$ values within the sapropel equivalent intervals seems to be the most feasible in the assessment of the general chronological framework of the hole, even if it may be objected (cf. Rohling, 1999).

Age model

The above discussed integrated stratigraphy, summarised in Fig. 1.5, allowed to propose for PRAD1-2 borehole an age-depth model plotted in Fig. 1.6 and based on the control points reported on Table 1.5

PRAD1-2 age-depth model			
mbsf	event	age (kyr BP)	reference
0	modern time	0	
0,6	LO G. inflata	6	from Ariztegui et al. (2000)
1,288	S1	8,5	from Lourens (2004)
1,8	top YD	12	from Asioli et al. (1999)
5,976	^{14}C AMS	17,3	this study
7,8	^{14}C AMS	19,2	this study
13,4	^{14}C AMS	27.6	this study
14.8	^{14}C AMS	33.4	this study
16.39	^{14}C AMS	41.6	this study

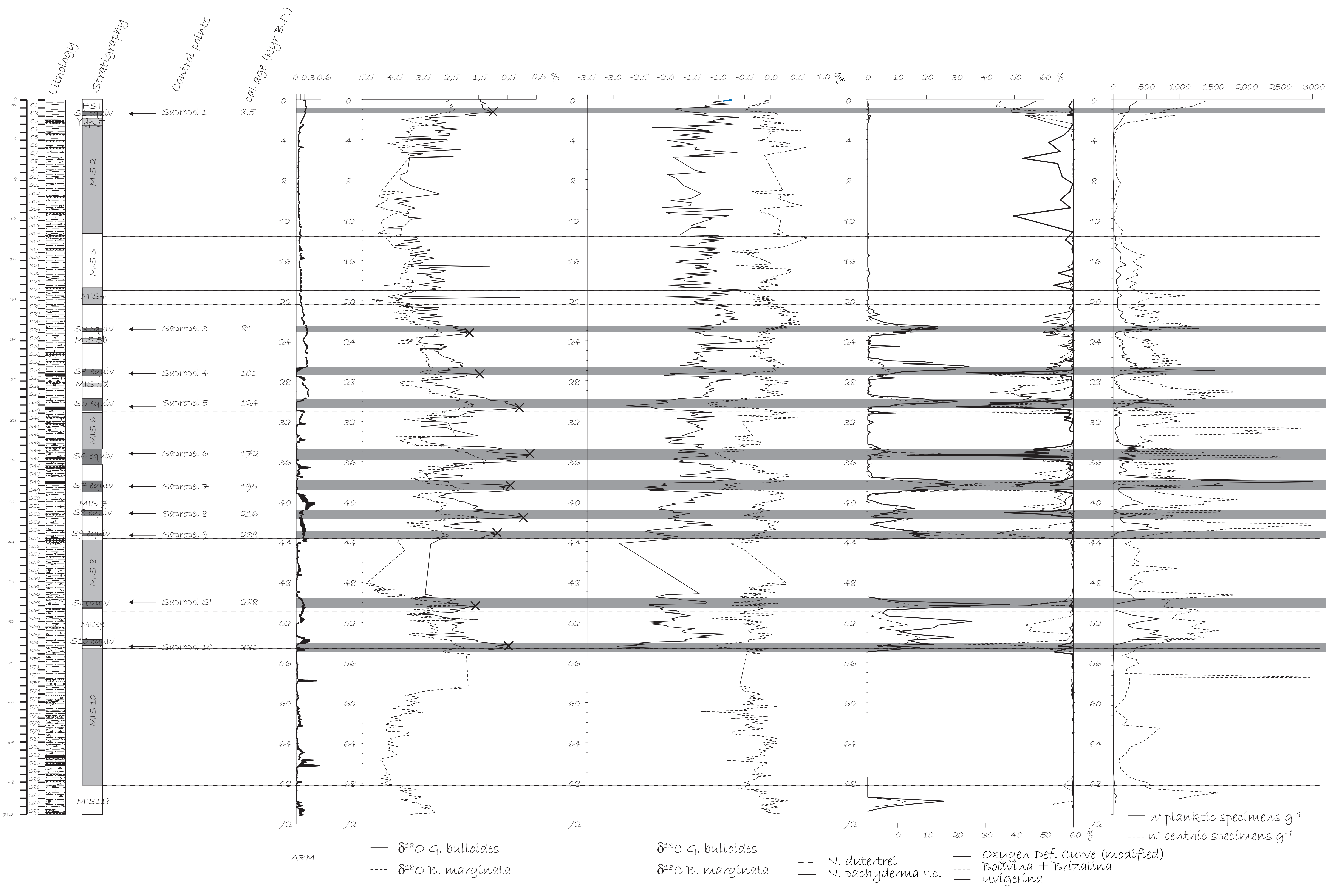

Fig. 1.4. Most representative proxies for PRAD1-2 sapropel equivalents' detection. X correspond to the control points of the lightest δ18O values for each sapropel equivalent (according to Lourens, 2004)

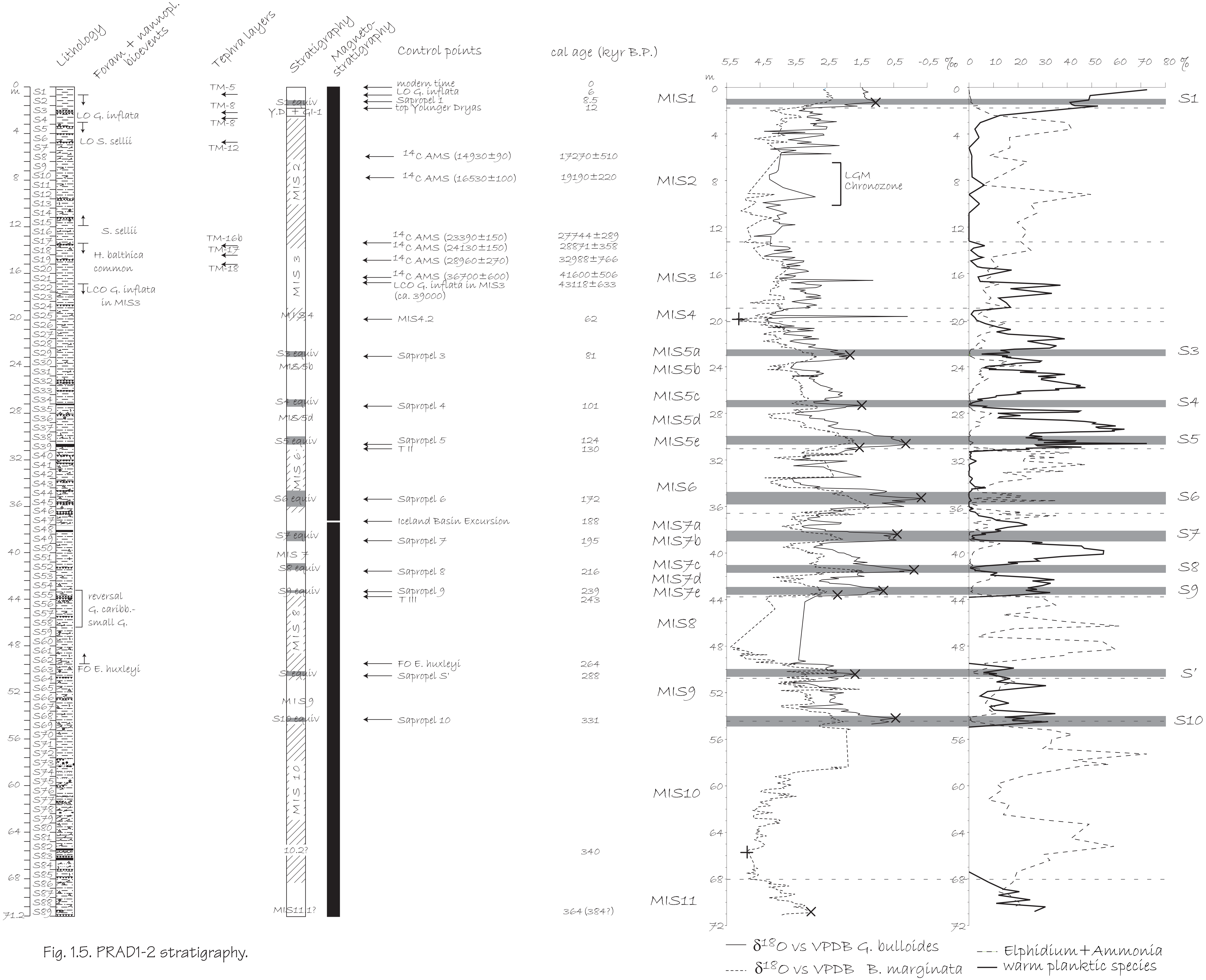

Fig. 1.5. PRAD1-2 stratigraphy.

16.9	^{14}C AMS (LCO G. inflata in MIS3)	43.1	from Asioli (1996)
19,99	MIS4.2	62	from Bassinot et al. (1994)
23,059	S3	81	from Lourens (2004)
27,3	S4	101	from Lourens (2004)
30,6	S5	124	from Lourens (2004)
30,95	T II	130	from Lisieki and Raymo (2005)
35,3	S6	172	from Lourens (2004)
37,32	IBE	188	from Lourens (2004)
38,4	S7	195	from Lourens (2004)
41,5	S8	216	from Lourens (2004)
43,2	S9	239	from Lourens (2004)
43,65	T III	243	from Lisieki and Raymo (2005)
49,551	FO E. huxleyi	264	from Lourens (2004)
50,4	S'	288	from Lourens (2004)
54,2	S10	331	from Lourens (2004)
65,696	MIS 10.2?	340	from Bassinot et al. (1994)
70,8	MIS 11.1	364	from Bassinot et al. (1994)

Table 1.5. Control points concurring in the definition of the age-depth model of borehole PRAD1-2.

The sedimentation rate curve for borehole PRAD1-2 derived from its age-depth model is illustrated in Fig. 1.7. Cattaneo and Trincardi (1999), analysing the relationship between sea level change and sediment supply in a semi-enclosed basin, such as the Central Adriatic, demonstrated that the higher the achieved stratigraphic resolution, the more inconstant the sedimentation rate is, especially as regards shelf deposits. The sedimentation rate tends to be more costant in the Mid-Adriatic slope setting. Yet, sea-level falls during glacial intervals caused the river mouths (in particular, the Po river mouth) to move closer to the edge of the Mid-Adriatic Deep (MAD), and that is the explanation of the enhanced sediment supply registered during the main glacial intervals (MIS10, MIS8 and MIS2, in particular).

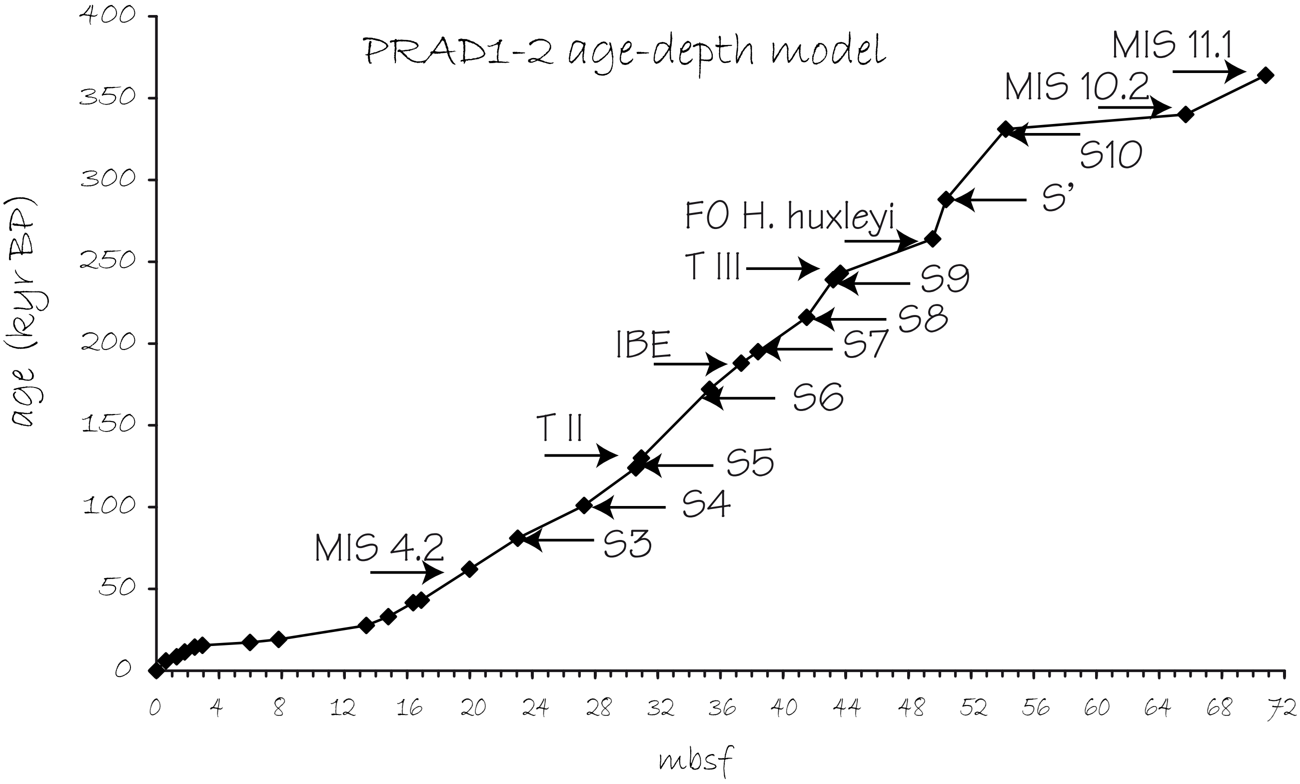

Fig. 1.6 Age-depth model calculated for borehole PRAD1-2.

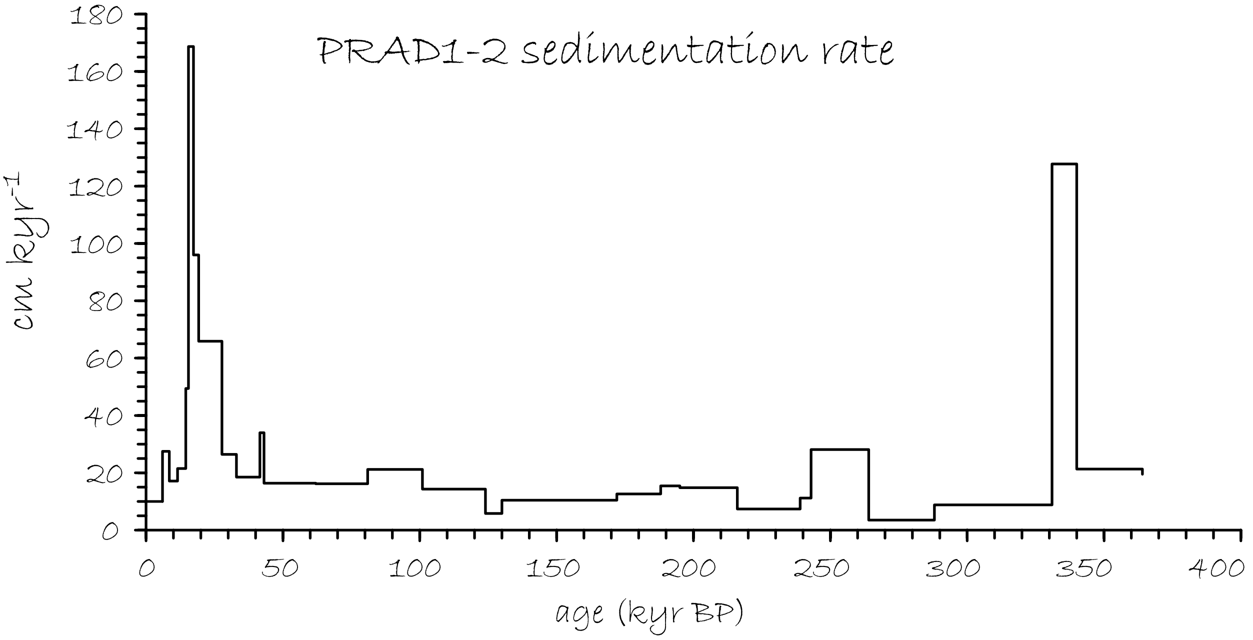

Fig. 1.7 Sedimentation rate curve derived from the age-depth model for borehole PRAD1-2.

CHAPTER II: PALEOENVIRONMENTAL RECONSTRUCTION

PRAD1.2 borehole spans five glacial oscillations (MIS10, MIS8, MIS6, MIS4, MIS2) and six interglacials (part of MIS11, MIS9, MIS7, MIS5, MIS3 and MIS1). These intervals will be first briefly described based on the most significant trends in the composition of planktic and benthic foraminifers' assemblages, and, later, some paleoenvironmental inferences will be derived from these results. The description of sapropelic layers will be treated in detail in another chapter (see chapter 3).

2.1 METHODS

To better define PRAD1-2 paleoenvironmental reconstruction, along with the abundances and the concentration of foraminifera, two indexes have been calculated based on planktic and benthic foraminifers' quantitative data, aiming at deriving information on the degree of diversification of the assemblage. In addition, such indexes allow discriminating whether an assemblage is dominated by few species or if taxa are more homogeneously distributed.

The Shannon and Weaver (1949) index monitors the taxonomic diversity of the assemblage. Its formula is:

$H(S)=-\Sigma^{S}_{i=1}\ (p_i*\ln p_i)$

Where $p_i=n_i/N$ is the proportion of i-taxon in the sample, with n_i corresponding to the number specimens of the i-taxon in the sample and N equal to the total number of specimens in the sample. S is the number of taxa present in the sample. $H(S)=0$ when $p_i=1$ (the lowest diversity corresponds to the presence of only one species). The maximum diversity value is reached when $H(S)=\ln S$, that is when all the taxa have the same proportions ($p_1=p_2=p_3\ldots=P_S$). This index gives a systematic error related to S and N values, which can be corrected according to Basharin (1959): $H(S)corr=H(S)sample-((S-1)/(N*2))$.

This correction is important when N is small (~50-80 specimens).The applicability limit of this index is, in fact, that few taxa with equal abundances can give the same result as many taxa with different abundances. For this reason, an alternative index has been calculated, in order to discern the homogeneity of the assemblage. The Equitability (Pielou, 1966) index:

$E=H(S)/H(S)max=H(S)/\ln S$

gives a value from 0 to 1, with E=0 when one species dominates, and E=1 when all the taxa are equally distributed. This index depends from N and S, and gives less reliable values when S is low (<10).

2.2 RESULTS

Glacial stages (Fig. 2.1a and 2.1b)

MIS10 is almost devoid of planktic microfauna, which is composed of very few specimens per sample (mainly of *Globigerina quinqueloba*). Benthic assemblage shows an overall homogeneous composition, although distinct species assemblages become dominant in successive stratigraphic levels; as an example, some layers are mainly characterised by *Islandiella islandica*, while others by *Elphidium* species (either *E. articulatum*, or *E. clavatum*[1], or *E. decipiens-granosum*); on the other hand, *Nonion depressulum* and *Nonion pauciloculum* are common and in some cases abundant throughout this cold interval. MIS10 is the only glacial period to show high abundance of *Bulimina* ex gr. *marginata*, and it is the only stage in the entire borehole characterized by the common presence of *Ammonia perlucida*. The upper portion of MIS10 interval also shows a peculiar level, located at about 58mbsf, composed by an exclusively benthic assemblage which is unique in the whole PRAD1-2 record (common *Ammonia beccarii*, *A. perlucida* and *N. depressulum*, abundant *E. articulatum*, *E. clavatum* and *E. decipiens*, dominant *B.* ex gr. *marginata,* presence of *Neoconorbina terquemi*); this stratigraphic interval is also characterised by the highest benthic concentration in the entire record.

During MIS8 the planktic assemblage is represented by very few specimens, mostly belonging to *G. quinqueloba*. Benthic microfauna is extremely oligotypic, and characterised by the alternating dominances of *I. islandica* and *E. articulatum*, while *N. depressulum* is common to abundant in two levels and *N. pauciloculum* becomes common in the upper part of MIS8 interval.

Planktic concentration within MIS6 is about one order of magnitude higher compared to those of the previous glacial periods (almost one hundred specimens versus less than ten during

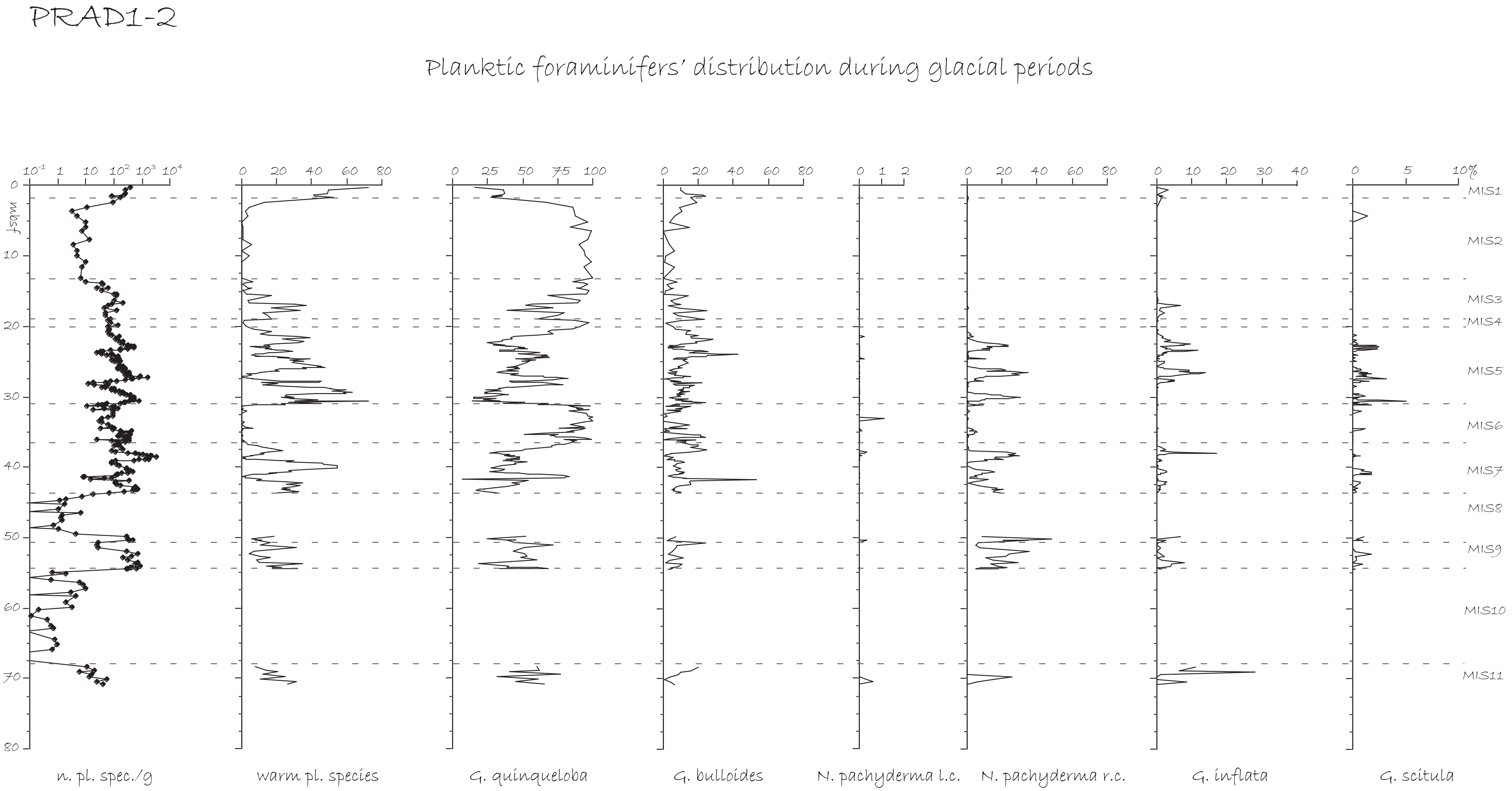

Fig. 2.1a Distribution of the main planktic foraminifers' species or groups in PRAD1-2 record during glacial periods.

PRAD1-2

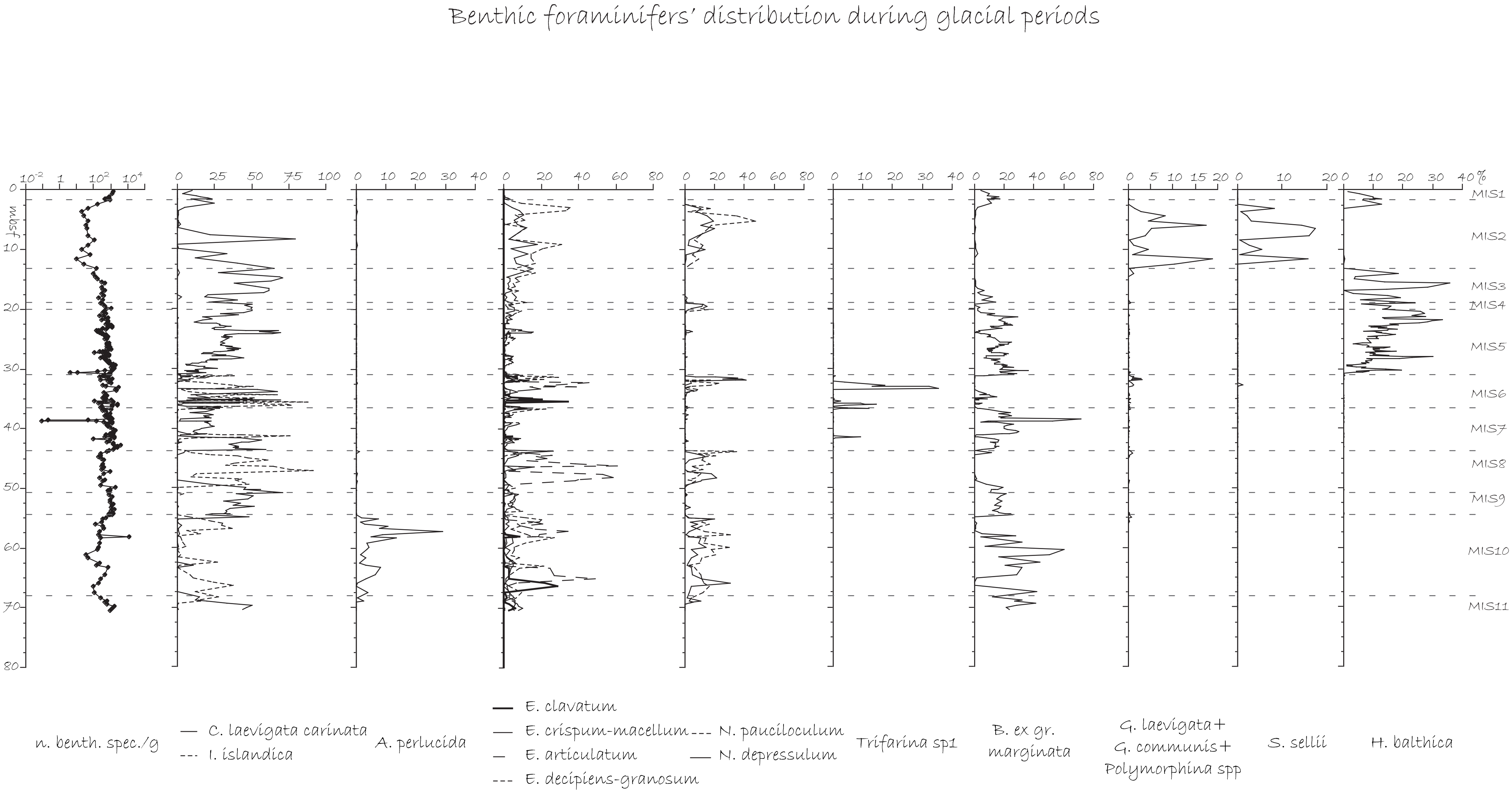

Fig. 2.1b. Distribution of the main benthic foraminifers' species or groups in PRAD1-2 record during glacial periods.

MIS10 and MIS8); in addition, the assemblage is more diversified: *G. quinqueloba* is highly dominant all over the stage, nevertheless it is possible to distinguish three distinct minor peaks, characterised by the presence of warm planktic species. Two of these levels also show the presence, although in small percentages, of *G. scitula*. *Globigerina bulloides* is common in two levels. *N. pachyderma* left coiled, typically very rare in the entire PRAD1.2 borehole, is present reaching its highest abundance in the upper part of the stage. Alternating abundances of *Cassidulina laevigata carinata* and *I. islandica*, of *E. articulatum* and *E. clavatum*, and of *Trifarina* sp1 dominate the benthic assemblage. *N. depressulum*, *N. pauciloculum* and *E. decipiens-granosum* are common to abundant in the upper part of the stage.

MIS4 planktic concentration reaches the same magnitude order as that of MIS6, but diversity is much lower, being strongly dominated by *G. quinqueloba*. As regards the benthic assemblage, *C. laevigata carinata* is very abundant (about 50%), with common to abundant *Hyalinea balthica* (this is the only glacial stage in which this species occurs), *N. pauciloculum* and *N. depressulum*. *E. crispum-macellum* is also common.

Planktic foraminifers' concentration is not very high during MIS2 (less than ten specimens per sample on average). *G. quinqueloba* is dominant, accompanied by the common presence of *G. bulloides*, and by the rare occurrence of sporadic warm planktic species. *G. scitula* occurs in a single peak in the upper part of MIS2. Alternating peaks of *C. laevigata carinata*, *N. pauciloculum* and *E. decipiens-granosum* dominate the benthic microfauna. *E. crispum-macellum* and *N. depressulum* are common all over the glacial interval. *Sigmoilina sellii*, common, occurs only within MIS2. *Glandulina laevigata* is common to abundant in two distinct levels.

Cool climate oscillations inside interglacial periods (MIS9.2, MIS7.4, MIS7.2, MIS5.4 and MIS5.2 stadial intervals) are characterised by a decrease in the planktic concentration, as well. The planktic assemblage is generally dominanted by *G. quinqueloba*, along with common to abundant *G. bulloides* (in particular during MIS7.4 and MIS5.2), while the benthic assemblage is characterised by levels of dominant *C. laevigata carinata* and by the common presence of *E. crispum-macellum* and *E. decipiens-granosum*.

---

[1] In this study, *E. clavatum* has been identified as a lump of *Elphidium excavatum* forma *excavata* and forma *clavata* (sensu Miller at al., 1982).

Lithologic descriptions bring new insights as regards the characterization of PRAD1-2 glacial periods. In fact, the silty fraction is generally more abundant during these cold intervals, and fine terrigenous sediment, mainly composed of mica and quarts grains, is visible in the analysis of the washed samples. During MIS10 grain size increases, and silty-sandy levels are more frequent. Finally, MIS2 is characterised by the abundant presence of oxidized clasts, whereas MIS10 and MIS8 show diffused pyritization of the sediment, affecting not only clasts and grains, but also foraminifers' tests.

Interglacial stages (Fig. 2.2a and 2.2b)

The very late MIS11 is represented by common warm planktic species, such as *Globigerinoides ex. gr. ruber*, *Orbulina* spp, *Zeaglobigerina rubescens* and *Globigerinoides tenellus*. *Globorotalia inflata* is common to abundant. *N. pachyderma* r.c. common in one level. The benthic assemblage is mostly dominated by *C. laevigata carinata*, along with *B.* ex gr. *marginata*. *Brizalina* and *Bolivina* spp. are rare.

The pervasive distribution of sapropelic layers inside MIS9, and its relatively short thickness, make the characterisation of this interglacial more difficult. Anyhow, non-sapropelic levels show common warm planktic species, along with common *G. inflata*. *Globorotalia truncatulinoides* and *G. scitula* are also present. *C. laevigata carinata* dominates the benthic assemblage, *B.* ex gr. *marginata* is abundant, as well. *Cibicidoides pachyderma* shows one distinct peak, *Trifarina angulosa* is present.

MIS7 is characterised by common to abundant warm planktic species, articulated in three distinct oscillations. In particular, the inner one shows higher percentages of *Orbulina* spp, abundant. In this substage *Globigerinoides* ex gr. *sacculifer* is also present. Globorotalids peak with little frequencies in each warm oscillation, and *G. inflata* is common in the upper one. Benthic *C. laevigata carinata* is generally abundant, dominant in the lower oscillation, *Brizalina*, *Bolivina*, *Bulimina* and *Uvigerina* groups, mainly characterising sapropelic levels, remain common also outside the anomalies. *T. angulosa* and *C. pachyderma* are common in all the three oscillations.

PRAD1-2

Planktic foraminifers' distribution during interglacial periods

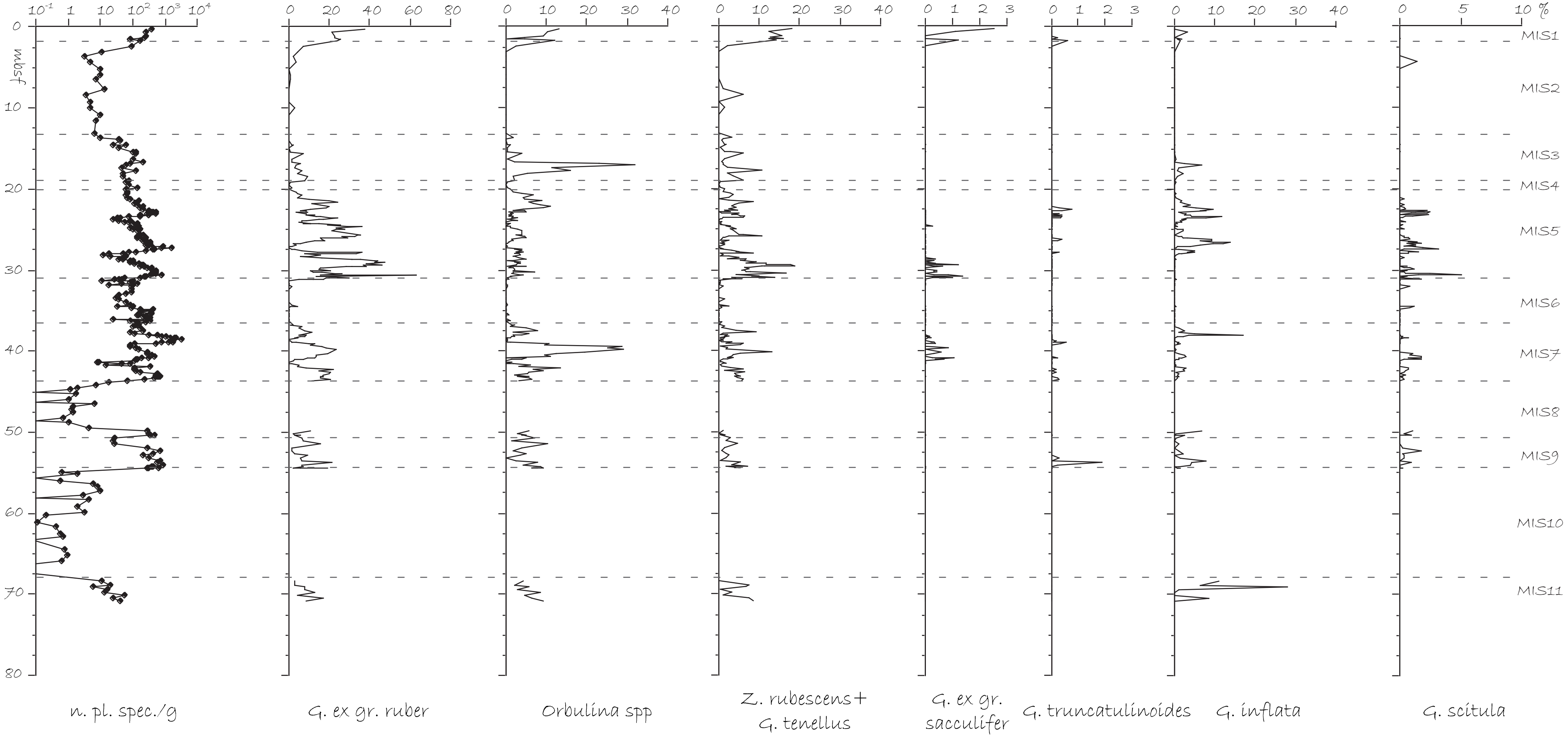

Fig. 2.2a. Distribution of the main planktic foraminifers' species or groups in PRAD1-2 record during interglacial periods.

PRAD1-2

Benthic foraminifers' distribution during interglacial periods

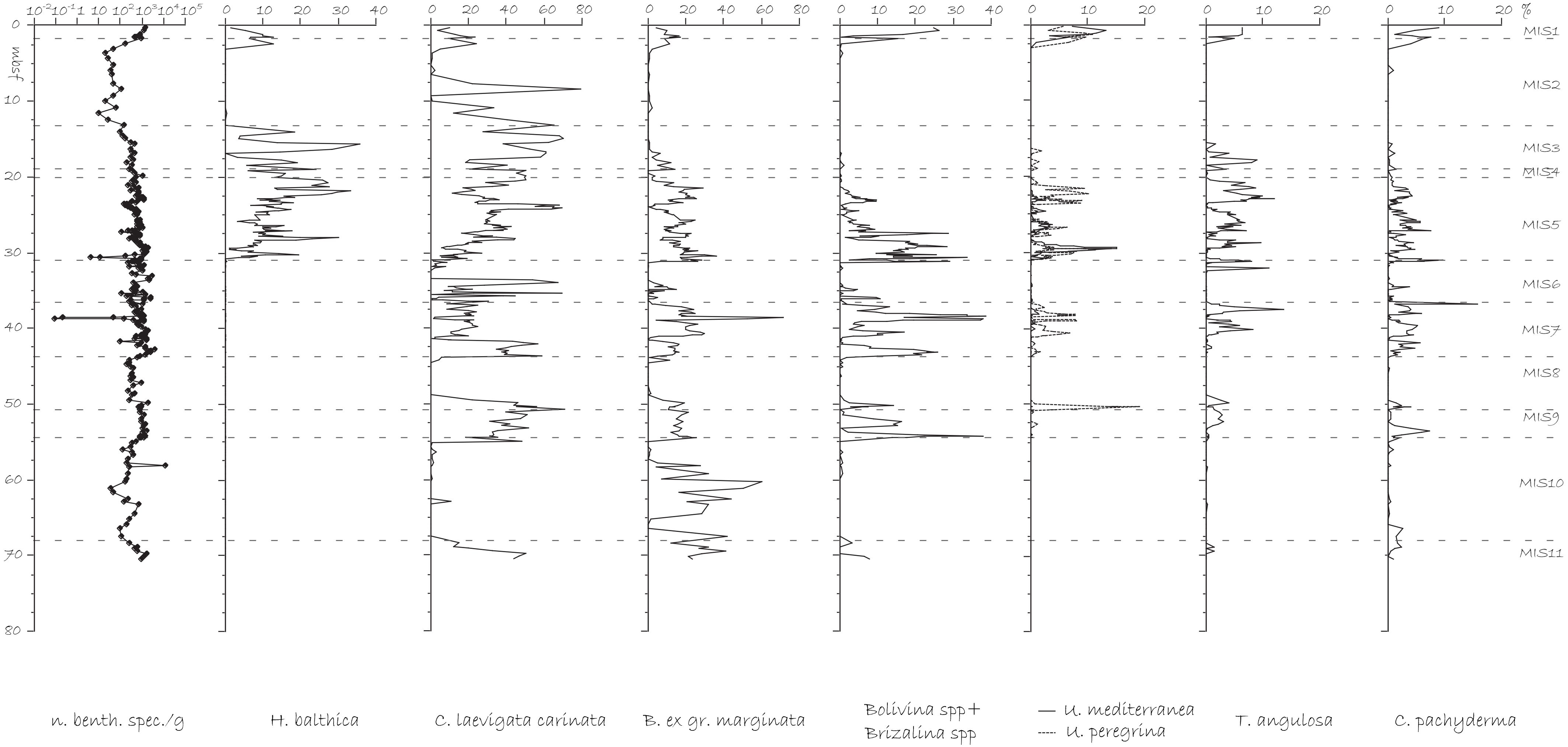

Fig. 2.2b. Distribution of the main benthic foraminifers' species or groups in PRAD1-2 record during interglacial periods.

MIS5 includes three warm substages which are dominated by warm planktic species: *G. ex gr. ruber* is very abundant, especially during MIS5e, *Orbulina* spp is common, and *Z. rubescens* is common to abundant. The presence of *G. ex gr. sacculifer* is mostly limited to MIS5e. Common *G. inflata* and rare *G. truncatulinoides* are present during MIS5c and MIS5a, *G. scitula* is present in all the three substages. The benthic assemblage shows a reversal in the frequencies of *C. laevigata carinata* + *H. balthica*, increasing upwards inside MIS5, versus a decreasing of *Brizalina*, *Bolivina*, and *Uvigerina* groups. *B.* ex gr. *marginata* is common in the three warm oscillations, as well as *T. angulosa* and *C. pachyderma*.

MIS3 warm planktic assemblage is mostly characterised by abundant *Orbulina* spp, while *G. inflata* is rare to common. Alternating levels of abundant *C. laevigata carinata* and *H. balthica* characterise the benthic assemblage. *T. angulosa* is common in the lower part of the stage.

PRAD1-2 is not the best record to study in detail MIS1, which appears to be rather condensed, compared to many other cores in the area and, in particular, to PRAD2-4, collected in 50 m water depth on the shelf. Moreover, the uppermost sections are contaminated by the presence of drilling mud. Therefore, this stage will not be treated here, and the reader is referred to the literature (Jorissen et al., 1993; Asioli, 1996; Asioli et al., 1999, 2001, Artizegui, 2000, Oldfield et al., 2003) for the Central Adriatic in general, as well as to Part II of this thesis (in particular as regards the last 6000 years).

2.3 PALEOCEANOGRAPHIC AND PALEOENVIRONMENTAL INFERENCES

Based on these results, it is possible to derive some observations about the expression of glacial and interglacial intervals in PRAD1-2 record.

First of all, every glacial cold interval shows a marked shift towards outer to inner shelf environments. The common background assemblage is typical of the shelf facies, and it is mainly characterised by the *Elphidium* group (Chierici et al., 1962; Jorissen, 1988; Murray, 1991), accompanied by cold water species such as *C. laevigata carinata* (Herman, 1981; Ross and Kennett, 1984; Williamson et al., 1984; Van Leeuwen, 1989; Murray, 1991) *I. islandica* (MIS10, MIS8 and MIS6) and *H. balthica* (MIS4). Nevertheless, each cold stage is represented by distinctive features. The common presence of species living today on the inner shelf, close to the shoreline, such as *A. perlucida* (Walton and Sloan, 1990; Murray, 1991; Vaiani and Venezia, 1999), characterises MIS10, accompanied by the lowest concentration of planktic specimens, indicating that the lowest paleobathymetry in PRAD1-2 record was achieved during this stage. Moreover, the abundant frequencies of *B.* ex gr. *marginata*, typical of sediments rich in organic matter (Phleger and Soutar, 1973; Van Weering and Qvale, 1983; Jorissen, 1988; Van der Zwaan and Jorissen, 1991; Jorissen et al., 1992; Barmawidjaja et al., 1992; Miao and Thunell, 1993; Rohling et al., 1993; Sen Gupta and Machain-Castillo, 1993; Rathburn and Corliss, 1994; Vaiani and Venezia, 1999) could be explained by an increased fluvial runoff, because of the closer position of the river mouths to the location of PRAD1.2. *E. clavatum*, which is common during glacial intervals and peaks in association with *B.* ex gr. *marginata*, has been generally ascribed to cold climate (Wilkinson, 1979; Williamson et al., 1984; Rodrigues and Hopper, 1982; Jennings et al., 2004) and considered as an opportunistic species (Linke and Lutze, 1993), which lives in cold (up to 5-7°C), turbid, shallow waters, with low salinity (Alve, 1995), and up to intertidal environments (Miller et al., 1982). The peculiar level found at about 58 mbsf has instead been interpreted as a not in situ layer. Therefore, MIS10 seems to be characterised by a proximal paleoenvironment, heavily influenced by continental influxes, characterised by cold water and by sporadic reworking mechanisms.

Late MIS10 (between about 57.8 and 55 mbsf) presents peculiar characteristics in PRAD1-2 record. As anticipated in the presentation on the isotope stratigraphy (Chapter I), benthic $\delta^{18}O$ values above 65.5 mbsf show a gradual trend towards lighter values (ca. +3.7‰), although punctuated by small fluctuations, culminating in an abrupt shift to values around +1.7‰ at 58.2 mbsf, quite close to the ones at the base of MIS9. This latter strong shift can be ascribed to a Termination trend. Nevertheless, this shift and the section above do not show a relative deepening trend, as it may be expected in the case of a Termination. Indeed, the very abundant benthic microfauna is composed, particularly in the interval between 57.8 and 55 mbsf, by a very proximal, inner shelf assemblage, dominated by *A. perlucida*, *I. islandica*, *E. articulatum* and *N. pauciloculum*. Some of these species, in particular *A. perlucida*, are presently known to inhabit the modern Adriatic muddy coastal zone (Jorissen 1988; Morigi et al., 2005), more or less directly influenced by fluvial runoff and characterised by water depths <20 m (the mean water depth when *A. perlucida* is dominant is <10 m, according to Morigi et al., 2005). The isotope trend does not seem, at present, to be ascribed to salinity variations, because the alchenones record parallels the oxygen isotope one (J. Grimalt personal communication, 2006). A temperature minimum (ca. 5°C) is centred at 62 mbsf, followed by a subsequent warming, reaching 10-12°C at 58 mbsf. Therefore, the silty clay sediment between 57.8 and 55 mbsf, characterized by scattered organic matter, deposited during a warming phase, and likely during Termination IV, but still under the influence of a significant sediment flux from the continent, capable to help the margin to keep pace with the relative sea-level rise. Progradational shelf deposit capable to outbuild during phases of sea level rise have been documented on several continental margins and, in the area, by Cattaneo and Trincardi (1999), even within the middle unit of the Transgressive System Tract, indicating a significant change in the supply regime between 14.8 and 11.3 cal years BP (including the Younger Dryas cold spell). Moreover, at 58.2-57.8 mbsf, the lithology is characterised by medium sand, shell remains, often broken; poorly preserved foraminifera tests dominate between 58.20 and 58.16 mbsf, and laminated mm-scale silty clay levels (typically 1-2 mm thick and light grey) dominate between 58.16 and 57.8 mbsf. The coarser interval likely represents the record of a phase of coastal to inner shelf wave reworking typical of the early phases of a base level rise.

MIS8 reflects a slightly deeper setting: plankton is very scarce, and a water depth lower than 25 m can be estimated particularly because of the occurrence of *E. articulatum* (Jorissen, 1988). Moreover, the oligotypic assemblage, dominated by four main benthic species, could be the expression of a stressed environment, cold and under a significant availability of organic matter.

MIS6 is more diversified, and also the planktic assemblage is richer. It is possible to distinguish three little warmer oscillations inside this glacial stage. In general, the low frequencies of warm planktic species, coupled with the presence of cold-climate, deep-water species *G. scitula* in the same levels, suggest that the warming was likely weak and confined to the shallower part of the water column, whereas deeper water masses remained cold (Bè and Hutson, 1977; Baumfalk et al, 1987; Hemleben et al., 1989). Moreover, the polar species *N. pachyderma* l.c. (Bè and Tolderlund, 1971) shows its highest abundances inside this stage, probably constraining the MIS6 glacial maximum. The benthic species, typical of a mid-inner shelf environment, are characterized by marked shifts in their abundances, which likely reflect shifts in the organic matter content within the sediment.

MIS4 records the deepest bathymetry, compared with all the other glacial intervals in PRAD1-2 record. This can be inferred not only by a conspicuous planktic concentration, but also because the benthic assemblage is composed by mid-outer shelf species, in contrast to the shallower-water associations of the other glacial intervals. The common presence of *H. balthica* can be interpreted as the signal of cold bottom waters, which appear better oxygenated if compared to the other glacial periods.

During MIS2 PRAD1-2 site returns to assemblages typical of mid-shelf environments. Scattered and low occurrences of warm planktic species within this interval alternate with peaks of cooler water species *G. bulloides*, likely recording high frequency climate oscillations. The peak of *G. scitula* inside this stage is a common feature all over the Adriatic basin, which consents to discriminate the onset of Greenland Stadial-2 (GS-2) climate oscillation. Other peculiar trends characterise the Adriatic benthic record inside MIS2. *S. sellii*, in fact, shows its first and last occurrence inside this stage, and deep infaunal, light-tested, ovoidal taxa, such as *G. laevigata*, *G. communis* and *Polymorphyna* spp, show two distinct peaks inside this stage. These species reflect high organic matter concentration at the sea floor and may suggest a very sluggish circulation (possibly reflecting a weakening in deep water formation). ^{14}C datings performed on these levels in PRAD1-2 seem to be consistent with the ages of the occurrence of Heinrich events 1 and (possibly) 2 in the East Atlantic ocean (Lebreiro et al., 1996), detected also in the Western Mediterranean (Rohling et al., 1998; Combourieu Nebout et al., 2002; Pérez-Folgado et al., 2003). PRAD1.2 results suggest that the climatic forcing controlling the Heinrich events in the Atlantic area overprinted also the shallow, peripheral Adriatic basin, a key area for deep water formation within the Mediterranean. This hypothesis, however, requires additional studies to be confirmed.

The boundary between MIS3 and MIS2 is approximated by the disappearance of *H. balthica*: the last occurrence of this benthic species, presently living in cold and well oxygenated waters, could be the consequence of a weakening of the deep water formation during this glacial interval.

As regards glacial periods, few other features can be discussed. The almost complete absence of *G. inflata* may be interpreted to reflect a severe weakening of the vertical mixing of the water mass, maybe the consequence of a decreased deep water production in the basin (Thunell, 1978; Pujol and Vergnaud-Grazzini, 1995). The reduced thickness of the water column during low stands cannot be the only explanation for the absence of this intermediate-deep water species: in fact, *G. inflata* results absent during these intervals also in the deeper Southern Adriatic basin, where the water depth is not a limiting factor (for instance during MIS2 in SAGA03 cores, see part III). The hypothesis of a reduced vertical mixing is strengthened by the evidence of a worse ventilation of the sea floor, resulting in the absence of oxic benthic species, such as *C. pachyderma* and *H. balthica* (Caralp, 1988; Hasegawa et al., 1990 among others) during MIS10, MIS8, MIS6 and MIS2.

Sub-polar deep species *N. pachyderma* r. c. never characterizes glacial stages in PRAD1-2 record, maybe because of the reduced thickness of the water column during these cold low stand periods. Instead, this species occurs in all the sapropelic anomalies registered in the borehole (except, obviously, Se1), where the water column was deep enough and its cool, deeper layer, rich in organic matter, was absolutely suitable to its life requests (Bè and Tolderlund, 1971; Bè and Hutson, 1977; Fairbanks and Wiebe, 1980; Faibanks et al., 1982; Reynolds and Thunell, 1986; Hemleben et al, 1989; Rohling and Gieskes, 1989). It may not be a case if *N. pachyderma* r. c. shows relatively low frequencies in Se6, which occurs inside glacial MIS6; in this case *N. pachyderma* r. c. is replaced by large amounts of *Neogloboqudrina dutertrei*, which lives in shallower levels within the water column (Bè, 1977).

Cool climate oscillations inside interglacial periods show distinct features compared to glacial periods, reflecting a relatively deeper water mass, characterised by the occurrence of upper slope and mid-outer shelf benthic species, where common to abundant *G. bulloides* could live (see, for instance, MIS5.2 and MIS7.4), coupled with *G. quinqueloba*. Significant peaks of these planktic species may reflect an increased productivity in shallow waters (Bè and Hutson, 1977; Hemleben et al., 1989; Rohling et al., 1993).

Planktic and benthic foraminifers' biodiversity (Fig. 2.3) is generally much lower during cold (glacial and stadial) intervals, compared to the interglacial periods, because the reduced water column and the possible weakened ventilation of the water mass (derived by the absence of Globorotalids), also resulting in an increase of the organic matter content (suggested by the dominance of planktic herbivorous species as *G. quinqueloba* and *G bulloides* and by the absence of oxic benthic species as *C. pachyderma* and *H. balthica*, except in MIS4), seriously hampered the microfauna to live and diversify; consequently, only opportunistic species could take advantage of such harsh conditions, and become dominant. These cold and oligotypic intervals are not necessarily coupled to an enhanced productivity, since the proximal shallow environment, characterising in particular MIS10 and MIS8, could also be affected by substantial variations in salinity as suggested by the low salinity species *N. depressulum, N. pauciloculum, A. perlucida* and *E. clavatum*, (Hageman, 1979; Walton and Sloan, 1990; Sgarrella and Mocharmont Zei, 1993 among others), as well as *G. quinqueloba* in the planktics (Bè and Hutson, 1977) because of high freshwater discharge from closer river mouths, limiting foraminifers' diversity.

Such a characterization is more difficult for interglacial periods, since the degree of similarity of their microfaunistic assemblages is higher, and it is not possible to distinguish each warm stage based on peculiar features. Anyhow, some paleoclimatic inferences can be derived, as well. For instance, warm planktic species reach (high) values of the same magnitude order in MIS7.3, MIS5.5 and MIS1 warm oscillations. These intervals also show the presence of tropical species *G.* ex gr. *sacculifer*, suggesting the onset of more oligotrophic and likely less rainy conditions (Bè and Tolderlund, 1971; Hemleben et al, 1989; Pujol and Vergnaud Grazzini, 1995). Nevertheless, it has to be noted that the peak of warm planktic species inside MIS7.3 mainly derives from the abundance of *Orbulina* spp, all the other warm planktic species being very poorly represented. For this reason it could be inferred that MIS7.3 climate condition were probably slightly colder compared to those of the Eemian (Thyrrhenian, MIS5.5) and of the present interglacial (MIS1). The same statement would bring to determine relatively less warm climate condition, compared to all the other interglacials, during MIS3, as well, since its peak of warm planktic species is mainly composed of *Orbulina* spp, too. Moreover, warm plantic species show a decreasing upward trend inside MIS3, characterised by repeated and alternating oscillations, consistent with isotopic shifts, which can possibly be the expression of high resolution climatic events, like the Dansgaard-Oeschger cycles, already found in the Mediterranean (Sànchez Goñi et al., 2002, Combourieu Nebout, 2002), in the Central Adriatic basin. This aspect, anyway, must be treated in more detail, possibly coupled to other proxies, like, for example, the pollen variation.

Other inferences can be derived as regards the ventilation of the water mass. Planktic species *G. inflata* and the deeper *G. truncatulinoides*, in fact, present only during interglacial periods in PRAD1-2 record, require a developed vertical mixing of the water column to live (Bè and Tolderlund, 1971; Hutson, 1977; Fairbanks et al., 1980; Van Leeuwen, 1989; Pujol and Vergnaud Grazzini, 1995). The enhancement of this vertical circulation also reflects in a well oxygenated bottom floor, testified by the common occurrence of epifaunal benthic species such as *C. pachyderma* and *H. balthica* (in MIS5 and MIS3).

The presence of *G. truncatulinoides* during MIS9, MIS7, MIS5 (and MIS1) interglacials also implies that the water column was thick enough to consent this deep water dweller to pass the Pelagosa sill and inhabit Central Adriatic. Globorotalids generally peak out of phase compared to the warm planktic species, suggesting that the vertical mixing probably occurred during temperate climate conditions. That could also reflect an intensification of the seasonal contrast, resulting in a well developed vertical mixing and in a better ventilation of the sea floor during winters, and in a more stratified and oligotrophic water in the summer season. Benthic assemblage during interglacials is generally composed by *C. laevigata carinata*, *B.* ex gr. *marginata*, *T. angulosa*,

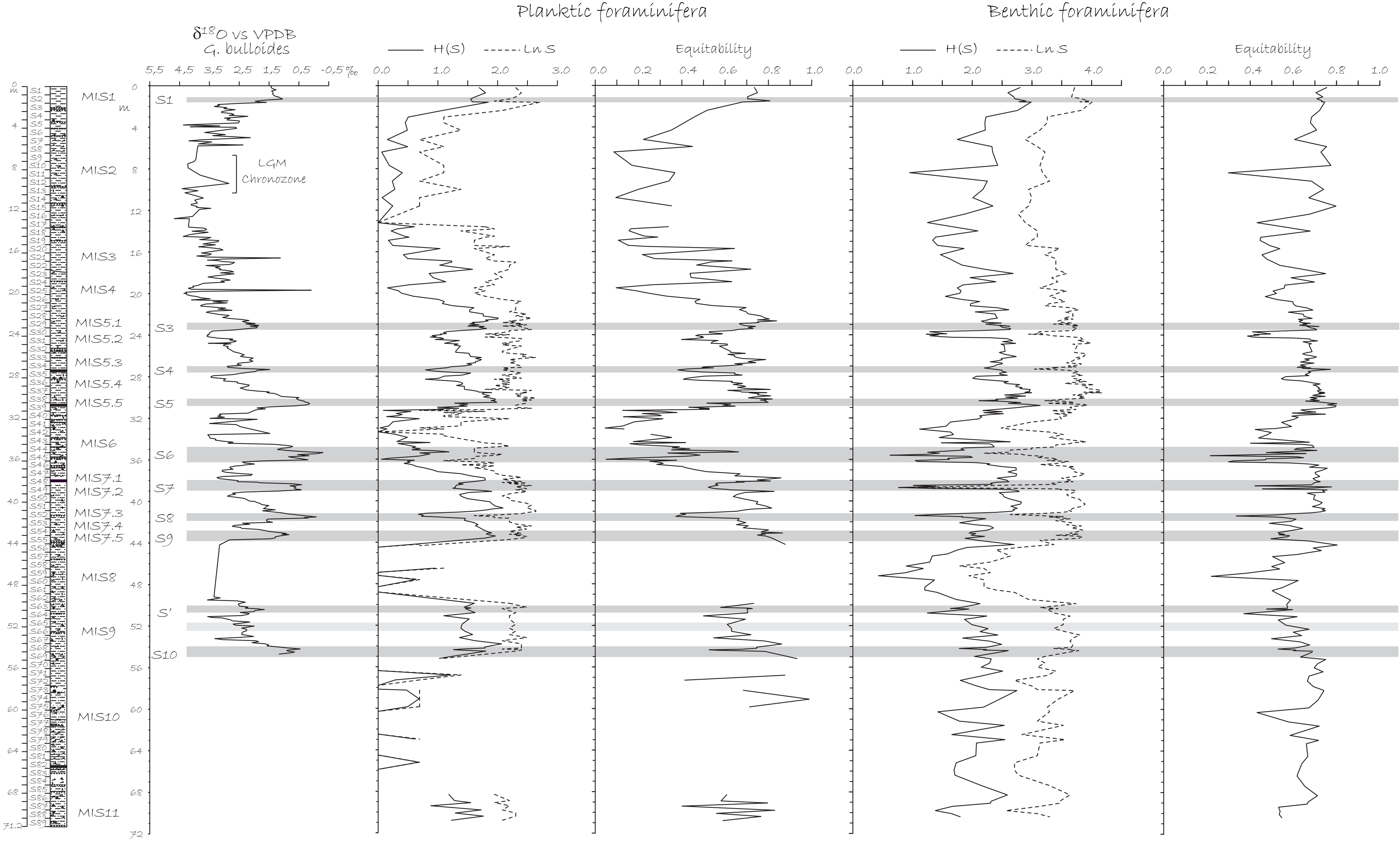

Fig. 2.3. Shannon-Weaver diveristy index H(S) plotted for planktic and benthic foraminifera. LnS represents the maximum values to which H(S) tends when the species have equal proportion. Equitability (Pielou index) is also reported. Grey areas represent Sapropel equivalent intervals. On the left the Oxygen isotope stratigraphy is shown.

Brizalina spp, *Bolivina* spp, *Uvigerina* spp, *C. pachyderma*, reflecting a mesotrophic environment typical of outer shelf to upper slope facies (Murray, 1991).

2.4 PALEOBATHYMETRIC RECONSTRUCTION

Depth can not be *per se* a limiting factor for the life of benthic foraminifera, as only pressure and light intensity are directly coupled to variation in depth (Van der Zwaan et al., 1999): food availability (flux) and oxygen content are considered some of the factors more limiting benthic foraminifera distribution (see Jorissen, 1999 for a review), then they should play a major role also in the bathymetric foraminifers' distribution. As individual species are never good paleodepth marker (except for high marsh assemblages), even if it is possible to distinguish species typical of deep waters and others of shelf environment, different assemblages will occur at a given depth depending on the oxygen/food supply combination (Van der Zwaan et al., 1999). The organic flux always decreases with depth, and plankton/benthos ratio consequently increases. Nevertheless, the reconstruction of a paleodepth record should be independent from organic flux. Van der Zwaan et al. (1990) proposed a quantitative method to obtain paleobathymetric estimates, using the P/B ratio corrected for the presence of genera with infaunal habitat (*Bulimina, Globobulimina, Bolivina, Uvigerina* and *Fursenkoina* (Murray, 1991; Sgarrella and Moncharmont Zei 1993; Jorissen 1999 among others)), as not directly influenced by the organic flux falling from the overlying water. In other words, this means that sapropel samples should not be included in the paleodepth estimate, as frequently dominated by infaunal species or even devoid of benthic fauna.

Van der Zwaan et al. (1990) proposed a formula for paleobathymetric estimate, that is:
$D=\ln(a+b\ \%P)$
with $D=$ depth, $a=3.58718$, $b=0.03534$; $\%P= P/P+(B\text{-infaunal})$, where $P=$ number of planktic foraminifera specimens and $B=$ number of benthic foraminifera specimens. The "a" and "b" values implies that if $P= 100$ the estimated paleobathymetry is 1250 m, while if $P=0$ D is 36 m. This implies that the application of this method is limited to this bathymetric range. Moreover, it has to be kept into account that 1) this method assumes negligible the dissolution of the tests (then, samples with dissolution traces should not be included in the calculation), and 2) reworked specimens should not be counted and used for this purpose.

Morigi et al. (2005) proposed the following different formula to estimate the paleodepth in records containing also mud belt environment:

$EWD = \Sigma (P_x * MWD_x) / \Sigma P_x \qquad x= 1, i$

where EWD= estimated weighted mean water depth, P=percentage of the i-species, MDW=mean weighted depth of the i-species calculated from the distribution of the species presently living in the Adriatic basin. As this method does not depend on planktic foraminifera abundance, it could be useful to estimate paleodepth in intervals out of the application range of Van der Zwaan et al. formula (for instance in environments shallower than 40m). However, the application of this method to pre-Holocene Adriatic records rises some doubt, in particular if the presence of mud belt environments is inferred in the record to be studied:

- the benthic species presently living in the modern mud belt, characterised by high organic matter supply and low oxygen content, present a bathymetric range depending on the modern spatial distribution of the muddy sediments, in turn function of the present riverine influence and of the circulation pattern, according to Van der Zwaan and Jorissen (1991). Then, a mud belt can change its depth and spatial distribution depending on several factors, such as the enhancement or decreasing of the riverine influence, the bottom topography on which it develops, the circulation pattern, and the available width of the shelf. Subsequently to these changes, benthic species typical of mud belt and present in a pre-Holocene record will surely indicate the presence of a mud belt environment (application of the taxonomic uniformitarism), but the paleodepth could be different compared to the present estimated mean weight depth for these species.
- the bathymetric resolution that this method can discriminate is not reported.

In PRAD1-2 borehole, this method could in theory be applied during the low stand intervals, when Van der Zwaan et al. curve reaches its minimum confidence value (36 m). Yet, the benthic assemblage found in glacial periods is deeply different from the assemblage presently living in the Adriatic shelf, since those cold periods were dominated by species such as *E. clavatum, E. articulatum, I. islandica*, *Trifarina* sp1, *Astrononion*, which are absent or poorly represented nowadays.

Then, for all the reasons above discussed, only the Van der Zwaan et al. (1990) method has been applied in PRAD1-2 record.

The main trend of the paleobathymetric index is shown in Fig. 2.4. As already observed, in Van der Zwaan et al. formula, sapropels levels should not be taken into account. Anyway, to have an idea of the aberrant (and not realistic) values obtained for these levels, the paleodepth has been calculated and the resulting values are reported as a stippled, black line, while the numbers aside each peak refer to the calculated value corresponding to each level. Additional not realistic values occur also during the two dysoxic levels inside MIS2, corresponding to peaks of *G. laevigata* + *Polymorphyna* spp.

The resulting paleobathymetric curve is represented in Fig. 2.4 as a solid black line. A 3 points-smoothing has then been applied to the curve, after neglecting the sapropel-like levels. The smoothed curve has been plotted also reporting the main paleoenvironments (shoreline, inner shelf, outer shelf, upper slope) the line crosses and their bathymetric boundaries. Paleodepths shallower than 36m (for instance during MIS 8 and 10) were inferred by the information available from the bathymetric range occupied by the modern benthic assemblage (e.g. Jorissen 1988) and they have been reported as a dashed black line.

The obtained paleobathymetric curve (Fig. 2.4) shows oscillations in the water depth from upper slope to inner shelf environments. That seems phased with the glacial/interglacial cyclicity indicated by the stable oxygen isotope curve, particularly the benthic one, and with indications derived from the bathymetric range occupied by the modern benthic assemblage.

Some sea-level curves for the last 4 climatic cycles are available in literature (e.g. Rohling et al. 1998; Siddall et al., 2003; Waelbroeck et al., 2002; SPECMAP curve by Imbrie et al., 1984). Waelbroeck et al. (2002) and Lambeck et al. (2002) curves have been reported for comparison in Fig. 2.4. These two sea-level curves are obtained by a stacked benthic oxygen stable isotope record and by sea-level data from different regions, respectively.

A general deepening trend is visible, comparing PRAD1-2 glacial periods, from MIS10 to MIS2, even if MIS2 water column results thinner than MIS4 and MIS6 ones. These outcomes find a good agreement with the concentration of planktic foraminifera, which results to be higher during MIS4 and 2, suggesting a relative deepening of the water column. Yet, this is in contrast with the global sea level curve (e.g Rohling et al., 1998; Waelbroeck et al., 2002), which assigns the lowest water depths (of the same magnitude order) to MIS10, MIS6 and MIS2, whereas MIS8 results a little deeper. These differences between the two record may imply a local control on PRAD1-2 estimated bathymetry, maybe affected by subsidence effects.

Quantitatively speaking, the bathymetric oscillations for glacial/interglacial boundaries (i.e. MIS10-9, MIS8-7, MIS6-5 and MIS4-3) are in the order of 120-130 m, not far from the estimates of the global sea level curve (Waelbroeck et al., 2002). A similar range results also for some substages, for instance during MIS7.5-4, MIS5.5-4, MIS5.4-2. These shifts, instead, result too wide, compared not only to those from the global sea level curve (Waelbreock et al. 2002) indicating, for MIS5.4, a 40m sea-level fall, but also to the sea-level data from Lambeck et al. (2002), indicating a 70m sea-level fall. Nevertheless, these bathymetric shifts can be considered qualitatively reliable, as geophysical evidences attest the presence of erosional or condensed surfaces on the shelf (in particular in correspondence to MIS5.4, MIS5.2 and MIS4): these geometries are in fact coherent with significant downward shifts of the shoreline. One possible explanation for these exaggerated paleobathymetric shifts could be that the expected lowering of the sea level affected Adriatic planktic and benthic foraminifera in such a way to decrease the diversity of the assemblage, and leading to the dominance of opportunistic taxa. This is the case of *C. laevigata carinata*, reaching highest abundances (>50%) during MIS7.4, MIS5.4, MIS5.2 and MIS4. Such oligotypic assemblages, reflecting an highly stressed environment, could somehow affect the paleodepth index, which should also be corrected whenever one single taxon shows a strong dominance.

The correlation between the paleobathymetry curve and the biodiversity index is shown in Fig. 2.5. the grey areas correspond to cold climate oscillations with shifts in the paleodepth wider than expected. Cold substages inside MIS7 have not been highlighted, since sapropelic layers partially alter the signal.

Moreover, as also reported by Luning et al. (1998), P/B ratio, which Van der Zwaan et al. index is an improvement of, could give unrealistic results because of an increase of the productivity of the water mass, affecting the abundance of the planktic assemblage. That may imply some additional corrections in the index formula, not only for the benthic assemblage, but also as regards planktic exceptional variations linked to productivity.

The correlation of PRAD1-2 paleobathymetric record with other Mediterranean (punctual and scattered) sea-level reconstructions (e. g. Antonioli et al., 2004) shows a good consistency for some interglacial oscillations (for instance, MIS5.1 and 7.3 result in the order of -21m in Antonioli

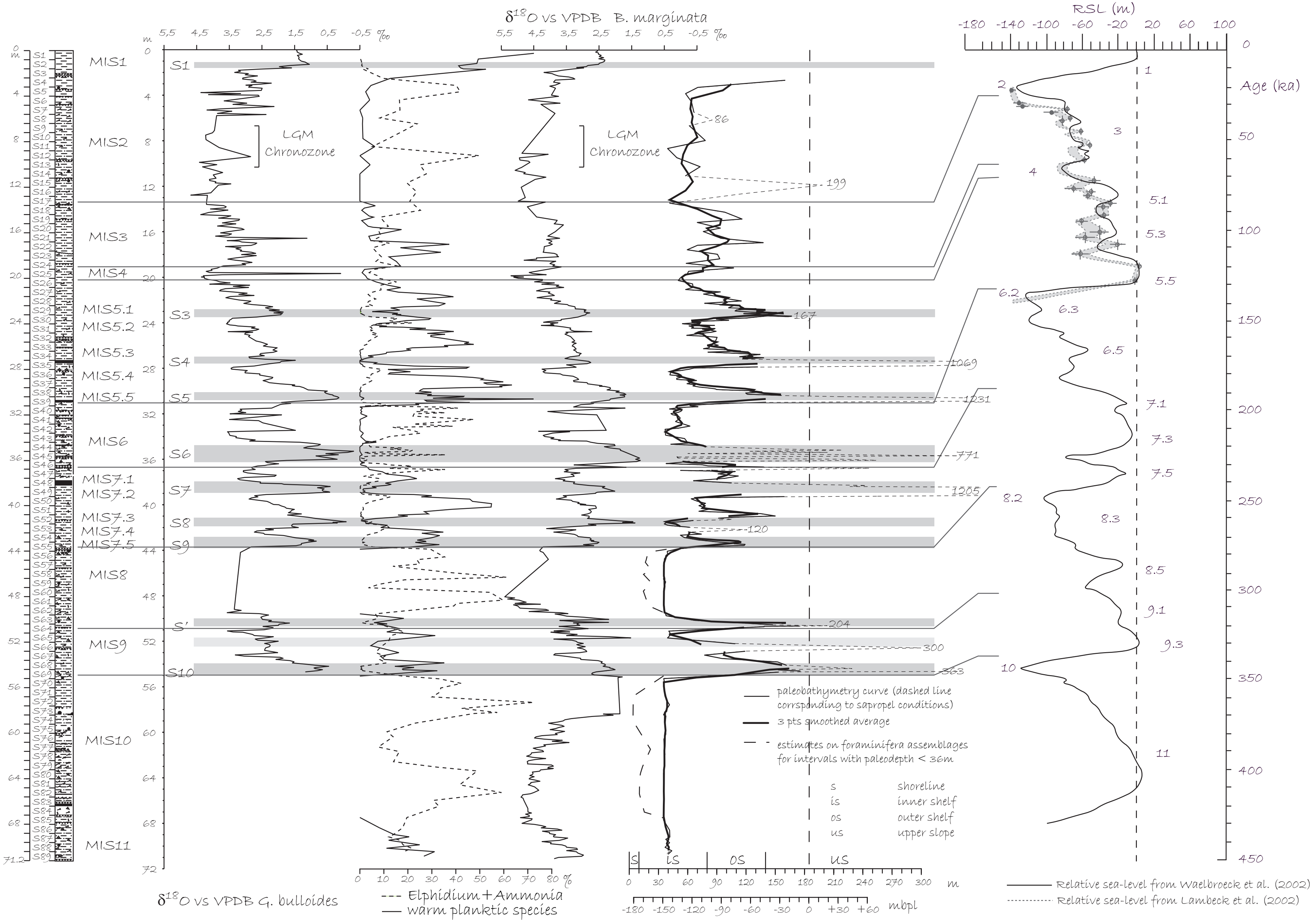

Fig. 2.4. Paleobathymeric curve according to Van der Zwaan et al. index. Planktic and benthic isotopic curves and foraminifers' climate cyclicity are reported for correlations, as well as global sea-level records. The grey areas correspond to sapropelic events.

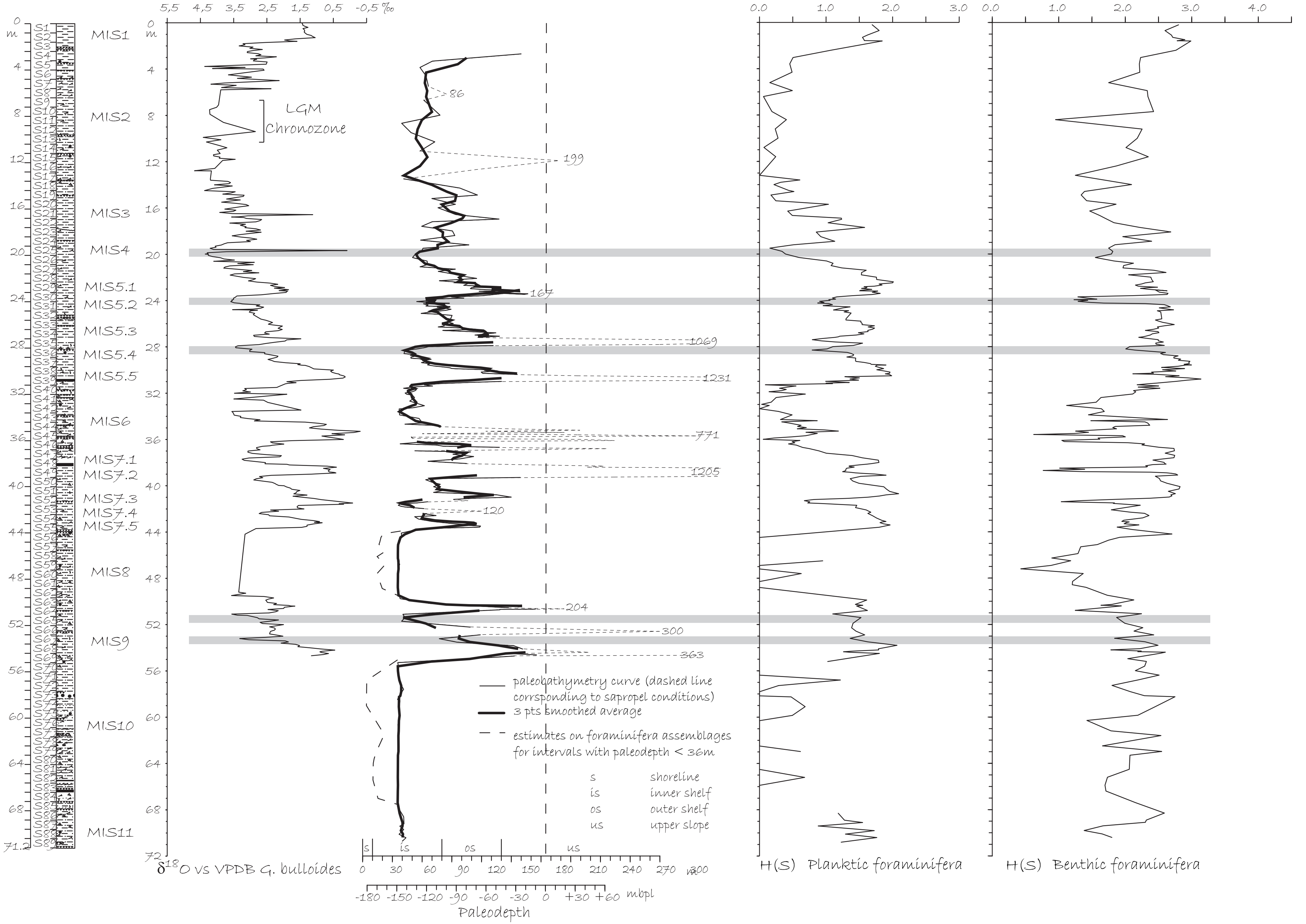

Fig. 2.5. Correlation between the paleobathymeric curve and the H(S) Shannon biodiversity index. The isotopic curve is reported on the left. The grey areas correspond to cold climate oscillations with paleobathymetric shifts wider than expected.

et al. record, and of about -25, -30m in PRAD1-2). This may imply that the observed paleo-depth anomalies are mainly located in the cold substages.

Looking in more detail, it is possible to note a general delay between the warmest climate conditions derived from foraminifers' climate cyclicity and the deepest tracts of the paleobathymetric curve (for instance during MIS7 and MIS5 warm substages). In particular, it seems that warm climate conditions affected the water column when the regressive trend had already begun. Comparing these curves with other temperature-dependent proxies, it is possible to observe a recurrent sequence of peaks, which consents to infer how oceanographic changes are first registered by the oxygen stable isotope curve (that is observed when temperature-linked peaks are distinguishable from peaks caused by salinity, for instance during MIS7.3 and MIS5.3), and by the alchenones record (Grimalt, personal oral communication, 2006), and then by the planktic foraminifers' assemblage.

Finally, it must be considered that also the use of global sea level curves imply to take some major cautions. In fact, these curves are strictly depending from the different age models adopted. Moreover, even if the Terminations are consistently determined, it cannot be completely ruled out an underestimation of minor order climatic shifts, because of stratigraphic (low sedimentation rates) and chronologic (events' identification) resolution problems.

CHAPTER 3: SAPROPELS

3.1. INTRODUCTION

The PRAD1-2 expanded stratigraphic record includes many intervals that can be considered as sapropel equivalents. These layers grant the possibility to perform a high resolution stratigraphic study based on the detection of events from planktic and benthic foraminifers' quantitative analyses and from stable isotope data. This chapter aims to analyse in detail the structure and the characteristics of each sapropel-equivalent layer recovered in PRAD1-2 borehole, in order to reconstruct the paleoceanographic setting which occurred during these peculiar events, and thereafter making comparisons through time (among PRAD1-2 sapropels) and space (between PRAD1-2 and other Eastern Mediterranean records available from literature). Before presenting the new results in Adriatic, a synthesis of the main mechanisms proposed in the literature for sapropel formation is provided, along with a review of the main proxies to detect sapropelic events.

Hypothesis on sapropel origin

Sapropel levels record peculiar oceanographic events in the depositional history of a sedimentary basin. These dark-coloured, organic-rich layers, first discovered in the eastern Mediterranean by Kullenberg, (1952), are a peculiarity of many silled marginal seas (e.g. Japan Sea and Red Sea) (Emeis et al., 1996). The mechanisms leading to a sapropelic environment include an increase in the rainfall frequency (Rohling and Gieskes, 1989; Kallel et al., 1997, 2000), and consequently also in river runoff, which would have caused the establishment of a shallow freshwater layer. This decrease in surface water salinity and density prevented the sinking of oxygenated surface water in the basin: that would have reflected in a decrease in the ventilation of the water mass, and therefore in the increased preservation of organic matter at the bottom floor, because of dysoxic condition and of a reductive environment (Olausson, 1961; Ryan, 1972; Cita et al., 1977; Vergnaud-Grazzini et al., 1977; Thunell, 1979; Cita and Grignani, 1982; Rossignol-Strick et al., 1982; Rossignol-Strick, 1983, 1985; Vergnaud-Grazzini, 1985; Thunell and Williams, 1989; Béthoux, 1993; Tang and Stott, 1993). A distinctive increase in the primary productivity in the photic zone, producing a marked stratification of the water column, is another frequent aspect of the sapropel paleoceanographic characteristics (Calvert, 1983; De Lange and Ten Haven, 1983; Parisi, 1987; Boyle and Lea, 1989; Pedersen and Calvert, 1990; Violanti et al., 1991; Calvert et al., 1992; Van Os et al., 1994). These two sapropelic features, once considered mutually exclusive, could instead combine and interact in the deposition of these peculiar paleoceanographic events (Rohling and Gieskes, 1989; Castradori, 1993; Sancetta, 1994).

A close connection between sapropelic dysoxic to anoxic environments and climate has been largely demonstrated in the literature, by assessing the correlation of these peculiar paleoceanographic events with northern hemispheric insolation maxima and periods of decreasing ice volume (Cita et al.,1977; Vergnaud-Grazzini et al., 1977; Rossignol-Strick, 1983; Hilgen, 1991; Lourens et al., 1996; Langereis et al., 1997). Nevertheless, the climatic mechanism that led to hydrographic changes and sapropel formation is still under debate.

One of the first theories about the onset of sapropelic conditions involved a reversal of the Mediterranean circulation pattern from antiestuarine to estuarine, caused by a low-salinity surface layer in the eastern Mediterranean (Stanley et al, 1975; Calvert, 1983; Thunell et al., 1983, 1984; Muerdter and Kennett, 1984; Ten Haven, 1986; Buckley and Johnson, 1988; Thunell and Williams, 1989). The estuarine circulation regime would have acted as a trap for nutrients, resulting in an increased production of organic matter, and in a consequent oxygen consumption at bottom levels of the water mass. Subsequent studies, anyhow, demonstrated that the deep Mediterranean outflow occurred continuously during the last 140 kyr, and that the antiestuarine regime was never reversed, but only weakened or reduced at times of sapropel formation in the eastern Mediterranean basin (Ross and Kennett, 1984; Zahn and Sarnthein 1987).

Another popular theory trying to explain sapropel formation involves changes in humidity related to an enhanced activity of the insolation-driven African monsoon, which would have caused huge freshwater runoff through the Nile River catchment (Rossignol-Strick et al., 1982; Rossignol-Strick, 1983, 1985; Lourens et al., 1996). Anyhow, as reported by Emeis et al. (2003), "the extent of freshwater discharge by the Nile river during some sapropel events is rather well constrained, suggesting that it was too small, or the effect too local, to alone explain the long-lasting enhanced stratification or the extent of isotope anomalies" (see also Jenkins and Williams, 1983, Focault and Stanley, 1989, Béthoux, 1993, Rohling and Bigg, 1998, Rohling and de Rijk, 1999, Krom et al., 1999).

Béthoux and Pierre (1999) pointed out that the presence of synchronous sapropel layers found both in the western and in the eastern Mediterranean, during ODP Legs 161 and 160, respectively, could be a consequence of decreased salinity of inflowing surface Atlantic water, reduced density of Mediterranean intermediate water forming in the eastern Mediterranean, and reduced density difference of intermediate water masses at the Gibraltar Strait.

Finally, it must be considered that other forcing mechanisms can have concurred in strengthening the orbital forcing effects: for instance, abrupt climate shifts had a strong impact on the late Quaternary Mediterranean circulation and freshwater runoff (Schilman et al., 2001; Rohling et al., 2002; Casford et al., 2003).

Proxies in sapropel identification

In general, sapropels are easily recognizable on single or, more typically, integrated multi-proxies. The proxies most frequently used to recognise sapropels are:

- Lithology. The identification of sapropel darker-looking layers at the visual lithologic exam has already been discussed in the sapropel stratigraphy paragraph (Chapter 1), where the risks of underestimation were shown to depend on oxidative processes affecting the organic matter at the upper boundary of the dark layer itself.
- Colour reflectance. This analysis provides a numerical quantification of the chromatic variations of the sediment, allowing a better resolution in case of laminated sediments and composite events. This is also a precious tool to constrain the culminating phase inside a sapropelic event (Lourens, 2004). This method has been used in some ODP sites as well (e.g. Leg 160). Nevertheless, caution has to be paid because this parameter may reflect grain size variations, specially in the presence of tephra layers.
- Stable O and C isotopes in carbonates. Sapropel levels present minima in $\delta^{18}O$ and $\delta^{13}C$ isotopic composition. Though oxygen isotopic values result from a combination of signals mainly deriving from temperature, salinity and ice volume effects, the parameter most affecting sapropelic conditions and therefore characterising marked shifts in the isotopic curve is represented by oscillations in salinity. Light $\delta^{18}O$ values, in fact, reflect a period of increased rainfall and river run-off. The proximity to river mouths, especially during glacial intervals, resulted not only in enhanced amounts of freshwater (Vergnaud-Grazzini et al., 1977; Thunell and Williams, 1989; Fontugne and Calvert, 1992; Tang and Stott, 1993; Emeis et al., 1998) but also, consequently, in increased sedimentation rates, in particular during the deposition of multiple layered Se6 cold sapropel and in Se5, (that is more than 100 cm thick in PRAD1-2 record).

Minima in the $\delta^{13}C$ isotopic record result from the establishment of reductive conditions which allow preservation of the organic matter on the sea floor during sapropel events, seriously hampering life conditions because of dysoxic to anoxic environment (Vergnaud-Grazzini et al., 1977; Fontugne et al., 1989; Emeis et al., 1998).

- Paleontologic indicators.

  Plankic foraminifera. Sapropels usually show a marked increase of planktic specimens and a corresponding depletion in the benthic assemblage, since life conditions at the sea floor become more critical. Several authors noticed a marked increase in the average size of foraminifers' tests during sapropelic events (Muerdter and Kennett, 1983-1984; Baumfalk et al., 1987; Violanti et al., 1991; Cita et al., 1996; Capotondi et al., 2006).This increase appears to be linked to both enhanced preservation and productivity, or to an ecological adaptation to changing physical-chemical parameters (temperature, salinity, pH) of the upper part of the water column (Violanti et al., 1991; Negri et al., 1999).

  As regards planktic microfauna, in the whole Eastern Mediterranean all the late-Quaternary sapropels except S1 are characterized by strong peaks in Neogloboquadrinids (Rohling and Gieskes, 1989; Castradori, 1993). *N. pachyderma* r. c. and *N. dutertrei* are herbivorous planktic foraminifera, which use to graze phytoplankton (diatoms and coccolithophorids) close to the Deep Chlorophill Maximum (Rohling and Gieskes, 1989; Thunell and Sautter, 1992), just at the base of the photic zone. The high amounts of Neogloboquadrinids are therefore a consequence of an increase in planktic primary productivity and reflect a concurrent stratification of the water column. *N. dutertrei* has already been considered, in the literature, as a bio-indicator for salinity changes of the water mass, since its eurythermal and euryaline nature (13-33°C, 25-46‰; Hemleben et al., 1989) allows this species to show wide shifts in its percentage in correspondence of sapropel events all over the Eastern Mediterranean (Ryan, 1972; Cita et al., 1973, 1977, 1996; Vergnaud-Grazzini et al., 1977; Thunell et al., 1977; Thunell, 1978; Muerdter et al., 1984). Although it has been demonstrated that this species well adapts to low salinity waters, also in the Atlantic Ocean (Ruddiman, 1971; Fairbanks and Wiebe, 1980; Fairbanks et al., 1982), nonetheless it seems too hazardous to use a single *taxon* as a proxy for freshwater influxes, since its variations in abundance could also be affected by other independent factors concurring in limiting its life. Another planktic proxy for the warmest sapropel is given by the common presence of *G. ruber* in its pink variety (Negri et al., 1999); this warm water (16-31°C; Bè and Tolderlund, 1971; Fairbanks et al., 1982), oligotrophic, *Zooxantellae*-bearing species, tolerates variations in salinity; within sapropel-like intervals, this species is characterized by thinner test (compared to *G. ruber white*) and inflated chambers, suggesting an adaptation of its shell to increase buoyancy and float in fresher water (Negri et al., 1999). Principato et al. (2006) study the deposition of sapropel S1 in a 2302 m deep core recovered in the Florence Rise (Levantine Basin), reporting the same thinning of planktic foraminifera (mainly for *G. ruber* s.s.). Yet, they consider this decrease in weight, common to more planktic species during the S1 deposition, as the result of dissolution and they reject the morphological characteristics (thin, foraminiferal shells with large pores) described by Capotondi et al. (1999) as a primary species-specific phenotypic variation. However, Principato et al (2006) do not take into account Negri et al (1999) paper, where optical and SEM pictures are reported for these morphologic characteristics. Then, aiming to verify whether carbon dissolution could be considered, as Principato et al. (2006) propose, the main cause of these modifications of the shells (inflated chambers, enlarged secondary apertures and thin test), which are present in Se5 and Se7 in PRAD1-2, planktic foraminifers' tests belonging to several planktic species (*G. ruber*, *G. bulloides*, *G. sacculifer* and *Orbulina*) were selected from one of the most intense Central Adriatic sapropel equivalents, Se5. The specimens were checked at the Scanning Electron Microscope (SEM). The tests, yet, appear well preserved and no trace of dissolution was found (see pictures in the plates reported at the end of the volume). Consequently, the observed morphologic characteristics of the shells of shallow-water-dweller planktic foraminifera are considered in this PhD thesis as a real adaptation of those species to variations in the density of the water mass.

Benthic foraminifera register a progressive deterioration of the oxygenation conditions at the sea floor, and the assemblage is mainly composed by dysoxic, deep-infaunal opportunistic species, typical of environments highly rich in organic matter. Anyway, a variety of settings can show dissimilar microfaunas, because of the water depth and in response to local variety in margin physiography. Anoxic conditions generally occur in deeper water depths, when deep water currents become sluggish or stop. Benthic foraminifera can be subdivided based on their ecological and environmental needs (Parisi and Cita, 1982; Vismara-Schilling and Coulbourn, 1991; Jorissen, 1999; Casford et al., 2003), and pre-sapropel, sapropel and post-sapropel benthic faunas show the paleoenvironmental evolution immediately before, during and after each sapropel (Schmiedl et al., 2003). Up to now, unfortunately, most studies on benthic foraminifers' assemblages in sapropelic environments have been carried out in deep water basins, partially limiting correlations with shallower records. Few papers report some data on benthic assemblage in more proximal settings, as regards Sapropel1 (Vigliotti et al., 1999) and Sapropel5 (Borsetti et al., 1995), the latter, however, in a rather discontinuous record.

Calcareous nannoplancton shows a decrease in *Syracosphaera* sp1 and an increase in the abundance of the genus *Rhabdosphaera* and of *Helicosphaera carteri*, of *Florisphaera profunda* and of the reworked specimens in correspondence of sapropel levels (Negri et al., 1999). In particular, *Florisphaera profunda* seems to be the only species of calcareous nannoplancton to inhabit the lower part of the photic zone, concurring in composing the Deep Chlorophyll Maximum (Castradori, 1993).

Pollen and dynoflagellate record. Sapropel layers also result in high pollen concentrations (Cheddadi and Rossignol-Strick, 1995; Rossignol-Strick and Paterne, 1999), because organic carbon preservation is much improved. Moreover, at least for the best known sapropel S1, *Pistacia* and the Mesophilous trees group seem to characterise the pollen assemblage (Rossignol-Strick et al., 1992; Rossignol-Strick, 1995, 1999).

Also dinoflagellates can provide information about sapropelic events: heterotrophic dinocysts' concentration is in fact a good indicator for productivity (e.g. Reichart and Brinkhuis, 2003), and the autotrophic species *Polysphaeridium zoharyi* dominates the sapropel 5 assemblage in the eastern Mediterranean (Sangiorgi et al., 2006).

- Magnetic properties. The Anhysteretic Remnant Magnetization (ARM) is a magnetic parameter that also helps defining sapropels (Langereis et al., 1997, Van Santvoort et al., 1997, Sangiorgi et al., 2003). ARM in fact reflects the presence of magnetite in the sediment. During sapropels, though, the reductive conditions at the sea floor consume this oxide, making it no more available. The result is that the best developed sapropels layers coincide with minima in ARM values. Anyhow, the lower boundary of the minimum interval in the ARM curve must be taken with cautions knowing that the reductive processes occurring at the water-sediment interface may affect underlying "older" deposits. Therefore the minimum interval corresponding to sapropel formation may involve more material than that effectively corresponding to the actual time of sapropel deposition (Larrasoaña et al., 2003).
- Geochemical proxies. The analysis of organic C, Ba and S content is also an important method to assess the presence of not visible, "ghost" sapropels, that would otherwise be considered as missing (Van Santvoort et al., 1997; Langereis et al. 1997). The development of

XRF technique allows the use of several other elements (e.g. V, Cu, Mo, As, Mn, all expressed as ratio versus Al), whose concentrations sharply peak during sapropel events, when oxidative processes are strongly weakened (Mercone et al., 2001; Böttcher et al., 2003; Löwemark et al., 2006).

Based on these independent paleoenvironmental indicators, it is possible to constrain the paleoceanographic anomalies characteristic of sapropelic conditions beyond the recognition of visible darker layers, and to spot a sapropelic event even when dark sediment is not apparent in the macroscopic lithologic scrutiny.

3.2. RESULTS

PRAD1-2 sapropel equivalents will be here briefly described, based on lithologic evidences, colour reflectance, $\delta^{18}O$ and $\delta^{13}C$ values, ARM paleomagnetic data, and quantitative analyses of planktic and benthic foraminifera.

Se1 is poorly represented in PRAD1-2 record, and will not be taken into exam in this section. Nevertheless, the Adriatic expression of this sapropelic event is quite well known from other cores, studied in detail in very expanded successions in the Central Adriatic (Ariztegui et al., 2000) and in the Southern Adriatic (Fontugne et al., 1989; Rossignol-Strick et al., 1992; Rohling et al., 1997; Rossignol-Strick, 1999; Sangiorgi et al., 2003).

Se3 (22.7-23.4 mbsf; Fig. 3.1).

Sapropel equivalent Se3 has no obvious expression in lithology, colour reflectance, or in the ARM values. Planktic $\delta^{18}O$ reaches a minimum value of +1.85‰, and planktic $\delta^{13}C$ a minimum value of -1.62‰. Planktic foraminifera are characterised by low amounts of *Globorotalia inflata*; warm species are present in detectable quantities; peaks in *Globigerina quinqueloba* and *Globigerina bulloides* at the base are replaced by *Neogloboquadrina dutertrei* and *Neogloboquadrina pachyderma* r.c. upsection. Benthic foraminifera are present throughout the interval: *Cassidulina laevigata carinata* common, increase in intermediate infaunal taxa as *Bulimina*, *Bolivina* and *Brizalina* and *Uvigerina*. Oxic species, such as *Hyalinea balthica*, are common.

Se4 (26.8-27.6 mbsf; Fig. 3.2).

Visible slightly darkened and partially laminated layer, marked by a change in colour reflectance values and by a minimum in the ARM curve. Planktic $\delta^{18}O$ shows a minimum value of +1.48‰, and planktic $\delta^{13}C$ a minimum value of -2.04‰. Planktic foraminifers' assemblage shows low values of *Globorotalia inflata*, and an overall decrease in the abundance of warm species. The base of Se4 shows a peak of *Globigerina quinqueloba*, followed upsection by a peak of *Neogloboquadrina dutertrei* and *Globigerina bulloides*, then of *Neogloboquadrina pachyderma* r.c.. Benthic foraminifera are always present, though scarce, and are characterised by the common presence of deep infaunal *Fursenkoina* and *Stainforthia* in the culminating phase, proto-sapropel is characterized by the common presence of *Bulimina marginata*, *Bolivina* and *Brizalina*, post-sapropel is instead composed by *Cassidulina laevigata carinata*, *Bolivina* and *Brizalina* and *Uvigerina*. Oxic species are scarce. Benthic specimens concentration is lower than the planktic one.

Se5 (29.9-30.8 mbsf; Fig. 3.3).

Visible markedly dark layer with laminated sediment, low values of colour reflectance and minimum in the ARM values. Planktic $\delta^{18}O$ read a minimum value of +0.14‰, and the planktic $\delta^{13}C$ minimum is -2.77‰. Planktic foraminifers' assemblage is characterised by nearly absent *Globorotalia inflata*, and abundant warm species (common presence of *Globigerinoides ruber pink*). The assemblage also includes peaks of *Globigerina quinqueloba* and *Globigerina bulloides* at the base of the layer, while *Neogloboquadrina dutertrei* and of *Neogloboquadrina pachyderma* r.c. dominate upsection. Benthic foraminifera are very scarce and almost complete absent in the culminating phase: deep infaunal taxa, *Bulimina marginata*, *Bolivina* and *Brizalina*, dominate just before and after the benthic extinction; proto and post-sapropelic phases are also composed by *Cassidulina laevigata carinata* and *Uvigerina*. Oxic species are very scarce.

Se6 (34.8-36.2 mbsf; Fig. 3.4).

Markedly visible dark and laminated sediment, articulated in multiple events. Colour reflectance values are low, and ARM values are close to zero. Planktic $\delta^{18}O$ reaches a minimum value of -0.31‰, whereas planktic $\delta^{13}C$ registers its minimum value at: -1.87‰. Planktic foraminifera are charecterised by the nearly absence of *Globorotalia inflata* and of warm species, and by peaks of *Globigerina quinqueloba* at the onset of sapropelic conditions, and subsequently of *Globigerina*

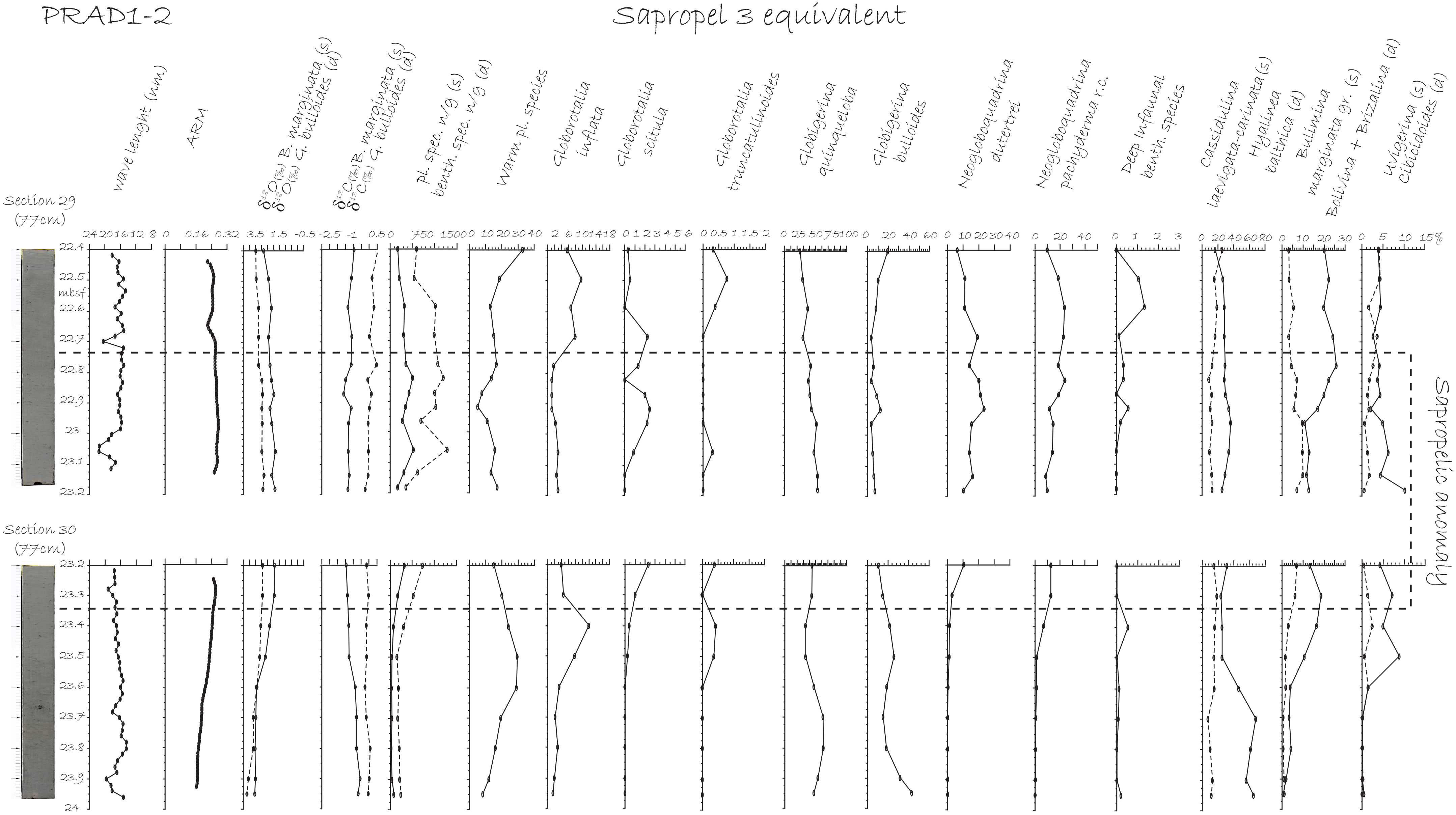

Fig. 3.1. Main results for Se3 (s is for solid line, d for dashed line).

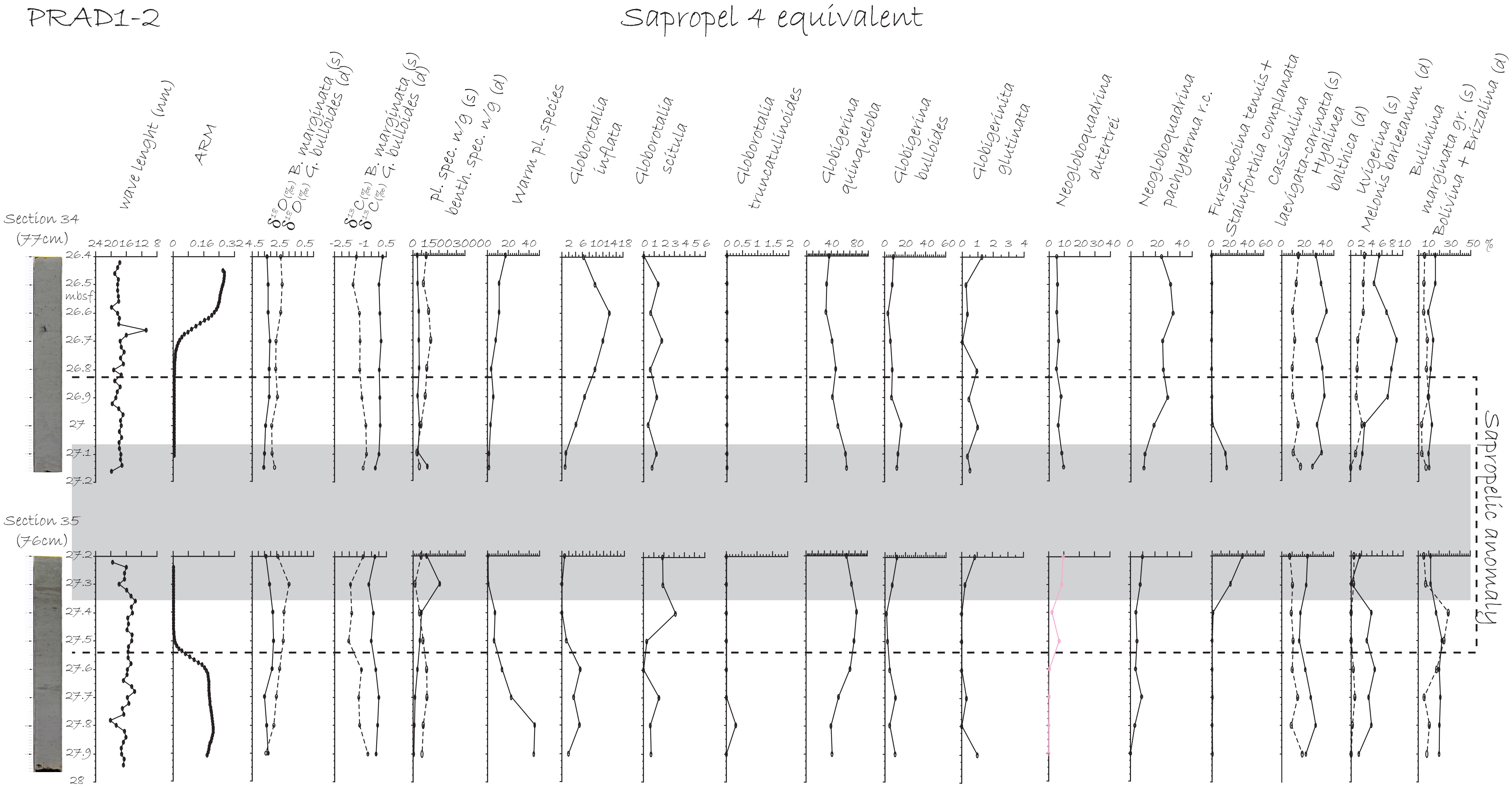

Fig. 3.2. Main results for Se4 (s is for solid line, d for dashed line). The grey band corresponds to the lithologically visible darker layer.
]

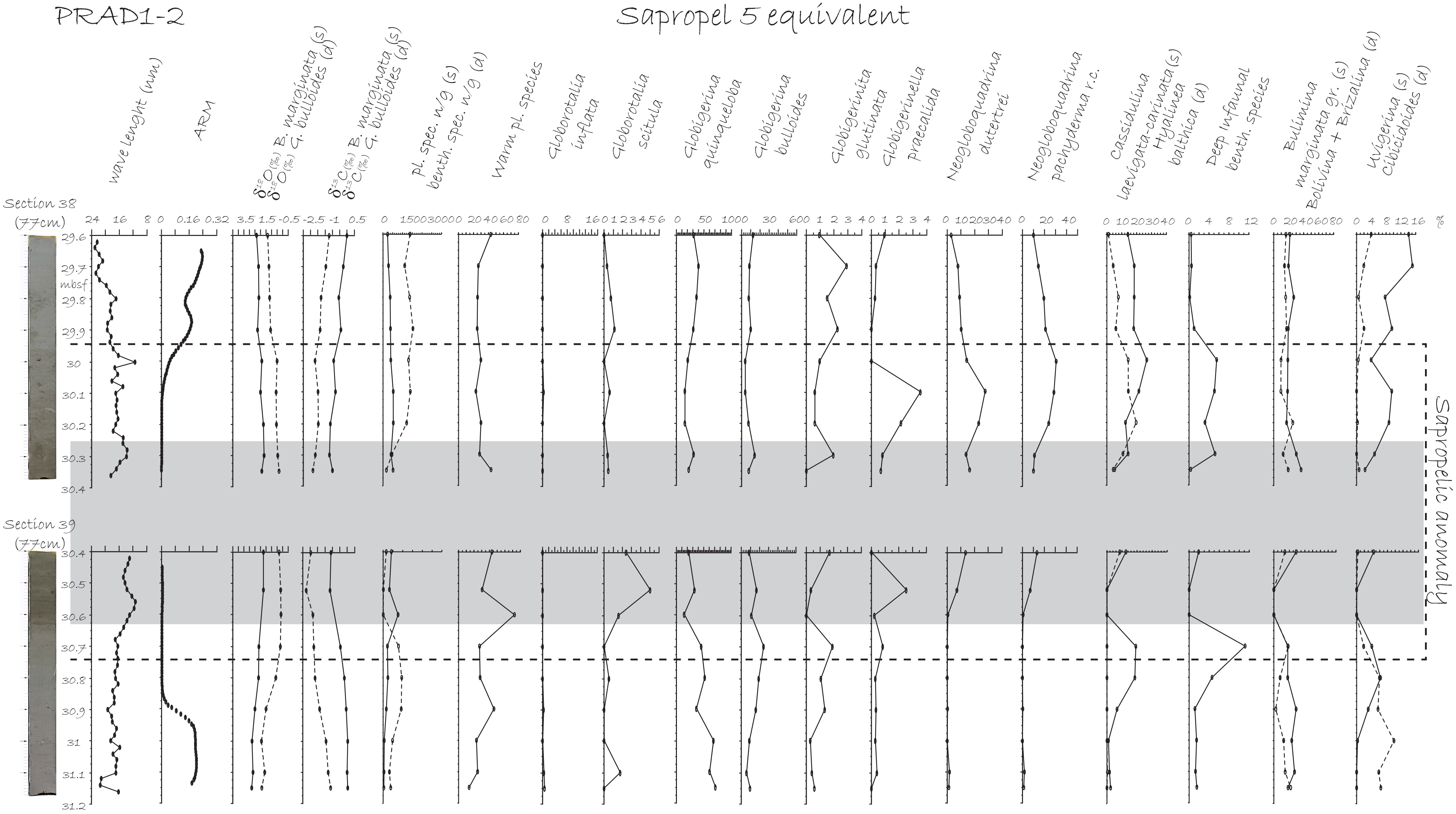

Fig. 3.3. Main results for Se5 (s is for solid line, d for dashed line). The grey band corresponds to the lithologically visible darker layer.

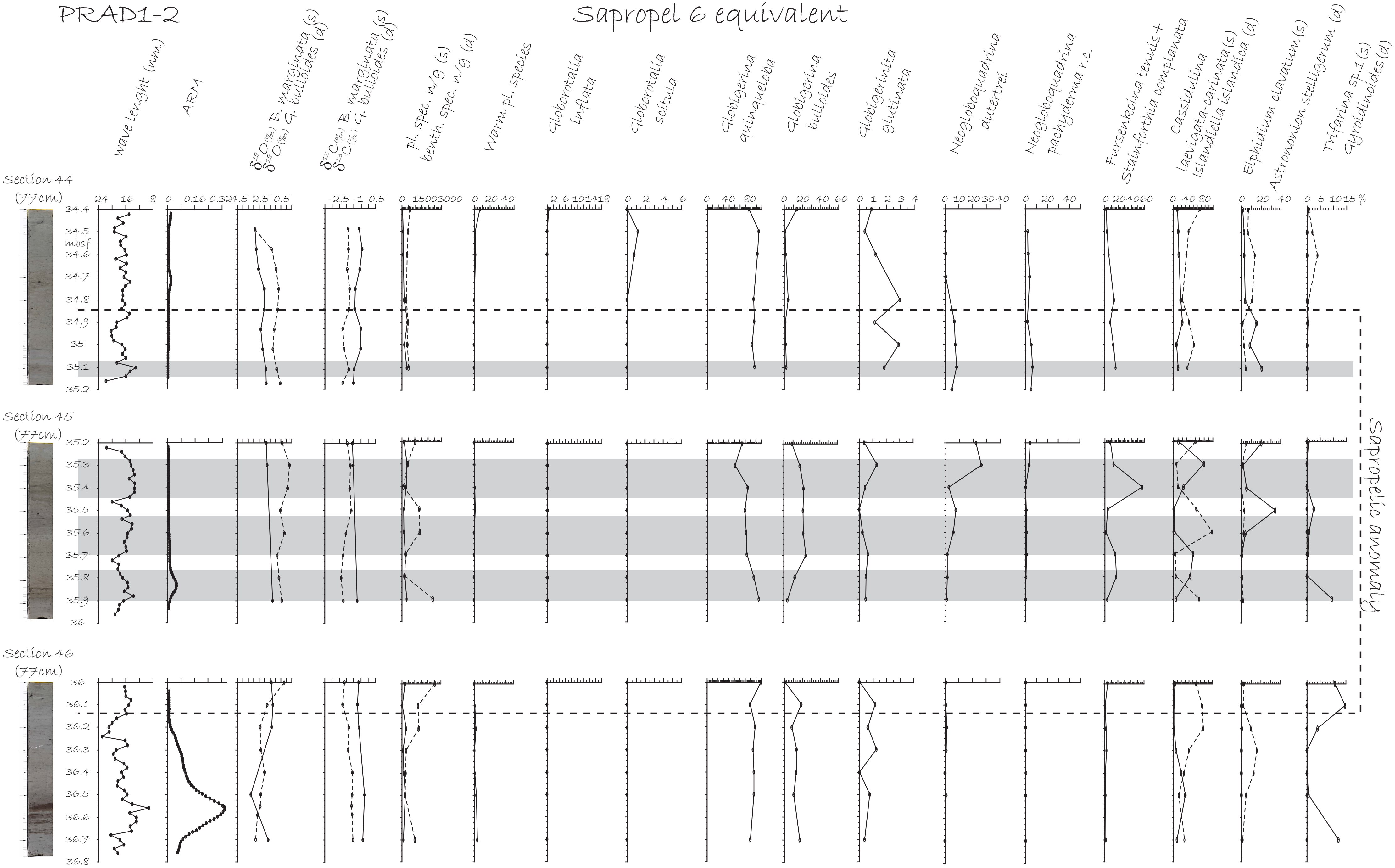

Fig. 3.4. Main results for Se6 (s is for solid line, d for dashed line). The grey bands correspond to lithologically visible darker layers.

bulloides, *Neogloboquadrina dutertrei* and of *Neogloboquadrina pachyderma* r.c.. Benthic foraminifera are always present, but with oscillating frequencies: peaks of *Fursenkoina* and *Stainforthia*, *Islandiella* and *Cassidulina laevigata carinata* with alternating trends characterise the most intense phase, *Trifarina* sp1 peaks in the early part of the sapropel, and *Elphidium excavatum* forma *clavata* in the latter part. The proto-sapropel shows the occurrence of *Astrononion stelligerum*, and the post-sapropel of *Astrononion stelligerum* and *Gyroidinoides*. Oxic species result very scarce. Benthic specimens concentration is lower than the planktic one in two cases.

Se7 (38.1-39 mbsf; Fig. 3.5).

Visible markedly dark and laminated sediment. This level also registers the lowest values of colour reflectance in PRAD1-2 record, and ARM values are close to zero. Planktic $\delta^{18}O$ has its minimum value at +0.41‰., and planktic $\delta^{13}C$ minimum value at -2.44‰. Planktic foraminifera are very abundant: *Globorotalia inflata* is nearly absent, whereas warm species are present, *Globigerinoides ruber pink occurs*; *Globigerina quinqueloba* and *Neogloboquadrina dutertrei* peak in the lower part of the sapropelic anomaly, *Neogloboquadrina pachyderma* r.c. upsection. Benthic foraminifera are very scarce, till an almost complete absence in the culminating phase: *Bulimina marginata*, *Bolivina* and *Brizalina* dominate the benthic assemblage just before and after the anoxic level; proto and post-sapropelic phase are also composed by *Cassidulina laevigata carinata* and deep infaunal taxa. Oxic species are nearly absent.

Se8 (41-41.9 mbsf; Fig. 3.6).

Visible darker sediment, resulting in low values of colour reflectance. Nevertheless, the minimum in the ARM curve is very short. Planktic $\delta^{18}O$ shows a minimum value of -0.08‰, and planktic $\delta^{13}C$ reaches a minimum value of -2.13‰. Planktic foraminifera are present in low concentrations: *Globorotalia inflata* and warm species are nearly absent, and cold planktic species are organized in two phases, the first composed by *Globigerina quinqueloba*, followed by *Globigerina bulloides*, *Neogloboquadrina dutertrei* and *Neogloboquadrina pachyderma* r.c.; the second constituted by a peak of *Globigerina quinqueloba*, and subsequent peaks of *Neogloboquadrina dutertrei*, *Globigerina bulloides* and finally *Neogloboquadrina pachyderma* r.c.. Benthic foraminifera are always present, with two minimum intervals: *Fursenkoina* and *Stainforthia*, *Islandiella*, *Trifarina* sp1 and *Astrononion stelligerum* characterise the most intense phase. Proto-sapropel and post-sapropelic assemblage are composed by *Gyroidinoides*, *Bolivina* and *Brizalina* and *Cassidulina laevigata carinata*. Oxic species are scarce. Benthic specimens concentration is never lower than the planktic one.

Se9 (42.6-43.7 mbsf; Fig. 3.7).

Not visible neither in the lithologic exam, nor in the colour reflectance; the minimum in the ARM curve is very short. Planktic $\delta^{18}O$ has its minimum value at +0.84‰, and planktic $\delta^{13}C$ minimum value attests at -2.39‰. Planktic foraminifera consist of *Globorotalia inflata*, present in low frequencies, common warm species, and of peaks of *Globigerina quinqueloba*, followed upsection by *Neogloboquadrina dutertrei* and *Neogloboquadrina pachyderma* r.c.. Benthic foraminifera are always very abundant: *Cassidulina laevigata carinata* is common, and intermediate infaunal taxa as *Bulimina*, *Bolivina* and *Brizalina* increase. Oxic species are scarce. The concentration of benthic specimens is always higher than the planktic one.

Se' (50.1-50.5 mbsf; Fig. 3.8).

Not visible neither in the lithologic exam, nor in the colour reflectance curve, the ARM curve presents a very short minimum. Planktic $\delta^{18}O$ reaches its minimum value at +1.66‰, planktic $\delta^{13}C$ minimum corresponds to a value of -2.32‰. Planktic foraminifera are composed by *Globorotalia inflata*, present in low amounts, common warm species, and by peaks of *Globigerina quinqueloba* and *Globigerina bulloides* at the onset of sapropelic conditions, followed upsection by *Neogloboquadrina dutertrei* and *Neogloboquadrina pachyderma* r.c.. Benthic foraminifera are always very abundant: *Cassidulina laevigata carinata* is abundant, intermediate infaunal taxa, as *Bulimina*, *Bolivina* and *Brizalina* and *Uvigerina* increase. Oxic species are scarce. The concentration of benthic specimens is always higher than the planktic one.

Se10 (54.1-54.5 mbsf; Fig. 3.9).

Though slightly visible in the visual lithologic exam, and poorly appreciable from the colour reflectance, this anomalous level shows a minimum in the ARM curve. Planktic $\delta^{18}O$ reaches its minimum value at +0.46‰, and planktic $\delta^{13}C$ has its minimum value at -2.96‰. Planktic foraminifers' assemblage is composed by *Globorotalia inflata*, present in low frequencies, by

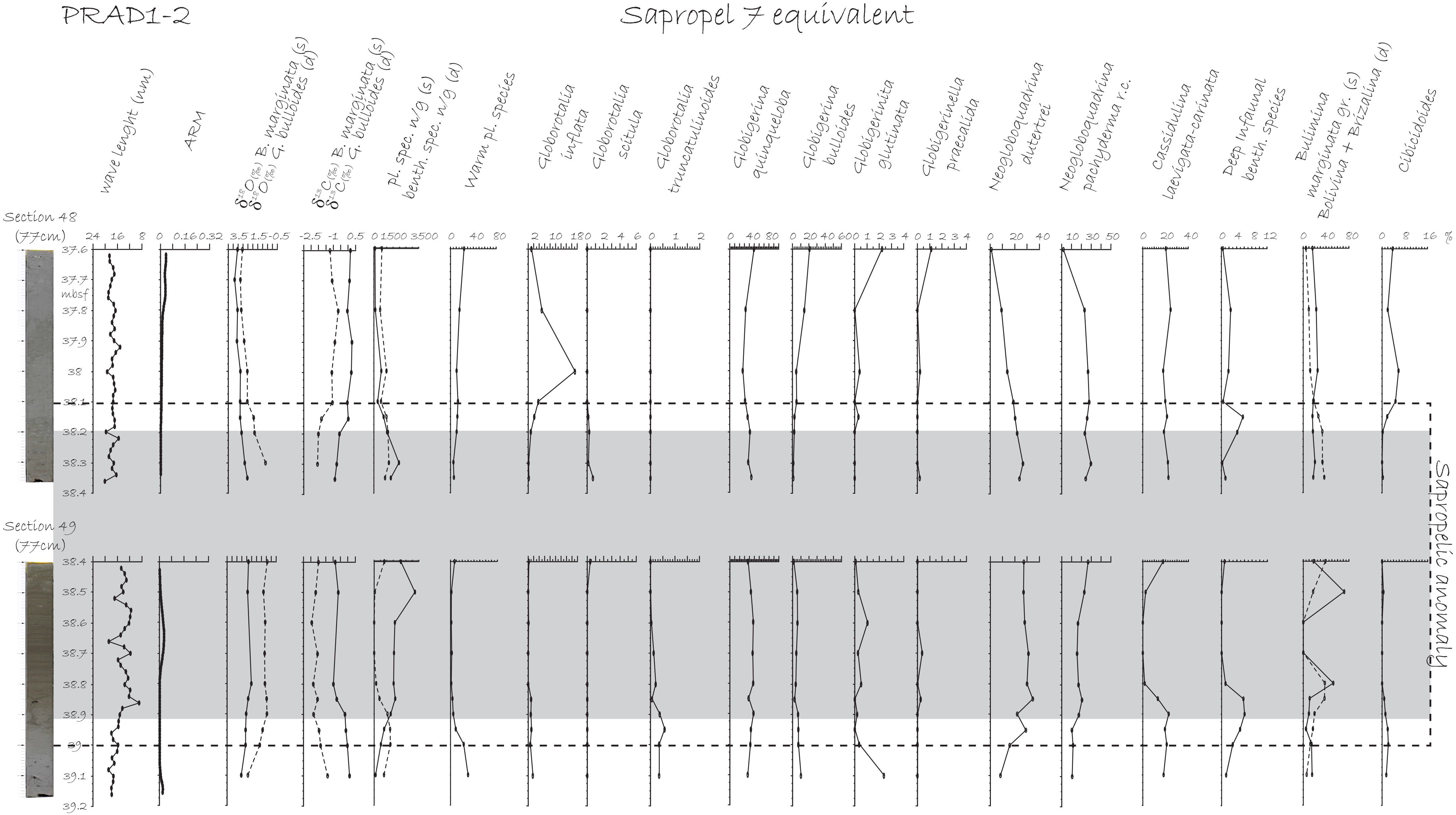

Fig. 3.5. Main results for Se7 (s is for solid line, d for dashed line). The grey band corresponds to the lithologically visible darker layer.

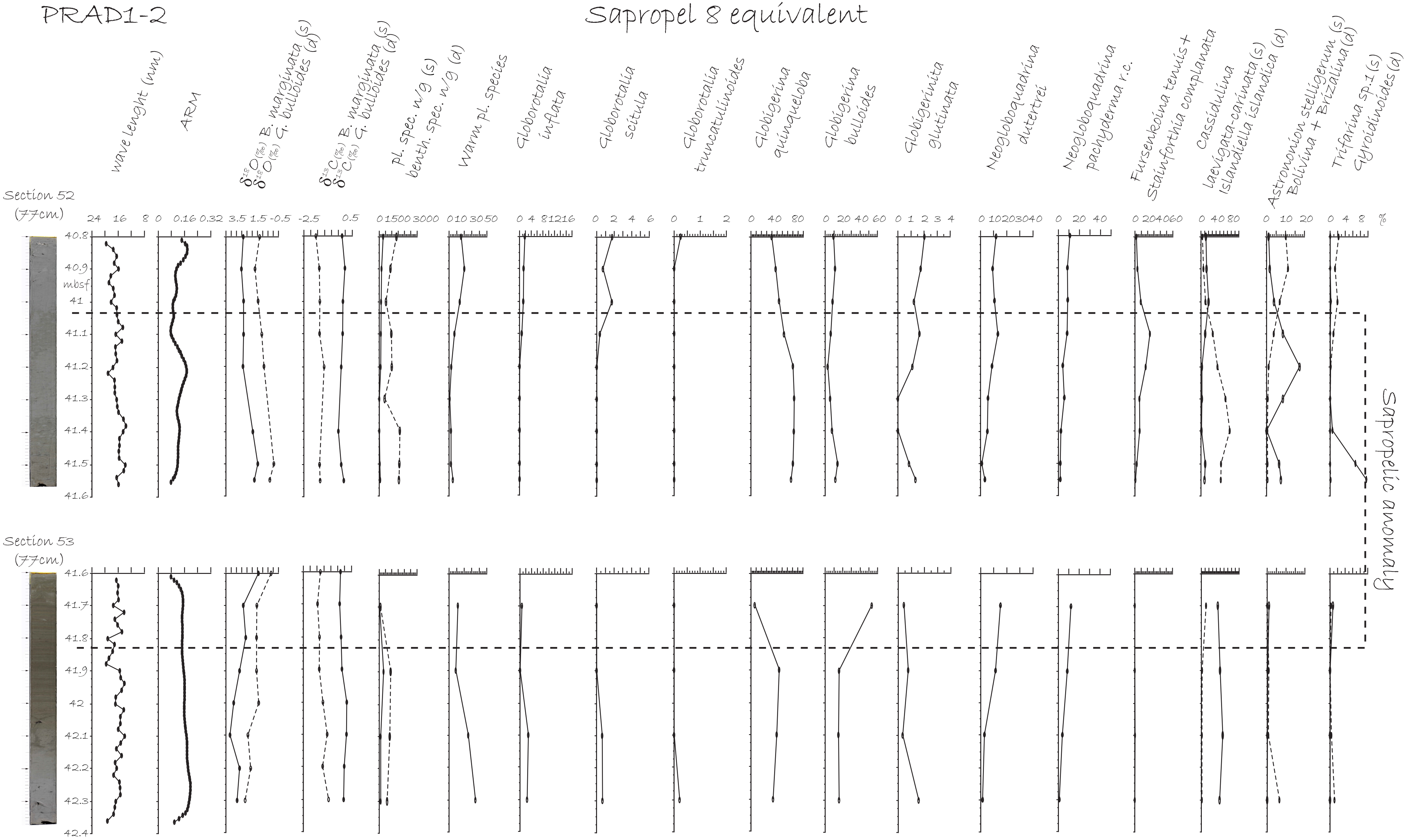

Fig. 3.6. Main results for Se8 (s is for solid line, d for dashed line).

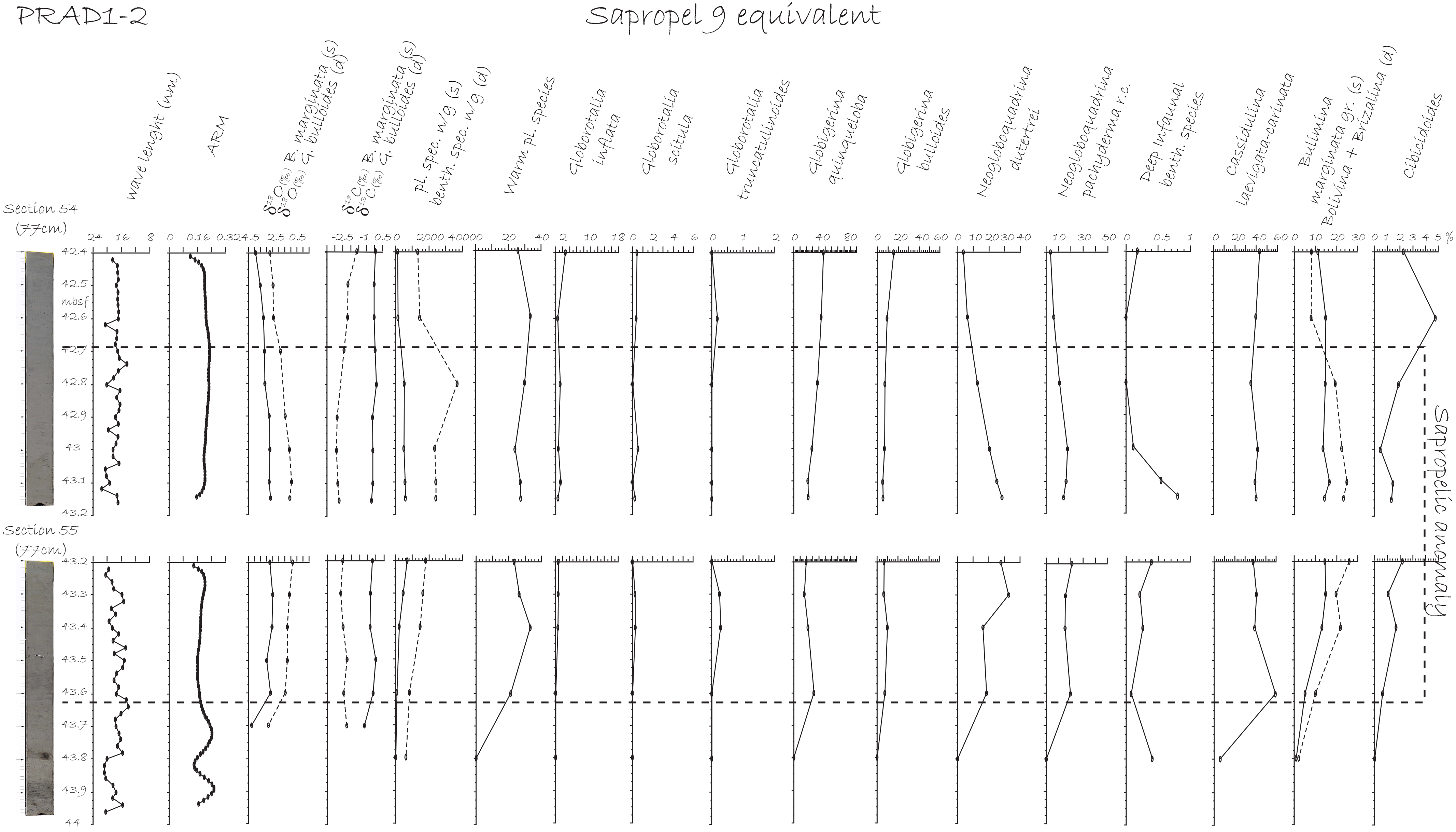

Fig. 3.7. Main results for Se9 (s is for solid line, d for dashed line).

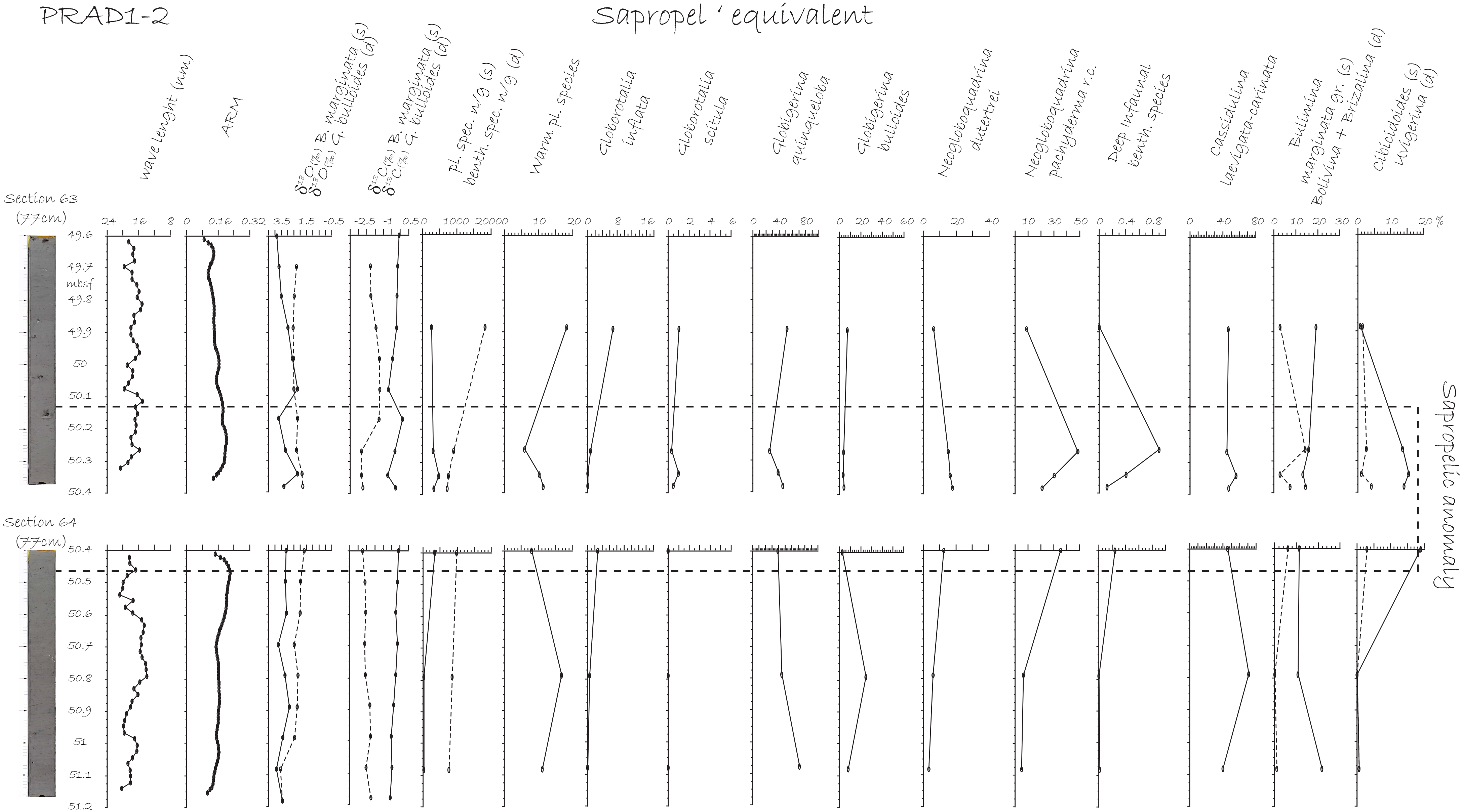

Fig. 3.8. Main results for Se' (s is for solid line, d for dashed line).

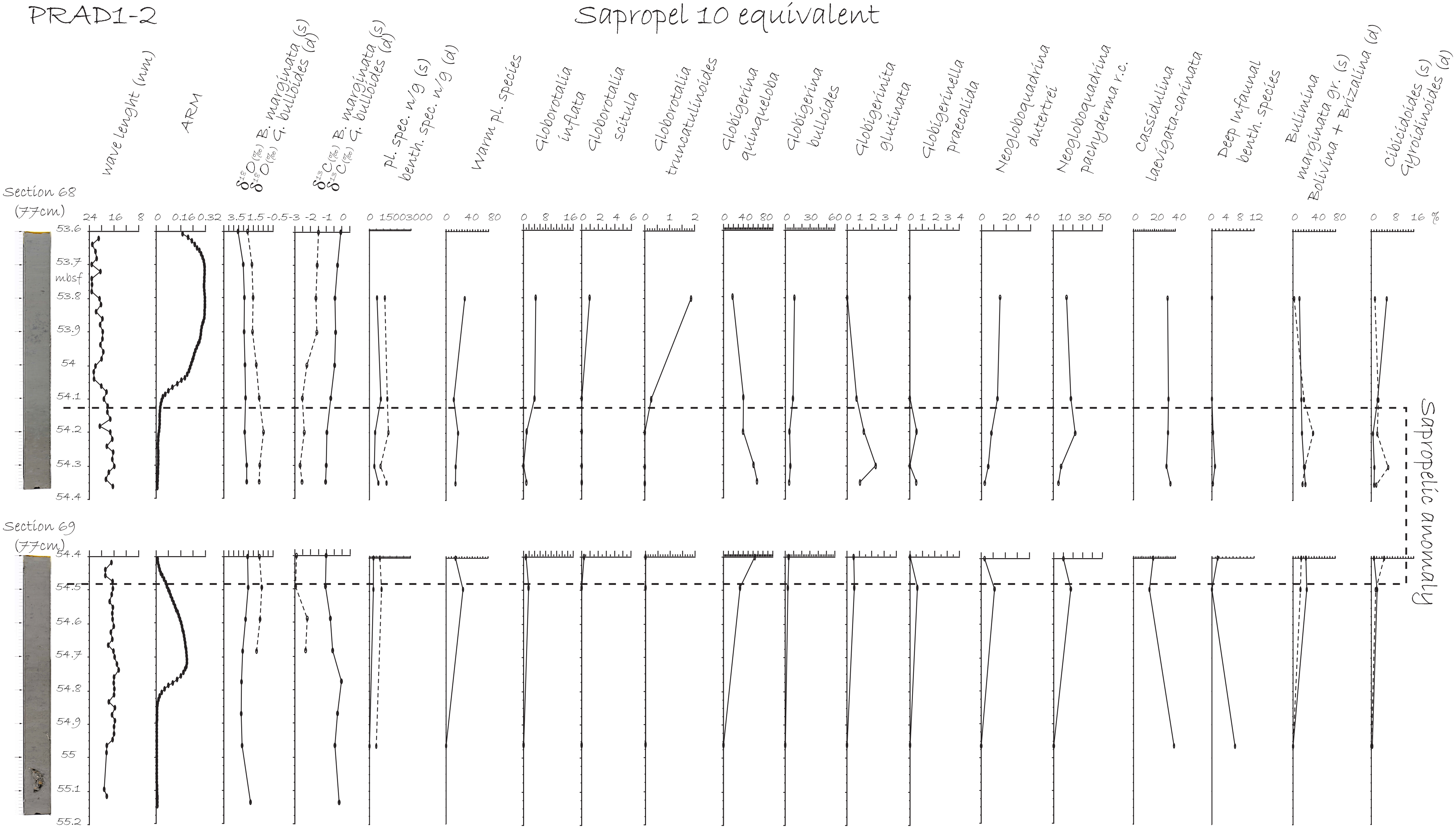

Fig. 3.9. Main results for Se10 (s is for solid line, d for dashed line).

common warm species, and by peaks of *Globigerina quinqueloba*, followed upsection by *Neogloboquadrina pachyderma* r.c., *Neogloboquadrina dutertrei* and *Globigerina bulloides*. Benthic foraminifera are always abundant: *Cassidulina laevigata carinata* is common, intermediate infaunal taxa, as *Bolivina* and *Brizalina* and *Bulimina*., increase Oxic species are scarce. The concentration of benthic specimens is always higher than the planktic one.

3.3 DISCUSSION

This section focuses on the correlation of the sapropelic levels within and beyond the Central Adriatic record, discussing the conditions that lead to the establishment of an individual sapropel in different areas, and then assessing similarities and differences among sapropel equivalents within the PRAD1.2 record.

3.3.1 SAPROPEL CHRONOLOGIC CORRELATIONS THROUGH SPACE

State of the art

Such a methodology has been recently applied, to the study of a possible lateral connection in the Eastern Mediterranean during sapropel 5, by Cane et al. (2002) and Capotondi et al. (2006). These studies adopted the following assumptions, as reported by Cane et al. (2002):

a) to select correlation levels from records of proxies that reflect different environmental processes (planktonic foraminiferal abundance records, and $\delta^{18}O$ and $\delta^{13}C$);

b) to use only unambiguous events as correlation levels (e. g. last or first zero abundance levels);

c) to avoid carefully circular reasoning through assessment of all potential correlations without any a priori assumption of synchroneity;

d) to restrict the application of the correlation framework to a basin of rather limited dimensions.

These assumptions can be strictly followed in the attempt of comparing the S5 event between the Adriatic and the eastern Mediterranean records, in order to test a possible wider-scale synchroneity. In fact Cane et al. (2002) assume that, if all sites show a virtually identical sequence of events, with remarkably similar thickness and spacing, it is not realistic to call on a systematically diachronous relationship between the records, even because this would imply that:

a) proxies reflecting a variety of biological and physic-chemical parameters would all have responded with identical phase shifts, and b) there also were the same phase relationships among surface and subsurface signals, so that the studied proxies could react in the same way in different records.

Cane et al. (2002) defined a series of isotopic and faunistic events occurring inside S5 in four different Eastern Mediterranean records (from the Ionian Basin, from Napoli mud volcano, South of Crete and from Erathosthenes Seamount, in the Levantine Basin), and all recurrent following almost the same succession. Moreover, an order of confidence (either primary or secondary) was assigned to each event. Almost all the primary confidence events occur inside the visible black layer, the base of which seems to correspond to the benthic extinction level in all cases. All the sites taken into exam by Cane et al. (2002) are quite deep, being collected in a range of water depths between 2026 and 2554 m.

Foraminifers' events defined inside S5 by Cane et al. (2002) are reported in Table 3.1.

Table 3.1

Event	Description	Confidence
f1	*G. scitula* faunal last sample before species reappears in detectable quantities	primary
f2	*G. sacculifer* faunal last sample before species reappears in detectable quantities	primary
f3	*O. universa* faunal last sample before species reappears in detectable quantities after short absence	primary
f4	*G. scitula* faunal species no longer present in detectable quantities (zero abundance)	primary
f5	*G. sacculifer* faunal species no longer present in detectable quantities (zero abundance).	primary
f7	*O. universa* faunal species no longer present in detectable quantities after large abundance at sapropel base.	primary
f6	*N. pachyderma* faunal last sample before species reappears in detectable quantities after short absence	primary
f8	*G. inflata* faunal species no longer present in detectable quantities (zero abundance).	primary
f9	pink *G. ruber* faunal last sample before species appears in detectable quantities	primary
f10	*N. pachyderma* faunal prominent peak below sapropel preceding sharp drop in abundance	primary
f11	*N. pachyderma* faunal lowest abundance of species after sapropel formation	secondary
f12	*G. sacculifer* faunal last sample before species reappears in detectable quantities after short dramatic decline	secondary
f13	G. glutinata faunal species no longer present in detectable quantities (zero abundance) within sapropel	secondary
f14	*G. siphonifera* faunal last sample before species appears in detectable quantities.	secondary

The study by Capotondi et al., (2006) was carried out in a transect of seven deep cores (933-3008 m w.d.) from the Ionian to the Levantine Basin. Quantitative analyses of planktic foraminifers' assemblages were conducted both on the 63 μm and on the 150 μm size fractions, in order to state if different mesh sizes could generate differences in the definition of the base and top of each faunistic event. Only the primary confidence events defined by Cane et al. (2002) were taken into account by Capotondi et al. (2006). In order to avoid ambiguities, an exact reference value was attributed, ranging in a percentage interval from 0.5% and 1%, clarifying the "detectable quantities" criterion used by Cane et al. (2002). This study pointed out anomalies for f5, f6 and f7 faunistic events, since their stratigraphic position did not occur always in the same sequence. Moreover, it was possible to constrain the base of the sapropel, expressed as a visible change in colour, between the first local occurrence of *G. ruber* var. *rosea* (f9) and the last local occurrence of *G. inflata* (f8). It must also be noted that, in both the papers, some events did not occur in all the records analysed, but only sometimes.

Application to PRAD1-2 record (Fig. 3.10)

Taking advantage of the continuous and expanded record in PRAD1-2 Se5, the same basic methodology and assumptions have been applied, to test whether the succession of events, recognised in the eastern Mediterranean, can be identified in the Adriatic. This is done not only for stratigraphic purposes, but also to discern different paleoceanographic responses in different locations. The correlation exercise among sapropelic events in different areas was necessarily restricted to the Se5 event, since this is one of the most expanded sapropelic equivalents in PRAD1-2, and because such kind of analysis has never been attempted for other late-Quaternary sapropels. The different nature of the Adriatic basin, shallower and closer to the mainland, necessarily resulted in some dissimilarities, especially concerning the thickness of the visible dark layer, which cannot be taken as a proxy of the effective sapropelic interval, since the oxidative processes, immediately subsequent to the end of the sapropel deposition, could have partially altered the organic matter constituting the dark layer itself. For this reason, the effective extent of Se5 in PRAD1-2 has been defined on the combination of all the other proxies available.

Almost all the faunistic events proposed by Cane et al. (2002) and Capotondi et al., (2006) occur consistently ordered within the PRAD1-2 Se5 anomaly, and are plotted in Fig. 3.10. Moreover, also the secondary confidence events pointed out by Cane et al. (2002) seem to occur in a coherent position. Yet, it must be noted that the benthic foraminifers' extinction match the base of the visible black layer, that is slightly above the sapropelic anomaly. This level seems to be constrained between events f9 and f8, as defined by Capotondi et al. (2006), but the two events are inverted. Nevertheless, it must be said that a) *G. inflata* frequency along Se5 is extremely low and recorded by very few specimens. Although this seems to be sufficient to determine its Last Occurrence, the risk of an uncorrect positioning of the event cannot be completely ruled out; b) *G. ruber pink* distribution for PRAD1-2 is based on semi-quantitative analyses. Based on those statements, events f8 and f9 must be considered with caution. Events f3 and f7 were defined by Cane et al. (2002) as delimiting an interval during which *O. universa* is not visible in detectable quantities, which Capotondi et al. (2006) quantified for their records as lower than 1%. It is possibile to individuate a similar paracme zone in *O. universa* distribution in the Se5 record of PRAD1-2, but the confidence value for the detectable quantities should be extended at least at 1.8%. If such an extension can be accepted, f3 and f7 events would occur in coherent positions. Event f4 seems to occur in an inconsistent (delayed) position in PRAD1-2 with respect to the other eastern Mediterranean records. Finally, it has not been possible to operate correlations between PRAD1-2 and the other eastern Mediterranean isotopic records shown by Cane et al., (2002) and Capotondi et al., (2006), since the analyses were performed on different planktic species (*G. bulloides* in the present study, *G. ruber and N. pachyderma* in the others).

Stratigraphic and paleoenvironmental inferences

Despite the few discrepancies mentioned above, an overall coherency can be pointed out in the correlation between PRAD1-2 record and the Eastern Mediterranean ones. Based on the assumption proposed by Cane et al. (2002), it seems more realistic to infer a syncroneity in the timing of these events: this would consent to widen the validity of this method at a wider scale, involving all the eastern Mediterranean, and granting an oceanographic evolution of Adriatic S5e similar to that of the other deeper eastern Mediterranean records. Anyway, the differences arisen in this event correlation could be generated by the peculiar oceanographic setting of the Adriatic basin. For instance, the position of the level corresponding to the extinction of the benthic fauna, after the beginning of the sapropelic anomaly, could suggest a delay of the most critical sapropelic phase in the Adriatic, where bottom currents, though weakened, managed to ventilate the basin floor, at least for a while.

Also the above discussed reversal of events f8 and f9 in PRAD 1-2 record could find an explanation linked to the minor thickness of the Central Adriatic water column. In fact, whereas in deeper basins *G. ruber* pink and *G. inflata* could live in the same water mass for a while, if this latter species confined itself at deeper water depths, such a life strategy could not occur in such a shallow basin as the Central Adriatic, forcing *G. inflata* to disappear before the freshwater layer definitely set, allowing *G. ruber* pink to live. Another reason for this difference in the event stratigraphy could be associated to the ecological needs of *G. inflata*, strictly depending on the vertical mixing of the water mass (Pujol and Vergnaud-Grazzini, 1995). This would mean that Adriatic deep water production would have likely shut down slightly before than in the other Eastern Mediterranean deep water production sites, like, for instance, the Aegean Sea; *G. inflata*, could therefore have lived just a little longer in the Eastern Mediterranean, and would have been forced to disappear in the Adriatic, as soon as vertical mixing (indicating deep water production) would have been hampered.

Finally, it must be observed that the restrictive application of the stratigraphic method proposed by Cane et al. (2002) by means of sharp Last Occurrence events cannot be strictly followed in all the records, because dissimilar settings and different analytic procedures necessarily oblige to make some minor corrections (for instance as regards the "detectable quantities" concept), in order to see the same succession of events. Such an event stratigraphy technique, applied at a so high degree of detail, must therefore be thought as the individuation of *relative* decreases in the abundance of the major species (instead of Last Occurrence events).

On the other hand, such a problem was already pointed out by Cane et al. (2002), who stated that the synchronism among the events was valid only for small basins. Widening the study area necessarily results in a loss of confidence in assuming the synchronism among different locations. A complete synchronism among the Adriatic and the Ionian-Levantine basins' sapropels, therefore, needs other independent evidences to be surely demonstrated, for instance, by means of the individuation of (macro- and micro-) tephra layers, which have the potential to act as time-lines.

Corselli et al. (2002) identify four planktic foraminifera assemblage zones (PFAZI-PFAZIV) inside Sapropel 5 in the Urania Basin, Eastern Mediterranean. The first and the fourth assemblage zones are defined based on the disappearance and on the re-appearance, respectively, of *G.inflata*. This species is poorly represented, for the reasons explained above, during the deposition of the Central Adriatic Se5, but it is possible to recognise its disappearance at the onset of sapropelic conditions (f8 event described by Cane et al., 2002 and Capotondi et al., 2006). Consequently, a correspondence with PFAZI assemblage zone can be found. *G. inflata*, yet, does not reappear in the Central Adriatic at the very end of Se5, (PFAZIV assemblage zone cannot be recognized in the area), maybe because of different paleoceanografic settings between the two basins. Nonetheless, it is important to observe that the reoccurrence of *G. inflata* at the very end of Sapropel 5 is not a robust biomarker to be taken, since it shows different trends in different areas (Cane et al., 2002;

Capotondi et al., 2006) depending on their paleoceanographic context. PFAZIV assemblage zone, therefore, should likely be restricted to a more local scale. On the other hand, the second and the third assemblage zones, characterised by the common presence of *G. ruber* var. *alba* and *G. scitula* (PFAZII) and of *G. glutinata*, *G. bulloides* and Neogloboquadrinids (PFAZIII), respectively, consistently match the record of borehole PRAD1-2. PFAZII assemblage zone has been interpreted as an interval of significant seasonal contrast and, in particular, the acme of *G. scitula* could correspond to the cold and dry event occurring in the Mid-Eemian (122 kyr) (Maslin et al., 1998; Adams et al., 1999). The common presence of herbivorous taxa during PFAZIII assemblage zone allowed the inference of an increased primary productivity, supported by nutrient-rich cool water and, consequently, causing a shoaling of the thermocline (Corselli et al., 2002).

3.3.2 SAPROPEL COMPARISON THROUGH TIME

As regards the comparison among different sapropelic events in the same location, aims and methodologies necessarily change, since what can be highlighted are similarities and differences in the onset and evolution of the sapropels equivalents. Moreover, planktic and benthic foraminifers' assemblage may change through time, because sapropels did not always occur during the same climate and environmental (and sea level) conditions. Comparisons, therefore, rely on the recognition of event successions, looking at the highest frequencies of the most abundant and characterising species.

The most pronounced PRAD1-2 sapropel equivalents were identified and analysed in detail; based on similar characteristics, two distinct groups were identified, and called respectively "cold sapropels" and "warm sapropels" (Fig. 3.11). This kind of subdivision has already been applied in the literature (see references below).

- The "Cold sapropels" group includes Se4, Se6 and Se8 equivalents. In particular, S6 and S8 were already defined in literature as "glacial sapropels", and are characterised by microfossils and pollen assemblages indicating cold and arid conditions in the Eastern Mediterranean, and globally low sea level (Cita et al., 1977, Vergnaud-Grazzini et al., 1977, Rossignol-Strick, 1983, 1985, Rossignol-Strick et al., 1998, Emeis et al., 2003). These events are characterized by the extreme scarcity or absence of warm planktic species. Planktic assemblage is instead composed by cold water and herbivorous species, such as *G. quinqueloba*, *G. bulloides*, *G. glutinata*, *N. dutertrei* and *N. pachyderma*. Apart from *G. glutinata*, an opportunistic species that never reaches high abundances, and which is more abundant outside the sapropelic intervals, the other species show a

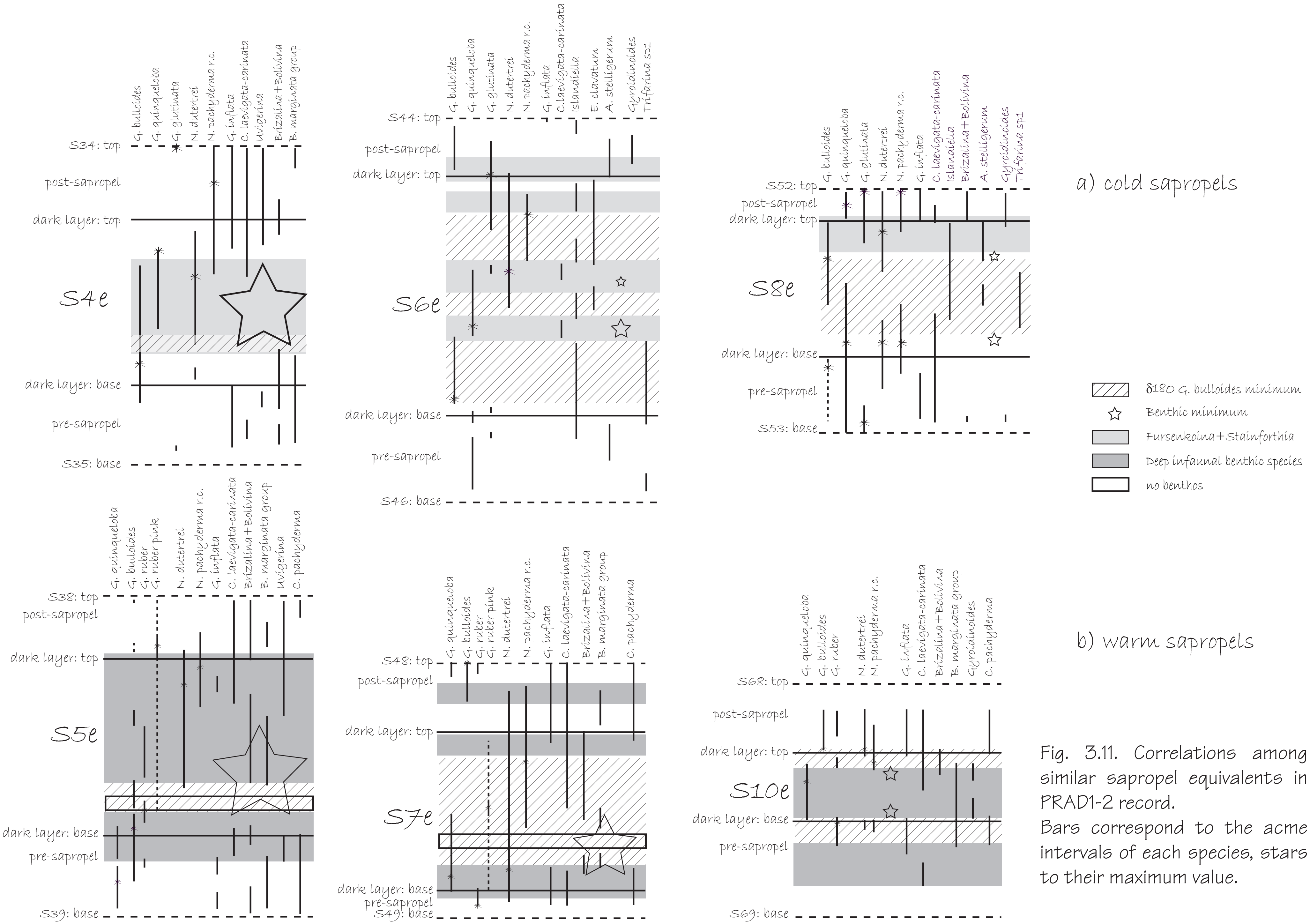

Fig. 3.11. Correlations among similar sapropel equivalents in PRAD1-2 record.
Bars correspond to the acme intervals of each species, stars to their maximum value.

coherent trend inside the "cold sapropels" group: shallower water species *G. quinqueloba* peaks at the base, replaced by intermediate waters species *G. bulloides* and *N. dutertrei*, and finally by slightly deeper *N. pachyderma* at the top. Apart from some exceptions (see in particular the discussion of Se7, below), the same sequence of cold water herbivorous species can be found also in the other PRAD1-2 sapropel equivalents, reflecting a progressive deepening of the chlorophill maximum. As regards the benthic assemblage, the "cold sapropels" group is characterised by the common presence of deep infaunal opportunistic *taxa* such as *Fursenkoina* and *Stainforthia*, which appear to be articulated in multiple events during Se4, Se6 and Se8 show the lightest $\delta^{18}O$ values of the entire isotopic record of PRAD1-2: the absence of warm waters planktic species allows to rule out a possible temperature effect to explain the isotopic record, and to ascribe the isotopic anomaly to salinity oscillations caused by increased freshwater influxes. Anyway, differences among the three cold sapropel equivalents can be found, considering the fact that Se6 occurs within a glacial period, being characterised by higher abundances of cold water species and by cold water shelf benthic dwellers. Moreover, Se4, occurring during a cold climatic oscillation within MIS5, is characterised by peculiar faunistic features, such as the presence of deep water planktic species *G. scitula* and of the oxic benthic *taxon H. balthica*. These species, common during the entire MIS5, including also sapropel equivalents Se3 and Se5, suggest interglacial conditions characterised by a thick water column and by a bottom floor barely but almost constantly ventilated. Finally, Se8 equivalent's planktic assemblage results split in two distinct phases, which occur in correspondence of two minima in the benthic concentration.

- The "Warm sapropels" group includes Se5, Se7 and Se10 (Fig. 3.11). Warm planktic species, though showing a decrease, remain common in all three sapropelic records. The "warm sapropels" group is characterised by a marked minimum in the $\delta^{13}C$, reflecting an increased organic matter concentration in the water column, progressively stocked at the sea floor. Such low $\delta^{13}C$ values are also the consequence of anoxic conditions at the sea floor, hampering benthic microfauna to colonize the sediment during Se5 and Se7. These two sapropel equivalents are also characterised by the presence of warmer, oligotrophic species *G. ruber pink*, which reaches its highest abundances after the most critical sapropelic phase. Sapropel Se7 shows also a different succession in the dominance of herbivorous planktic species: *G. quinqueloba* is in fact rapidly replaced by *N. dutertrei* (*G. bulloides* scarce), probably testifying an abrupt deepening of the chlorophyll maximum. This sapropel equivalent is also characterised by the highest concentration of planktic specimens per gram of the entire PRAD1-2 record, likely a consequence of the large availability of nutrients during that peculiar sapropelic anomaly. Moreover, infaunal species *Bulimina marginata* and *Brizalina* and *Bolivina*, represented by their thinnest tested and widest pored morphotypes, characterise the sapropelic benthic assemblage in both Se5 and Se7. Se10, instead, shows different features in the foraminifers' assemblage, making it more similar to weaker sapropel equivalents, despite from isotopic values.

3.3.3 PALEOCEANOGRAPHIC SETTING DURING THE DEPOSITION OF CENTRAL ADRIATIC SAPROPELIC EQUIVALENTS

All the independent but complementary evidences presented here permit to infer some hints for the depositional model of the main sapropel equivalents in the Central Adriatic (Fig. 3.12):

- Although not discussed in terms of results, it seems important to recall what so far interpreted in the literature in terms of paleoceanographic reconstruction as regards Sapropel 1 deposition. It consists of a double-phased event, interrupted by a break, during which the ventilation of the water mass improved. This feature is well known and visible all over the Eastern Mediterranean record (Mercone et al., 2000, 2001). Yet, this interval shows peculiar characteristics in the Central Adriatic, beside the absence of Neogloboquadrinids, implying that the Deep Chlorophyll Maximum (DCM) did not develope, as already known for the Eastern Mediterranean (Rohling and Gieskes, 1989, Castradori, 1993, Principato et al., 2006). The peculiarity of Se1 is that the water mass was instead inhabited by oligotrophic species, such as those belonging to the *Globigerinoides* group, although *G. ruber*'s pink variety is rare, testifying and steadying a weak freshwater influx in this area. Levantine planktic species *Z. rubescens* is instead common-abundant, and characterizes this interval. Anyhow, the main difference characterising Se1 Central Adriatic equivalent from the S1 record of other Eastern Mediterranean basins results from the oxygenation conditions at the sea floor. Oxic benthic fauna was not rare during the deposition of Se1 equivalent in the Central Adriatic (presence of *H. balthica*), implying that North Adriatic Dense Waters (NAdDW) formed in this period in the Northern Adriatic, and contributed to some degree to the ventilation of this epicontinental shelf. Yet, the 160 m deep Pelagosa sill, separating Central and Southern Adriatic basins, should have represented an impassable barrier for NAdDW, since evidences from Southern Adriatic cores testify a strongly dysoxic environment at the sea floor during S1 event (see Fig. 3.13). Another explanation could be that NAdDW managed to reach

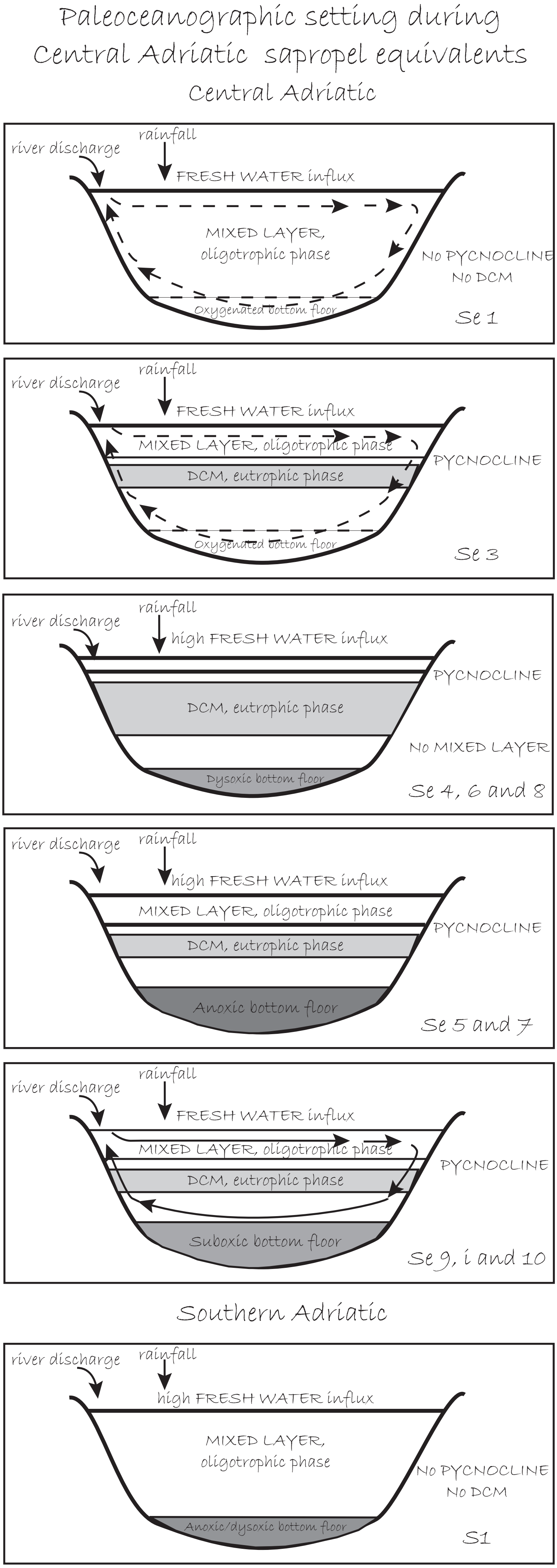

Fig. 3.12. Paleoceanographic models of PRAD1-2 sapropel equivalents and of S1 in Southern Adriatic.

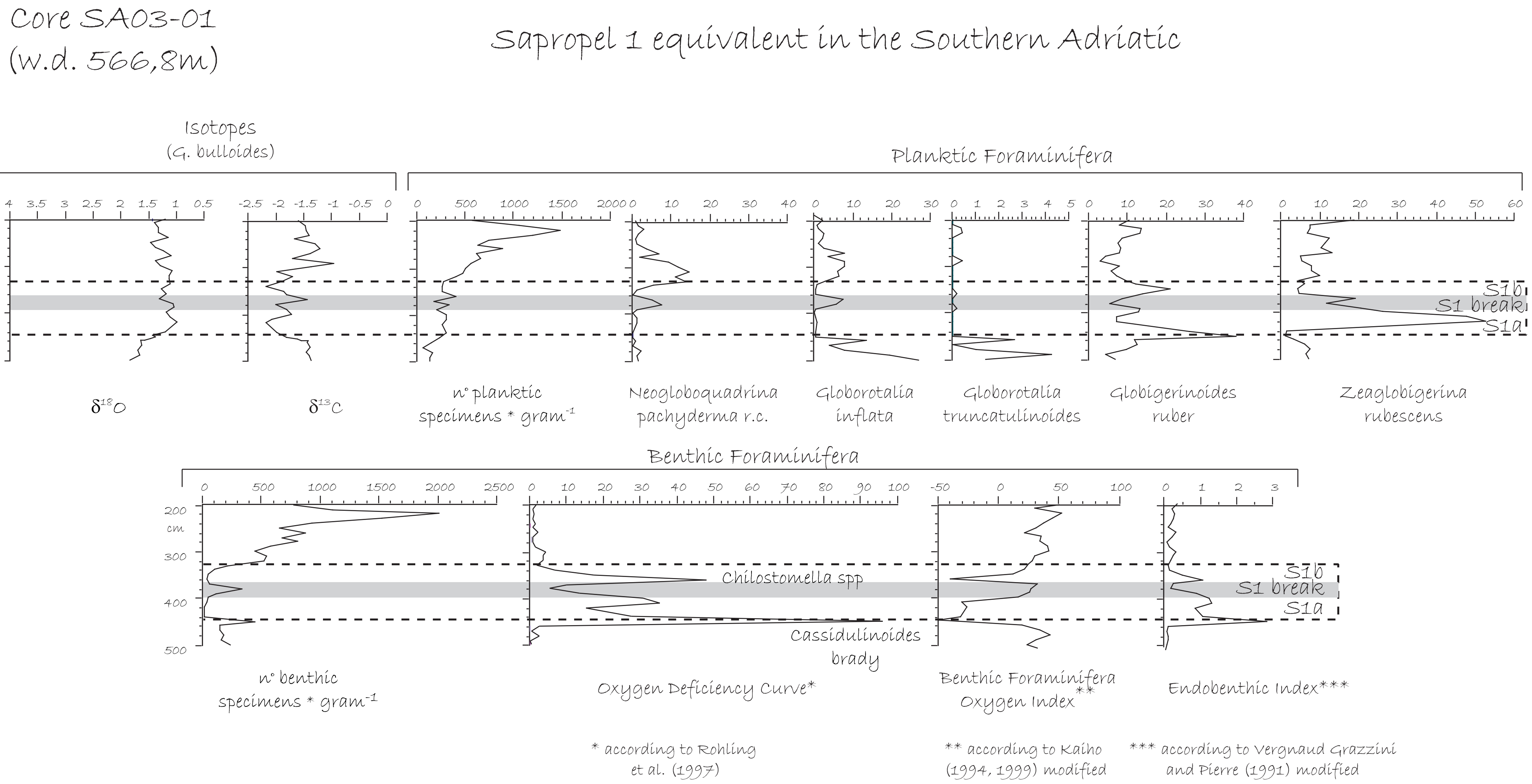

Fig. 3.13. Results for S1 equivalent in a deeper Southern Adriatic core. The light grey stripe corresponds to the S1 interruption.

the Southern Adriatic, but remained confined in shallower water depths. Evidences for that could be found by analysing cores collected in the Southern Adriatic shelf. At the present time, though, such shallow cores are not available in literature. This hypothesis is consistent with *G. ruber* pink being more abundant in the Southern Adriatic basin, witnessing a well formed oligotrophic mixed layer, and therefore a higher freshwater influx in this area.

- Despite the presence of the DCM, pointed out by peaks in Neogloboquadrinids, Se3 Central Adriatic equivalent shows similarities with S1, particularly as regards the oxic conditions of the sea floor. Even though the water mass was somehow more stratified, NAdDW could therefore form as well during Se3 equivalent.

- Sapropel equivalents Se4, Se6 and Se8 all occurred during cold climate conditions, and show common features: firstly, cool waters did not allow warm species from *Globigerinoides* group to establish in the area, and hampered the development of the oligotrophic mixed layer. Secondly, the planktic microfauna is strongly composed by herbivorous species (Neogloboquadrinids and, in shallower layers, *G. bulloides* and *G. quinqueloba*), indicating a well developed eutrophic phase, in correspondence of the DCM. Sapropel equivalents Se6 and Se8 show the lightest values in $\delta^{18}O$ in the region (lighter than 0.5‰ in the planktic record), which evidence a huge freshwater influx, likely reflecting the influence of the Po River, at times when the Po delta was closer to the Central Adriatic. The benthic microfauna was dominated by the dysoxic, eutrophic species *Fursenkoina tenuis* and *Stainforthia complanata*, implying that NAdDW formation was significantly weakened during these events. Finally, Se6 and Se8 equivalents show multiple events also in the Adriatic, consistently with literature (Emeis et al., 1998; Schmiedl et al., 2003; Casford et al., 2003) and implying repeated changes in the structure of the water column.

- Se5 and Se7 equivalents both occurred during temperate to warm climate conditions (Ganssen and Troelstra, 1987; Ten Haven et al., 1987), and share similar characteristics: the water mass was strongly stratified, because of the almost concurrent presence of both an eutrophic phase, evidenced by the development of the DCM, indicated by repeated peaks in the Neogloboquadrinids, and of an oligotrophic one. The mixed layer was in fact dominated by warm water species such as those from the *Globigerinoides* group, and *G. ruber* pink, particularly abundant in some levels. The $\delta^{18}O$ values are light (almost -0.5‰ in the planktic curve), and all these features suggest a strong freshwater influx. During these sapropelic equivalents, the benthic assemblage is very rare and in some cases even absent. Concurrently, $\delta^{13}C$ registers the lowest values (-3.5‰ in the benthic record). These proxies indicate that the NAdDW did not form during these events, and that this stop in the ventilation of the sea floor brought to the formation of reductive conditions, which allowed the organic matter to stock, even generating laminated sediments.

- Se9, Se' (originally identified as *ghost* sapropel by Langereis et al., 1997) and Se10 equivalents show intermediate features compared to the other sapropelic events. The planktic microfauna is characterised by temperate-climate assemblages, with common *Globigerinoides* group but rare *G. ruber* pink, as well as by marked peaks in Neogloboquadrinids. That reflects in a layered structure of the water column, consisting of both an oligotrophic and a eutrophic phase. On the other hand, the benthic assemblage is mainly composed of pre-sapropelic dysoxic species, such as those belonging to the genera *Uvigerina*, *Bolivina* and *Brizalina*. Therefore, though markedly weakened, it seems that dense water production was still active during these sapropelic events.
- Sapropelic-like conditions seem to occur in a peculiar level, inside MIS9.1, between Se' and Se10 equivalents. Evidences for that are given by many proxies (see Fig. 3.14), ranging from low values of ARM rock-magnetic parameter, to minima in O and C stable isotopic composition, to sharp peaks of Neogloboquadrinids and of dysoxic benthic microfauna (i.e. *Brizalina*). Similar features consistently occur in Se9, Se' and Se10 sapropel equivalents. Anyhow, up to now, such an event has never been either identified or described in literature.

3.4 CONCLUDING REMARKS

The Central Adriatic depositional and paleoceanographic history provides a continuous record of sapropel-equivalent deposits back to the base of MIS9 (sapropel Se10). Sapropel-equivalent layers in the Adriatic can be clustered in three distinct groups, each characterized by peculiar features (resumed in fig. 3.15). During the time corresponding to the deposition of Se10, Se' and Se9 equivalents (Fig. 3.15d), all independent proxies suggest climate conditions not so extreme to hamper life of the benthic microfauna. On the contrary, Se8, Se7, Se6, Se5 and Se4 (Figg. 3.15b-c) show a more severe paleoceanographic context with exceptionally rainy conditions, that is possibly the consequence of a northward shift of the African monsoon, resulting in a dysoxic to anoxic sea floor environment. Finally, deposition during recent Se3 and Se1 events (Fig. 3.15a) reflects a markedly different paleoceanographic setting in the Central Adriatic, compared to the other

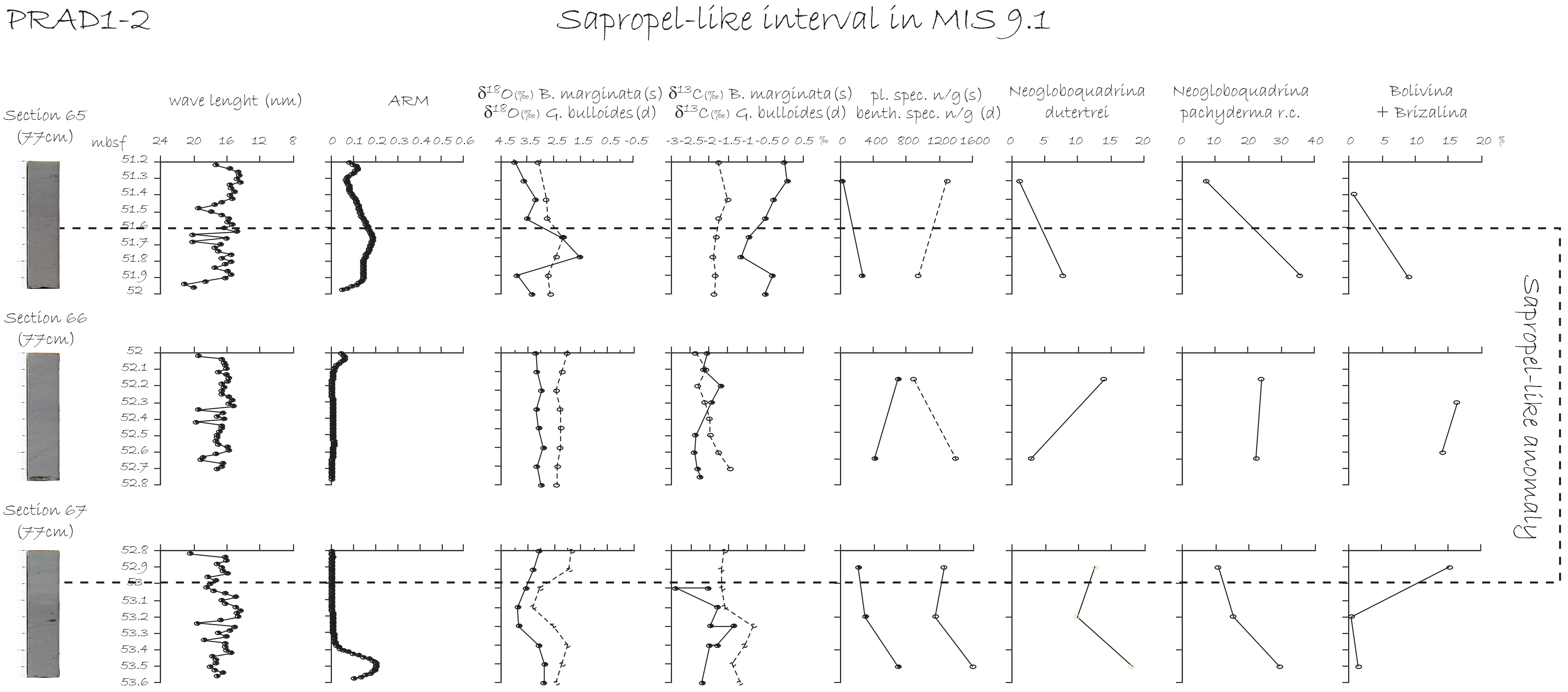

Fig. 3.14. Main results for the sapropel-like unterval during MIS9.1.

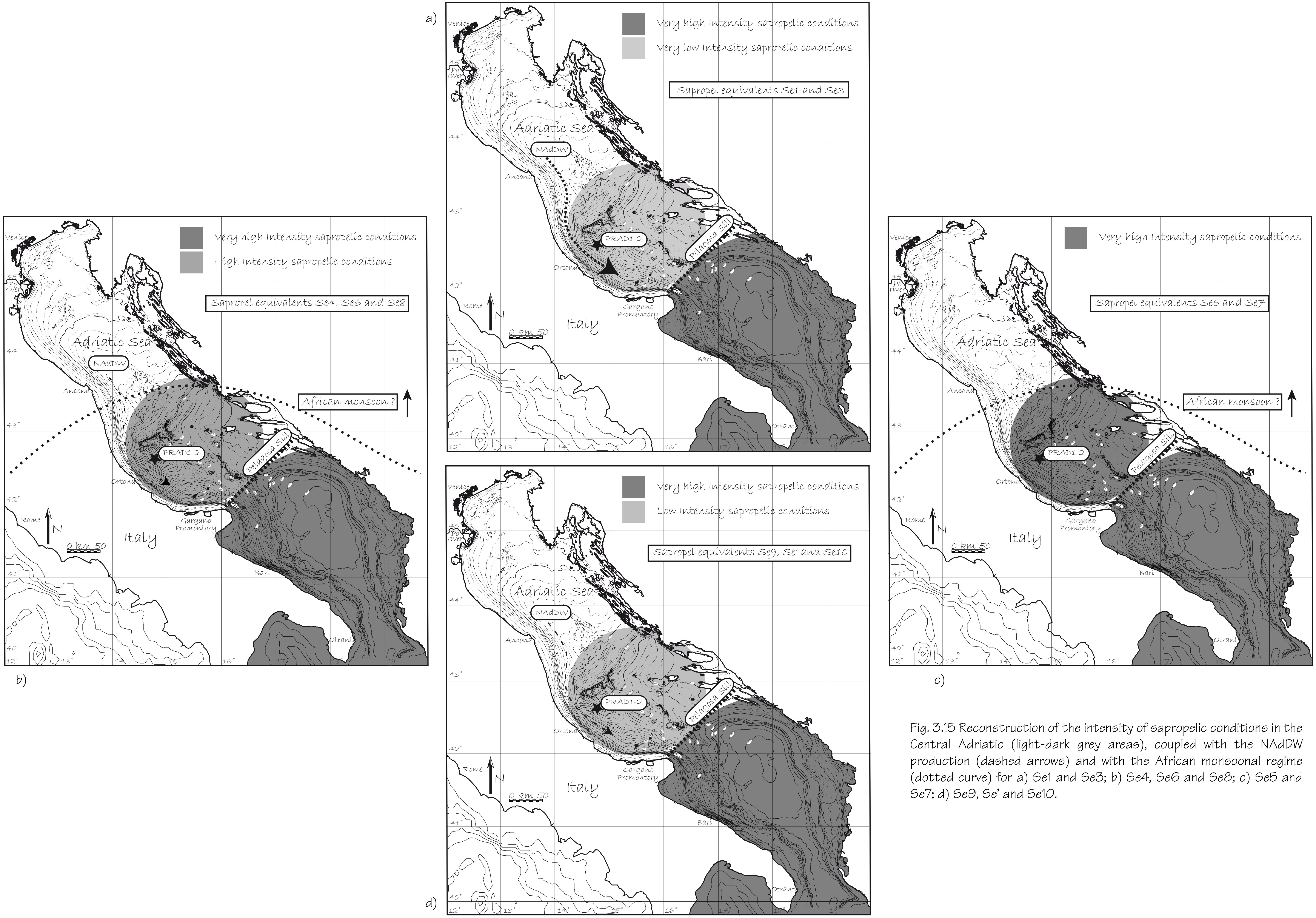

Fig. 3.15 Reconstruction of the intensity of sapropelic conditions in the Central Adriatic (light-dark grey areas), coupled with the NAdDW production (dashed arrows) and with the African monsoonal regime (dotted curve) for a) Se1 and Se3; b) Se4, Se6 and Se8; c) Se5 and Se7; d) Se9, Se' and Se10.

Eastern Mediterranean sites. These latest Central Adriatic sapropels depict the scenario of a more isolated basin, weakly linked to the rest of the Eastern Mediterranean, allowing benthic life even when conditions became critical in the adjacent deeper water basins. Two possible non-mutually-exclusive explanations can be suggested to explain this evidence: 1) since the time of S3 formation the North Adriatic was already filled to define a shallow shelf where deep waters were able to form through winter cooling and densification; in this case, some degree of bottom oxygenation was granted by the passage of these dense bottom-hugging currents. 2) The progressive infill of the Mid Adriatic Deep from the Po low stand delta resulted both in a shallowing of the site where PRAD1.2 is located and in the increased shedding of sediment-laden currents disturbing the sapropel formation.

References

Abbott, P. M. (2005). Towards a tephrochronology for a Southern Adriatic deep marine sequence. *Masters Thesis of Science Degree in Quaternary Science,Royal Holloway,* University of London.107 pp.

Adams, J., M. Maslin, and E. Thomas (1999). Sudden climate transitions during the Quaternary, *Progr. Phys. Geogr.*, 23, 1-36.

Alve, E. (1995). Benthic foraminiferal responses to estuarine pollution: a review. *Journal of Foraminiferal Research*, 25 (3), 190-203.

Amorosi, A., M. L. Colalongo, F. Fusco, G. Pasini, and F. Fiorini (1999). Glacio-eustatic Control of Continental–Shallow Marine Cyclicity from Late Quaternary Deposits of the Southeastern Po Plain, Northern Italy. *Quaternary Research*, 52, 1-13.

Amorosi, A., M. L. Colalongo, F. Fiorini, F. Fusco, G. Pasini, S. C. Vaiani, G. Sarti (2004). Palaeogeographic and palaeoclimatic evolution of the Po Plain from 150-ky core records. *Global and Planetry Change*, 40, 55-78.

Ariztegui, D., A. Asioli, J. J. Lowe, F. Trincardi, L. Vigliotti, F. Tamburini, C. A. Accorsi, M. Bandini Mazzanti, A. M. Mercuri, S. Van Der Kaars, C. Chondrogianni, J. A. Mckenzie, F. Oldfield (2000). Palaeoclimatic reconstructions and formation of sapropel S1: inferences from Late Quaternary lacustrine and marine sequences in the Central Mediterranean region. *Palaeoclimatology. Paleoecology, Paleogeography*, 158 (3/4), 215-240.

Asioli, A. (1996) High resolution foraminifera biostratigraphy in the Central Adriatic basin during the last deglaciation: a contribution to the PALICLAS Project, in *Palaeoenvironmental Analysis of Italian Crater Lake and Adriatic Sediments*, edited by F. Oldfield and P. Guilizzoni*, Memorie dell'Istituto Italiano di Idrobiologia*, 55, 197 – 218.

Asioli, A., F. Trincardi, J. J. Lowe and F. Oldfield (1999). Rapid Communication Short-term climate changes during the Last Glacial–Holocene transition: comparison between Mediterranean records and the GRIP event stratigraphy. *Journal of Quaternary Science* 14, 373-381.

Asioli, A., F. Trincardi, J. J. Lowe, D. Ariztegui, L. Langone, and F. Oldfield (2001). Sub-millennial scale climatic oscillations in the central Adriatic during the Lateglacial: palaeoceanographic implications. *Quaternary Science Reviews* 20, 1201-1221.

Barmawidjaja, D. M., F. J. Jorissen, S. Puskaric, and G. J. Van der Zwaan (1992). Microhabitats selection by benthic foraminifera in the northern Adriatic Sea. *Journal of Foraminiferal Research*, 22,(4), 297-317.

Bassinot, F. C., L. D. Labeyrie, E. Vincent, X. Quidelleur, N. J. Shackleton, and Y. Lancelot (1994). The astronomical theory of climate and the age of the Brunhes Matuyama magnetic reversal. *Earth Planet. Sci. Lett.*, 126, 91–108.

Baumfalk, Y. A., S. R. Troelstra, G. Ganssen, M. Van Zanen (1987). Phenotypic variation of *Globorotalia scitula* (foraminiferida) as a response to Pleistocene climatic fluctuation. *Marine Geology* 75, 231–240.

Basharin, G. P. (1959). On a statistical estimate for the entropy of a sequence of independent random variables, p. 333-336. In: N. Artin (Ed.), *Theory of probability and its applications*. Vol. IV. Translation of Teoriya Veroyatnostei i ee Primeneniya). Society for Industrial and Applied Mathematics, Philadelphia.

Bé, A. W. H., D. S. Tolderlund (1971). Distribution and ecology of living planktonic Foraminifera in surface waters of the Atlantic and Indian Oceans. In: Funnell, B.M., Riedel, W.R. (Eds.), *The Micropaleontology of the Oceans*. pp. 105–149.

Bè, A. W. H. (1977). An ecological, zoogeographic and taxonomic review of recent planktonic foraminifera. In: Ramsay, A.T.S. (ed.), *Oceanic Micropaleontology*, 1, chap. 1, London, 1-100.

Bè, A. W. H., and W. H. Hutson (1977). Ecology of planktonic foraminifera and biogeographic patterns of life and fossil assemblages in the Indian Ocean. *Micropaleontology*, 23, 369-414.

Béthoux, J. –P. (1993). Mediterranean sapropel formation, dynamic and climatic viewpoints. *Oceanological Acta* 16 (2), 127-133.

Béthoux, J. –P., and C. Pierre (1999). Mediterranean functioning and sapropel formation : respective influences of climate and hydrological changes in the Atlantic and the Mediterranean. *Marine Geology* 153, 29-39.

Borsetti, A. M., L. Capotondi, F. Cati, A. Negri, C. Vergnaud-Grazzini, C. Alberini, P. Colantoni, and P. V. Curzi (1995). Biostratigraphic events and late Quaternari tectonics in the Dosso Gallignani (central-southern Adriatic Sea). *Giornale di Geologia*, ser. 3, 57 (1-2), 41-58.

Böttcher, M. E., J. Rinna, B. Warning, R. Wehausen, M. W. Howell, B. Schnetger, R. Stein, H. –J. Brumsack, J. Rullkötter (2003). Geochemistry of sediments from the connection between the western and the eastern Mediterranean Sea (Strait of Sicily, ODP Site 963). *Palaeoclimatology. Paleoecology, Paleogeography*, 190, 165-194.

Bourne, A.J. (2006). An initial tephrochronology for the Adriatic core Prad 1-2 for 40ka BP. Masters of Science Degree in Quaternary Science, Royal Holloway, University of London, 172 pp.

Boyle, E .A., D. W. Lea (1989). Cd and Ba in planktonic foraminifera from the Eastern Mediterranean: evidence for river outflow and enriched nutrients during sapropel production.*Trans. Am. Geophys. Union* 70, 101-134.

Buckley, H. A., and L. R. Johnson (1988). Late Pleistocene to Recent sediment deposition in the central and western Mediterranean. *Deep Sea Research*, 35, 749-766.

Butzin, M., M. Prange and G. Lohmann (2005). Radiocarbon simulations for the glacial ocean: the effects of wind stress, Southern Ocean sea ice and Heinrich events. *Earth & Planetary Science Letters*, 235, 45-61.

Calvert, S. E. (1983). Geochemistry of Pleistocene sapropels and associated sediments from the eastern *Mediterraneanean Oceanological Acta* 6, 255-267.

Calvert, S. E., B. Nielsen, B., M. R. Fontugne (1992). Evidence from nitrogen isotope ratios for enhanced productivity during formation of eastern Mediterranean sapropels. *Nature* 359, 223– 225.

Cane, T., E. J. Rohling, A. E. S. Kemp, S. Cooke, R. B. Pearce (2002). High-resolution stratigraphic framework for Mediterranean sapropel S5: defining temporal relationships between records of Eemian climate variability. *Palaeoclimatology. Paleoecology, Paleogeography*, 183, 87-101.

Cao, L., R.G. Fairbanks, M. Butzin and N. Naik (2007). The marine radiocarbon reservoir age. *Radiocarbon*, in prep.

Capotondi, L., A. M. Borsetti, and C. Morigi (1999). Foraminiferal ecozones, a high resolution proxy for the late Quaternary biochronology in the central Mediterranean Sea. *Marine Geology,* 153, 253–274.

Capotondi, L., M. S. Principato, C. Morigi, F. Sangiorgi, P. Maffioli, S. Giunta, A. Negri, C. Corselli (2006). Foraminiferal variations and stratigraphic implications to the deposition of sapropel S5 in the eastern Mediterranean. *Palaeoclimatology. Paleoecology, Paleogeography*, 235, 48-65.

Caralp, M. H. (1988). Late Glacial to Recent deep-sea benthic foraminifera from the northeastern Atlantic(Cadiz Gulf) and Western Mediterranean (Alboran Sea); Paleoceanografy results. *Marine Micropaleontology*, 13, p. 255-267.

Casford, J. S. L., E. J. Rohling, R. H. Abu-Zied, C. F. Fontanier, J. Jorissen, M. J. Leng, G. Schmiedl, J. Thomson (2003). A dynamic concept for eastern Mediterranean circulation and oxygenation during sapropel formation. *Palaeogeography, Palaeoclimatology, Palaeoecology* 2962, 1-17.

Castradori, D. (1993), Calcareous nannofossil biostratigraphy and biochronology in eastern Mediterranean deep-sea cores, *Rivista It. Paleontol. Stratigr.,* 99(1), 107– 126.

Cattaneo, A., and F. Trincardi (1999). The late-Quaternary transgressive record in the Adriatic epicontinental sea: basin widening and facies partitioning. In: Bergman, K.M., Snedden, J.W. (Eds.), *Isolated Shallow Marine Sand Bodies: Sequence Stratigraphic Analysis and Sedimentological Interpretation*. SEPM Special Publication, 64, 127–146.

Cheddadi, R., M. Rossignol-Strick (1995). Improved preservation of organic-matter and pollen in eastern Mediterranean sapropels. *Paleoceanography* 10, 301-309.

Chierici, M. A., M. T. Busi, and M. B. Cita (1962). Contribution a une étude ecologique des foramifères dans la Mer Adriatique. *Revue de Micropaleontologie*, 5, (2), 123-142.

Cita, M. B., M. A. Chierici, G. Ciampo, M. Moncharmont Zei, S. D'Onofrio, W. B. F. Ryan, R. Scaziello (1973). The Quaternary record in the Tyrrhenian and Ionian basins of the Mediterranean Sea. *Initial Reports DSDP* 13, 1263–1298.

Cita, M. B., C. Vergnaud Grazzini, C. Robert, H. Chamley, N. Ciaranfi, S. D'Onofrio (1977). Paleoclimatic record of a long deep sea core from the eastern Mediterranean. *Quaternary Research* 8, 205–235.

Cita, M. B., and D. Grignani (1982). Nature and origin of late Neogene Mediterranean sapropels. In: *Nature and Origin of Createaceous Carbon-Rich Facies*, edited by S. O. Schlanger and M. B. Cita, Academic, San Diego, California, pp. 165-196.

Cita, M. B., E. Erba, R. Lucchi, M. Pott, R. Van der Meer, L. Nieto (1996). Stratigraphy and sedimentation in the Mediterranean Ridge diapiric belt. *Marine Geology* 132, 131–150.

Colmenero-Hidalgo, E., J., A. Flores and F. J. Sierro (2002). Biometry of *Emiliania huxleyi* and its biostratigraphic significance in the eastern north Atlantic Ocean and Western Mediterranean Sea in the last 20,000 years. *Marine Micropaleontology*, 46, 247– 263.

Colmenero-Hidalgo, E., J. and A. Flores (2005). Coccolithophores and calcareous nannofossils abundance in Hole PRAD1-2 from PROMESS1 cruise. In: Bernè, S., Shipboard Scientific Party (2004): PROMESS1 Summary cruise Report: past global changes investigated by drilling Mediterranean continental margins, *Unpublished Cruise report, Research Institute for Exploitation of the Sea (IFREMER), Brest, France.*

Combourieu Nebut, N., J. L. Turon, R. Zahn, L. Capotondi, L. Londeix, and K. Pahnke (2002). Enhanced aridity and atmospheric high-pressure stability over the western Mediterranean during the North Atlantic cold events of the past 50 k.y.. *Geology*, 30 (10), 863-866.

Corselli, C., M. S. Principato, P. Maffioli, D. Crudeli (2002). Changes in planktonic assemblage during sapropel S5 deposition: Evidence from Urania Basin area, eastern Mediterranean. *Paloceanography*, 17 (3), 10.1029/2000PA000536.

Cramp, A., G. O' Sullivan (1999). Neogene sapropels in the Mediterranean: a review. *Marine Geology*, 153, 11-28.

De Lange, G. J., H. L. Ten Haven (1983). Recent sapropel formation in the eastern Mediterranean. *Nature* 305, 797–798.

Emeis, K.C., Shipboard Scientific Party of Leg 160 (1996). Paleoceanography and sapropel introduction. *Proc. ODP Init. Rep.* 160, 21–27.

Emeis, K. –C., H. M. Schulz, U. Struck, T. Sakamoto, H. Doose, H. Erlenkeuser, M. Howell, D. Kroon and M. Paterne (1998). Stable isotope and alkenone temperature records of sapropels from sites 964 and 967: constraining the physical environment of sapropel formation in the eastern Mediterranean Sea. Robertson, A.H.F., Emeis, K.-C., Richter, C., and Camerlenghi, A. (Eds.) *Proceedings of the Ocean Drilling Program, Scientific Results,* 160, 309-331.

Emeis, K. –C., H. Schulz, U. Struck, M. Rossignol-Strick, H. Erlenkeuser, M. W. Howell, D. Kroon, A. Mackensen, S. Ishizuka, T. Oba, T. Sakamoto, and I. Koizumi (2003). Eastern Mediterranean surface water temperatures and $\delta^{18}O$ composition during deposition of sapropels in the late Quaternary. *Paleoceanography*, 18, 1, 5, 1-18.

Fairbanks, R. G., P. H. Wiebe (1980). Foraminifera and chlorophyll maximum: vertical distribution, seasonal succession, and paleoceanographic significance. *Science* 209, 1524–1526.

Fairbanks, R. G., P. H. Wiebe, and A. W. H. Bè (1980). Vertical Distribution and Isotopic composition of Living Planktonic Foraminifera in the Western North Atlantic. *Science*, 207, 61-63.

Fairbanks, R. G., M. Sverdlove, R. Free, P. H. Wiebe, A. W. H. Bé (1982). Vertical distribution of living planktonic foraminifera from the Panama Basin. *Nature* 298, 841–844.

Fairbanks, R. G., R. A. Mortlock, Tzu-Chien Chiu, L. Cao, A. Kaplan, T. P. Guilderson, T. W. Fairbanks and A.L. Bloom, (2005). Marine Radiocarbon Calibration Curve Spanning 0 to 50,000 Years B.P. Based on Paired $^{230}Th/^{234}U/^{238}U$ and ^{14}C Dates on Pristine Corals. *Quaternary Science Reviews*, 24, 1781-1796.

Flores, J.-A., R. Gersonde and F. J. Sierro (1999). Pleistocene fluctuations in the Agulhas current retroflections based on the calcareous plankton record. *Marine Micropaleontology*, 37, 1 – 22.

Focault, A., and D. A. Stanley (1989). Late Quaternary paleoclimatic oscillations in East Africa recorded by heavy minerals in the Nile delta. *Nature* 339, 44-46.

Fontugne, M. R., M. Paterne, S. E. Calvert, A. Murat, F. Guichard, and M., Arnold (1989). Adriatic deep water formation during the Holocene : implication for the reoxygenation of the deep eastern Mediterranean Sea. *Paleoceanography* 4 (2), 199-206.

Fontugne, M., and S. E. Calvert (1992). Late Pleistocene variability of the carbon isotopic composition of organic matter in the eastern Mediterranean Sea: monitor of changes in carbon sources and atmospheric CO_2 concentrations, *Paleoceanography*, 7, 1-20.

Ganssen, G. M. and S. R. Troelstra (1987). Paleoenvironmental change from stable isotopes in planktonic foraminifera from eastern Mediterranean sapropels. *Marine Geology* 75, 210-218.

Guilizzoni, P. and F. Oldfield (Guest Editors) (1996). Palaeoenvironmental Analysis of Italian Crater Lake and Adriatic Sediments. *Mem. Ist. ital. Idrobiol.*, 55.

Hageman, J. (1979). Benthic foraminiferal assemblage from Plio-Pleistocene open bay to lagoonal sediments of the Western Peloponnesus (Greece). *Utrecht Micropaleontology Bullettin*, 20, 171 pp.

Hasegawa, J., R. Sprovieri, and A. Poluzzi (1990). Quantitative analysis of benthic foraminiferal assemblage from Plio-Pleistocene sequences in the Tyrrhenian Sea, ODP Leg 107. *Proceedings ODP, Scientific Results*, 107, p. 461-478.

Hemleben, C., M. Spindler and O. R. Anderson (Eds.), (1989) *Modern planktic foraminifera*, Springer-Verlag, New York.

Herman, Y. (1981). Paleoclimatic and paleohydrologic record of Mediterranean deep-sea cores based on Pteropods, Planktonic and Benthonic Foraminifera. *Revista Española de Micropaleontologia*, 13, (2), 171-200.

Hilgen, F. J. (1991). Astronomical calibration of Gauss to Matuyama sapropels in the Mediterranean and implication for the geomagnetic polarity time scale, *Earth Planet. Sci. Lett.*, 104, 226– 244.

Hine, N. and Weaver, P.P.E. (1998). Quaternary. In: *Calcareous Nannofossil Biostratigraphy* (P.R. Bown, ed.), *Chapman & Hall*, London, 266-283.

Howell, M. W., R. C. Thunell, E. Di Stefano, R. Sprovieri, E. J. Tappa, and T. Sakamoto (1998). Stable isotope chronology and paleoceanographic history of Sites 963 and 964, eastern Mediterranean Sea. *Proceedings of the Ocean Drilling Program, Scientific Results,* Robertson, A.H.F., Emeis, K.-C., Richter, C., and Camerlenghi, A. (Eds.), 160, 167-180.

Hughen, K. A., M. G. L. Baillie, E. Bard, J. W. Beck, C. J. H. Bertrand, P. G. Blackwell, C. E. Buck, G. S. Burr, K. B. Cutler, P. E. Damon, R. L. Edwards, R. G. Fairbanks, M. Friedrich, T. P. Guilderson, B. Kromer, G. McCormac, S. Manning, C. B. Ramsey, P. J. Reimer, R. W. Reimer, S. Remmele, J. R. Southon, M. Stuiver, S. Talamo, F. W. Taylor, J. van der Plicht, C. E. Weyhenmeyer (2004). Marine04 Marine Radiocarbon Age Calibration, 0–26 Cal kyr BP. *Radiocarbon*, 46, 3, 1059-1086.

Hutson, W. H. (1977). Transfer functions under no-analog condition: experiment with Indian Ocean planktonic Foraminifera. *Quaternary Research* , 8, 355-67.

Imbrie, J., J. D. Hays, D. G. Martinson, A. McIntyre, A. C. Mix, J. J. Morley, N. G. Pisias, W. L. Prell, and N. J. Shackleton (1984). The orbital theory of Pleistocene climate: support from a revised chronology of the marine δ^{18}Orecord. In: *Milankovitch and Climate* (edited by A. Berger, J. Imbrie, J. Hays, G. Kukla & B. Saltzman), Reidel, Dordrecht, 269-306.

Jenkins, J. A., D. F. Williams, (1983/84). Nile water as a cause of eastern Mediterranean sapropel formation: evidence for and against. *Marine Micropaleontology* 9, 521– 534.

Jennings, A. E., N. J. Weiner, G. Helgadottir, and J. T. Andrews (2004). Modern foraminiferal faunas of the Southwestern to Northern Iceland shelf: oceanographic and environmental controls. *Journal of Foraminiferal Research*, 34 (3), 180-207.

Jorissen, F. J. (1988). Benthic foraminifera from the Adriatic Sea; principles of phenotypic variation. *Utrecht Micropaleontological Bullettins*, 37, 174 pp.

Jorissen, F. J., D. M. Barmawidjaja, S. Puskaric, G. J. Van der Zwaan (1992). Vertical distribution of benthic foraminifera in the northern Adriatic Sea: the relation with the organic flux. *Marine Micropaleontology*, 19, 131-146.

Jorissen, F. J., A. Asioli, A. M. Borsetti, L. Capotondi, J. P. De Visser, F. J. Hilgen, E. J. Rohling, K. Van Der Borg, C. Vergnaud-Grazzini and W. J. Zachariasse (1993). Late Quaternary central Mediterranean biochronology. *Marine Micropaleontology,* 21, 169–189.

Jorissen, F.J. (1999). Benthic foraminiferal successions across Late Quaternary Mediterraenan sapropels. *Marine Geology* 153, 91-101.

Kallel, N., M. Paterne, L. Labeyrie, J. –C. Duplessy, M. Arnold (1997). Temperature and salinity records of the Tyrrhenian Sea during the last 18,000 years. *Palaeoclimatology. Paleoecology, Paleogeography*, 135, 97-108.

Kallel, N., J. –C. Duplessy, L. Labeyrie, M. Fontugne, M. Paterne, M. Montacer (2000). Mediterranean pluvial periods and sapropel formation over the last 200000 years. *Palaeoclimatology. Paleoecology, Paleogeography*, 157, 45-58.

Kidd, R. B., M. B. Cita, W. B. F. Ryan (1978). Stratigraphy of eastern Mediterranean sapropel sequences recovered during Leg 42A and their paleoenvironmental significance. *Initial Report DSDP* 42A, 421–443.

Krom, M., A. Michard, R. A. Cliff, and K. Strohle (1999). Sources of sediment to the Ionian Sea and western Levantine basin of the Eastern Mediterranean during S-1 sapropel times. *Marine Geology* 160, 45-61.

Kroon, D., I. Alexander, M. Little, L. J. Lourens, A. Matthewson, A. H. F. Robertson and T. Sakamoto (1998). Oxygen isotope and sapropel stratigraphy in the eastern Mediterranean during the last 3.2 Million years. *Proceedings of the Ocean Drilling Program, Scientific Results,* Robertson, A.H.F., Emeis, K.-C., Richter, C., and Camerlenghi, A. (Eds.), 160, 181-189.

Kullenberg, B. (1952). On the salinity of the water contained in marine sediments. *Medd. Oceanogr. Inst. Göteborg* 21, 1-38.

Lambeck, K., Y. Yokoyama, T. Purcell (2002). Into and out of the Last Glacial Maximum: sea-level change during Oxygen Isotope Stages 3 and 2. *Quaternary Science Reviews*, 21, 343-360.

Langereis, C. G., M. J. Dekkers, G. J. De Lange, M. Paterne, and P. J. M. Van Santvoort (1997). Magnetostratigraphy and astronomical calibration of the last 1.1 Myr from an eastern Mediterranean piston core and dating of short events in the Brunhes, *Geophys. J. Intern.*, 129, 75– 94.

Larrasoaña, J. C., A. P. Roberts, J. S. Stoner, C. Richter, R. Wehausen (2003). A new proxy for bottom-water ventilation in the eastern Mediterranean based on diagenetically controlled magnetic properties of sapropel-bearing sediments. *Palaeoclimatology. Paleoecology, Paleogeography*, 190, 221-242.

Lebreiro, S. M., J. C. Moreno, I. N. McCave, P. P. E. Weaver (1996). Evidence for Heinrich layers off Portugal (Tore Seamount: 39°N, 12°W). *Marine Geology*, 131, 47-56.

Linke, P., and G. F. Lutze (1993). Microhabitat preferences of benthic foraminifera-a static concept or a dynamic adaptation to optimize food acquisition? *Marine Micropaleontology*, 20, 215-234.

Lisiecki, L. E. and M. E. Raymo (2005). A Pliocene-Pleistocene stack of 57 globally distributed d180 records. *Paleoceanography*, 20, PA1003.

Lourens, L. J., A. Antonarakou, F. J. Hilgen, A. A. M. Van Hoof, C. Vergnaud-Grazzini, and W. J. Zachariasse (1996). Evaluation of the Plio-Pleistocene astronomical timescale. *Paleoceanography,* 11, 391-413.

Lourens, L. J. (2004). Revised tuning of Ocean Drilling Program Site 964 and KC01B (Mediterranean) and implications for the D180, tephra, calcareous nannofossil, and geomagnetic reversal chronologies of the past 1.1 Myr. *Paleoceanography*, 19, PA3010.

Löwemark, L., Y. Lin, H. –F. Chen, T. –N. Yang, C. Beier, F. Werner, C. –Y. Lee, S. –R. Song, S. –J. Kao (2006). Sapropel burn-down and ichnological response to Late Quaternary sapropel formation in two -400ky records from the Eastern Mediterranean Sea. *Palaeoclimatology. Paleoecology, Paleogeography*, 239, 406-425.

Martini, E. (1971). Standard Tertiary and Quaternary calcareous nannoplankton zonation. *In* Farinacci, A. (Ed.), *Proc. 2nd Int. Conf. Planktonic Microfossils Roma:* Rome (Ed. Tecnosci.), 2, 739–785.

Maslin, M. A., M. Sarnthein, J. J. Knaack, P. Grootes, and C. Tzedakis (1998). Intra-interglacial cold event: An Eemian-Holocene comparison, in *Geological Evolution of the Ocean Basin: Results From the Ocean Drilling Program*, edited by A. Cramp et al., Geol. Soc. Spec. Publ., 131, 91– 99.

Massari, F., D. Rio, R. Serandrei Barbero, A. Asioli, L. Capraro, E. Fornaciari, P. P. Vergerio (2004). The environment of Venice area in the past two million years. *Palaeoclimatology. Paleoecology, Paleogeography*, 202, 273-308.

Mercone, D., J. Thomson, I. W. Croudace, G. Siani, M. Paterne, S. Troelstra (2000). Duration of S1, the most recent sapropel in the eastern Mediterranean Sea, as indicated by accelerator mass spectrometry radiocarbon and geochemical evidence. *Paleoceanography*, 15, 336-347.

Mercone, D., J. Thomson, R. H. Abu-Zied, I. W. Croudace, E. J. Rohling (2001). High-resolution geochemical and micropalaeontological profling of the most recent eastern Mediterranean sapropel. *Marine Geology* 177, 25-44.

Miao, Q., and R. C. Thunell (1993). Recent deep sea benthic foraminiferal distribution in the South China and Sulu Seas. *Marine Micropaleontogy*, 22, 1-32.

Miller, A. A. L., D. B. Scott, and F. S. Medioli (1982). *Elphidium excavatum* (Terquem): ecophenotypic versus subspecific variation. *Journal of Foraminiferal Research*, 12 (2), 116-144.

Morigi, C., F. J. Jorissen, S. Fraticelli, B. J. Horton, M. Principi, A.Sabbatini, L. Capotondi, P. V. Curzi, A. Negri (2005). Benthic foraminiferal evidence for the formation of the Holocene mud-belt and bathymetrical evolution in the central Adriatic Sea. *Marine Micropaleontology*, 57, 25-49.

Muerdter, D.R., and J. Kennett, 1983-84. Late Quaternary planktonic foraminiferal biostratigraphy, Strait of Sicily, Mediterranean Sea. *Marine Micropaleontology* 8, 339–359.

Muerdter, D. R., J. Kennett, R. C. Thunell (1984). Late Quaternary sapropel sediments in the Eastern Mediterranean Sea: faunal variations and chronology. *Quaternay Research* 21, 385–403.

Murray, J. W. (1991). Ecology and paleoecology of benthic foraminifera. Longman Scientific e Technical Ed.

Negri , A., L. Capotondi and J. Keller (1999). Calcareous nannofossils, planktonic foraminifera and oxygen isotopes in the late Quaternary sapropels of the Ionian Sea, Mar. Geol., 157, 89– 103.

Olausson, E. (1961). Studies of deep-sea cores: *Reports of the Swedish Deep-Sea Expedition, 1947–1948*, 8, 323–438.

Oldfield, F., A. Asioli, C. A. Accorsi, A. M. Mercuri, S. Juggins, L. Langone, T. Rolph, F. Trincardi, G. Wolff, Z. Gibbs, L. Vigliotti, M. Frignani, K. van der Post, N. Branch (2003). A high resolution late Holocene palaeo environmental record from the central Adriatic Sea. *Quaternary Science Reviews* 22, 319–342.

Parisi, E., M. B. Cita (1982). Late Quaternary paleoceanographic changes recorded by deep-sea benthos in the western Mediterranean rigde. *Geogr. Fis. Diatom. Quat.* 5, 102-114.

Parisi, E. (1987). Carbon and oxygen isotope composition of *Globigerinoides ruber* in two deep sea cores from the Levantine Basin (Eastern Mediterranean). *Marine Geology* 75, 201–219.

Pedersen, T. F., S. E. Calvert (1990). Anoxia vs. productivity: what controls the formation of organic-carbon rich sediments and sedimentary rocks? *AAPG Bulletin* 74 (4), 454– 466.

Pérez-Folgado, M., F. J. Sierro, J. A. Flores, I. Cacho, J. O. Grimalt, R. Zahn, N. Shackleton (2003). Western Mediterranean planktonic foraminifera events and millennial climatic variability during the last 70 kyr. *Marine Micropaleontology*, 48, 49-70.

Phleger, F. B., and A. Soutar (1973). Production of benthic foraminifera in three east Pacific oxygen minima. *Micropaleontology*, 19, 1, p. 110-115.

Pielou, E. C. (1966). The measurement of diversity in different types of biological collections. *Journal of Theoretical Biology*, 13, 131-144.

Pierre, C., P. Belanger, J. F. Saliege, M. J. Urrutiaguer and A. Murat (1999). Paleoceanography of the western Mediterranean during the Pleistocene: Oxygen and Carbon isotope records at Site 975. *Proceedings of the Ocean Drilling Program, Scientific Results,* Zahn, R., Comas, M.C., and Klaus, A. (Eds.), 161, 481-488.

Principato, M. S., D. Crudeli, P. Ziveri, C. P. Slomp, C. Corselli, E. Erba, G. J. de Lange (2006). Phyto- and zooplankton paleofluxes during the deposition of sapropel S1 (eastern Mediterranean): Biogenic carbonate preservation and paleoecological implications. *Palaeogeography, Palaeoclimatology, Palaeoecology* 235, 8 –27.

Pujol, C. and C. Vergnaud Grazzini (1995). Distribution patterns of live planktic foraminifera as related to regional hydrography and productive systems of the Mediterranean sea. *Marine Micropaleontology,* 25, 187–217.

Rathburn, A. E., and B. H. Corliss (1994). The ecology of living (stained) deep-sea benthic foraminifera from the Sulu Sea. *Paleoceanography*, 9, (1), 87-150.

Reichart, G. J., and H. Brinkhuis (2003). Late Quaternary *Protoperidinium* cysts as indicators of paleoproductivity in the northern Arabian Sea. *Marine Micropaleontolo*gy 49, 303–315.

Reynolds, L. A., and R. C. Thunell (1986). Seasonal production and morphologic variation of *Neogloboquadrina pachyderma* (Ehrenberg) in the Northeast Pacific. *Micropaleontology*, 32, 1-18.

Ridente, D. and F. Trincardi (2002). Eustatic and tectonic control on deposition and lateral variability of Quaternary regressive sequences in the Adriatic basin (Italy). *Marine Geology* 184 (2002) 273-293

Ridente, D. and F. Trincardi (2006). Active foreland deformation evidenced by shallow folds and faults affecting late Quaternary shelf–slope deposits (Adriatic Sea, Italy). *Basin Research*, 8, 2, 171-188,

Rio, D., I. Raffi and G. Villa (1990). Pliocene-Pleistocene calcareous nannofossil distribution patterns in the Western Mediterranean. *In* Kastens, K.A., Mascle, J., et al., *Proc. ODP, Sci. Results,* 107, College Station, TX (Ocean Drilling Program), 513–533.

Rodrigues, C. G., and K. Hopper (1982). The ecological significance of *Elphidium clavatum* in the Gulf of St. Lawrence, Canada. *Journal of Paleontology*, 56 (2), 410-422.

Rohling, E. J. and W. W. C. Gieskes (1989). Late Quaternary changes in Mediterranean intermediate water density and formation rate. P*aleoceanography* 4, 531-545.

Rohling, E. J. H. C. De Stigter, C. Vergnaud Grazzini, and R. Zaalberg (1993). Temporary repopulation by low-oxygen tolerant benthic foraminifera within an Upper Pliocene sapropel: Evidence for the role of oxygen depletion in the formation of sapropel. *Marine Micropaleontogy*, 22, 207-219.

Rohling, E. J., F. J. Jorissen, H. C. de Stigter (1997). 200 year interruption of Holocene sapropel formation in the Adriatic Sea. *Journal of Micropaleontology* 16, 97-108.

Rohling, E. J., and G. R. Bigg (1998). Paleosalinity and δ^{18}O: a critical assessment. *Journal of Geophysical Research* 103, 1307-1318.

Rohling, E. J., M. Fenton, F. J. Jorissen, P. Bertand, G. Ganssen, and J. P. Caulet (1998). Magnitudes of sea-level lowstands of the past 500,000 years. *Nature*, 394, 162-165.

Rohling, E. J., A. Hayes, S. De Rijk, D. Kroon, W. J. Zachariasse, and D. Eisma (1998). Abrupt cold spells in the northwestern Mediterranean. *Paleoceanography*, 13 (4), 316-322.

Rohling, E. J. (1999). Environmental controls on salinity and δ^{18}O in the Mediterranean. *Paleoceanography*, 14, 706-715.

Rohling, E. J., S. De Rijk (1999). Holocene climate optimum and last glacial maximum in the Mediterranean: the marine oxygen isotope record. *Marine Geology* 153, 57-75.

Rohling, E. J., P. A. Mayewski, R. H., Abu-Zied, J. S. L., Casford, A. Hayes (2002). Holocene atmosphere-ocean interactions: records from Greenland and The Aegean Sea. *Climate Dynamics* 18, 587-593.

Ross, C. R., and J. P. Kennett (1984). Late Quaternary paleoceanography as recorded by benthonic foraminifera in Strait of Sicily sediment sequencies. *Marine Micropaleontology*, 8, 315-337.

Rossignol-Strick, M., W. Nesteroff, P. Olive, C. Vergnaud-Grazzini (1982). After the deluge: Mediterranean stagnation and sapropel formation. *Nature* 364, 319– 321.

Rossignol-Strick, M. (1983). African monsoons, an immediate climate response to orbital insolation. *Nature* 304, 46–49.

Rossignol-Strick, M. (1985). Mediterranean Quaternary sapropels, an immediate response of the African monsoon to variations of insolation. *Palaeogeography, Palaeoclimatology, Palaeoecology* 49, 237–263.

Rossignol-Strick, M., M. Paterne, F. C. Bassinot, K. -C. Emeis, and G. J. De Lange (1988). An unusual mid-Pleistocene monsoon period over Africa and Asia. *Nature*, 392, 269-272.

Rossignol-Strick M., N. Planchais, M. Paterne, D. Duzert (1992). Vegetation dynamics and climate during the last deglaciation in the South Adriatic basin from a marine record. *Quaternary Science Reviews* 11: 415–423.

Rossignol-Strick M. (1995). Sea-land correlation of pollen records in the Eastern Mediterranean for the Glacial-Interglacial transition: biostratigraphy versus radiometric time-scale. *Quaternary Science Review* 14, 893-915.

Rossignol-Strick M. (1999). The Holocene climatic optimum and pollen records of sapropel 1 in the eastern Mediterranean, 9000–6000 BP. *Quaternary Science Reviews* 18: 515–530.

Rossignol-Strick M., and M. Paterne (1999). A synthetic pollen record of eastern Mediterranean sapropels of the last 1 Ma: implications for the time-scale and formation of sapropels. *Marine Geology* 153, 221-238.

Ruddiman, W. F. (1971). Pleistocene sedimentation in the equatorial Atlantic: stratigraphy and climatology. *Geol. Soc. Am. Bull.*, 82, 283-302.

Ryan, W. B. F. (1972). Stratigraphy of Late Quaternary sediments in the Eastern Mediterranean. In: *Stanley, D.J. (Ed.), The Mediterranean Sea. Dowden, Hutchinson and Ross, Stroudsburg, PA*, pp. 149–169.

Sancetta, C. (1994). Mediterranean sapropels: seasonal stratification yields high production and carbon flux. *Paleoceanography* 9, 195–196.

Sànchez Goñi, M. F., I. Cacho, J.-L. Turon, J. Guiot, F. Sierro, J.-P. Peypouquet, J. O. Grimalt, N. J. Shackleton (2002). Synchroneity between marine and terrestrial responses to millennial scale climate variability during the last glacial period in the Mediterranean region. *Climate Dynamics*, 19, 95-105.

Sangiorgi F., L. Capotondi, N. Combourieu Nebout, L. Vigliotti, H. Brinkhuis, S. Giunta, A. F. Lotter, C. Morigi, A. Negri, and G. –J. Reichart (2003). Holocene seasonal sea-surface temperature variations in the southern Adriatic Sea inferred from a multiproxy approach. *Journal of Quaternary Science* 18 (8), 723-732.

Sanvoisin, R. , S. D'Onofrio, R. Lucchi, D. Violanti and D. Castradori (1993), 1 Ma paleoclimatic record from the eastern Mediterranean- Marflux project: First results of a micropaleontological and sedimentological investigation of a long piston core from the Calabrian Ridge, Il Quat., 6(2), 169– 188.

Sbaffi, L., C. W. Forese, N. Kallel, M. Paterne, I. Cacho, P. Ziveri, N. J. Shackleton (2001). Response of the pelagic environment to paleoclimatic changes in the central Mediterranean Sea during the Late Quaternary. *Marine Geology* 178, 39-62.

Schilman, B. A. Almogi-Labin, M. Bar-Matthews, L. Labeyrie, M. Paterne, B. Luz (2001). Long- and short-term carbon fluctuations in the eastern Mediterranean during the Holocene. *Geology* 29, 1099-1102.

Schmiedl, G., C. Hemleben, J. Keller, M. Segl (1998). Impact of climatic changes on the benthic foraminiferal fauna in the Ionian Sea during the last 330,000 years. *Paleoceanography* 13, 5, 447-458.

Schmiedl, G., A. Mitschele, S. Beck, K. –C. Emeis, C. Hemleben, H., Schulz, M., Sperling, S., Weldeab (2003). Benthic foraminiferal record of ecosystem variability in the eastern Mediterranean Sea during times of sapropel S5 and S6 deposition. *Palaeogeography, Palaeoclimatology, Palaeoecology* 190, 139–164.

Sen Gupta, B. K., and M. L. Machain-Castillo (1993). Benthic foraminifera in oxygen-poor habitats. *Marine Micropaleontology*, 20, 183-204.

Sgarrella, F., and M. Moncharmont Zei (1993). Benthic Foraminifera of the Gulf of Naples (Italy): systematics and autoecology. *Bollettino della Società Paleontologica Italiana*, 32, (2), 145-264.

Shannon, C. E., and W. Weaver (1949). The Mathematical Theory of Communication. *Urbana, University of Illinois Press*, 117 pp.

Siani, G., M. Paterne, M. Arnold, E. Bard, B. Mètivier, N. Tisnerat, F. Bassinot (2000). Radiocarbon reservoir ages in the Mediterranean Sea and Black Sea. *Radiocarbon*, 42, 2, 271-280.

Siddal, M., E. J. Rohling, A. Almogi-Labin, C. Hemleben, D. Meischner, I. Schmelzer, and D. A. Smeed (2003). Sea-level fluctuations during the last glacial cycle. *Nature*, 423, 853-858.

Sprovieri, R., E. Di Stefano, A. Incarbona, M. E. Gargano (2003). A high-resolution record of the last deglaciation in the Sicily Channel based on foraminifera and calcareous nannofossil quantitative distribution. *Palaeogeography, Palaeoclimatology, Palaeoecology* 202, 119-142.

Stanley, D. J., A. Maldonado, and R. Stuckenrath (1975). Strait of Sicily depositional rates and patterns, a possible reversal of currents in the late Quaternary. *Palaeogeography, Palaeoclimatology, Palaeoecology* 18, 279-291.

Strohle K., and M. D. Krom (1997). Evidence for the evolution of an oxygen minimum layer at the beginning of S-1 sapropel deposition in the eastern Mediterranean. *Marine Geology*, 140, 231-236.

Stuiver, M. and P. J. Reimer (1993). Extended ^{14}C data base and revised CALIB 3.0 ^{14}C age calibration program. *Radiocarbon* 35, 215-230.

Tang, C. M., L. S. Stott (1993). Seasonal salinity changes during mediterranean sapropel deposition 9000 years B.P.: evidence from isotopic analyses of individual planktonic foraminifera. *Paleoceanography* 8, 473–493

Ten Haven, H. L., M. Baas, M. Kroot, J. W. De Leeuw, P. A. Schenck and J. Ebbing (1986). Late Quaternary Medirreanean sapropels. III: Assessment of source of input and paleotemperature as derived from biological markers. *Geochimica et Cosmochimica Acta*, 51, 803-810.

Thierstein, H.R., K. Geitzenauer, B. Molfino and N. J. Shackleton (1977). Global synchroneity of late Quaternary coccolith datum levels: validation by oxygen isotopes. *Geology*, 5, 400–404.

Thunell, R. C., D. F. Williams, J. P., Kennett (1977). Late Quaternary paleoclimatology, stratigraphy, and sapropel history in eastern Mediterranean deep-sea sediments. *Marine Micropaleontology*, 2, 371-388.

Thunell, R. C. (1978). Distribution of recent planktonic foraminifera in surface sediments of the Mediterranean Sea. *Marine Micropaleontology* 3, 147–173.

Thunell, R. C. (1979). Pliocene–Pleistocene paleotemperature and paleosalinity history of the Mediterranean Sea: results from DSDP Sites 125 and 132. *Marine Micropaleontology* 4, 173–187.

Thunell, R. C., D. F. Williams, and M. B. Cita (1983). Glacial anoxia in the eastern Mediterranean. *Journal of Foraminiferal Research*, 13, 283-290.

Thunell, R. C., D. F. Williams, and P. R. Belyea (1984). Anoxic events in the Mediterranean Sea in relation to the evolution of late Neogene climates. *Marine Geology*, 59, 105-134.

Thunell, R. C., D. F. Williams (1989). Glacial–Holocene salinity changes in the Mediterranean Sea: hydrographic and depositional effects. *Nature*, 338 493-496.

Thunell, R. C., L. R. Sautter (1992). Planktonic foraminiferal faunal and stable isotopic indices of upwelling: a sediment trap study in the San Pedro Basin, Southern California Bight. In: Summerhayes, C.P., Prell, W.L., Emeis, K.C. (Eds.), Upwelling Systems: Evolution since the Early Miocene. *Geological Society Special Publication* 64, 77–91

Trincardi F., A. Cattaneo, A. Asioli, A. Correggiari and L. Langone (1996) Stratigraphy of the late-Quaternary deposits in the central Adriatic basin and the record of short-term climatic events, in *Palaeoenvironmental Analysis of Italian Crater Lake and Adriatic Sediments*, edited by F. Oldfield and P. Guilizzoni, Memorie dell'Istituto Italiano di Idrobiologia, 55, 39-70.

Vaiani, S. C., and P. Venezia (1999). La sezione pleistocenica del Lamone (Appennino Romagnolo): associazioni a foraminiferi ed evoluzione paleoambientale. *Bollettino della Società Paleontologica Italiana* 38 (1), 39-57.

Van der Zwaan, G. J., F. J. Jorissen, and H. C. de Stigter (1990). The depth dependency of planktonic/benthic foraminiferal ratio: Constraints and applications. *Marine Geology*, 95, 1-16.

Van der Zwaan, and G. J., F. J. Jorissen (1991). Biofacial patterns in river –induced anoxia. In: *R. Tyson and Th. Pearson Eds.), Modern and ancient continental shelf anoxia. Geological Society of London Special Publication*, 58, 65-82.

Van der Zwaan, G. J., I. A. P. Duijnstee, M. den Dulk, S. R. Ernst, N. T. Jannink, T. J. Kouwenhoven (1999). Benthic foraminifers: proxies or problems? A review of paleoecological concepts. *Earth-Science Reviews*, 46, 213-236.

Van Leeuwen, R. J. W. (1989). Sea-floor distribution and Late Quaternary faunal patterns of planktonic and benthic foraminifers in the Angola Basin. *Utrecht Micropaleontology Bullettin*, 38, 287 pp.

Van Os, B. J. H., L. J. Lourens, F. J. Hilgen, G. J. Delange, L. Beaufort(1994). The formation of Pliocene sapropels and carbonate cycles in the Mediterranean - diagenesis, dilution, and productivity. *Paleoceanography* 9, 601-617.

Van Santvoort, P. J. M., G. J. De Lange, C. G., Langereis, M. J., Dekkers, M. Paterne (1997). Geochemical and paleomagnetic evidence for the occurrence of “missing” sapropels in eastern Mediterranean sediments. *Paleoceanography* 12, 773– 786.

Van Weering, T. C. E., and G. Qvale (1983). Recent sediments and foraminiferal distribution in the Skagerrack, Northeastern North Sea. *Marine Geology*, 52, 75-99.

Vergnaud-Grazzini, C., W. B. F. Ryan, M. B. Cita (1977). Stable isotope fractionation, climate change and episodic stagnation in the Eastern Mediterranean during the Late Quaternary. *Mar. Micropaleontol.* 2, 353-370.

Vergnaud-Grazzini, C. (1985). Mediterranean late Cenozoic stable isotope record: stratigraphic and paleoclimatic implications. In: *Geological Evolution of the Mediterranean Basin*, edited by D. J. Stanley and F. C. Wezel, Springer-Verlag, New York,pp.413-451.

Vergnaud-Grazzini, C. and C. Pierre, (1992) Fresh water discharge in the Adriatic Sea since 17000 years: influence on organic carbon recycling and deep water ventilation rates. *Rapports Commission Internationale pour l'Exploration Scientifique de la Mer Mediterranee*, 33, 327.

Vigliotti, L., L. Capotondi, and M. Torii (1999). Magnetic properties of sediments deposited in suboxic–anoxic environments: relationships with biological and geochemical proxies. In: *Tarling, D.H., Turner, P.(Eds.), Palaeomagnetism and Diagenesis in Sediments, Vol.151. Geological Society of London Special Publication*, pp.71–83.

Villanueva, J., Flores, J.-A. and Grimalt, J.O. (2002). A detailed comparison of the Uk'$_{37}$ and coccolith records over the past 290 kyears: implications to the alkenone paleotemperature method. *Organic Geochemistry*, 33, 897-905.

Violanti, D., G. Grecchi, D. Castratori (1991). Paleoenvironmental interpretation of core Ban 88-11 GC (Eastern Mediterranean, (Pleistocene–Holocene) on the grounds of Foraminifera, Thecosomata and calcareous nannofossils. *Quaternario* 4, 13–39.

Vismara Schilling, A., W. T. Coulbourn (1991). Benthic foraminiferal thanatofacies associated with late Pleistocene to Holocene anoxic events in the eastern Mediterranean Sea. *Journal of Foraminiferal Research* 21 (2), 103– 125.

Voelker, A. H. L., workshop participants (2002). Global distribution of centennial-scale records for Marine Isotope Stage (MIS) 3: a database. *Quaternary Science Reviews* 21, 1185-1212.

Von Grafenstein, R., R. Zahn, R. Tiedemann and A. Murat (1999). Planktonic $\delta^{18}O$ records at Sites 976 and 977, Alboran Sea: stratigraphy, forcing, and paleoceanographic implications. *Proceedings of the Ocean Drilling Program, Scientific Results,* Zahn, R., Comas, M.C., and Klaus, A. (Eds.), 161, 469-479.

Waelbroeck, C. L. Labeyrie, E. Michel, J. C. Duplessy, J. F. McManus, K. Lambeck, E. Balbon, M. Labracherie (2002). Sea-level and deep water temperature changes derived from benthic foraminifera isotopic records. *Quaternary Science Reviews*, 21, 295-305.

Walton, W. R., and B. J. Sloan (1990).The genus *Ammonia* BRUNNICH, 1772: its geographic distribution and morphology variability. *Journal of Foraminiferal Research*, 20, (2), 128-156.

Williamson, M. A., C. E. Keen, and P. J. Mudie (1984). Foraminiferal distribution on the continental margin off Nova Scotia. *Marine Micropaleontology*, 9, 219-239.

Wilkinson, I. P. (1979). The taxonomy, morphology and distribution of the Quaternary and recent foraminifer *Elphidium clavatum* Cushman. *Journal of Paleontology,* 53 (3), 628-641.

Zahn, R., and M. Sarnthein (1987). Benthic isotope evidence for changes of the Mediterranean outflow during the late Quaternary. *Paleoceanography*, 2 (6), 543-559.

PART II

The last 6000 years in the Adriatic

1. INTRODUCTION

The purpose of this part is to evaluate the Adriatic expression of the short-term climatic oscillations, registered for the last 6000 years, and to determine whether and to what extent anthropogenic factors could have influenced them.

Another aim is to significantly improve the resolution of the ecobiostratigraphy for this time interval, which encompasses the deposition of the late Holocene HST in the Adriatic (Cattaneo et al., 2003; 2004), having the chance to study extremely expanded cores where the paleoceanographic impact of short-term climatic events can be resolved at century to decadal scales.

In particular, the correlation between the cores analysed aims at: 1) defining a regional scale connection of events within comparable depositional environments (characterised by the same facies associations and similar water depth), 2) finding the impact of the same environmental signals within shallow and deeper-water settings, and 3) checking whether the observed events have a regional extent, involving other basins beyond the Adriatic.

The cores analysed here were collected within EC-EURODELTA and EC-EUROSTRATAFORM (the reader is referred to the preface for a more detailed presentation of these projects) and are compared to the results of PALICLAS.

Setting and description of the cores

The cores selected for this study come from complementary depositional settings (from shallow shelf to open slope), span almost three degrees in Latitude, and parallel the pathway of the NAdDW, flowing from the North Adriatic shallow shelf to the Southern Adriatic Basin. This paper builds on previous results from core RF93-30, collected in 77 m water depth on the western flank of the Central Adriatic (Lat. 42° 03' 95"N; Long. 15° 40' 00"E). The core is on the seaward pinch-out of the 35-m-thick Late Holocene mud wedge and, analysed following a multi-proxy approach (Oldfield et al., 2003), revealed century to millennial-scale environmental changes over the last 6000 years. These results are reconsidered in this paper, and extended both latitudinally, within the same depositional environment, and into deeper-water settings, to ascertain whether a super-regional extent can be proved. In particular, core AN97-15 (Lat. 43° 45' 21"N; Long. 13° 38' 46"E) was raised in 55.1 m water depth, from the Late Holocene muddy prodelta, 300 km north of core

RF93-30. Both the shallow-water cores come from a mud belt environment, where sediment is typically delivered through hypopycnal floods and storm-related re-suspension. Consequently, the core is uniformly muddy and structure-less (Correggiari et al., 2001).

The study was extended to slope settings where sediment accumulation rates are high and the planktic record fully accounts for paleoceanographic changes. Core AMC99-1 was collected in the Mid-Adriatic Deep (Lat. 42° 51' 80"N; Long. 14° 45' 67"E) at 260 m water depth and spans about the last 14000 years, although the discussion is here restricted to the last 6000 years. Core SA03-09 was collected in the Southern Adriatic basin (Lat. 41° 21' 70"N; Long. 17° 19' 02"E), in 712 m water depth, in a slope environment impacted by off-shelf cascading cold waters (Trincardi et al., 2007 in press; Turchetto et al., 2007 in press). Consequently, this latter core presents a variable component of material from shallower environments, but this feature does not alter the relevance of all the paleoenvironmental results. The studied cores, therefore, come from sites that are complementary from a geographic and bathymetric point of view. The core location is reported in Fig. 1.

2. MATERIALS AND METHODS

The four cores have been analysed in detail for biostratigraphic and chronologic purposes.

Reference core RF93-30, has already been studied by Oldfield et al. (2003): the reader is referred to the materials and methods paragraph in that paper.

Cores AN97-15 and SA03-09 were sampled every 10 cm, whereas core AMC99-1 was processed with a sampling interval of 3 cm (yet, foraminifers' assemblages were analysed every 6 cm). Each sample consisted of a 1 cm-thick mud slice, on average, corresponding to a volume of about 30 cc. Samples were processed and analytically counted according to the same method described in Part I, chapter 1 (for PRAD1-2 borehole). The taxa are quantified as percentages of the total number of planktic and benthic foraminifera, while the concentration is reported as number of specimens per gram.

Oxygen and carbon stable isotope analyses were conducted on the $CaCO_3$ of the shells of selected monospecific specimens of foraminifers, in cores SA03-09 and AMC99-1. In particular, twenty specimens (on average) of planktic species *Globigerina bulloides* and *Globigerinoides sacculifer* (only in the case of core AMC99-1) were picked from the size fraction >180μm. The

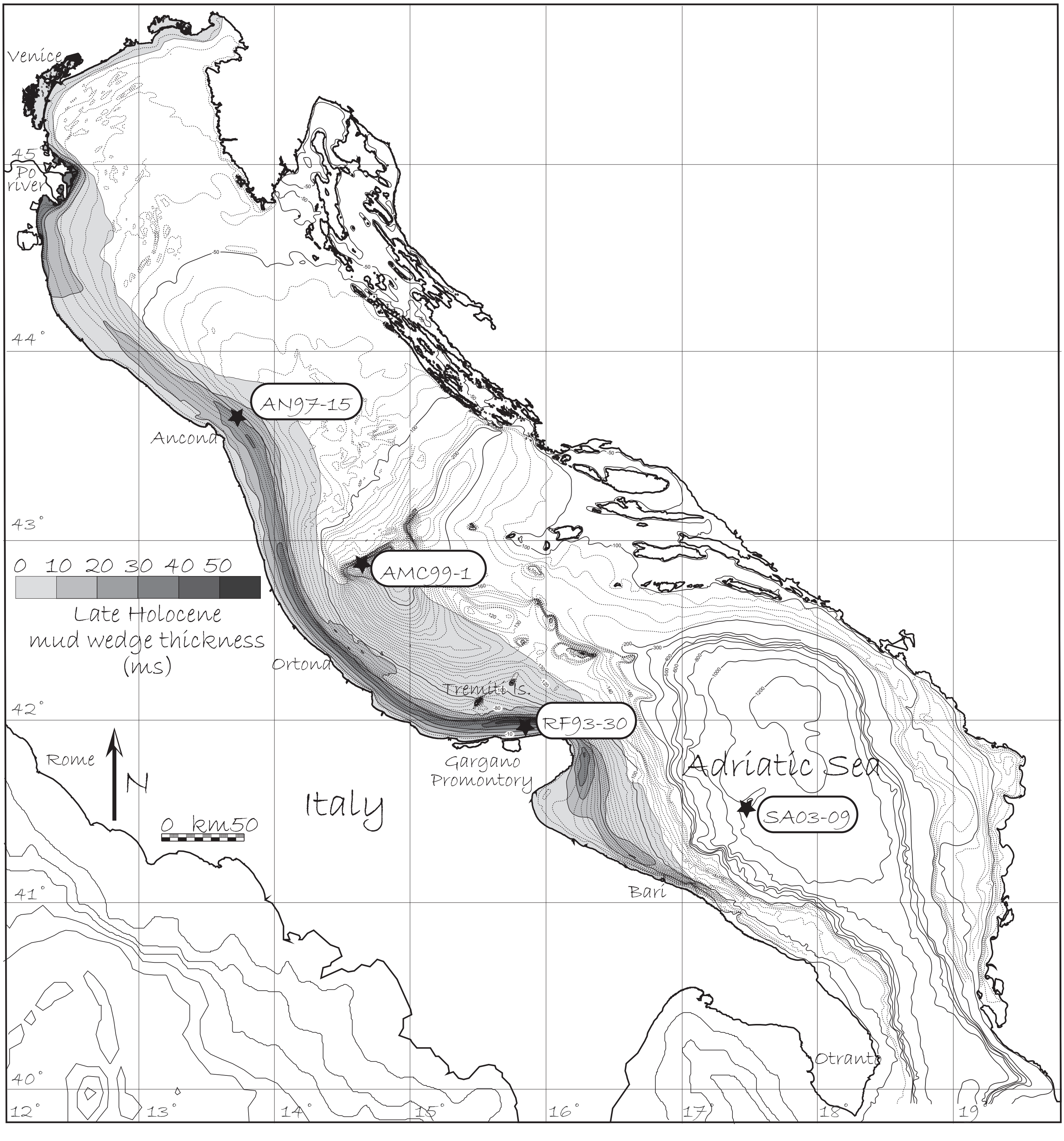

Fig. 1. Location of the cores analysed in this Part.

analyses were performed at the Leibniz Laboratory for Radiometric Dating and Stable Isotope Research, CAU Kiel, Germany, by means of a MAT 251 mass spectrometer.

^{14}C AMS ages were obtained in cores AMC99-1 and SA03-09 on (mixed) planktic and benthic samples (monospecific *Cibicidoides pachyderma*, mixed with *Uvigerina peregrina* in one sample) at the Poznan Radiocarbon Laboratory, Poland, from the size fraction >250μm. The data were then calibrated using Calib 5.0.2 Radiocarbon Calibration Program (Stuiver & Raimer, 1993). In addition, two analyses were performed on a benthic sample from core AN97-15 at the Lawrence Livermore National Laboratory (University of California).

In order to calculate the ΔR (reservoir), two sites on the western side of the Adriatic were selected from the Calib 5.0.2 database, from Northern Adriatic (Rimini) and Southern Adriatic (Barletta), neglecting data from Dalmatia and Croatia (Rovigne). The calculated weighted mean ΔR value is 135.8 with a standard deviation of 40.8. The calibrated age ranges are reported in years BP and referred to 2σ. Table I reports the ^{14}C AMS datings available and their respective calibrated ages. As regards core RF30-30, Oldfield et al. (2003) rejected all the ^{14}C AMS datings; anyhow, the reader is referred to that paper for a more detailed discussion. The ^{14}C AMS available for core AN97-15 has been calibrated according to the updated Calib 5.0.2 program.

Sample name	Lab N°	Age ^{14}C	Material	Calibrated Age range (yr BP, 2σ)	
				from	To
AMC99-1 21-22	Poz- 16133	1405±30	*C. pachyderma*	701	917
AMC99-1 117-118	Poz-16134	2880±40	*C. pachyderma*	2326	2662
AMC99-1 222-223	Poz-16135	4200±40	*C. pachyderma*	3918	4278
AMC99-1 258-259 P	Poz-16136	4750±50	Mixed planktic	4432	4794
AMC99-1 258-259 B	Poz-16137	4745±35	*C. pachyderma*	4651	4972
SA03-09 50-51	Poz-16139	1825±30	Mixed planktic	1133	1343
SA03-09 110-114 B	Poz- 17324	2435±35	Mainly *Uvigerina+ C. pachyderma*	1775	2064
SA03-09 110-114 P	Poz- 17326	2990±35	Mixed planktic	2435	2739
SA03-09 215-216	Poz- 16140	3870±50	Mixed planktic	3478	3832
SA03-09 315-316	Poz- 17327	4730±40BP	Mixed planktic	4625	4961
AN97-15 205-207		1070±50	Mixed benthic	450	644
AN97-15 421-428	CAMS 55345	4520±50	Mixed benthic	4385	4774

Table I. Dataset of calibrated ^{14}C AMS datings used in this part.

3. CHRONOLOGIC FRAMEWORK

- A regional bioevent, nevertheless occurring all over the Adriatic, is represented by the Last Occurrence of the planktic species *Globorotalia inflata*, dated around 6kyrs and approximating the maximum flooding surface, that is the base of the HST.

  Oldfield et al. (2003) managed to trace a sharp ecobiostratigraphic reconstruction as regards foraminifers' assemblages, indeed for core RF93-30, supported by a very robust chronology. Even if the proximal mud belt environment in which the core was collected forced the ecobiozonation to rely mainly on benthic foraminifera, nevertheless the variations of the poorly represented planktic community are quite visible and the resulting signal can be compared with the other cores. Core RF93-30 can boast of an extremely sharp chronological framework, involving also pollen data, tephrostratigraphy and tephrochronology, the secular variation paleomagnetic curve, ^{210}Pb analyses and many ^{14}C datings (all the results are fully described in Oldfield et al., 2003). For this reason, core RF93-30 plays an important role as reference core for the HST deposition in the Adriatic.
- Also the other cores analysed have been implemented with several ^{14}C datings, mainly concentrated in the deeper ones, aiming to check if the signal visible in the chronologically robust shallow reference core, was visible in a more distal environment.

  It has also been noted that the ages <3000 years BP, obtained on benthic foraminifers' shells, are systematically older, as far as 300 years, in the shallower cores. For this reason it was chosen not to implement the proximal cores with other datings, whose interpretation would have been difficult because of a too wide range of variation. However, two ^{14}C ages are available from literature (Correggiari et al., 2001) for core AN97-15, to give an idea of the magnitude of the error. ^{14}C ages performed in core RF93-30 (rejected in Oldfield et al., 2003 and not reported in Fig. 5) provided results comparable with that reported for core AN97-15, yet.

  ^{14}C datings performed in core AMC99-1 mainly rely on the analyses of benthic foraminifers samples (all monospecific and performed on the same epifaunal species, *C. pachyderma*). Yet, one level has been analysed both on planktic and benthic foraminifers. A time lag of almost 200 years resulted. For this reason, it was chosen to subtract 200 years to all the other ^{14}C AMS datings of core AMC99-1 performed on benthic foraminifers. This assumption allows a better correlation with the ^{14}C datings of the other cores.

- The secular variation curve is available for core AMC99-1 (data available by Vigliotti, oral personal communication), as well, though with less detail than that of core RF93-30, giving independent and additional ages.
- A really intense volcanic activity occurred in the last 5.5kyrs in the Italian region. Many tephra layers have been individuated in the cores analysed. Unfortunately, the occurrence of multiple events at really contiguous times hampered the possibility of recognizing each volcanoclastic event. A Master thesis is presently trying to separate the different origin of the single eruptions, in order to discriminate them. Anyway, the position of the tephra layers found in the cores, in relation with the foraminifers' ecobiostratigraphy and with the tephrochronological data existing for core RF93-30, helped in the event correlation, giving indirect age evidences. As regards core AMC99-1, the tephra layer present at 200-300 cm can probably correspond to an event linked to Agnano Monte Spina multiple eruption, consistently with the calibrated age of 4610 years BP at 258 cm. This would be in good agreement with the tephrochronological data available from core CM93-42 (Asioli, 1996), collected in the same area. Anyhow, the absence of geochemical analyses does not allow to surely individuate this volcanic event.
- Estimates of the sedimentation rate for the last 100 years have been obtained by means of ^{210}Pb profiles (Frignani et al., 2005) in a core collected in the same site of AN97-15 using a SW104 corer, which preserves the sediment-water interface. The analyses indicate an average sedimentation rate of about 2.7 mm per year, resulting in an approximated age of 100 years at 27 cm below the sea floor. This level registers the sharp decline of *V. complanata*. These kind of estimates via ^{210}Pb have been conducted also for a set of cores collected in the same area of core AMC99-1, stating an approximated age of 100 years BP at about 10 cm. (Frignani et al., 2005).

Matching the dataset deriving from all these proxies, it has been possible to achieve the following age-depth models for cores AMC99-1 and SA03-09:

Core AMC99-1		
Level (cm bsf)	Corresponding age (years BP)	Source
0	0	
10	100	^{210}Pb
21	610	^{14}C AMS$^{\#}$
90	1800	event δ inclination*
117	2295	^{14}C AMS$^{\#}$
127	2350	event e declination*
148	2750	event f declination*
184	3525	event ε inclination*
222	3900	^{14}C AMS$^{\#}$
258	4610	^{14}C AMS
323	6000	LO *G. inflata*§

\# calibrated ^{14}C AMS age deriving on benthic foraminifers' sample: 200 years subtracted.

* events deriving from the secular geomagnetic curve (Vigliotti, oral personal communication)

§ from literature (Asioli, 1996; Ariztegui et al., 2000)

Core SA03-09		
Level (cm bsf)	Corresponding age (years BP)	Source
0	0	
50	1235	^{14}C AMS
112	1920	^{14}C AMS
215	3655	^{14}C AMS
315	4790	^{14}C AMS
350	6000	LO *G. inflata*§

§ from literature (Asioli, 1996; Ariztegui et al., 2000).

As regards the age-depth model of core RF93-30, the reader is referred to literature (Oldfield et al., 2003). Core AN97-15 presents few control points, among which two ^{14}C AMS datings performed on mixed benthic foraminifers. Because of the problems above discussed linked to the reliability of these ages, it has been chosen not to estimate the age of bioevents from this core.

4. RESULTS

The most significant results in the biostratigraphic record of the cores analysed are briefly presented, taking into particular account the distribution of two foraminifers' species, already employed in the study of HST deposits in previous papers (Jorissen et al., 1993; Asioli, 1996;

Capotondi et al., 1999; Ariztegui et al., 2001, Oldfield et al., 2003): the planktic *Globigerinoides sacculifer* and the benthic *Valvulineria complanata*, living in the shallow shelf settings, within the mud belt.

- Core AN97-15 (Fig.2) can be divided into two ecobiozones, the lower of which presenting high frequencies of *G. sacculifer* in the planktic assemblage: this species shows an oscillating trend, and it becomes occasionally dominant, though it is not possible to define distinct peaks. The upper ecobiozone is completely devoid of this form, showing instead a sensible increase in the abundance of benthic *V. complanata*, rare in the lower ecobiozone, which presents at least two distinct peaks. *Elphidium decipiens* and epiphytic forms show an apparent decrease in frequencies from the lower to the upper zone. The very top of the core is characterised by a decrease in *V. complanata* in favour of *Brizalina spathulata* and *Nonionella turgida*.
- Core RF93-30 shows a similar trend compared to core AN97-15, but it presents two distinct peaks of *G. sacculifer* in the lower ecobiozone. Moreover, a significant increase in the frequencies of *V. complanata* occurs during the minimum in between the two peaks of the planktic biomarker. The upper ecobiozone shows instead at least two separate peaks of *V. complanata*, where *G. sacculifer* is absent. A more detailed description of the results of this core can be found in Oldfield et al. (2003).
- Core AMC99-1 (Fig. 3) is a deeper core, collected outside the clay belt environment: for this reason the frequencies of *V. complanata* cannot be taken into account, as they do not appear consistent and significant. The distribution of *G. sacculifer* shows instead a similar trend to the shallower cores, though the upper ecobiozone, in which the species does not occur, is restricted to the very first 20 cm. The very expanded lower ecobiozone presents three distinct peaks of *G. sacculifer*, separated by two minima. The other warm water planktic species (i.e. *Globigerinoides* ex gr. *ruber*, *Zeaglobigerina rubescens* and *Orbulina universa*) show a rather uniform trend, and a visible decrease in frequencies at the very top of the core. The benthic assemblage is uniform, as well, with the exception of a reversal between *Brizalina spathulata* and *Cassidulina laevigata carinata*.
- Deeper-water core SA03-09 (Fig.4) presents an extremely reduced uppermost ecobiozone,: *G. sacculifer* is in fact absent from the uppermost 10 cm. On the other hand, four peaks in the abundance of this species are clearly apparent in the lower ecobiozone. Despite the proximity of this core location to the Bari canyon, resulting in a higher abundance of reworked material

compared to all the time-equivalent cores, the succession of events is still clearly apparent and well preserved in the stratigraphic record of the core. The benthic assemblage at this water depth and in this sedimentary environment, instead, does not show a meaningful trend.

It is important to consider that the frequency of *G. sacculifer* appears inversely related to the water depth: in fact, the deeper the bathymetry, the lower the abundances of this planktic biomarker. This is not surprising, taking into account that planktic microfauna increases in its abundance and becomes more diversified with the deepening of the water column. Nevertheless, although really different frequencies, related to the water depth, and a different number of peaks, due to the sedimentation rate, *G. sacculifer* presents a similar trend in all the cores here analysed. As regards the benthic assemblage, the two cores collected inside the mud belt environment show a good and consistent correlatability, by means of *V. complanata*: although this topic clearly has a local value, moreover restricted to a peculiar environment, nonetheless the signal can be recognized in an area at least 300 km wide. In the end, it has not yet been possible to individuate another benthic biomarker for deeper environments.

Other planktic and benthic foraminiferal proxies are discussed later in this chapter, as regards their paleocanographic inferences.

5. DISCUSSION

5.1 CLIMATE SHORT TERM OSCILLATIONS: A REVIEW

Although Holocene climate is considered anomalously stable (Broecker, 1994), even more than during the last Interglacial (Eemian, Euthyrrenian) (Fronval and Jansen, 1997), nevertheless, a higher and higher number of evidences, from both the marine and the continental records, testify the undoubt occurrence of high frequency oscillations inside the latest 12000 years.

Increasing studies on Holocene short-term climate shifts, aim at understanding the mechanisms which control sub-Milankovitch millennial to centennial (and, in some cases, even decadal) fluctuations, their timing and amplitude. This improved understanding may shed light on the key forcing factors which controlled short-term climate change and better define possible scenarios brought about by similar climate evolutions in the future (see for instance Berger and Loutre, 2002). Though its origin is not yet fully known, it seems that a weak quasi-periodic forcing

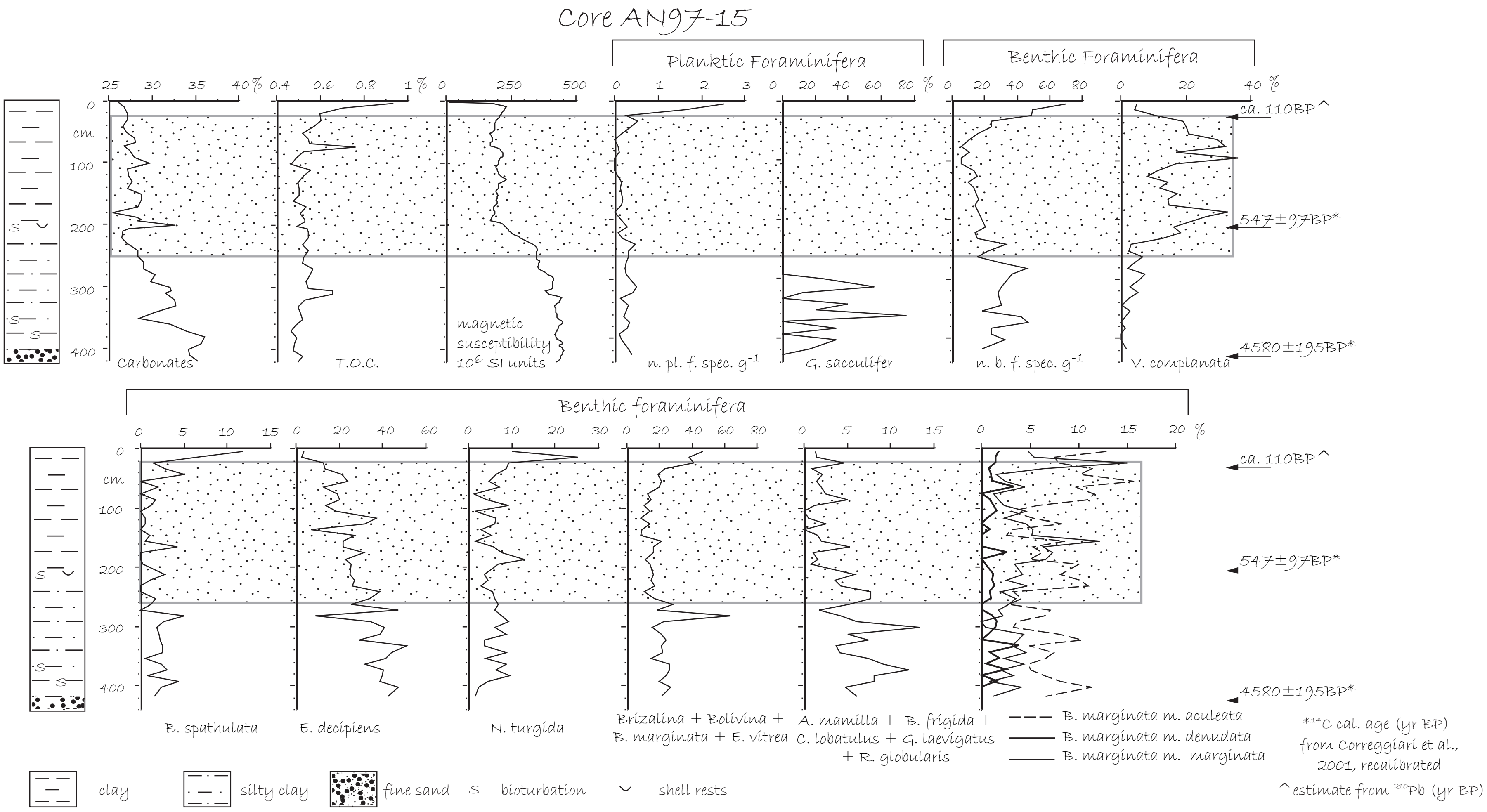

Fig. 2. Main planktic and benthic species for core AN97-15. The dotted area corresponds to the ecozone devoid of G. sacculifer (Little Ice Age)

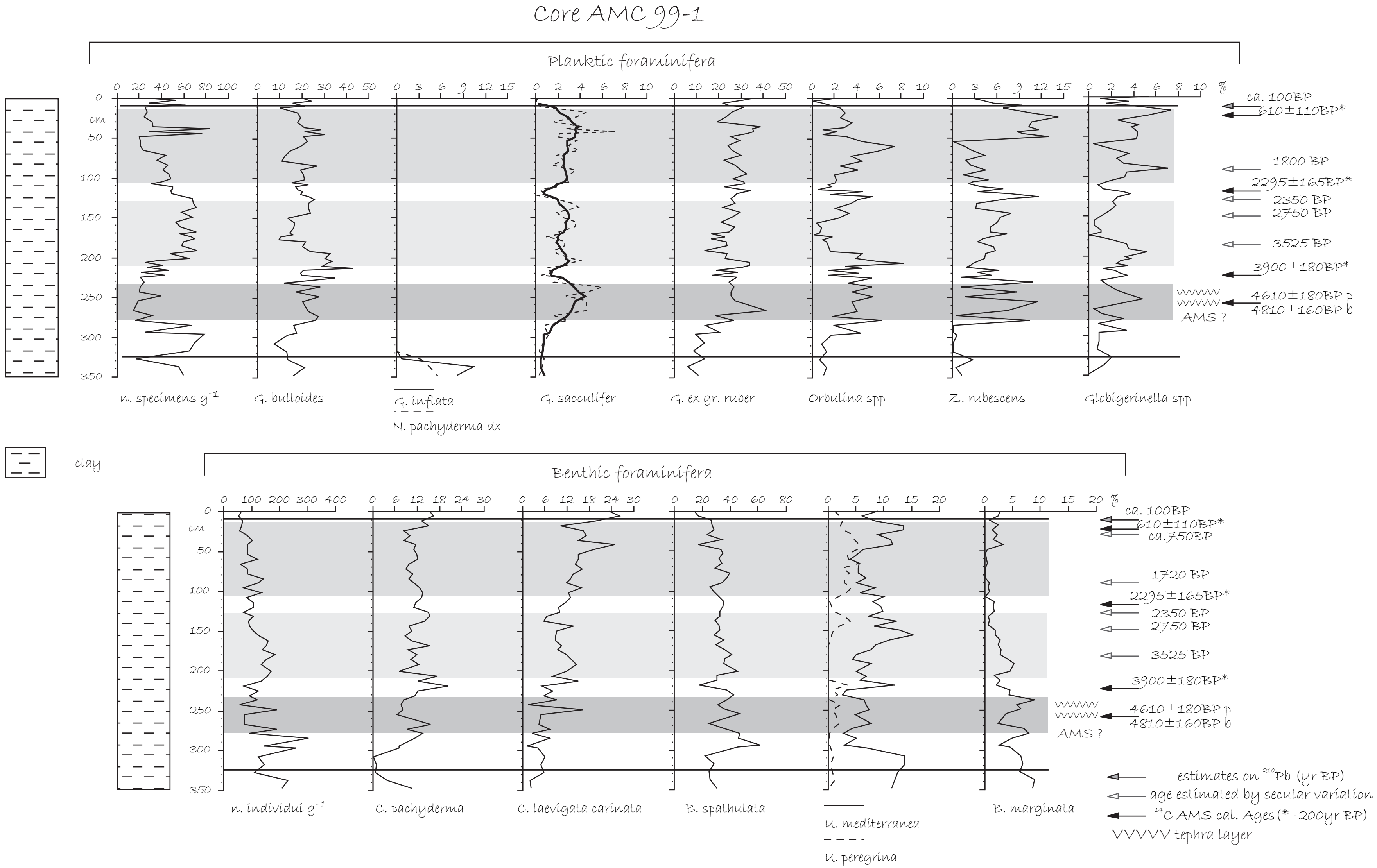

Fig. 3. Main planktic and benthic species for core AMC99-1. The grey areas mark the peaks in the abundance of G. sacculifer

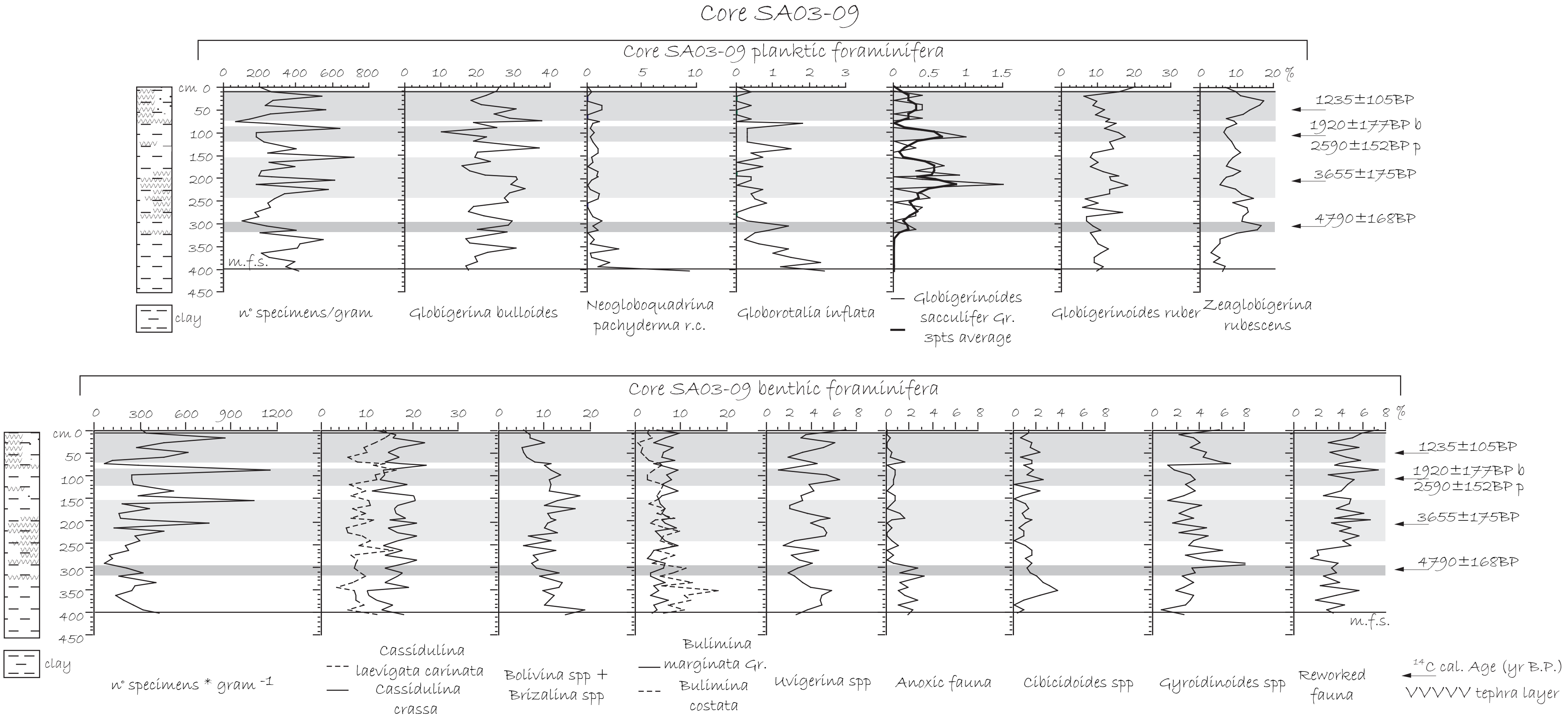

Fig. 4. Main planktic and benthic species for core SA03-09. The grey areas mark the peaks in the abundance of G. sacculifer

(1500±500 years) drove this sub-Milankovitch climate variability (Campbell et al., 1998, McDermott et al., 2001). Some authors (Bond et al., 1997, Alley, 1998, Bianchi and McCave, 1999, Bond et al., 2001) suggested that, at least the North Atlantic region, experienced a succession of climate changes that probably reflects the same periodicity as the Dansgaard-Oeschger oscillations, which are paced around 1450 years, though with a substantially attenuated expression during the Holocene.

In the continental record, important evidence is given by the analysis of the expansion and retreat of mountain glaciers (Mayr, 1964; Veggiani, 1986), by the reconstruction of stable-isotope records from speleothems (McDermott et al., 2001), by spectral analyses on stalagmites (Frisia et al., 2003), or by estimates of the dust content (Thompson et al., 2002) and green-house gasses, even in ice-cores. Other complementary proxies help defining changes in the hydrological cycle, including: the precipitation regime (Renssen et al., 2006), the recurrence and intensity of storm events (Noren et al., 2002), the periodicity of drought episodes (deMenocal, 2001), and the paleohydrological excursions of lacustrine and fluvial flows (Campbell et al., 1998; Magny et al., 2002; Marchant and Hooghiemstra, 2004). Precious additional paleoenvironmental information come from the exam of tree rings and varved lake sediments (Overpeck et al., 1997), together with the pollen content record (Marret et al., 2006).

On the other hand, deep and shallower marine records rely on several complementary proxies, such as planktic foraminifers' assemblages, SST estimates, IRD content, (Alley, 1998; deMenocal et al., 2000), hematite-stained grains content and the stable isotope record (Bond et al., 1997; Bond et al., 2001; Hong et al., 2003). Isotopic anomalies (Hendy et al., 2002), can be compared with alkenone-derived paleotemperatures (Sbaffi et al., 2001; Arz et al., 2003), changes in bottom current intensity expressed by sortable silt (Bianchi and McCave, 1999), and benthic foraminifers (Diz et al., 2002; Murdmaa et al., 2004; Bartels-Jònsdòttir et al., 2006).

About eight major cool oscillations have been recognised during the Holocene (Bond et al., 1997; deMenocal et al., 2000), three of which occurred during the last 5500 years. During this interval, historical accounts and phenological records document the occurrence of the Little Ice Age, the most dramatic cold oscillation in the last centuries (Matthes, 1939). Possibly-synchronous changes impacting on hemispheric scale include the dramatic climate change bringing Eurasia into cool and wet conditions around 700 years BC (van Geel et al., 1996). In general, however, the latest climate oscillations occurring during the second half of the Holocene, appear somehow more diachronous, in particular during the last 1000 years. For instance, the Medieval

Warm Period (MWP), first defined by Lamb (1965), registered warm climate conditions in the Northern Hemisphere between 800 and 1400AD (Johnes and Mann, 2004), especially in the Mediterranean and North African areas (Schilman et al., 2001), in the Cariaco Basin (Haug et al., 2001), in California, where drought episodes occurred (Stine, 1994) and as far as high latitudes in the North Atlantic, where the retreat of Arctic glaciers allowed the colonization of Greenland coastlands by the Vikings. Anyhow, this warm oscillation was not synchronous (Hughes and Diaz, 1994), since it occurred earlier (1000-600AD) in China and Antarctica, and affected only part of the Southern Hemisphere (Cook et al., 2002). The atmospheric connection which regulates these climate oscillations could indeed be responsible of delays and different intensities and even opposite behaviours between the two hemispheres.

The Little Ice Age (LIA), instead, can boast of a better time constraint, because its impact on human life, which caused floodings, swampings, interment of the harbours, damages to agriculture, crises in fishing and economic activities, lead to drought, famine, poorness, diseases and plague, (Veggiani, 1986), and it is testified by several historical, artistic, literary, economic and scientific evidences. A relative coherent cooling is registered between 1550 and 1850AD, despite spatial and temporal variations in detail (Bradley and Johnes, 1992), and it caused mountainous glaciers to advance and broaden all over the world, from the Alps to Sierra Nevada, from Rocky Mountains to the Andes, from eastern Africa to the Himalayas, from New Guinea to New Zealand (Crowley and North, 1991). The expansion of marine ice around Iceland seriously damaged fishing activities and isolated the colonies sprung up in Greenland (Dansgaard, 1975). The paleotemperature record registered in Paris marked the winter nature of this cooling phenomenon in Europe (Pfister, 1985). Tree rings exam point out summer drought conditions in North America (Cook and Jacoby, 1979; Stahle et al., 1985, 1988; Stahle and Cleaveland, 1988). Droughts and dust storms (Zhang, 1984) occurred more frequently in China, as well, together with episodes of enhanced flooding (Zheng and Feng, 1988). LIA cool oscillations in the northern hemisphere result mostly synchronous with those reported in the records of cave deposits from New Zealand, of geomorphic features in Southern Georgia Island and of Eastern Antarctic ice cores (Wilson et al., 1979; Mosley-Thompson and Thompson, 1982; Morgan, 1985; Clapperton et al., 1989; Domack et al., 1993, 2003). Moreover, peri-Antarctic Ross Sea registered episodes of upwelling longside of its coasts, index of the occurrence of a regime of strong winds, which hampered the expansion of the sea ice in this area, respect to the Weddell Sea (Parkinson, 1990). Seemingly opposite trends were registered in the 19th century in Australia, where lake levels got higher (Churchill et al., 1978), and in

Southern Chile, where dryer conditions were registered: these phenomena are explained by a southward shift of the atmospheric circulation, which moved the subtropical high pressure to higher latitudes (Lamb, 1969). The LIA seems to have been a particularly humid period, which brought wetter conditions even in the sub-Saharan African region (Nicholson, 1978). Evidences from the Andes, from China and from North America would bring to reconstruct cool and moist conditions in the first phase, from 1450 to 1700AD, and a cool and dry period in the second, from 1700 to 1880AD. Sea records from coastal cores and corals analyses testify lower SSTs and stronger winds in the East Pacific (Pisias, 1979; Juillet-Leclerc and Schrader, 1987), and stormy periods (especially in the 1690s) in the North Atlantic (Lamb, 1979).

The combination of solar and volcanic forcing can account for almost all the temperature variability at hemispheric or global level over the last 300 to 1000 years (Crowley and Kim, 1999; Free and Robock, 1999; Crowley, 2000; Amman et al., 2003; Bradley, 2003; Broccoli et al., 2003; Jones and Mann, 2004). In fact, explosive eruptions release a so huge quantity of ash and dust material, ejected in the stratosphere, to cause severe repercussions on climate, such as wind anomalies and cooler surface temperatures (Shindell et al., 2004), above all because of the conversion of sulphur volatiles in sulphuric acid, resulting in the cooling of the lower troposphere by backscattering of incoming long-wave radiation (Devine et al., 1984). For example, the eruption of the Tambora volcano, in Indonesia, on April 10th-12th, 1815 (Stothers, 1984), causing 92000 victims, ash falls, tsunami, diseases and starvation, was also the main responsible of the so called *year without a summer* during the subsequent 1816. Although the effects following an eruption can be perceived only for a couple of years, the ice-albedo feedback affecting sea ice cover or multiple closely spaced eruptions could result in a longer effect, sensible over decades (Crowley and North, 1991). It has also to be taken into account that only eruptions occurring at equatorial latitudes have the potential to be transmitted via upper atmosphere winds to higher latitudes of both hemispheres (Legrand and Delmas, 1987). Anyway, high latitude eruptions may explane inter-hemispheric differences due to a localized forcing (Crowley and North, 1991). It is therefore more and more believed that explosive volcanic activity can amplify climatic changes that are already underway trough the operation of a complex series of both positive and negative feedback loops (Lowe and Walker, 1997).

Moreover, another forcing factor which could have regulated these short term climatic oscillations is given by variations in the solar activity. It has been demonstrated a 11, 22-year (Hale cycles), 88-year (Geisberg cycles), and almost 200 and 2500-year (Rind and Overpeck, 1993) periodicity of solar variability, as regards solar magnetic cycles, sunspots, aurora and ^{14}C variations (Gleissberg, 1966; Feynman and Fougere, 1984; Stuiver and Braziunas, 1988, 1989), maybe related to changes in the structure of the sun in response to magnetic field variations (Kuhn et al., 1988), or maybe linked to variations in the solar radius (Ribes, 1990). Four distinct minima in the solar activity, regarding in particular the solar irradiance and the co-varying sunspots (Pittock, 1983; Sofia, 1984) have been individuated: these are the Dalton (1830-1810AD), Maunder (1715-1645AD), Spörer (1540-1420AD) and Wolf (1325-1285) solar activity minima. Both Dalton and Maunder minima correspond to the most severe phases inside the LIA (Grove, 1988). Wolf and Spörer minima could instead reflect the deterioration of climate condition after the end of MWP. Moreover, numerous and severe eruptions, occurring in correspondence of the Maunder minimum, may have given rise to longer-lasting climate impacts (Bradley, 2003). Recent studies showed a link between the strenght of cosmic-ray flux (which is negatively correlated with solar activity) and the formation of cloud condensation nuclei in the atmosphere (Svensmark and Friis-Christensen, 1996; Marsh and Svensmark, 2000). This would have resulted in a reduction in temperature due to cloudier conditions.

Anyway, several of the most dramatic changes in Holocene climate can only be explained when feedbacks from the cryosphere, oceans and terrestrial biosphere are fully taken into account (Oldfield, 2005). An example is given by the feedback caused by the ocean-atmosphere system (Broecker et al., 1999; Bond et al., 1999; Keigwin and Boyle, 2000), and the resulting millennial scale fluctuations of the North Atlantic Deep Water (NADW) (Boyle and Keigwin, 1987), by which decreased NADW production would be associated with colder events. Internal feedback mechanisms therefore concur in amplifying external forcing mechanisms (Lowe and Walker, 1997).

5.2 STRATIGRAPHIC EVIDENCES

Matching ecobiostratigraphic and chronologic results gave surprising results in the event stratigraphic correlation of the cores analysed. The three major peaks of *G. sacculifer* visible in core AMC99-1 (FIgg. 3, 5) have been dated respectively around 4600-4800 years BP, at almost 3500-3600 years BP and between 2000 and 1200 years BP. This latter peak, which seems to be slightly uniform in core AMC99-1 and instead double phased in core SA03-09, has been tentatively split in two distinct periods. *G. sacculifer*'s Last Occurence occurs between 500 and 600 years BP (about 550 years BP). This age corresponds to the average of the interpolated calibrated ages obtained in the records of cores RF93-30, AMC99-1, and SA03-09. Also the minima in the abundances of this planktic foraminifer were dated, and the ages gave consistent values. Moreover, the two peaks of *V. complanata* visible in the shallower cores were dated, as well, and they correspond to an age of 1865AD and 1689AD, respectively, according to the secular variation curve. These datings are in good agreement in all the cores analysed, and consent to define the stratigraphic framework plotted in Fig. 5.

The identification of the same ecobiostatigraphic events in cores collected several hundreds kilometers apart one from the other, at very different water depths, in dissimilar environmental conditions and in two distinct basins gives strength to the ecobiozonation here presented, which assumes a regional value. Moreover, it is now apparent that in the Adriatic more than one peak of *G. sacculifer* can be identified in the HST ecobiozone. This statement implies higher caution in correlating not so expanded records, reporting only one major peak of this biomarker (Capotondi et al., 1999; Sbaffi et al., 2001; Sprovieri et al., 2003).

5.3 PALEOCEANOGRAPHIC INFERENCES

The ecobiostratigraphic events recognized in foraminifers' abundances have also a significant paleoclimatic and paleoceanographic meaning. Each species has in fact peculiar life styles, derived from climatic and trophic limiting factors. High frequencies of one particular species are therefore the consequence of the fact that climatic and oceanographic conditions were perfectly suitable with its life needs at that time.

G. sacculifer is an oligotrophic, shallow water dweller, typical of warm, tropical environments, characterised by low turbidity of the water column and by poor runoff (Bè and Tolderlund, 1971; Hemleben et al., 1989; Pujol and Vergnaud Grazzini, 1995). For this reason, the peaks of this species during the HST deposition have been interpreted as periods of Climatic Optimum, the latest two of which corresponding to the Medieval Warm Period-Roman Age, and to the late Bronze Age, respectively (in consequence of ^{14}C datings)(Fig. 5).

Following the same criterion, it seems fair to assume that its LO, dated around 1400 AD, approximates the base of the Little Ice Age. Schilman et al. (2001, 2003) report the bioevent LO *G. sacculifer* ranging between 800 and 850 yr BP in two cores collected in the slope off Israel. Although this event appears to occur slightly earlier in the Levantine Basin, in comparison with the cores of this study, this disappearance can not be considered a bioevent restricted to the Adriatic basin, and it may represent the planktic foraminifers' bioevent best approximating the base of the Little Ice Age in the whole Eastern Mediterranean.

Moreover, in the Southern Adriatic deep core SA03-09, it has been observed a peculiar trend in the frequencies of another planktic foraminifer, *Globigerinoides ruber* pink. The curve of the abundances of this species shows in fact an opposite trend in respect of that of *G. sacculifer* (Fig. 6). *G. ruber* is another oligotrophic, shallow water inhabitant, indicating warm climate, and its pink variety shows a modification of the shell, presenting a thinner test and inflated chambers (Bè and Tolderlund, 1971; Fairbanks et al., 1982; Negri et al., 1999). Since *G. ruber* pink reached its highest abundances in the Levantine basin, in correspondence of the deposition of recent sapropel layers (for instance Sapropel 1), and these peculiar paleoceanographic events are assumed to have been humid periods, with strong rainfall and enhanced fluvial runoff, it seems reliable to consider *G. ruber* pink as a biomarker of relatively wetter conditions. The modification of the shell can in fact be explained by the need of being buoyant and floating in a water mass become less dense because of freshwater influxes. Although it is apparent that no sapropelic event occurred during the HST deposition, nevertheless this statement results in good accordance with the observation about the opposite trends of the two *Globigerinoides* species here analysed. They could indeed reflect humidity changes in the weather conditions, drier during Climatic Optima and wetter and slightly cooler in between.

On the other hand, *V. complanata* is a benthic opportunistic species, presently living in the mud belt extreme environment, characterised by strong amounts of organic matter, mainly of continental origin, brought by river runoff, and by a consequently poorly oxygenated bottom floor (Blanc-Vernet, 1969; Jorissen, 1988; Murray, 1991; Sgarrella and Moncharmont Zei, 1993; Rathburn and Corliss, 1994). The two distinct peaks of this species registered in the shallower cores analysed, occur inside the ecobiozone devoid of *G. sacculifer*, and therefore inside the Little Ice Age. Moreover, the ages corresponding to these two peaks reflect the occurrence of the most critical phases of the LIA, which glaciologic literature defined the Fernau (1590-1630AD) and the Napoleon (1810-1820AD) Stadia (Veggiani, 1986). High frequencies of *V. complanata* could therefore be linked to cold and humid periods, which would have caused such huge river discharges. A concurring depletion in the frequencies of benthic epiphythic species (*Asterigerinata mamilla*, *Buccella granulata frigida*, *Cibicides lobatulus*, *Gavelinopsis laevigatus* and *Rosalina globularis*) inside the interval corresponding to the LIA could suggest an increase in the turbidity of the water mass, because of enhanced rainfall and fluvial runoff (Jorissen, 1988; Murray, 1991; Sgarrella and Moncharmont Zei, 1993). The end of the LIA is characterized, in core RF93-30, by an increase of benthic species such as *Bulimina marginata*, *Epistominella vitrea*, and those belonging to the

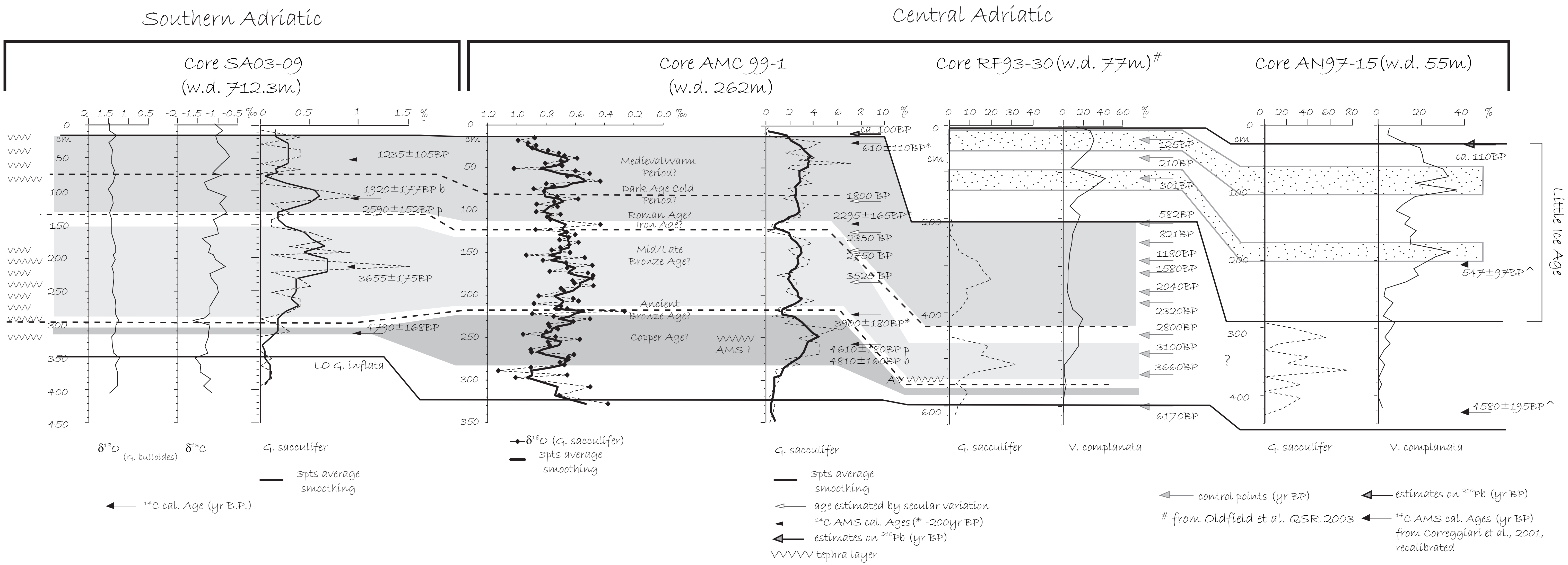

Fig. 5. Ecobiostratigraphic correlation of the main marker species among the cores analysed. Grey areas mark the peaks in the abundance of G. sacculifer, dashed lines point out the minima of this species. Dotted areas mark the peaks in the abundance of V. complanata

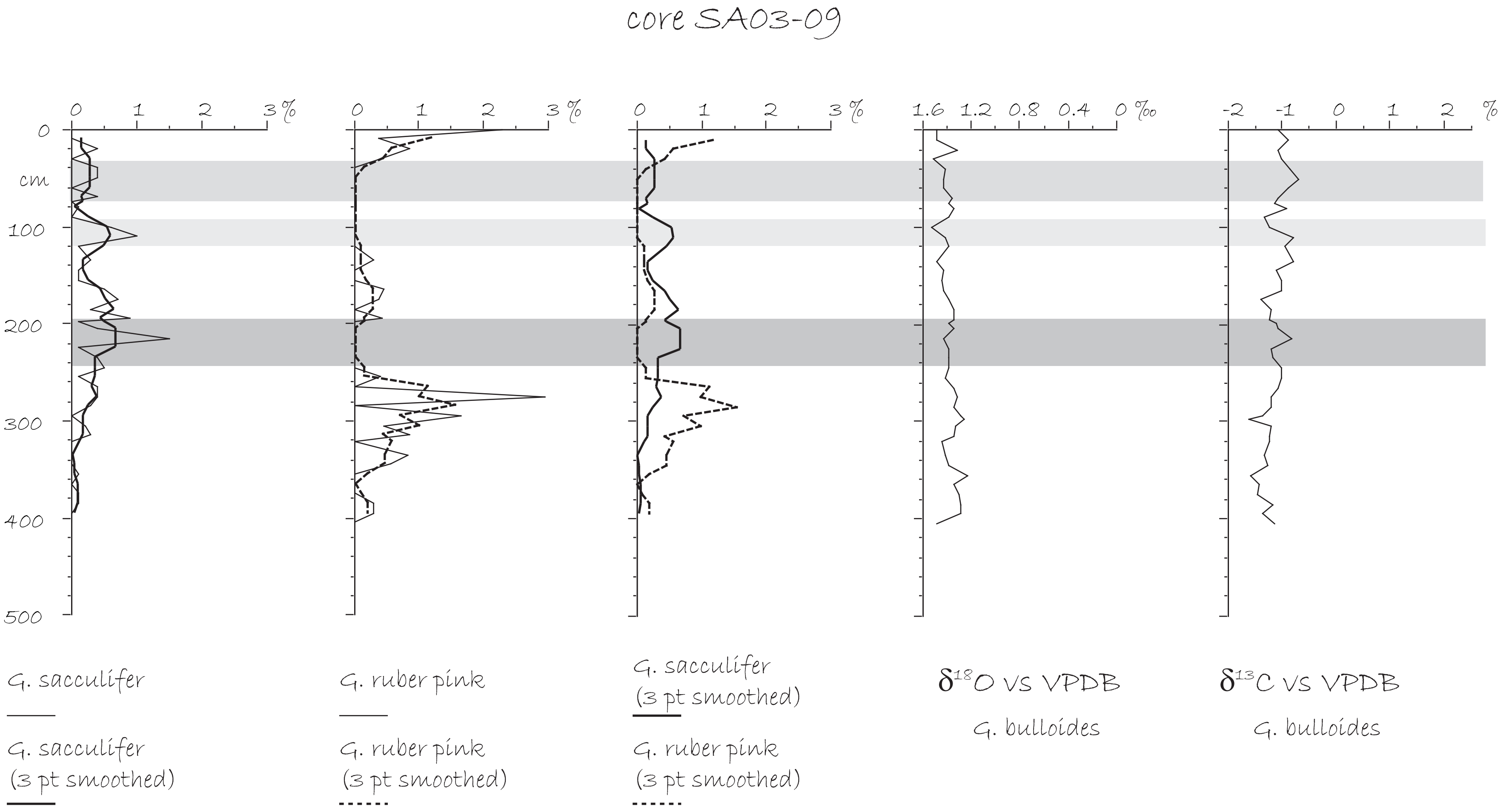

Fig. 6. Results of the main marker planktic species and of the isotope curves for core SA03-09.

genera *Brizalina* and *Bolivina*, to the detriment of *V. complanata*. According to Barmawidjaja et al. (1992), these species are potentially infaunal foraminifera, rather mobile and able to shift their microhabitat from infaunal to epifaunal, somehow reflecting seasonal variability. Therefore, an increase in those species could be the signal of a higher frequency of dysoxic episods or of a more intense seasonal contrast of oxygenation conditions (Phleger and Soutar, 1973; Hermelin and Shimmield, 1990; Jorissen et al., 1992; Miao and Thunell, 1993; Sen Gupta and Machain Castillo, 1993; Rathburn and Corliss, 1994).

Deeper cores give more complete information about the planktic foraminifers' assemblage during the last 6kyrs, which is typical of warm-temperate climate, as reported in previous literature, and it is characterised by species like *G.* ex gr. *ruber*, *G. sacculifer*, *Orbulina* spp, *Zeaglobigerina rubescens* and *Globigerinella* spp (Hemleben et al., 1989). The LIA, poorly represented because of scarce sedimentation rate, cannot be fully described at greater water depths. The benthic assemblage is typical of mesotrophic environment in both the deeper cores. The frequencies of the main taxa are generally constant, except from minor oscillations. The most visible shift in frequencies, specially in core AMC99-1, is given by a small decrease of *Bolivina-Brizalina* group, in favour of *Cassidulina laevigata carinata*; this slight reversal could be interpreted as a relative improvement of bottom floor oxygenation conditions, and, regarding *C. laevigata carinata*, an increase in bottom water salinity (Verhallen, 1991). Nevertheless, in the two deeper cores no benthic taxon clearly varies in its frequencies according to *G. sacculifer*'s trend. That could mean that the oscillations registered in surface waters would not have been sufficiently strong/long-lasting to cause significant variations on the bottom floor at high water depths, and that these oscillations would have had a stronger impact at lower w.d., where sediment supply is higher and fluvial influence is more intense, according to the general trend in the Adriatic circulation.

The oxygen and carbon stable isotope curves performed on the intermediate-waters dweller *G. bulloides* appear somewhat steady in core SA03-09 (Fig. 5), suggesting a uniform water mass. On the other hand, stable isotope analyses performed on shallower-water dwellers *G. ruber* and *G. sacculifer*, respectively in cores RF93-30 and AMC99-1 (Figg. 5, 7b), reveal a consistent behaviour of the shallower layer of the water column. Lighter $\delta^{18}O$ and heavier $\delta^{13}C$ values generally match *G. sacculifer's* peaks, suggesting slightly warmer intervals and reduced content in organic matter during the Climatic Optima, and *vice versa* cooler and denser waters, richer in organic matter, during the cold climate oscillations. Two significant events, at about 2300 and 5800 years BP, are recorded by the isotope trends derived by shallow water species, indicated both by $\delta^{18}O$ and $\delta^{13}C$ minima. These levels have been interpreted as river floods, discharging large amounts of freshwater and organic matter into the basin. This interpretation is consistent with the signal being best recorded in the proximal core RF93-30, and that shows a lighter overprint in the more distal core AMC99-1. Moreover, *G. sacculifer* is absent during these levels, not because of an actual climatic cooling, but because the environmental conditions were no longer suitable.

The bioevents recognised through the analysis of the variations in the relative abundance of both planktic and benthic foraminifera are a regional faunal expression of short-term climate changes during the middle-late Holocene, when the HST mud wedge was deposited. The two peaks in the frequencies of *V. complanata*, in fact, well match with the most severe and coldest intervals during the LIA, as identified by SST anomalies. Moreover, minima in the abundance of *G. sacculifer* can be easily interpreted as a faunal expression of late Holocene cooling events. The Adriatic stratigraphic record here analysed has been compared with several other climatic records based on different proxies in several locations worldwide (see Table II, below). Even though the synchronism of these cooling events in each particular area needs to be better investigated, no doubt exists that an atmospheric-climate connection is the most likely link among these distant depositional basins, offering the possibility to achieve a super-regional correlation of events. The trends of the main biomarkers, expressed both as percentages and as fluxes, plotted versus time (Fig. 7a and 7b), consistently define all the major short-term climatic shifts, which are roughly correspondent to archaeological intervals, and constrain few additional climatic oscillations during the last 6000 years, granting the chance to achieve a more detailed framework as regards climatic change. Anyhow, it cannot be ruled out that these additional climatic shifts may have a more local significance. The warm-climate, arid oscillations and the colder and more rainy ones pointed out by peaks and low amounts in *G. sacculifer*'s (and warm planktic species) abundance, respectively, find good consistency with the available pollen data (Fig. 7a, Lowe et al., 1996; Oldfield et al., 2003), which show an increase in humidity-related aquatic herbs/hygrophytes pollen when *G. sacculifer* decreases. In particular, aquatic herbs, consisting of Limnophytes and Thelmatophytes, represent the herbaceous pollen component, first occurring during humidity intervals, whereas hygrophytes (*Alnus, Salix* and *Populus*), reach their acme when the humid phase already set. Hygrophytes' trend can be desumed in Fig. 7a by the difference between the humidity-related pollen sum and the aquatic herbs. The tree pollen curve obtained by Oldfield et al. (2003) and reported in

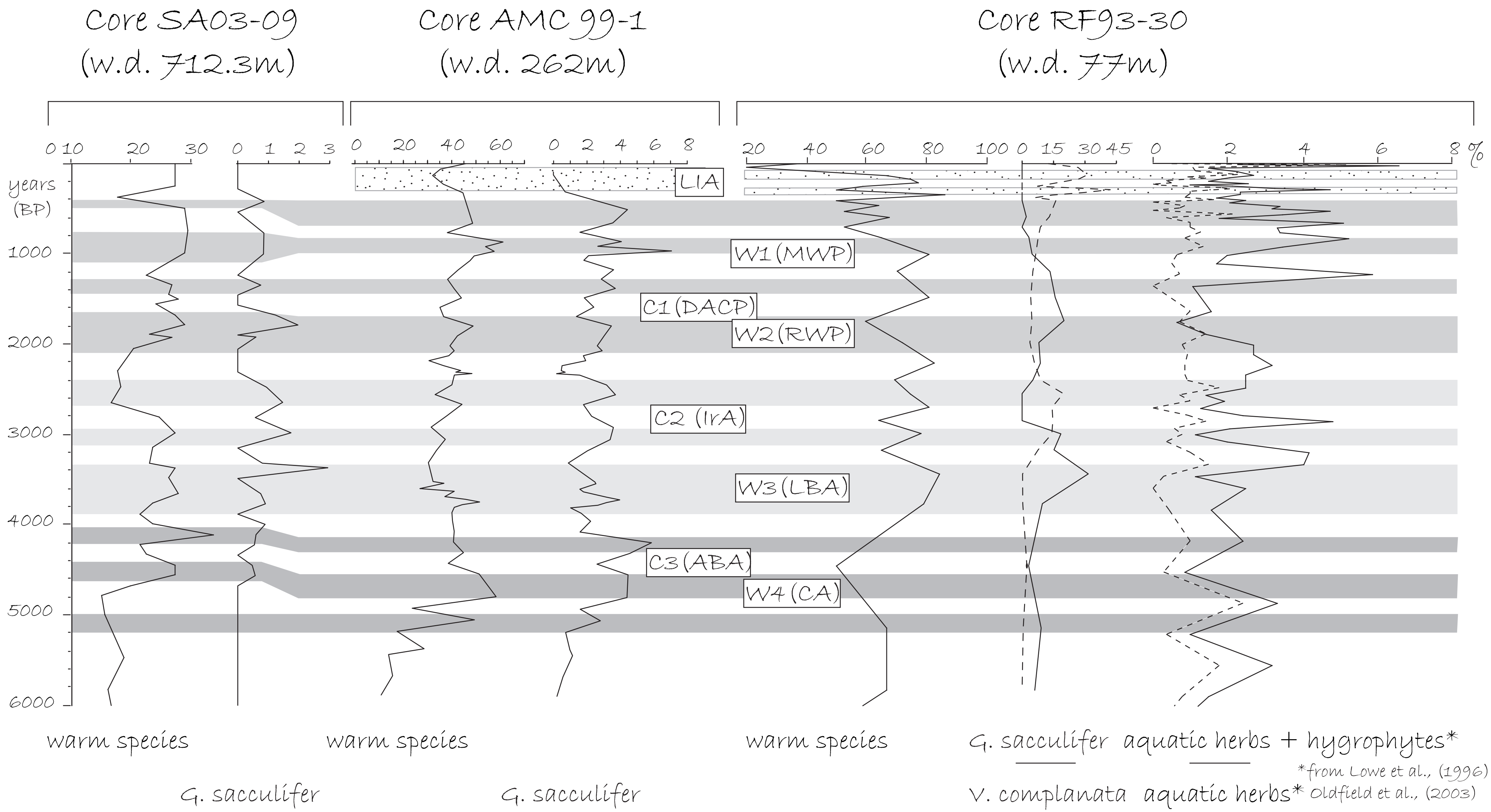

Fig.7a Climate oscillations in the Adriatic record: temperature and humidity proxies. The grey areas highlight the warm-climate, arid phases; rainy, cold-climate periods in white. The dotted stripes mark the Little Ice Age. C1-C3 and W1-W4 correspond to cold and warm-climate oscillations, according to Bond et al. (1997) and Bond (2001). LIA=Little Ice Age; MWP=Medieval Warm Period; DACP=Dark Age Cold Period; RWP=Roman Warm Period; IrA=Iron Age; LBA=Late Bronze Age; ABA=Ancient Bronze Age; CA=Copper Age.

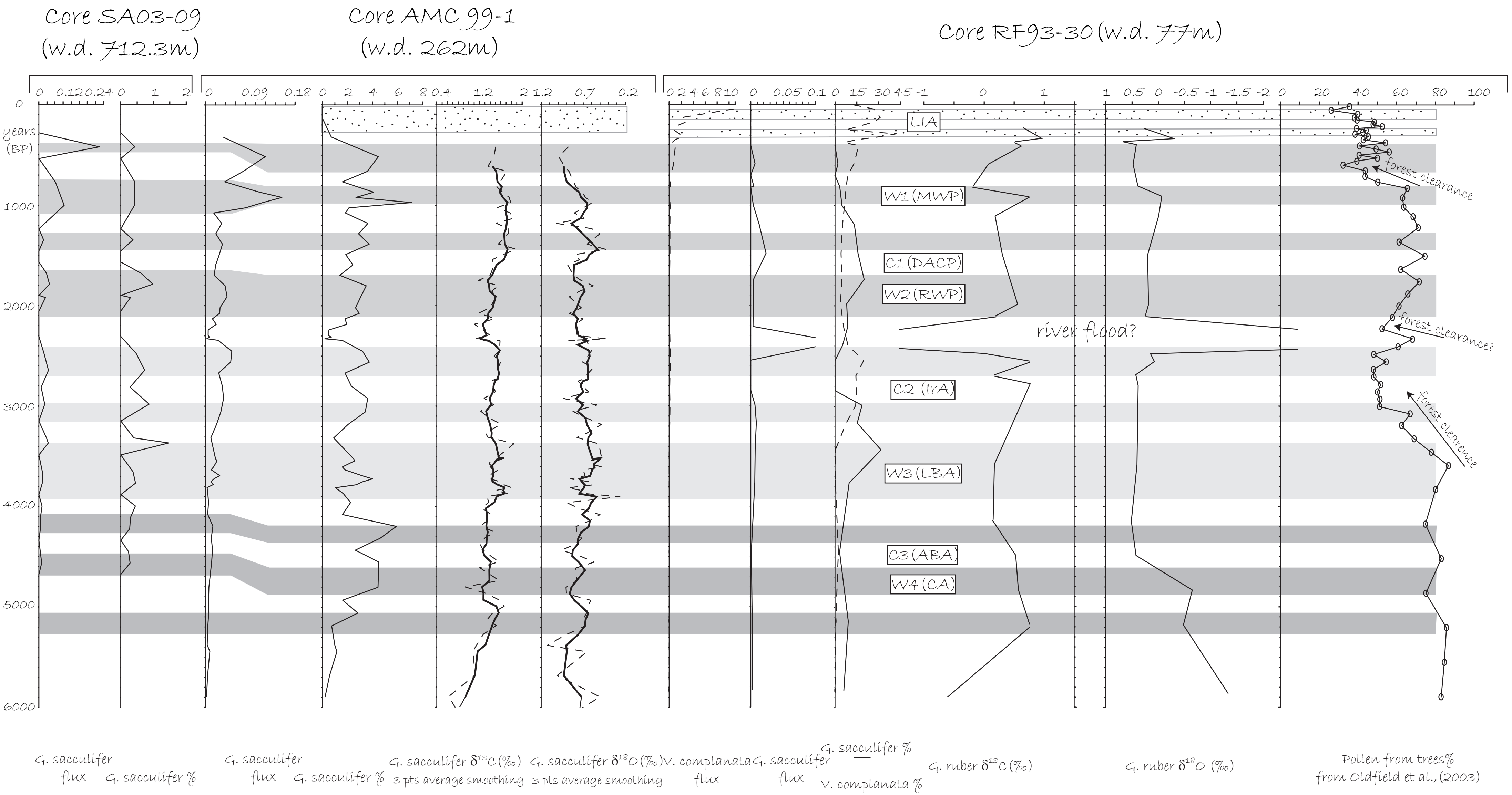

Fig.7b Climate oscillations in the Adriatic record and proxies for human impact (pollen) and abrupt events (stable isotopes). The grey areas highlight the warm-climate, arid phases; rainy, cold-climate periods in white. The dotted stripes mark the Little Ice Age. C1-C3 and W1-W4 correspond to cold and warm-climate oscillations, according to Bond et al. (1997) and Bond (2001). LIA=Little Ice Age; MWP=Medieval Warm Period; DACP=Dark Age Cold Period; RWP=Roman Warm Period; IrA=Iron Age; LBA=Late Bronze Age; ABA=Ancient Bronze Age; CA=Copper Age.

Short term oscillations	Adriatic Sea	Western Mediterranean (Sbaffi et al., 2001)	North Atlantic (de Menocal et al., 2000)	Tirol (Veggiani, 1986, Mayr, 1964)	North Atlantic (Bond, 2001)	SW Ireland (Bond et al., 1997)	North America? (Campbell et al., 1998)	SW Ireland (McDermott et al., 2001)	Tagus prodelta (Bartels-Jònsdòttir et al., 2006)	North Atlantic (Bianchi & McCave 1999)	Alps (Frisia et al., 2003)	NADW-HE (Alley, 1998)	Bermuda Rise (Keigwin and Pickart, 1999)	Overall (Crowley & North, 1991)	Overall (Mayewski et al., 2004)	Forcing events
LIA1 (Little Ice Age)	1865AD	-	1870AD	1820-1810AD	1850-1350AD	-	1900-1500AD	1800-1650AD	1350-1850AD	-	1840-1798AD	-	1850-1600AD	1890-1810AD	-	1883AD Krakatoa eruption, 1815AD Tambora eruption, 1830-1810AD Dalton minimum
LIA2 (Little Ice Age)	1689AD	-	1500AD	1630-1590AD		-		1550-1350AD		1550AD	1698-1650AD	-		1690-1650AD	since 1350AD	1715-1645AD Maunder minimum
C0 (transition)	1400-1200AD	-	-	1250-1150AD	-	-	-	-	1400-1000AD	-	-	-	1400-1200AD	-	-	1325-1285 Wolf minimum
W1 (MWP) (Medieval Warm Period)	1200-600AD	-	1300-800AD	1150-750AD	1350-1000AD	-	1500-600AD	1350-750AD	1000-500AD	1250-900AD	-	-	1100-800AD	1300-1100AD/1000-600AD	-	-
C1 (DACP) (Dark Age Cool Period)	600-350AD	1000-400AD	800AD-0	750-400AD	1000-400AD	550AD	600AD-150BC	750-300AD	500-400AD	1000-500AD	-	1200-600AD	800-200AD	1000-500AD	750-950AD	536AD Rabaul eruption; end of Maya civilization
W2 (RWP) (Roman Warm Period)	350AD-150BC	400AD-0	0-800BC	400AD-300BC	400AD-600BC	-	150-1050BC	300AD-1000BC	400AD-150BC	100AD	-	-	-	-	-	-
C2 (Iron Age)	750-950BC	0-1600BC	800-1400BC	900-700BC	600-1350BC	750-850BC	650-800BC/1050-1300BC	1000-2600BC?	-	-	-	300-1000BC	-	500-2500BC	550-1550BC	-
W3 (Mid/Late Bronze Age)	1350-1800BC	1600-2800BC	1400-2300BC	-	1350-1650BC	-	-		-	-	-	-	-		-	1470BC Santorini eruption
C3 (Ancient Bronze Age)	2300-2550BC	2800-3000BC	2300-2700BC	-	1650-2700BC	2150-2350BC	1650-1800BC		-	-	-	1800-2300BC	-		1850-2250BC	End of Accadian and Egyptian civilizations
W4 (Copper Age/Eneolithic)	2550-2800BC	-	2800-3300BC	-	2700-3200BC	-	-	2600-3000BC	-	-	-	-	-	-	-	-
C4 (m.f.s./Final Neolithic)	3500BC	-	3500BC onset of more arid conditions	-	3200-4000BC (C4)	3850-3950BC (C4)	-	-	-	-	-	3300-3900BC (C4)	-	-	3000-4000BC (C4)	-

Table II. The climatic oscillations defined for the Adriatic have been compared with records derived from other areas. Coherent time intervals inside the main cooling phases are shaded in grey. Ages are expressed as years AD/BC. C0-C4 refer to cool climate oscillations, W1-W4 to warm climate oscillations, according to Bond et al., 1997.

Fig. 7b, provide information about the anthropogenic signal, identifying intervals of forest clearance around 3600, 2400 and 700 years BP. The possible role of human impact during these intervals does not find a similarly well-defined expression in deeper and distal areas, and probably affects only relatively proximal environments. In fact, the occurrence of a rather uniform and steady benthic microfauna in both AMC99-1 and SA03-09 cores suggests that the sea floor in the basins was not perturbed by terrigenous inputs of continental origin. Moreover, in these distal contexts only the surface-water dweller planktic foraminifers display some oscillations in their relative abundances. These variations appear to match with the climate variability on super-regional extents. Therefore, even if any anthropogenic signal reached more distal areas, their intensity would have been hardly appreciable and difficult to disentangle from the climatic overprint. The local signal in the Mid Adriatic Deep records detectable changes only in the case of abrupt and catastrophic events, like, for instance, the major river floods discussed above. Therefore, the distal and less river-affected records provide precious archives, preserving the climatic signal in great detail.

References

Alley, R. B. (1998). Icing the North Atlantic. *Nature*, 392, 335-337.

Amman, C. M., G. A. Meehl, and W. M. Washington (2003). A monthly and latitudinally varying volcanic forcing dataset in simulations of twentieth century climate. *Geophysical Research Letters*, 30 (12), 1657.

Ariztegui, D., A. Asioli, J. J. Lowe, F. Trincardi, L. Vigliotti, F. Tamburini, C. Chondrogianni, C. A. Accorsi, M. Bandini Mazzanti, A. M.Mercuri, S. Van der Kaars, J. A. McKenzie, F. Oldfield (2000). Paleoclimate and the formation of sapropel S1: inferences from Late Quaternary lacustrine and marine sequences in the central Mediterranean region. *Paleoceanography, Paleoclimatology, Paleoecology*, 158, 215-240.

Arz, H. W., F. Lamy, J. Pätzold, P.J. Müller, M. Prins (2003). Mediterranean Moisture Source for an Early-Holocene Humid Period in the Northern Red Sea. *Science*, 300, 118-121.

Asioli, A. (1996). High resolution Foraminifera biostratigraphy in the Central Adriatic basin during the Last Deglaciation: a contribution to the PALICLAS project. In*: Guilizzoni, P., Oldfield, F. (Eds.), Palaeoenvironmental Analysis of Italian Crater lake and Adriatic Sediments (PALICLAS). Memorie del'Istituto Italiano di Idrobiologia* 55, 197–218.

Barmawidjaja, D. M., F. J. Jorissen, S. Puskaric, G. J. Van Der Zwaan (1992). Microhabitats selection by benthic foraminifera in the northern Adriatic Sea. *Journal Foraminifera Research*, 22 (4), 297-317.

Bartels-Jónsdóttir, H. B., K. L. Knudsen, F. Abrantes, S. Lebreiro, J. Eiríksson (2006). Climate variability during the last 2000 years in the Tagus Prodelta, western Iberian Margin: benthic foraminifera and stable isotopes. *Marine Micropaleontology* 59, 83–103.

Bé, A. W. H., D. S. Tolderlund (1971). Distribution and ecology of living planktonic Foraminifera in surface waters of the Atlantic and Indian Oceans. In: Funnell, B.M., Riedel, W.R. (Eds.), *The Micropaleontology of the Oceans*. pp.105–149.

Berger A., and M. F. Loutre (2002). An Exceptionally Long Interglacial Ahead?. Science 297, 1287-1288.

Bianchi, G. G., N. McCave (1999). Holocene periodicity in North Atlantic climate and deep-ocean flow south of Iceland. *Nature* 397, 515–517.

Blanc-Vernet, L. (1969). Contribution à l'étude des foraminifères de Méditerranée. These. Rec. Trav. Mar. Endoume. 64, 281 pp.

Bond, G., W. Showers, M. Cheseby, R. Lotti, P. Almasi, P. deMenocal, P. Priore, H. Cullen, I. Hajdas, G. Bonani (1997). A pervasive millennial-scale cycle in North Atlantic Holocene and Glacial Climates. *Science* 278, 1257–1266.

Bond, G. B., W. Showers, M. Elliot et al. (1999). The North Atlantic's 1-2 kyr climate rhythm: relation to Heinrich events, Dansgaard-Oeschger cycles and the Little Ice Age. In: *Clark, P. U., Webb, R. S. and Keigwin, L.D. (eds.). Mechanisms of Global Climate Change at Millennial Time Scales.* Washington DC, AGU, pp. 35-58.

Bond, G., B. Kromer, J. Beer, R. Muscheler, M. N. Evans, W. Showers, S. Hoffmann, R. Lotti-Bond, I. Hajdas, G. Bonani (2001). Persistent solar influence on North Atlantic climate during the Holocene. *Nature*, 294, 2130-2136.

Boyle, E. A., and L. D. Keigwin (1987). North Atlantic thermoaline circulation during the past 20,000 years linked to high-latitude surface temperatures. *Nature* 330, 35-40.

Bradley, R. S., and P. D. Jones (1992). When was the "Little Ice Age"? In: *Mikami, T. (ed.). Proceedings of the International Symposium on the Little Ice Age Climate*. Tokyo, Dept. of Geography, Tokyo Metropolitan University, pp. 1-4.

Bradley, R. S. (2003). Climate forcing during the Holocene. In Mackay, A., Battarbee, R. W., Birks, H. J. B. and Oldfield, F. (eds.). Global Change in the Holocene. London, Arnold, pp.10-19.

Broccoli, A. J., K. W. Dixon, T. L. Delworth, T. R. Knutson, and R. J. Stouffer (2003). Twentieth-century temperature and precipitation trends in ensemble climate simulations including natural and anthropogenic forcing. *Journal of Geophysical Research* 108, ACL 16-1-16-13.

Broecker, W. S. (1994). Massive iceberg discharges as triggers for global climate change. *Nature*, 372, 421-424.

Broecker, W. S., S. Sutherland, and T. –H. Peng (1999). A Possible 20th Century Slowdown of Southern Ocean Deep Water Formation, *Science*, 286, 1132-1135.

Campbell, I. D., C. Campbell, M. J. Apps, N. W. Rutter, A. B. G. Bush (1998). Late Holocene ~1500 yr climatic periodicities and their implications. *Geology* 26 (5), 471-473.

Capotondi, L., A. M. Borsetti, C. Morigi (1999). Foraminiferal ecozones, a high resolution proxy for the late Quaternary biochronology in the central Mediterranean Sea. *Marine Geology* 153, 253-274.

Cattaneo, A., A. Correggiari, L. Langone, and F. Trincardi (2003). The late-Holocene Gargano subaqueous delta, Adriatic shelf: Sediment pathways and supply fluctuations. *Marine Geology*, 193, 61-91.

Cattaneo, A. , F. Trincardi, L. Langone., A. Asioli, P. Puig (2004). Clinoform Generation on Mediterranean Margins. Oceanography, vol. 17, n. 4, pp. 104-117.

Churchill, D. M., R. W. Galloway, and G. Singh (1978). Closed lakes and the paleoclimatic record. In: *Climatic Change and Variability, A Southern Perspective*. A. B. Pittock, L. A. Zillman (Eds.). Cambridge Univ. Press, Cambridge, p.264.

Civitarese, G. M. Gacic, V. Cardin, and V. Ibello (2005). Winter Convection Continues in the Warming Southern Adriatic. *Eos*, v. 86, n. 45, 8, pp. 445-451.

Clapperton, C. M., D. E. Sugden, J. Birnie, and M. J. Wilson (1989). Late glacial and Holocene glacier fluctuations and environmental change on South Georgia, Southern Ocean. *Quaternary Research* 31, 210-228.

Cook, E. R., J. G. Palmer, and R. D. D'Arrigo (2002). Evidence for a "Medieval warm Period" in a 1100 year tree-ring reconstruction of past austral summer temperatures in New Zealand. *Geophysical Research Letters* 29 (14), 12-1-12-4.

Cooke, E. R., and G. C. Jacoby (1979). Evidence for quasi-periodic July drought in the Hudson Valley, New York. *Nature* 282, 390-392.

Correggiari, A., F. Trincardi, L. Langone, M. Roveri (2001). Styles of failure in heavily sedimented highstand prodelta wedges on the Adriatic shelf. *Journal of Sedimentary Research* 71/2, 218–236.

Crowley, T. J., and G. R. North (1991). Paleoclimatology. *Oxford Monographs on Geology and Geophysics* #18.

Crowley, T. J., and K., -Y. Kim (1999). Modeling the temperature response to forced climate change over the last six centuries. *Geophysical Research Letters* 26, 1901-1904.

Crowley, T. J. (2000). Causes of climate change over the past 1000 years, *Science* 289, 270-277.

Dansgaard, W., S. J. Johnson, N. Reeh, N. Gundestrup, H. B. Clausen, and C. U. Hammer (1975). Climate changes, Norsemen, and modern man. *Nature* 255, 24-28.

de Menocal, P., J. Ortiz, T. Guilderson, M. Sarnthein (2000). Coherent high- and low-latitude climate variability during The Holocene warm period. *Science* 288, 2198– 2202.

de Menocal, P. (2001). Cultural responses to climate change during the late Holocene. *Science* 292, 667-673.

Devine, J. D., H. Sigurdsson, A. N. Davis, and S. Self (1984). Estimates of sulphur and chlorine yield to the atmosphere from volcanic eruptions and potential climatic effects. *Journal of Geophysical Research* 89, 6309-6325.

Diz, P., G. Francés, C. Pelejero, J. O. Grimalt, F. Vilas (2002). The last 3000 years in the Ría de Vigo (NW Iberian Margin): climatic and hydrographic signals. *Holocene* 12, 459–468.

Domack, E. W., T. A. Mashiotta, L. A. Burkley, and S. E. Ishman (1993). 300 year cyclicity in organic matter preservation in Antarctic fjord sediments. In: *The Antarctic Paleoenvironment: A Perspective on Global Change, Part 2*, edited by J. P. Kennett, J. and D. A. Warnke, *Antarctic Research Service*, 60, American Geophysical Union, Washington D.C., 265-272.

Domack, E. W., A. Leventer, S. Root, J. Ring, E. Williams, D. Carlson, E. Hirshorn, W. Wright, R. Gilbert, and G. Burr (2003). Marine sedimentary record of natural environmental variability and recent warming in the Antarctic Peninsula. In: *Antarctic Peninsula Climate Variability. Historical and Paleoenvironmental Perspectives*, edited by E. W. Domack, A. Leventer, A. Burnett, R. Bindschadler, P. Convey, and M. Kirby, *Antarctic Research Service*, 79, American Geophysical Union, Washington D.C., 205-224.

Fairbanks, R. G., M. Sverdlove, R. Free, P. H. Wiebe, A. W. H. Bé (1982). Vertical distribution of living planktonic foraminifera from the Panama Basin. *Nature* 298, 841–844.

Feynman, J., and P. F. Fougere (1984). Eighty-eight year periodicity in solar-terrestrial phenomena confirmed. *J. Geophys. Res.* 89, 3023-3027.

Free, M., and A. Robock (1999). Global warming in the context of the Little Ice Age. *Journal of Geophysical Research-Atmospheres* 104, 19057-70.

Frignani, M., L. Langone, M. Ravaioli, D. Sorgente, F. Alvisi, S. Albertazzi (2005). Fine-sediment mass bilance in the western Adriatic continental shelf over a century time scale. *Marine Geology*, 222-223, 113-133.

Frisia, S., A. Borsato, N.Preto, F. McDermott (2003). Late Holocene annual growth in three Alpine stalagmites records the influence of solar activity and the North Atlantic Oscillation on winter climate. *Earth and Planetary Science Letters* 216, 411-424.

Fronval, T., and E. Jansen (1996). Rapid changes in ocean circulation and heat flux in the Nordic seas during the last interglacial period. *Nature* 383, 806-810.

Gleissberg, W. (1966). Ascent and descent in the eighty-year cycle of solar activity. *J. Br. Astron. Assoc.* 76, 265-268.

Grove, J. M. (1988). *The Little Ice Age.* Methuen, New York.

Haug, G. H., K. A. Hughen, D. M. Sigman, L. C. Peterson, and U. Rohel (2001). Southward migration of the intertropical convergence zone through the Holocene. *Science* 293, 1304-1308.

Hemleben, C., M. Spindler and O. R. Anderson (Eds.), (1989) *Modern planktic foraminifera*, Springer-Verlag, New York.

Hendy, E. J., M. K. Gagan, C. A. Alibert, M. T. McCulloch, J. M. Lough, P. J. Isdale (2002). Abrupt decrease in tropical Pacific sea surface salinity at end of Little Ice Age. *Science* 295, 1511-1514.

Hermelin, J. O. R., and Shimmield, G. B. (1990). The importance of the oxygen minimum zone and sediment geochemistry in the distribution of recent benthic foraminifera in the Northwest Indian Ocean. *Marine Geology*, 91, 1-29.

Hong, Y. T., B. Hong, Q. H. Lin, Y. X. Zhu, Y. Shibata, M. Hirota, M. Uchida, X. T. Leng, H. B. Jiang, H. Xu, H. Wang, L. Yi (2003). Correlation between Indian Ocean summer monsoon and North Atlantic climate during the Holocene. *Earth and Planetary Science Letters* 211, 371-380.

Hughes, M. K., and H. F. Diaz (1994). Was there a "Medieval Warm Period" and if so, where and when?*Climatic Change* 26, 109-142.

Jones, P. D., and M. E. Mann (2004). Climate over past millennia. *Review of Geophysics* 42.

Jorissen, F. J. (1988). Benthic foraminifera from the Adriatic Sea; principles of phenotypic variation. *Utrecht Micropaleontological Bullettins*, 37, 174 pp.

Jorissen, F. J., D. M. Barmawidjaja, S. Puskaric, G. J. Van der Zwaan (1992). Vertical distribution of benthic foraminifera in the northern Adriatic Sea: the relation with the organic flux. *Marine Micropaleontology*, 19, 131-146.

Jorissen, F. J., A. Asioli, A. M. Borsetti, L. Capotondi, J. P. De Visser, F. J. Hilgen, E. J. Rohling, K. Van Der Borg, C. Vergnaud-Grazzini, W. J. Zachariasse (1993). Late Quaternary central Mediterranean biochronology. *Marine Micropaleontology* 21, 169–189.

Juillet-Leclerc, A., and H. Schrader (1987). Variations of upwelling intensity recorded in varved sediment from the Gulf of California during the past 3,000 years. *Nature* 329, 146-149.

Keigwin, L. D. and E. A. Boyle (2000). Detecting Holocene changes in thermohaline circulation. *Proceedings of the National Academy of Sciences USA*, 97: 1343-1346.

Kuhn, J., K. G. Libbrecht, and R. Dicke (1988). The surface temperature of the sun and changes in the solar constant. *Science* 242, 908-911.

Lamb, H. H. (1965). The early Medieval warm epoch and its sequel. *Paleoceanography, Paleoclimatology, Paleoecology*, 1, 13-37.

Lamb, H. H. (1969). Climatic fluctuations. In: *World Survey of Climatology*, v. 2. H. E. Landsberg (Ed.). Elsevier, Amsterdam, pp. 173-249.

Lamb, H. H. (1979). Climatic variation and changes in the wind and ocean circulation: The Little Ice Age in the North Atlantic. *Quaternary Research* 11, 1-20.

Legrand, M., R. J. Delmas (1987). A 220-year continuous record of volcanic H_2SO_4 in the Antarctic ice sheet. *Nature* 327, 671-676.

Lowe,J. J., C. A. Accorsi, M. Bandini Mazzanti, A. Bishop, S. Van der Kaars, L. Forlani, A. M. Mercuri, C. Rivalenti, P. Torri, and C. Watson (1996). Pollen stratigraphy of sediment sequences from lakes Albano and Nemi (near Rome) and from the central Adriatic, spanning the interval from oxygen isotope Stage 2 to the present day. In*: Guilizzoni, P., Oldfield, F. (Eds.), Palaeoenvironmental Analysis of Italian Crater lake and Adriatic Sediments (PALICLAS). Memorie del'Istituto Italiano di Idrobiologia* 55, 71–98.

Lowe, J. J., and M. J. C. Walker (1997). *Reconstructing Quaternary Environments*, 2nd edn. Harlow, Pearson Prentice Hall.

Magny, M., C. Miramont, O. Sivan (2002). Assessment of the impact of climate and anthropogenic factors on Holocene Mediterranean vegetation in Europe on the basis of palaeohydrological records. *Palaeogeography, Palaeoclimatology, Palaeoecology* 186, 47-59.

Marchant, R., and H. Hooghiemstra (2004). Rapid environmental change in African and South American tropics around 4000 years before present: a review. *Earth-Science Reviews* 66, 217–260.

Marret, F. J. Maley, J. Scourse (2006). Climatic instability in west equatorial Africa during the Mid- and Late Holocene. *Quaternary International* 150, 71–81.

Marsh, N. D., and H. Svensmark (2000). Low cloud properties influenced by cosmic rays. *Physics Review Letters* 85, 5004-5007.

Matthes, F. E. (1939). Report of committee on glaciers. *Trans. Am. Geophys. Union* 20, 518-523.

Mayr, F. (1964). Untersuchungen über Ausmass und Folgen der Klima und Gletscherschwankungen seit dem Beginn der postglazialen Wärmezeit, *Zeitschrift für Geomorphologie*, N. F. Bd. 8, H. 3, Berlin, pp.257-285.

McDermott, F., D. P. Mattey, C.Hawkesworth (2001). Centennial-scale Holocene climate variability revealed by a high-resolution speleothem $\delta^{18}O$ record from SW Ireland. *Science* 294, 1329-1331.

Miao, Q., and R. C. Thunell (1993). Recent deep sea benthic foraminiferal distribution in the South China and Sulu Seas. *Marine Micropaleontogy*, 22, 1-32.

Morgan, V. I. (1985). An oxygen isotope climate record from the Law Dome, Antarctica. *Climate Change* 7, 415-426.

Mosley-Thompson, E., and L. G. Thompson (1982). Nine centuries of microparticle deposition at the South Pole. *Quat. Res.* 17, 1-13.

Murdmaa, I., L. Polyak, E. Ivanova, N. Khromova (2004). Paleoenvironments in Russkaya Gavan' Fjord (NW Novaya Zemlya, Barents Sea) during the last millennium. *Palaeogeography, Palaeoclimatology, Palaeoecology* 209, 141–154.

Murray, J. W. (1991). Ecology and paleoecology of benthic foraminifera. Longman Scientific e Technical Ed.

Negri , A., L. Capotondi and J. Keller (1999). Calcareous nannofossils, planktonic foraminifera and oxygen isotopes in the late Quaternary sapropels of the Ionian Sea, Mar. Geol., 157, 89– 103.

Nicholson, S. E. (1978). Climatic variations in the Sahel and climate predictability. In: *Milankovitch and Climate*. A. L. Berger, J. Imbrie, J. Hays, G. Kukla, and J. Saltzman (Eds.). D. Reidl, dordrecht, Netherlands, pp. 637-652.

Noren, A. J., P. R. Bierman, E. J. Steig, A. Lini, and J. Southron (2002). Millennial-sacle storminess variability in the northeastern United States during the Holocene epoch. *Nature* 419, 821-824.

Oldfield, F., A. Asioli, C. A. Accorsi, A. M. Mercuri, S. Juggins, L. Langone, T. Rolph, F. Trincardi, G. Wolff, Z. Gibbs, L. Vigliotti, M. Frignani, K. van der Post, N. Branch (2003). A high resolution late Holocene palaeo environmental record from the central Adriatic Sea. *Quaternary Science Reviews* 22, 319–342.

Oldfield, F. (2005). *Environmental Change, key issues and Alternative Approaches*. Cambridge University Press.363pp.

Overpeck, J., K. Hughen, D. Hardy, R. Bradley, R. Case, M. Douglas, B. Finney, K. Gajewski, G. Jacoby, A. Jennings, S. Lamoureux, A. Lasca, G. MacDonald, J. Moore, M. Retelle, S. Smith, A. Wolfe, G. Zielinski (1997). Arctic environmental change of the last four centuries. *Science* 278, 1251-1256.

Parkinson, C. L. (1990). Search for the Little Ice Age in Southern Ocean sea ice records. *Ann. Glac.* 14, 221-225.

Phleger, F. B., and A. Soutar (1973). Production of benthic foraminifera in three east Pacific oxygen minima. *Micropaleontology*, 19, 1, p. 110-115.

Pisias, N. G. (1979). Model for paleoceanographic reconstructions of the California Current during the last 8000 years. *Quaternary Research* 11, 373-386.

Pittock, A. B. (1983). Solar variability, weather and climate: an update. *Quart. J. R. Met. Soc.* 109, 23-55.

Pfister, C. (1985). *CLIMHIST: A weather data bank for Central Europe*. Meteostat, Bern, 1525-1863.

Pujol, C. and C. Vergnaud Grazzini (1995). Distribution patterns of live planktic foraminifera as related to regional hydrography and productive systems of the Mediterranean sea. *Marine Micropaleontology,* 25, 187–217.

Rathburn, A. E., and B. H. Corliss (1994). The ecology of living (stained) deep-sea benthic foraminifera from the Sulu Sea. *Paleoceanography*, 9, (1), 87-150.

Renssen, H., V. Brovkin, T. Fichefet, H. Goosse (2006). Simulation of the Holocene climate evolution in Northern Africa: the termination of the African Humid Period. *Quaternary International* 150, 95–102.

Ribes, E. (1990). Astronomical determinations of solar variability. *Philosophical Transactions of the Royal Society*, A330, 487-497.

Rind, D., and J. Overpeck (1993). Hypothesized causes of decade-to-century-scale climatic variability: climate model results.*Quaternary Science Reviews* 12, 357-374.

Sbaffi, L., F. C. Wezel, N. Kallel, M. Paterne, I. Cacho, P. Ziveri, N. Shakleton (2001). Response of the pelagic environment to paleoclimatic changes in the central Mediterranean Sea during the late Quaternary. *Marine Geology* 178, 39-62.

Schilman, B., M. Bar-Matthews, A. Almogi-Labin, and B. Luz (2001). Global climate instability reflected by eastern Mediterranean marine records during the late Holocene. *Palaeogeography, Palaeoclimatology, Palaeoecology* 176, 157-176.

Schilman, B., A. Almogi-Labin, M. Bar-Matthews, and B. Luz (2003). Late Holocene productivity and hydrographic variability in the eastern Mediterranean inferred from benthic foraminiferal stable isotopes. *Paleoceanography*, 18 (3), 1064, doi:10.1029/2002PA000813.

Sen Gupta, B. K., and M. L. Machain-Castillo (1993). Benthic foraminifera in oxygen-poor habitats. *Marine Micropaleontology*, 20, 183-204.

Sgarrella, F., and M. Moncharmont Zei (1993). Benthic Foraminifera of the Gulf of Naples (Italy): systematics and autoecology. *Bollettino della Società Paleontologica Italiana*, 32, (2), 145-264.

Shindell, D. T., G. A. Schmidt, M. E. Mann, and G. Faluvegi (2004). Dynamic winter climate response to large tropical volcanic eruptions since 1600. *Journal of Geophysical Research* 109, D05104.

Sofia, S. (1984). Solar variability as a source of climate change. In: *Climate Processes and Climate Sensitivity*. J. E. Hansen and T. Takahashi (Eds.). Geophys. Mono 29. Am. Geophys. Union, Washington, D. C., pp. 202-206.

Sprovieri, R., E. Di Stefano, A. Incarbona, M. E. Gargano (2003). A high-resolution record of the last deglaciation in the Sicily Channel based on foraminifera and calcareous nannofossil quantitative distribution. *Palaeogeography, Palaeoclimatology, Palaeoecology* 202, 119-142.

Stahle, D. W., M. K. Cleaveland, and J. G. Hehr (1985). A 450-year drought reconstruction for Arkansas, United States. *Nature* 316, 530-532.

Stahle, D. W., M. K. Cleaveland, and J. G. Hehr (1988). North Carolina climate changes reconstructed from tree rings: A.D. 372 to 1985. *Science* 240, 1517-1519.

Stahle, D. W., and M. K. Cleaveland, (1988). Texas drought history reconstructed and analyzed from 1698 to 1980. *J. Clim.* 1, 59-74.

Stine, S. (1994). Extreme and persistent drought in California and Patagonia during medieval time. *Nature* 369, 546-549.

Stothers, R. B. (1984). The great Tambora eruption in 1815 and its aftermath. *Science* 224, 1191-1198.

Stuiver, M., and T. F. Braziunas (1988). The solar component of the atmospheric ^{14}C record. In: *Secular Solar and Geomagnetic Variations in the Last 10,000 Years.* F. R. Stephenson and A. W. Wolfendale (Eds.). Kluwer, Dordrecht, Netherlands, pp. 245-266.

Stuiver, M., and T. F. Braziunas (1989). Atmospheric ^{14}C and century-scale solar oscillations. *Nature* 338, 405-408.

Stuiver, M. and P. J. Reimer (1993). Extended ^{14}C data base and revised CALIB 3.0 ^{14}C age calibration program. *Radiocarbon* 35, 215-230.

Svensmark, H., and E. Friis-Christensen (1996). Variation of cosmic ray flux and global cloud coverage –a missing link in solar-climate relationships. *Journal of Atmospheric and Solar-Terrestrial Physics* 59, 1225-1232.

Thompson, L. G., E. Mosley-Thompson, M. E. Davis, K. A. Henderson, H. H. Brecher, V. S. Zagorodnov, T. A. Mashiotta, P. -N. Lin, V. N. Mikhalenko,D. R. Hardy, J. Beer (2002). Kilimanjaro ice core records: evidence of Holocene climate change in tropical Africa. *Science* 298, 589-593.

Trincardi, F., F. Foglini, G. Verdicchio, A. Asioli, A. Correggiari, D. Minisini, A. Piva, A. Remia, D. Ridente, M. Taviani (2007). The impact of cascading currents on the Bari Canyon System, SW-Adriatic Margin (Central Mediterranean). *Marine Geology*, in press.

Turchetto, M., A. Boldrin, L. Langone, S. Miserocchi, T. Tesi and F. Foglini (2007). Particle transport in the Bari canyon (southern Adriatic Sea). *Marine Geology*, in press.

Van Geel, B., J. Buurman, H. T. Waterbolk (1996). Archaeological and palaeoecological indications of an abrupt climate change in The Netherlands, and evidence for climatological teleconnections around 2650 BP. *Journal of Quaternary Science* 11, 451–460.

Veggiani, A. (1986). Le fluttuazioni del clima dal XVIII al XX secolo. I cicli di Bruckner. *Bollettino della società Torricelliana di Scienze e Lettere*, 37, 1-56, Faenza.

Verhallen, P. J. J. M. (1991). Late Pliocene to Early Pleistocene Mediterranean mud-dwelling foraminifera; influence of changing environment on community structure and evolution. *Utrecht Micropal. Bull.* 40, 187 pp.

Wilson, A. T., C. H. Hendy, and C. P. Reynolds (1979). Short-term climatic changes and New Zealand temperatures during the last millennium. *Nature* 279, 315-317.

Zhang, D. (1984). Synoptic-climate studies of dust fall in China since historic times. *Scientia Sinica (Ser. B)* 27, 825-836.

Zheng, S., and L. Feng (1986). Historical evidence of climatic instability above normal in cool periods in China. *Scientia Sinnica (Ser. B)* 29, 441-448.

PART III

Revised integrated foraminifera biostratigraphy for the last 60kyr in the Central and Southern Adriatic

1. INTRODUCTION

A biostratigraphy, based on evolutionary appearance and extinction events, is poorly applicable as regards the Late Quaternary foraminifera, because of the short duration of this time interval. Then, in literature, in particular for high resolution studies, a common approach is the definition of local bioevents, based on the detection of paleoenvironmental/paleoceanographic variations, defined by qualitative and quantitative changes in the foraminifera assemblages (e. g. warming, cooling of the water column).

Some attempts have been done in the recent literature (Jorissen et al., 1993; Asioli, 1996; Capotondi et al., 1999; Ariztegui et al., 2000; Asioli et al., 2001; Sbaffi et al., 2001; Oldfield et al., 2003; Sprovieri et al., 2003), trying to define a more and more detailed ecobiostratigraphy for the last 20 kyr. Indeed, a sequence of ecobiozones has been recognised for different Mediterranean basins (e.g. Central Adriatic, Southern Adriatic, Sicily Channel, Tyrrhenian Sea) characterised by different hydrological patterns. Therefore, each sequence of ecozones, the chronology of which is based on ^{14}C datings and oxygen isotope stratigraphy, must be viewed in a local contest.

However, the comparison of the local ecobiozones allowed to recognize common paleoceanographic trends during the Last Glacial-Interglacial Transition (LGIT) and Holocene in the Central Mediterranean, in spite of the dissimilarities in the local hydrology and of the different methods of analysis (such as different sieve meshes used by the authors, from 0.063 mm to 0.150 mm). Then, an (eco)biostratigraphy, based on a sequence of ecozones correlatable among them and to be interpreted as the response to a common paleoclimatic forcing, is presently available for the Central Mediterranean for the LGIT and Holocene.

Following this approach, this thesis, on the basis of cores collected within the EC-EUROSTRATAFORM project, in addition to the records already discussed in Parts I and II, can update and revise the presently available ecobiostratigraphy for the Adriatic. This updating, mainly based on foraminifers' analyses, is corroborated by several other independent proxies, obtained from the same material, such as radiocarbon datings, isotope stratigraphy, and tephrochronology. An extremely detailed seismic stratigraphic knowledge of the Adriatic basin allowed the collection of very expanded sediment successions, aiming to reach a highest degree of resolution for particular time intervals. These new detailed records, along with data available from literature (as regards time intervals not specifically analysed in the PhD thesis, for instance Younger Dryas and

Bølling-Allerød), consented to extend, improve and better constrain the present Adriatic ecostratigraphy of the last 60000 years.

2. MATERIALS AND METHODS

Table I reports the cores analysed in this thesis, whose location is shown in Fig. 1. As regards the Southern Adriatic basin, three cores have been selected among those collected during SAGA-2003 cruise, after the semi-quantitative analyses of all the dataset of cores. The choice favoured those cores presenting the most continuous and undisturbed record. Cores CM92-43 and A236P09, have been already studied and published, but the interval corresponding to the early Holocene (pre-Boreal) has been re-sampled in higher detail for the goal of this thesis, and these new results are here presented.

BASIN	CORES	LATITUDE	LONGITUDE	WATER DEPTH	CORE RECOVERY
Central Adriatic	PRAD1-2	42°40.347826'N	14°46.135565'E	185.5 m	71.2 m
Southern Adriatic	SA03-01	41°30.2516'N	17°10.7780'E	566.8 m	13.87 m
	SA03-03	41°56.8860'N	16°57.4564'E	470.7 m	10.44 m
	SA03-11	41°37.2444'N	17°28.4023'E	1125.9 m	15.98 m
Channel of Sicily	A236 P09	36°47.299'N	14°12.316'E	609.0 m	8 m
Adriatic literature	CM92-43	42°53.124'N	14°43.568'E	252 m	9.75 m

Table !. Location of the studied cores.

The proxies which concurred in defining the Adriatic stratigraphic framework are:

- Quantitative analysis on planktic and benthic foraminifers' assemblage. The procedure to achieve the washed samples and the methodology adopted for the analytical counting have been the same for the whole dataset of cores, and have already been discussed in Part I, chapter 1. Samples have been analysed every 10 cm on average in all the cores, except for cores CM92-43 and A236 P09, which have been analysed only in the interval corresponding to the Pre-Boreal period, every 3 cm on average. Core SA03-11 rely only on semi-quantitative data (courtesy of Asioli, 2004).

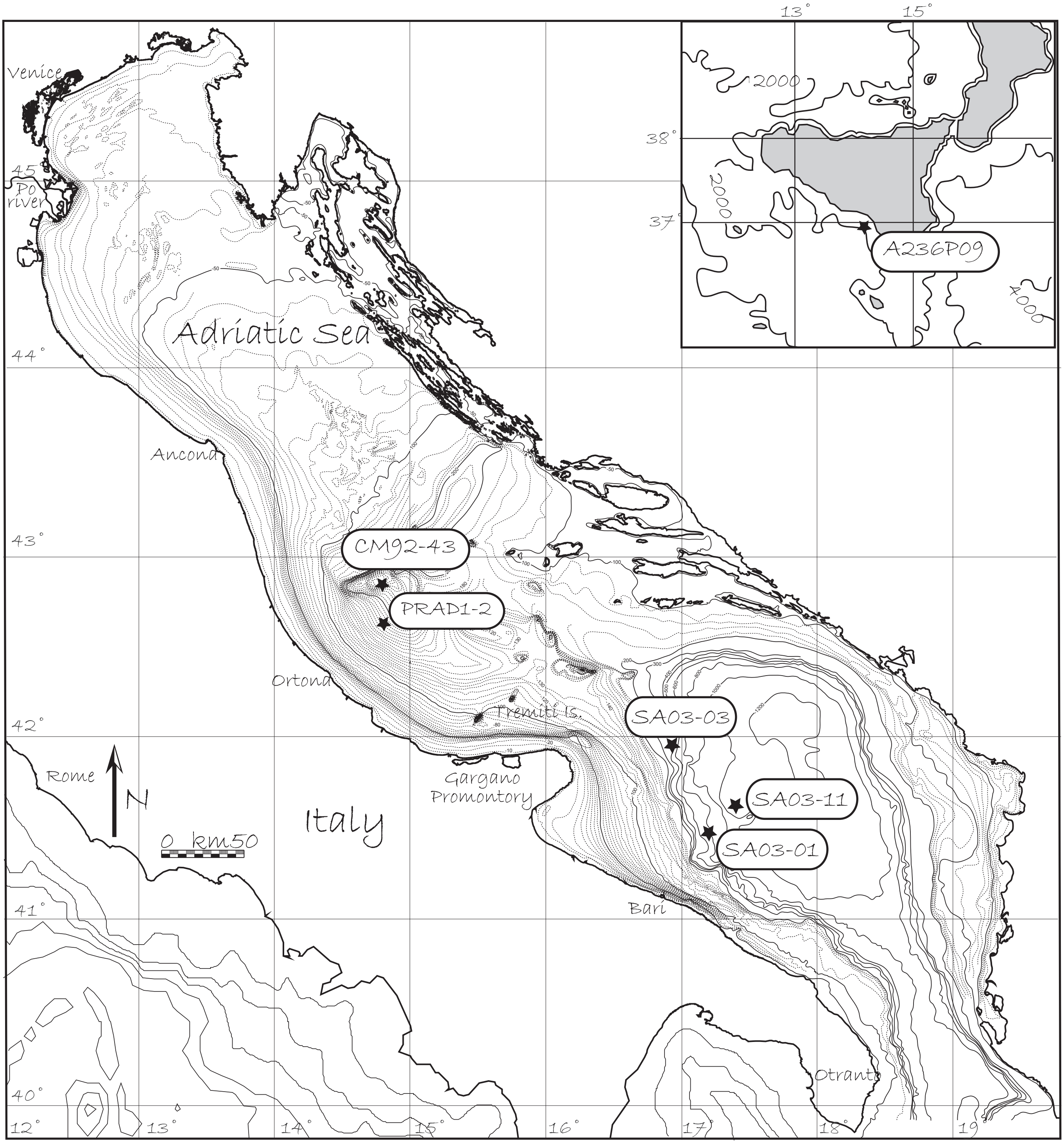

Fig. 1 Location of the cores analysed in this Part.

- Oxygen stable isotope stratigraphy. The analyses of the stable isotope record of borehole PRAD1-2 (planktic, *G. bulloides*, and benthic, *B. marginata*) and of cores SA03-01, SA03-03 and SA03-11 (only planktic, *G.* bulloides) have been performed at the Leibniz Laboratory for Radiometric Dating and Stable Isotope Research, CAU Kiel, Germany (Dr. Nils Andersen). As regards the analytical proceedings, the reader is referred to Part I, Chapter 1. Isotopic analyses (planktic, *G. ruber*) have also been performed for core A236 P09, at ETH, Zurich (Dr. Daniel Aritzegui) in 2001.
- Identification of tephra levels. Tephrochronologic information have been achieved by Abbott (2005), for core SA03-11, by Bourne (2006) for borehole PRAD1-2, and by Blockley (written personal communication, 2006), as regards the tephra layer positioned in core SA03-03, at cm 23-24.
- ^{14}C AMS datings were performed at the Poznan Radiocarbon Laboratory, Poland, (Dr. Tomasz Gozlar), from the size fraction >250 μm, on benthic monospecific samples (*Elphidium crispum* or *Hyalinea balthica*) as regards borehole PRAD1-2, on planktic monospecific samples (*G. bulloides*) for cores SA03-03 and SA03-11, as well as one level (cm 450-451, *G. ruber*) inside core SA03-01. ^{14}C AMS datings for cores A236 P09 and for the other samples of core SA03-01 have been performed on mixed planktic (and, only in one case benthic) foraminifers' assemblage. Samples from core A236 P09 were analysed at the Centre for Accelerator Mass Spectrometry, Lawrence Livermore National Laboratory, California, USA, in 2001 by Dr. Michaele Kashgarian. The obtained dataset was then processed using the recently published online calibration program by Fairbanks et al. (2005) (http://radiocarbon.LDEO.columbia.edu) for ages between 0 and 55000 years. Fairbanks et al. (2005), Butzin et al., (2005) and Cao et al., (2007) calculated reservoir output is 262 and 254 years for Rimini and Barletta sites, respectively. Then, a mean age of 258 years has been used for the calibration (^{14}C age minus 258=^{14}C age to be calibrated). The estimated reservoir age for the Sicily Channel (calculated on the geographic coordinates of core A236 P09) is 255 years. The calibrated ages are reported in years BP and referred to 2σ. The ^{14}C ages of core CM92-43 are published in literature (Asioli, 1996, Langone et al., 1996), but they have been recalibrated according to Fairbanks et al. (2005), Butzin et al., (2005), and Cao et al., (2007). Table II reports all the ^{14}C AMS datings available and their respective calibrated ages.

Sample name	Lab N°	Age ^{14}C	Material	Calibrated Age (yr BP, 2σ)	
				mean	std dev
PRAD1-2 S8 40-42	Poz- 16129	14930±90BP	*E. crispum*	17894	168
PRAD1-2 S10 60-62	Poz-16130	16530±100BP	*E. crispum*	19423	83
PRAD1-2 S17 60-62 H	Poz-16132	23390±150BP	*H. balthica*	27654	181
PRAD1-2 S17 60-62 E	Poz-16131	24130±150BP	*E. crispum*	28435	178
PRAD1-2 S19 40-42	Poz-17321	28960±270BP	*E. crispum*	33450	482
PRAD1-2 S21 40-42	Poz-17320	36700±600BP	*H. balthica*	41626	376
SA03-01 450-451	Poz- 16141	9080±50BP	*G.ruber*	9892	138
SA03-01 460-461	Poz- 16142	9360±50BP	Mixed planktic	10245	33
SA03-01 500-501	Poz- 16144	9860±60BP	Mixed planktic	10968	147
SA03-01 1330-1334 P	Poz- 17322	14300±70BP	Mixed planktic	16916	148
SA03-01 1330-1334 B	Poz- 17323	15030±80BP	Mixed benthic	18060	195
SA03-03 20-21	Poz- 16161	16140±120BP	*G. bulloides*	19079	142
SA03-03 100-101	Poz- 16162	19920±240BP	*G. bulloides*	23547	336
SA03-03 230-231	Poz- 16164	26070±180BP	*G. bulloides*	30970	158
SA03-03 360-361	Poz- 16165	32300±400BP	*G. bulloides*	36928	396
SA03-03 560-561	Poz- 16166	40000±800BP	*G. bulloides*	43998	670
SA03-11 1560-1561	Poz- 16160	30700±300BP	*G. bulloides*	35385	251
A236 P09 377-378	Poz- 16158	9340±120BP	Mixed planktic	10245	130
A236 P09 397-398	Poz- 16159	9910±110BP	Mixed planktic	11045	183
A236 P09 519-522	CAMS 75693	10870±40BP	Mixed planktic	12607	41
A236 P09 609-612	CAMS 75694	12460±40BP	Mixed planktic	14096	60

Table II. ^{14}C AMS calibrated ages (years BP).

3. RESULTS

3.1 Core SA03-01

All the main ecozones already defined in literature (Asioli et al., 2001) have been recognised in this core, from the upper GS-2 on (Fig. 2). The boundary between GS-2 and GI-1 ecozones is marked by the LCO of *G. scitula*. The GI-1 (Bølling-Allerød) ecozone is characterised by five climatic oscillations, the colder of which (GI-1d and GI-1b) showing peaks in *G. bulloides*. GI-1d cold oscillation is also characterised by the presence of deep infaunal taxa. Warm climate oscillations GI-1e, GI-1c and GI-1a are represented by higher abundances of *G.* ex gr. *ruber*, coupled with peaks in *G. inflata* and *G. truncatulinoides*. *N. pachyderma* r. c. is common with alternating abundances, as well as planktic and benthic foraminifers' concentrations, which show more populated warmer intervals and poorly represented colder oscillations. GS-1 (Younger Dryas) ecozone can be subdivided in an earlier phase, with common *N. pachyderma* r. c., a central part characterised by higher abundances of *G. bulloides* and *G. glutinata* and a later phase dominated by *G. quinqueloba*, also showing a reprise of *G.* ex gr. *ruber* and of *G. inflata*. The benthic microfauna is dominated by

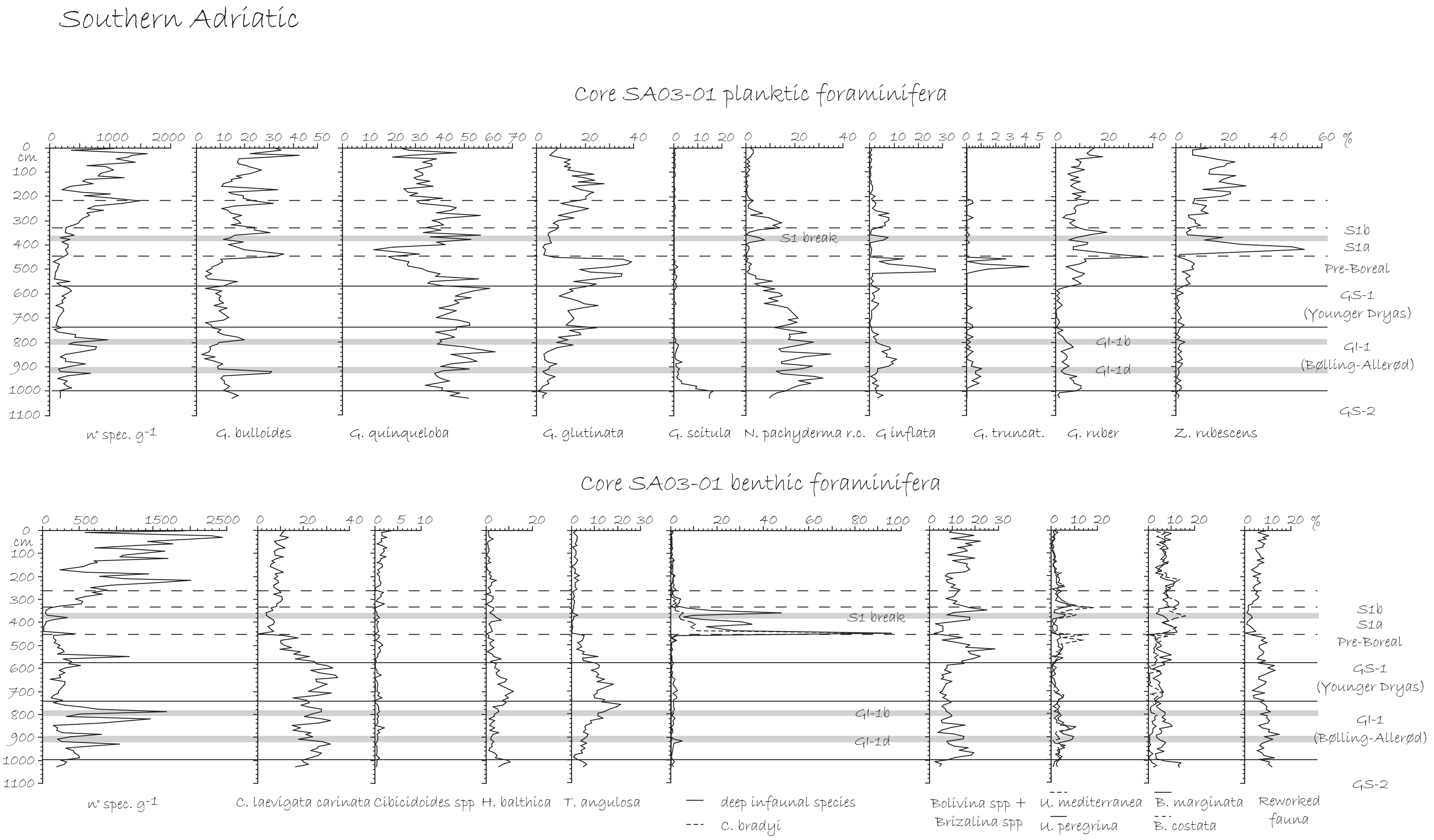

Fig. 2. Main results of foraminifers' quantitative analyses for core SA03-01.

C. laevigata carinata, associated with *H. balthica* in the early GS-1, and by *T. angulosa* in the mid- and upper- Younger Dryas. The base of the Holocene (Pre-Boreal ecozone) shows a sensible reprise of warm planktic species, such as *G.* ex gr. *ruber*, and by a decreasing-upwards trend in colder water species, like *G. quinqueloba* and *N. pachyderma* r. c.. Temperate climate planktic species characterise this ecozone, and *G. glutinata* shows two alternating peaks, in favour of two distinct intervals dominated by *G. inflata*, with common *G. truncatulinoides*. The benthic assemblage at the base of the Holocene shows a reversal between *C. laevigata carinata*, dominating the Younger Dryas, in favour of *B. dilatata*. The Sapropel 1 ecozone is splitted in two distinct phases, as already known from literature: the earlier, called S1a, presents more intense features, and it is characterised by highest abundances of warm planktic species like *Z. rubescens* and *G.* ex gr. *ruber*. This latter species shows the common occurrence of its pink variety, characterised by a thinner test and by inflated chambers. S1a phase is represented by a benthic assemblage dominated by deep infaunal dwellers. In particular, the base of the ecozone presents a level mainly (and almost only) composed by *Cassidulinoides bradyii*, occurring in the same position all over the Southern Adriatic. S1b phase shows similar features, although with lower percentages. *G. bulloides* peaks at the base and at the top of the ecozone. Globorotalids and *N. pachyderma* r. c., absent during the two sapropelic phases, characterise the Sapropel 1 break between them. The end of Sapropel 1 ecozone (top of S1b phase) shows a reprise of epifaunal benthic species, like *C. pachyderma*, as well as of *G. inflata* and *N. pachyderma* r. c.. The last (common) occurrence of these planktic species at the top of this ecozone, approximating the maximum flooding surface, shows the onset of the ecozone characterising the last 6000 years, corresponding to the deposition of the Highstand System Tract. This latter ecozone is dominated by warm planktic species, such as *G.* ex gr. *ruber* and *Z. rubescens*, and the benthic assemblage is mainly composed by *B. dilatata*, coupled with *C. laevigata carinata*. Even if the always common reworked benthic taxa oblige to take some caution in the ecobiostratigraphic reconstruction of this core, nevertheless all the ecozones are quite well identifiable and the signal, even if sometimes lightly disturbed, is always apparent.

3.2 Core SA03-03

The ecozone corresponding to MIS 5 is characterised by common *G.* ex gr *ruber*, coupled by common *G. inflata* and by the presence of *G. truncatulinoides*. The benthic microfauna shows sensible peaks of *Bolivina* and *Brizalina* spp, and common deep infaunal taxa. Moreover, it must be noted that the oxygen stable isotope record shows the presence of a very light peak at the base of the core, which seems to correspond, for comparison with PRAD1-2 isotopic record, to the 5.5 substage. This observation consent to infer a very condensed sedimentation for MIS5 in this core. For this reason, this warm isotope stage has not been considered in the following Adriatic ecobiozonation. The LO of *G. truncatulinoides* approximates the boundary between MIS5 and MIS4 ecozones. MIS4 is dominated by *G. quinqueloba*, and shows the presence of *N. pachyderma* l. c.. The benthic microfauna is composed by *C. laevigata carinata*, coupled with *H. balthica*. MIS3 shows a reprise of *G. inflata*, characterising the lower part of the ecozone, and having its LO at about halfway, where warm planktic species, present in a scattered trend, become more common. *N. pachyderma* r. c. presents an alternating trend (better pointed out by a 3 points average smoothing), mostly reversing with *G. bulloides*. The benthic microfauna is composed by *T. angulosa*, coupled with *H. balthica*. The upper MIS3 shows the presence of *N. pachyderma* l. c.. MIS2 is composed by abundant *G. quinqueloba*, with common *G. bulloides* and *G. scitula*. Benthos consists of *C. laevigata carinata* and *Bolivina* and *Brizalina* spp. Deep infaunal taxa show a scattered presence all over MIS3 and part of MIS2. The results are plotted in Fig. 3.

3.3 Core SA03-11

The characterization of the ecobiostratigraphy of the core only rely on semi-quantitative data (Fig. 4), and particularly focus on its lower tract (from 6 to 16 m), consisting of MIS3 and MIS2 ecozones. MIS3 is composed by *N. pachyderma* r. c., *G. scitula*, *G. bulloides*, *G. quinqueloba* and *G. glutinata*, with the scattered frequent presence of *G.* ex gr. *ruber*. MIS2 presents almost the same planktic assemblage, (*G. scitula*, *N. pachyderma* r. c., *G. bulloides*, *G. quinqueloba* and *G. glutinata*). *G. ruber* gr. occurs in rare percentages only in few levels. The benthic assemblage is composed by *C. pachyderma*, *U. peregrina*, *B. albatrossii*, *B. dilatata*, *H. elegans*, *S. sellii*, *C. laevigata carinata*. Several dysoxic levels, consisting of benthic *F. tenuis, S. complanata*, *G. affinis* and *Chilostomella* are present all over the ecozone. *S. sellii* extinguishes at the top of MIS2 ecozone.

3.4 Cores CM92-43 and A236 P09

Both the cores present the same peaks of *G. truncatulinoides* and *G. inflata* (Fig. 5) already discussed for core SA03-01. These peaks have been dated and show consistent ages, the lower

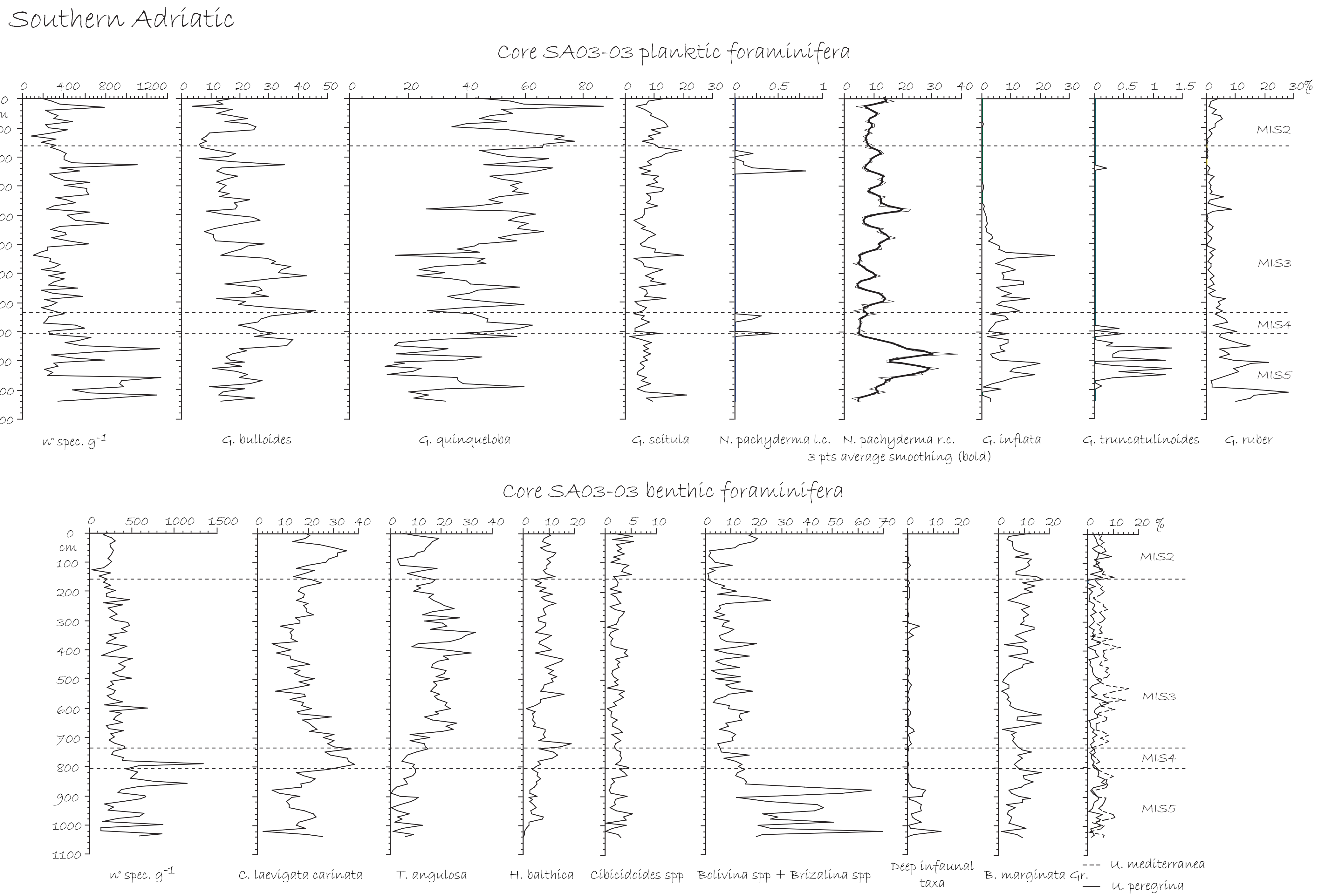

Fig. 3. Main results of foraminifers' quantitative analyses for core SA03-03.

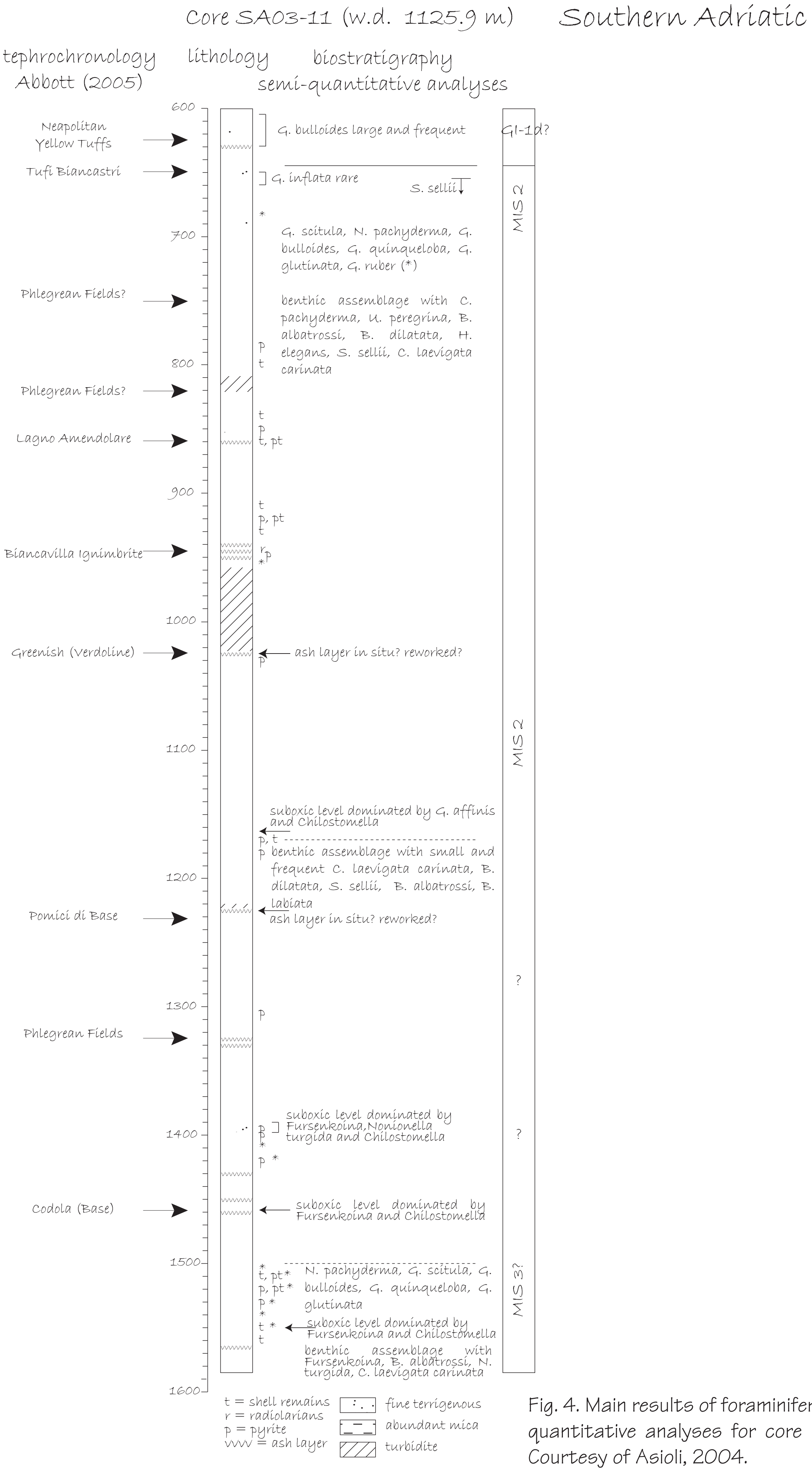

Fig. 4. Main results of foraminifers' semi-quantitative analyses for core SA03-11. Courtesy of Asioli, 2004.

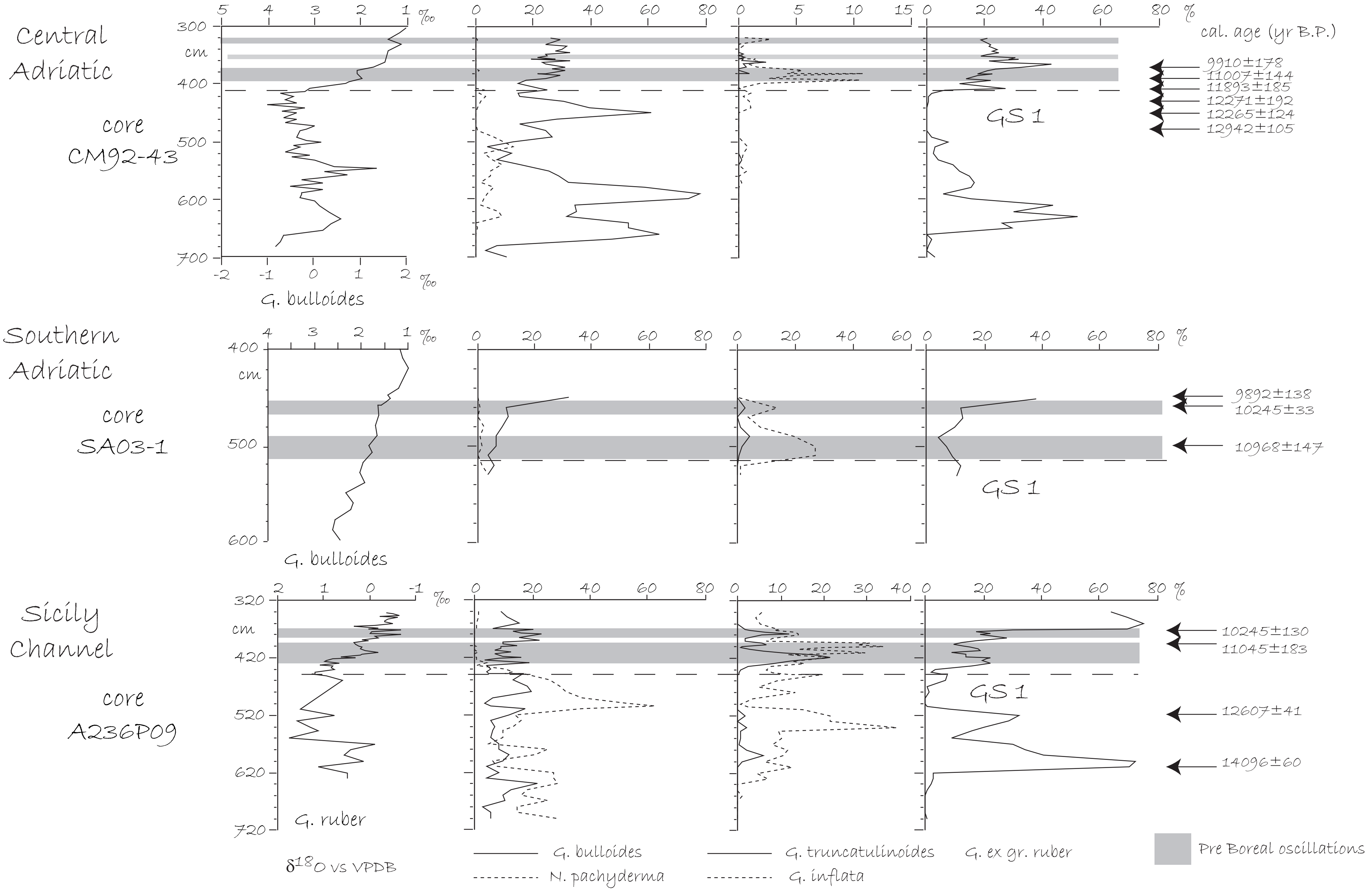

Fig. 5. Foraminifers' main trends for cores CM92-43, SA03-01 and A236 P09 as regards the Pre-Boreal ecobiozone.

attesting around 11000 years, the upper between 10000 and 9800 years. These peaks seem to be reversed with the abundances of *G.* ex gr. *ruber*; and appear to be coupled with light shifts towards heavier values of the $\delta^{18}O$ curve.

4 DISCUSSION

The methodology adopted to define the ecobiostratigraphic framework for the Southern Adriatic is here described; then a description of the main ecozones identified for Central and Southern Adriatic basins is presented.

4.1 Stratigraphic correlation between cores SA03-01, SA03-03 and SA03-11

Cores SA03-01 and SA03-03 have been analysed on a quantitative way as regards planktic and benthic foraminifers' assemblages, aiming to achieve a continuous succession of ecozones for the Southern Adriatic, spanning the last 60000 years (MIS4-MIS1). Unfortunately, though, foraminifers' assemblages are not so peculiar or diversified inside MIS2 to discern whether the two cores overlap or not. For this reason, this issue has been addressed to tephrochronology, coupled with ^{14}C datings, comparing and matching the obtained results with those deriving from core SA03-11, which present an impressively expanded MIS2, and which can boast of a detailed analytical study of the many macro- and micro- tephra levels present (Abbott, 2005).

The upper tephra layer of core SA03-03, located at cm 26-27, results geochemically similar to Greenish (Verdoline) eruption, approximately dated at 17560 years BP. One ^{14}C AMS dating, performed close to this level (20-21 cm), though, gives a slightly older age, that is 19079±142 years BP, suggesting that the volcano-clastic level of core SA03-03, does probably not correspond to the Greenish (Verdoline) event (Blockley, written personal communication, 2006), but could belong to the same volcanic series of eruptions. This tephra layer was anyhow geochemically compared to the lowest volcanic level present in core SA03-01, and they resulted to be quite different in their composition. Two ^{14}C AMS datings, performed on planktic and benthic foraminifers in correspondence of the tephra layer of core SA03-01, located at cm 1330-1334, gave an age of 16916±148 and 18060±195 years BP, respectively. The two tephra layers analysed were then compared and matched with those identified in core SA03-11. After this operation, it seems that the tephra analysed in core SA03-01 would occur in a coherent position in respect to tephra Y1 (Biancavilla Ignimbrite), dated at about 17000 years. This would suggest that the succession of ecozones of the two cores could be somehow continuous, or that the gap of lacking record would be very reduced. The stratigraphic framework for Southern Adriatic is summarised in Fig. 6.

4.2 Ecobiostratigraphy

The data achieved by different and independent proxies consented to define the following age-depth models for the cores analysed:

Core SA03-01			
Level (cm bsf)	Corresponding age (years BP)	Event	Source
0	0		
12	550	LO G. sacculifer	this study, part II
220	6000	LO G. inflata	literature (Asioli, 1996)
450	9892	Sapropel S1 base, ^{14}C AMS	this study
460	10245	PB, *G. inflata* peak 2 ^{14}C AMS	this study
500	10968	PB, *G. inflata* peak 1 ^{14}C AMS	this study
575	11987	Top GS-1	literature (Asioli, 1996), recalibrated
740	12943	Bottom GS-1	literature (Asioli, 1996), recalibrated
920	13634	GI-1d event	literature (Asioli, 1996), recalibrated
1332	16916	^{14}C AMS	this study

Table III: age-depth model for core SA03-01

Core SA03-03			
Level (cm bsf)	Corresponding age (years BP)	Event	Source
20	19079	^{14}C AMS	this study
100	23547	^{14}C AMS	this study
230	30970	^{14}C AMS	this study
360	36928	^{14}C AMS	this study
470	43118	LCO G. inflata in MIS3	this study, from PRAD1-2
560	43998	^{14}C AMS	this study
780	62000	MIS4.2	literature (Bassinot et al., 1998)

Table IV: age-depth model for core SA03-03

Core SA03-11			
Level (cm bsf)	Corresponding age (years BP)	Event	Source
0	550	LO *G. sacculifer*	this study, part II
200	6000	LO *G. inflata*	literature (Asioli, 1996)
373	9892	Sapropel S1 base, ^{14}C AMS	this study, from SA03-01

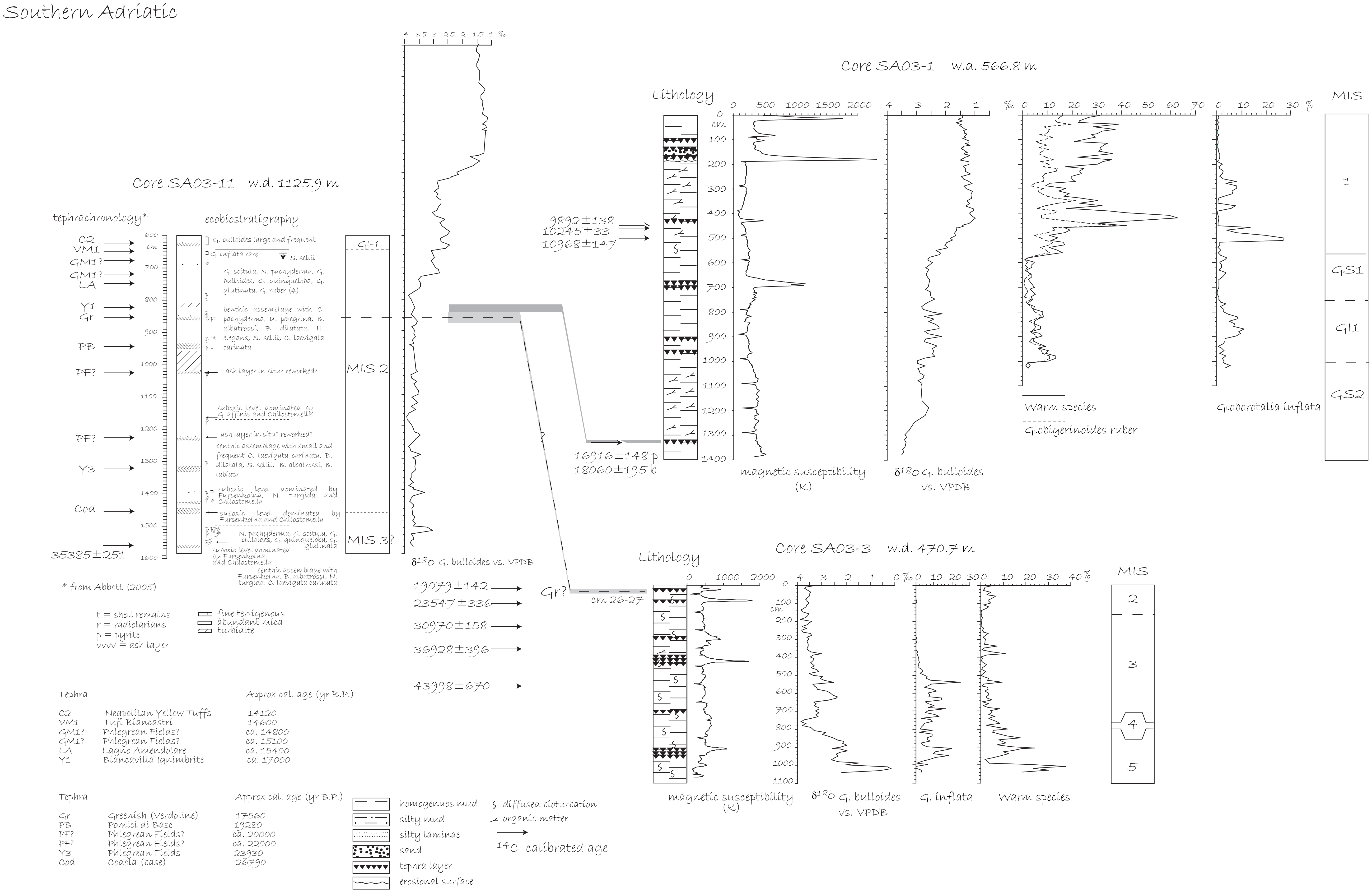

Tephra		Approx cal. age (yr B.P.)
C2	Neapolitan Yellow Tuffs	14120
VM1	Tufi Biancastri	14600
GM1?	Phlegrean Fields?	ca. 14800
GM1?	Phlegrean Fields?	ca. 15100
LA	Lagno Amendolare	ca. 15400
Y1	Biancavilla Ignimbrite	ca. 17000

Tephra		Approx cal. age (yr B.P.)
Gr	Greenish (Verdoline)	17560
PB	Pomici di Base	19280
PF?	Phlegrean Fields?	ca. 20000
PF?	Phlegrean Fields?	ca. 22000
Y3	Phlegrean Fields	23930
Cod	Codola (base)	26790

Fig. 6. Stratigraphic scheme on the correlation of Southern Adriatic cores.

379	10245	PB, *G. inflata* peak 2 ^{14}C AMS	this study, from SA03-01
390	10968	PB, *G. inflata* peak 1 ^{14}C AMS	this study, from SA03-01
420	11987	Top GS-1	literature (Asioli, 1996), recalibrated
490	12943	Base GS-1	literature (Asioli, 1996), recalibrated
610	13634	GI-1d event	literature (Abbott, 2005)
620	14120	C2 tephra layer	literature (Abbott, 2005)
650	14600	VM1 tephra layer	literature (Abbott, 2005)
750	15400	LA tephra layer	literature (Abbott, 2005)
820	17000	Y1 tephra layer	literature (Abbott, 2005)
860	17560	Gr tephra layer	literature (Abbott, 2005)
945	19280	PB tephra layer	literature (Abbott, 2005)
1022	20000	PF? tephra layer	literature (Abbott, 2005)
1233	22000	PF? tephra layer	literature (Abbott, 2005)
1324	23930	Y3 tephra layer	literature (Abbott, 2005)
1459	26790	Cod tephra layer	literature (Abbott, 2005)
1560	33385	^{14}C AMS	this study

Table V: age-depth model for core SA03-11

Core A236 P09			
Level (cm bsf)	Corresponding age (years BP)	Event	Source
377	10245	^{14}C AMS	this study
397	11045	^{14}C AMS	this study
455	11987	Top GS-1	literature (Asioli, 1996), recalibrated

Table VI: age-depth model for core A236 P09

Core CM92-43			
Level (cm bsf)	Corresponding age (years BP)	Event	Source
297	8826	^{14}C AMS	literature (Asioli, 1996), recalibrated
370	9910	^{14}C AMS	literature (Asioli, 1996), recalibrated
390.5	11007	^{14}C AMS	literature (Asioli, 1996), recalibrated
420	11893	^{14}C AMS	literature (Asioli, 1996), recalibrated
433.5	12265	^{14}C AMS	literature (Asioli, 1996), recalibrated

Table VII: age-depth model for core CM92-43

The age-depth model achieved for borehole PRAD1-2 is reported in part I, chapter 1. These age-depth models allowed the definition of the main bioevents and of 16 time-constrained correspondent ecobiozones for the last 60000 years in both the Central and the Southern Adriatic basins, summarised in Figg. 7 (ecobiozones (1-)3-8), 8 (ecobiozone 5) and 9 (ecobiozones

(1-)9-16), and described hereafter. As regards ecobiozones 1 and 2 (last 6000 years), the reader is referred to Part II for a more detailed description.

In Table VII the sequence of the ecozones recognised for Central and Southern Adriatic is summarised. As in some case the age boundary of some ecozone is apparently diachronous between the two basins, in brackets are reported the age boundaries relative to the Central Adriatic.

Ecozone	Description	Age boundary (cal kyr B.P.)
1	Corresponding to the cold climate oscillation known as Little Ice Age, whose base is approximated by the **Last Occurrence of *G. sacculifer***, dated at about 550 years BP. This ecozone has been treated and described in Part II.	0-0.550
2	Corresponding to the deposition in the Adriatic Sea of the Highstand System Tract, whose base, related to the maximum flooding surface, is approximated by the **Last Occurrence of *G. inflata***, dated in the Adriatic at about 6000 years BP. Planktic foraminifers' assemblage is dominated by warm climate-linked species, such as *Globigerinoides* ex gr. *ruber*, *Zeaglobigerina rubescens*, *Orbulina* and *Globigerinoides sacculifer*. *N. pachyderma* r. c. is absent. The reader is referred to Part II for a better description of this ecobiozone.	0.550-6
3	Characterised by the **re-occurrence of *G. inflata* and *N. pachyderma* r.c.**; *G.* ex gr. *ruber* is common (Fig. 7).	6-8
4	Reflecting the deposition of Sapropel1 equivalent in the Adriatic basin. **Its base is defined by the temporary disappearance of G. inflata and by the LO of G. truncatulinoides.** Splitted in two distinct phases, named respectively S1a and S1b, separated by a short break (Fig. 7). *G. inflata* and *N. pachyderma* r. c. are absent during S1 phases, and reappear during the break. The sapropelic intervals consist of a planktic assemblage dominated by *G.* ex gr. *ruber*, common in its *pink* variety, and show increases of *Globigerinella*, *Z. rubescens* and *Globigerinoides tenellus*. The increase in deep infaunal benthic taxa is more evident in the Southern Adriatic record than in the Central Adriatic one, characterised by the common presence of oxic, epifaunal benthic species, as well. The base of the ecozone is approximated in the Southern Adriatic by a level dominated by the benthic dysoxic species *Cassidulinoides bradyi*, event occurring on a local scale. The LO of *G. truncatulinoides* approximates the base of this ecozone, as well, all over the Adriatic basin and the Channel of Sicily. Yet, this boundary shows an apparent diachronism between the Central Adriatic (dated about 9500 years BP) and the Southern basin and the Sicily Channel (dated around 9900 years BP), (Fig. 7), suggesting that the onset of sapropelic conditions occurred later in the Central Adriatic (and in a weaker way).	8-9.5 (9.9)

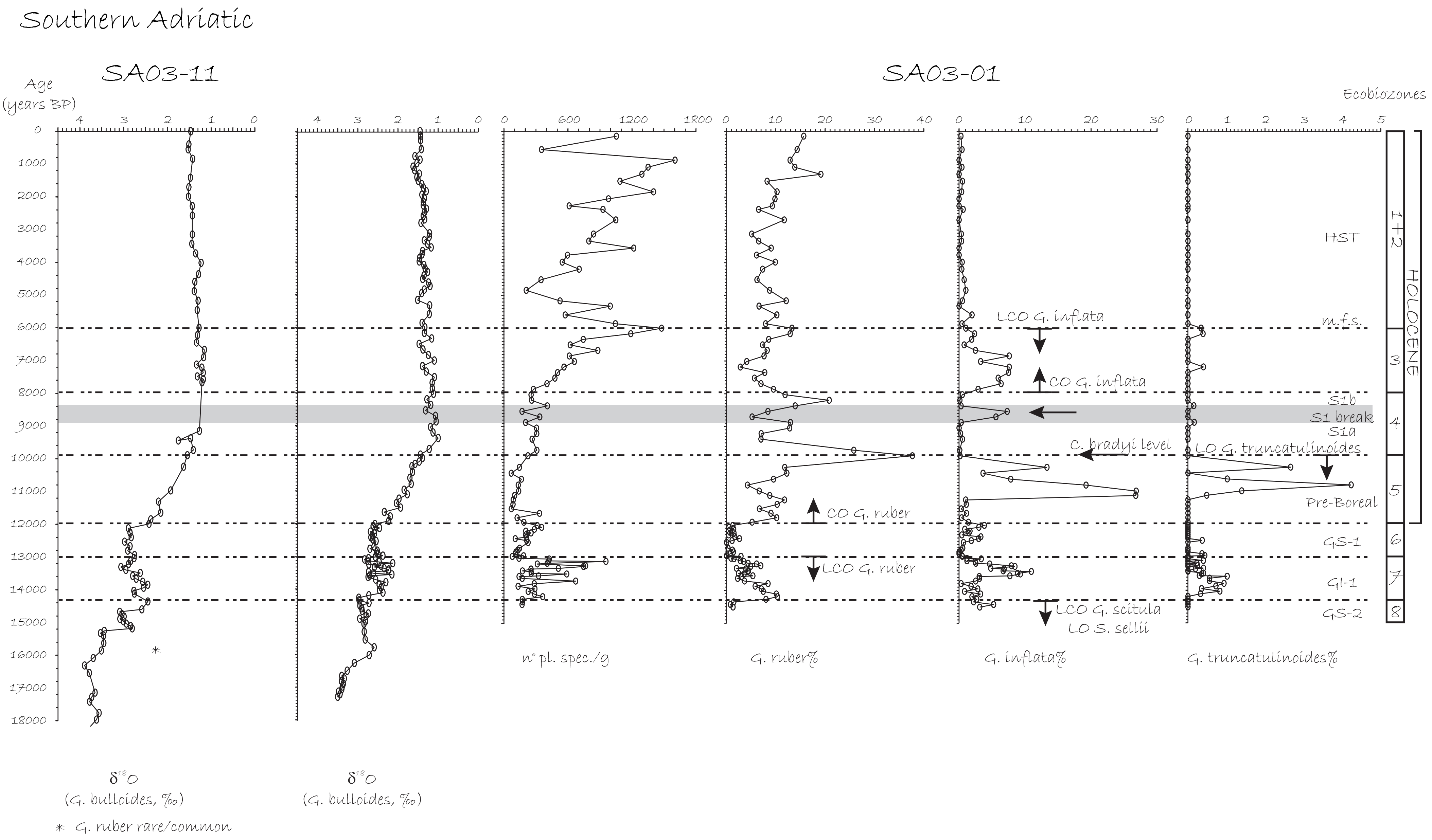

Fig. 7. Main Southern Adriatic ecobiozones for the last 15000 years BP.

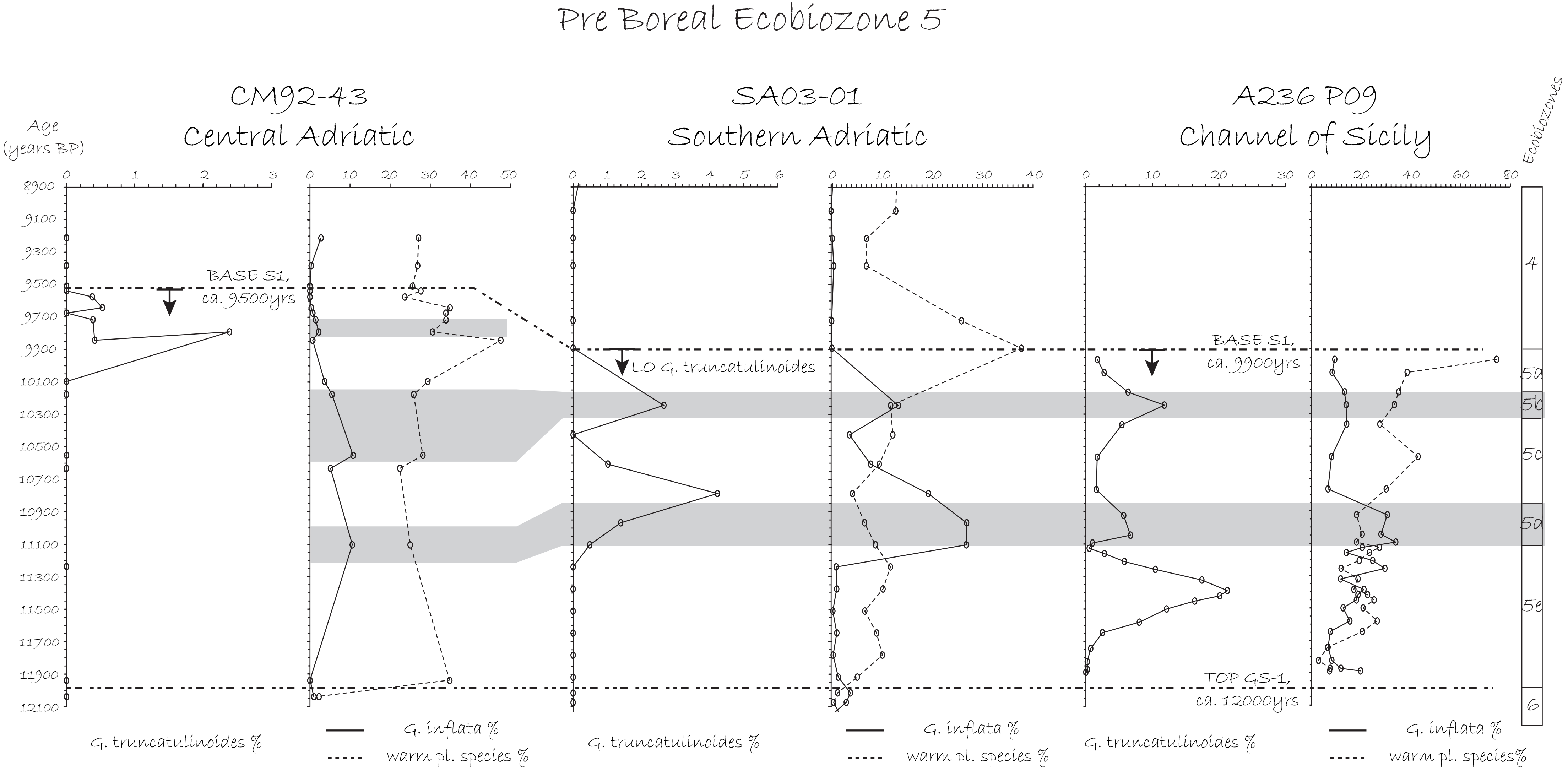

Fig. 8. Main subzones within Pre-Boreal Ecobiozone 5.

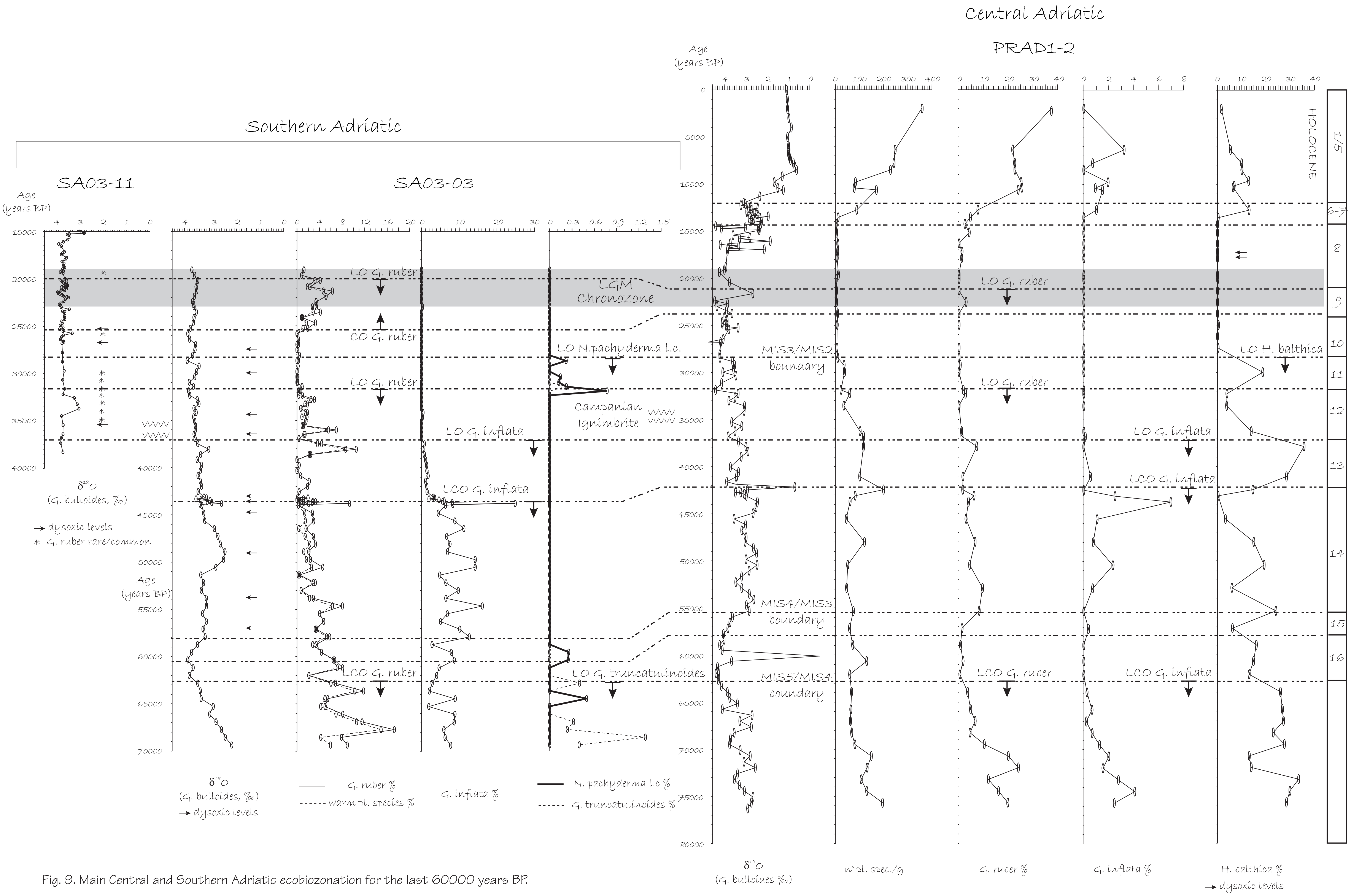

Fig. 9. Main Central and Southern Adriatic ecobiozonation for the last 60000 years BP.

5	Ecozone correspondent to the pre-Boreal interval, characterised by **peaks of *G. inflata***, in opposition of phase with warm planktic species, **and of *Globorotalia truncatulinoides***, and by the **common-abundant presence of *G.* ex gr. *ruber***, *Globigerinita glutinata* and *Globorotalia scitula*. The upper limit of the ecobiozone is diachronous, as described above. The ecobiozone has been subdivided into five subzones (Fig. 8), named 5a-e. Oscillations 5d and 5b are identified by peaks of *G. inflata*, and by a correspondent decrease of *G. ruber*, and have been dated in the Southern Adriatic and in the Sicily Channel at around 11100 and 10220 years BP, respectively. The Central Adriatic shows the same two oscillations, but their occurrence is somehow diachronous. Oscillations 5e, 5c and 5a show a reprise of warm planktic species compared to *G. inflata*; their abundances increase from 5e to 5a subzones. 5e oscillation shows the scattered presence of *G. inflata*, more abundant in the Sicily Channel, rarer in the Southern Adriatic. *G. inflata* is a species common in the Western Mediterranean, and its higher abundance in the Channel of Sicily is coherent. The base of the ecobiozone is dated around 12000 years BP, and correspond to an increase in frequencies of warm planktic species. *G. truncatulinoides* presents peaks, whose occurrence seems too diachronous to use it as a biomarker.	9.5 (9.9)-12
6	The cold climate conditions of Younger Dryas period reflect on the planktic assemblage, composed by abundant *Globigerina quinqueloba*, and by *Globigerina bulloides*, *N. pachyderma* r.c. and *G. glutinata*. *G. scitula* is very scarce. The upper boundary, separating MIS2 from the Holocene, is characterised by a marked increase of *G.* ex gr. *ruber*, and it is dated at around 12000 years BP. The lower boundary of this ecobiozone is dated at around 13000 years BP, and corresponds to the temporary disappearance of warm planktic species (Fig. 7). This ecobiozone has been already described for the Adriatic basin in literature (Asioli, 1996; Asioli et al., 1999; Capotondi et al., 1999).	12-13
7	The Bølling-Allerød ecozone is characterised by **common frequencies of *G.* ex gr. *ruber***, *Orbulina*, *G. bulloides*, **with peaks of *G. inflata* and *G. truncatulinoides*** (Fig. 7). Its subdivision into five distinct phases has already been demonstrated in literature (Asioli, 1996; Capotondi et al., 1999; Asioli et al., 1999, 2001). Event GI-1d, identified by a marked peak of *G. bulloides*, occurring in correspondence of Neapolitan Yellow Tuff (C2) tephra layer, has been dated in this work at 13630 years BP.	13-14.4
8	The ecozone corresponding to GS-2, that is the main phase of MIS2, is characterised by dominant frequencies of *G. quinqueloba*, and by common *G. bulloides, N. pachyderma* r. c. and ***G. scitula***. The **LCO** of this latter species, along with the **LO** of benthic ***Sigmoilina sellii***, characterize the upper limit of the ecobiozone, dated at about 14400 years BP (Fig. 7). ***G. inflata* is absent**. *G.* ex gr. *ruber* remains very rare and shows a scattered distribution. This ecozone also presents levels consisting of dominant deep infaunal taxa, such as the peaks of *Glandulina laevigata* in the Central Adriatic. Planktic specimens are very rare in Central Adriatic.	14.4-22(20)
9	The ecozone is very similar to the previous one, but, in comparison, presents **higher abundances of *G.* ex gr. *ruber***, particularly in the Southern Adriatic	22(20)-23.5(25)

	(Fig. 9) from 25000 to 20000 years BP. This ecozone includes most of the Last Glacial Maximum (LGM) Chronozone, constrained between 23000 and 19000 years BP. The higher abundance of *G.* ex gr. *ruber* during this time interval is a recurrent feature in the Western Mediterranean, as well (e. g. Capotondi et al., 1999, Sbaffi et al., 2001). Planktic specimens are very rare in Central Adriatic, even if an increase of *G. ruber* is detectable between 23.5 and 22 kyr B.P.. ***G. inflata*** **is absent.**	
10	The early MIS2 presents analogue microfaunistic characteristics compared with the other ecobiozones inside MIS2 (i.e. 9 and 8). Planktic specimens are very rare in Central Adriatic. *G.* ex gr. *ruber* is very rare. Scattered dysoxic levels occur in the Southern Adriatic. The lower boundary of this ecobiozone, dated at about 28200 years BP, is approximated by the **LO of benthic *Hyalinea balthica* in the Central Adriatic, and by the LO of planktic *N. pachyderma* l. c. in the Southern Adriatic** (Fig. 9). ***G. inflata*** **is absent.**	23.5(25)-28.2
11	Late MIS3 shows higher concentrations of planktic specimens compared to MIS2, but the assemblage is characterised by the occurrence of **rare *N. pachyderma*** l. c. **in the Southern Adriatic** and **common-abundant *H. balthica* in the Central Adriatic** (Fig. 9). *G.* ex gr. *ruber* is nearly absent, despite few and scattered levels, in which it occurs in very low abundances. ***G. inflata*** **is absent.**	28.2-31.5
12	This ecobiozone shows an additional increase in planktic specimens, and the planktic assemblage presents the **continuous, though rare, presence of *G.* ex gr. *ruber***. The temporary disappearance of this species, marking the upper boundary of this ecobiozone, has been dated at about 31500 years BP (Fig. 9). ***G. inflata*** **is absent.** Campanian Ignimbrite tephra layer, date around 34000-35000 years BP, occurs inside this ecobiozone.	31.5-37
13	The upper limit of this ecobiozone is approximated by the **LO of *G. inflata* inside MIS3**, occurring in correspondence of a marked peak of warm planktic species (*G.* ex gr. *ruber* and *Orbulina universa*), and dated around 37000 years BP. *G. inflata* and *G.* ex gr. *ruber* show a continuous and rare abundance inside the ecozone. *H. balthica* reaches high abundances in the Central Adriatic. The lower limit of the ecobiozone is characterised by a spike in the oxygen stable isotope curve, occurring in correspondence of a marked peak of *G. inflata* and of a minor peak of *G.* ex gr. *ruber*. (Fig. 9). This events, which seem synchronous in the Southern Adriatic, shows a little time lag in the Central Adriatic, maybe indicating a more condensed sedimentation in core SA03-03 in correspondence of this level. It must also be taken into account that ages often derive by interpolation, and that their precision is therefore less reliable. Anyhow, the lower limit of the ecobiozone occurs around 42000-43500 years BP.	37-43.5
14	***G. inflata*** **and *G. ruber* are continuous and common to abundant** along the whole ecobiozone (Fig. 9), which presents, like the whole MIS3, several sporadic events characterised by the occurrence of benthic dysoxic species. The boundary between ecozones 15 and 14 is inferred by the shift towards lighter values in the oxygen stable isotope curve, corresponding to the boundary between MIS4 and MIS3, and dated between 55000 and 58000 years BP.	43.5-55(58)

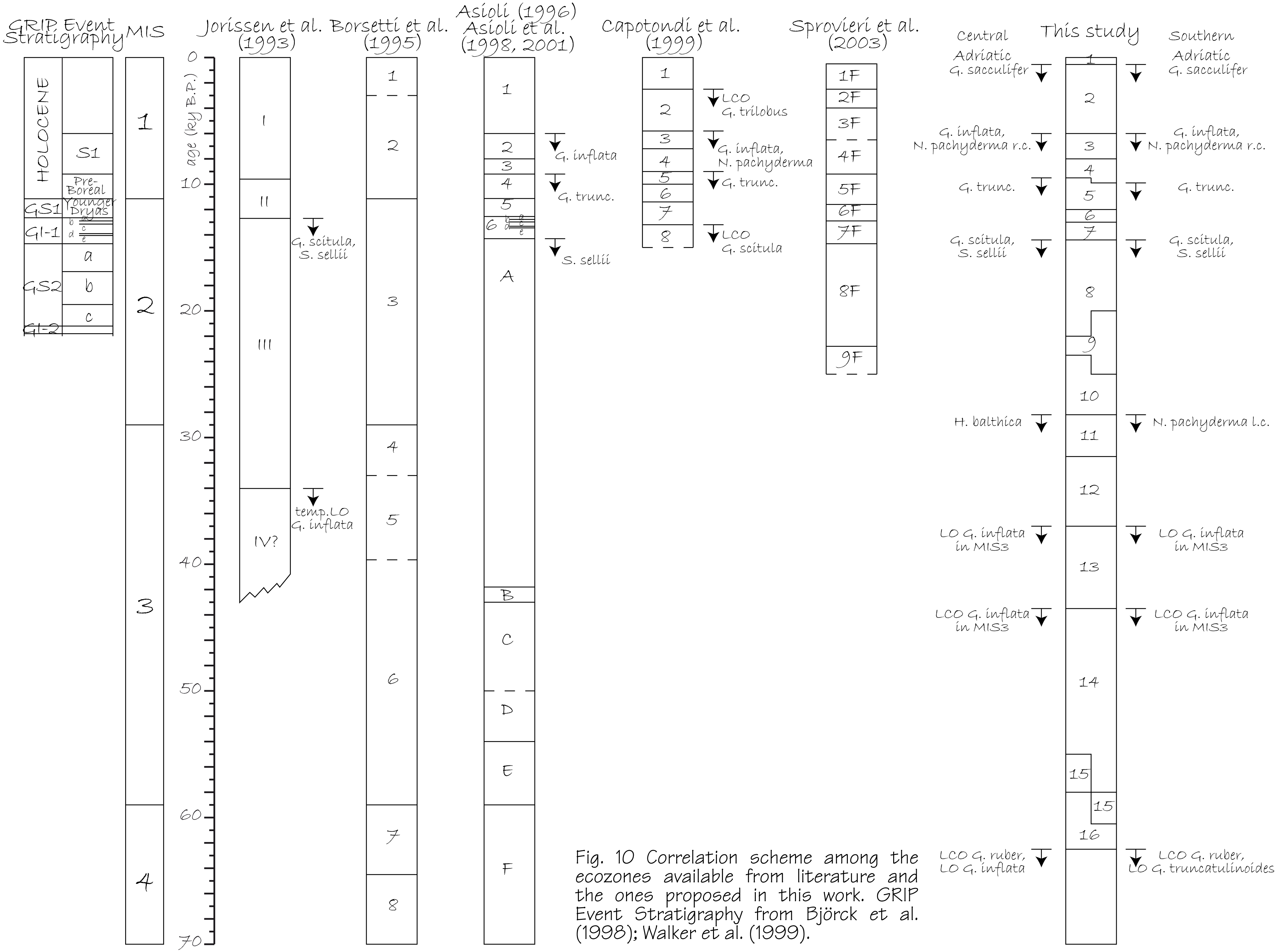

Fig. 10 Correlation scheme among the ecozones available from literature and the ones proposed in this work. GRIP Event Stratigraphy from Björck et al. (1998); Walker et al. (1999).

15	Ecozone 15 includes the late MIS 4, characterised by colder climate conditions than in the early part of the stage. The lower boundary is defined by the **occurrence of *N. pachyderma*** l. c. and by a **concurrent increase of *G. inflata* in the Southern Adriatic** (60.5kyr), and by the **re-occurrence of *G. inflata* in the Central Adriatic** (Fig. 9). Even if the diachronism of the re-occurrence of *G. inflata* in Central Adriatic may be real because of paleoceanographic conditions, it can not be ruled out that it is an artefact of the adopted age model.	55(58)-58(60.5)
16	The lower limit of the ecozone, that may approximate the boundary MIS5/MIS4, can be distinguished by the temporary **LO of *G. truncatulinoides*,** occurring at around 62500 years BP, and the **concurrent strong decrease of *G. ruber* in Southern Adriatic. In Central Adriatic** the boundary MIS5/MIS4 is characterised by the **disappearance of *G. ruber* and *G. inflata***. This ecozone also contains a spike of the oxygen record towards lighter values, which is well pronounced in the Central Adriatic, coupled with a relative increase of *G.* ex gr. *ruber* (Fig. 8) in both the basins. The age of this boundary does not find a correspondence with literature (in which it occurs between 76 and 70 kyr BP). That is likely due to the lack of a control point in the proposed age model, which could give a better time-constraint to this limit.	58(60.5)-62.5

Table VII. Description of the main ecobiozones identified in the Adriatic Basin

Fig. 10 reports the correlation scheme among the ecobiozones available from literature and the ones proposed in this work. The description of the ecozones identified by the other authors is not reported in detail, and the reader is referred to literature for their complete characterisation.

The most important new bioevents identified in this work are reported in Table VIII. Some of them are characteristic of a single basin, others occur all over the Adriatic region.

Area	Bioevent	Age	Description
Central Adriatic	LCO *H. balthica*	ca. 29 kyr BP	boundary MIS3/2
Central Adriatic	end paracme *H. balthica* (top MIS11?-MIS6)	ca. 125 kyr BP	boundary MIS6/5 (PRAD1-2, see part I)
Southern Adriatic	LO *N. pachyderma* l.c.	ca. 29 kyr BP	boundary MIS3/2
Adriatic	LO *G. sacculifer*	0.55 kyr BP	base LIA (see part II)
Adriatic	LO *G. inflata* in MIS3	ca. 37 kyr BP	D-O 8 (Denekamp), Y5 tephra

Table VIII. Main new bioevents identified in the Adriatic Basin

References

Abbott, P. M. (2005). Towards a tephrochronology for a Southern Adriatic deep marine sequence. *Masters Thesis of Science Degree in Quaternary Science,Royal Holloway,* University of London.107 pp.

Ariztegui, D., A. Asioli, J. J. Lowe, F. Trincardi, L. Vigliotti, F. Tamburini, C. A. Accorsi, M. Bandini Mazzanti, A. M. Mercuri, S. Van Der Kaars, C. Chondrogianni, J. A. Mckenzie, F. Oldfield (2000). Palaeoclimatic reconstructions and formation of sapropel S1: inferences from Late Quaternary lacustrine and marine sequences in the Central Mediterranean region. *Palaeoclimatology. Paleoecology, Paleogeography*, 158 (3/4), 215-240.

Asioli, A. (1996) High resolution foraminifera biostratigraphy in the Central Adriatic basin during the last deglaciation: a contribution to the PALICLAS Project, in *Palaeoenvironmental Analysis of Italian Crater Lake and Adriatic Sediments*, edited by F. Oldfield and P. Guilizzoni, *Memorie dell'Istituto Italiano di Idrobiologia*, 55, 197 – 218.

Asioli, A., J. J. Lowe, F. Trincardi, D. Ariztegui, L. Langone, G. Wolff, and F. Oldfield (1998). Paleoenvironmental reconstruction of the Central Adriatic Sea during the last 70 ka. PAGES (Past Global Changes) Open Science Meeting (London, UK, April, 20th-23rd, 1998). Abstract.

Asioli, A., F. Trincardi, J. J. Lowe, and F. Oldfield (1999). Rapid Communication Short-term climate changes during the Last Glacial–Holocene transition: comparison between Mediterranean records and the GRIP event stratigraphy. *Journal of Quaternary Science* 14, 373-381.

Asioli, A., F. Trincardi, J. J. Lowe, D. Ariztegui, L. Langone, and F. Oldfield (2001). Sub-millennial scale climatic oscillations in the central Adriatic during the Lateglacial: palaeoceanographic implications. *Quaternary Science Reviews* 20, 1201-1221.

Bassinot, F. C., L. D. Labeyrie, E. Vincent, X. Quidelleur, N. J. Shackleton, and Y. Lancelot (1994). The astronomical theory of climate and the age of the Brunhes Matuyama magnetic reversal. *Earth Planet. Sci. Lett.*, 126, 91–108.

Borsetti, A. M., L. Capotondi, F. Cati, A. Negri, C. Vergnaud-Grazzini, C. Alberini, P. Colantoni, P. Curzi (1995). Biostratigraphic events and Late Quaternary tectonics in the Dosso Gallignani (central-southern Adriatic Sea). *Giornale di Geologia* 57 (1–2), 41–58.

Björck, S., M. J. C. Walker, L. Cwynar, S. Johnsen, K. L. Knudsen, J. J. Lowe, B. Wohlfarth, and INTIMATE Members (1998). An event stratigraphy for the Last Termination in the North Atlantic region based on the Greenland ice-core record: a proposal by the INTIMATE group. *Journal of Quaternary Science* 13, 283-292.

Bourne, A.J. (2006). An initial tephrochronology for the Adriatic core Prad 1-2 for 40ka BP. Masters of Science Degree in Quaternary Science, Royal Holloway, University of London, 172pp.

Butzin, M., M. Prange and G. Lohmann (2005). Radiocarbon simulations for the glacial ocean: the effects of wind stress, Southern Ocean sea ice and Heinrich events. *Earth & Planetary Science Letters*, 235, 45-61.

Cao, L., R.G. Fairbanks, M. Butzin and N. Naik (2007). The marine radiocarbon reservoir age. *Radiocarbon*, in prep.

Capotondi, L., A. M. Borsetti, and C. Morigi (1999). Foraminiferal ecozones, a high resolution proxy for the late Quaternary biochronology in the central Mediterranean Sea. *Marine Geology,* 153, 253–274.

Fairbanks, R. G., R. A. Mortlock, Tzu-Chien Chiu, L. Cao, A. Kaplan, T. P. Guilderson, T. W. Fairbanks and A.L. Bloom, (2005). Marine Radiocarbon Calibration Curve Spanning 0 to 50,000 Years B.P. Based on Paired ^{230}Th/^{234}U/^{238}U and ^{14}C Dates on Pristine Corals. *Quaternary Science Reviews*, 24, 1781-1796.

Jorissen, F. J., A. Asioli, A. M. Borsetti, L. Capotondi, J. P. De Visser, F. J. Hilgen, E. J. Rohling, K. Van Der Borg, C. Vergnaud-Grazzini and W. J. Zachariasse (1993). Late Quaternary central Mediterranean biochronology. *Marine Micropaleontology,* 21, 169–189.

Langone, L., A. Asiooi, A. Correggiari and F. Trincardi (1996). Age-depth modelling through the late Quaternary deposits of the central Adriatic basin. in *Palaeoenvironmental Analysis of Italian Crater Lake and Adriatic Sediments*, edited by F. Oldfield and P. Guilizzoni, *Memorie dell'Istituto Italiano di Idrobiologia*, 55, 177-196.

Oldfield, F., A. Asioli, C. A. Accorsi, A. M. Mercuri, S. Juggins, L. Langone, T. Rolph, F. Trincardi, G. Wolff, Z. Gibbs, L. Vigliotti, M. Frignani, K. van der Post, N. Branch (2003). A high resolution late Holocene palaeo environmental record from the central Adriatic Sea. *Quaternary Science Reviews* 22, 319–342.

Sbaffi, L., C. W. Forese, N. Kallel, M. Paterne, I. Cacho, P. Ziveri, N. J. Shackleton (2001). Response of the pelagic environment to paleoclimatic changes in the central Mediterranean Sea during the Late Quaternary. *Marine Geology*, 178, 39-62.

Sprovieri, R., E. Di Stefano, A. Incarbona, M. E. Gargano (2003). A high-resolution record of the last deglaciation in the Sicily Channel based on foraminifera and calcareous nannofossil quantitative distribution. *Palaeoclimatology. Paleoecology, Paleogeography*, 202, 119-142.

Walker, M. J. C., S. Björck, J. J. Lowe, L. C. Cwynar, S. Johnsen, K. L. Knudsen, B. Wohlfarth, INTIMATE group (1999). Isotopic events in the GRIP ice core: a stratotype for the Late Pleistocene. *Quaternary Science Reviews* 18, 1143-1150.

CONCLUSION

- A multi-proxy stratigraphic framework has been achieved for borehole PRAD1-2, spanning a time interval from late MIS11 till the present interglacial, matching the results derived from many independent disciplines, such as planktic and benthic foraminfers' quantitative analyses, calcareous nannoplankton semi-quantitative data, oxygen and carbon stable isotope stratigraphy, magnetostratigraphy and sediment magnetic properties, ^{14}C AMS datings, tephrochronology and sapropel stratigraphy.

- Paleoenvironmental inferences have been derived from the micropaleontological content of the samples of PRAD1-2 borehole. Glacial periods show scarce or absent planktic microfauna, and are characterised by a marked shift towards outer to inner shelf bathymetries. Peculiar faunistic features, such as the oligotypic benthic assemblage during MIS8, or the characteristic assemblage of MIS10, reflecting proximal environments, prone to freshwater fluxes and distinctive of high organic matter availability, consent to discriminate each glacial interval. Interglacial periods show more diversified planktic and benthic foraminifers' assemblages, correspondent to mesotrophic upper slope environments. Moreover, these warmer periods show an enhanced vertical mixing of the water column, and a consequent better ventilation of the sea floor. MIS3 and MIS2 are characterised by peculiar faunistic assemblage, which could represent the Central Adriatic, proximal expression of Eastern Atlantic Heinrich events and Dansgaard-Oeschger cycles. This observation, though, needs more constraints by other proxies to be surely confirmed. Van der Zwaan et al. (1990) paleobathymetric index has been adopted to reconstruct the paleo-depth trend along borehole PRAD1-2, and it has then been compared with global sea-level curves, to test the results and to have an estimate of the reliability of this method, also possibly disentangling the global eustatic signal from features of more local origin. An overall deepening trend of glacial periods paleobatymetries has been pointed out, from MIS10 to the last glacial interval. Moreover, whereas bathymetric shifts in correspondence of the main isotopic Terminations are generally coherent with those reported on global sea-level estimates, paleo-depth excursions during minor climatic events (stadial-interstadial transitions) result sensibly wider than the expected ones. This could be explained both by local factors, linked to subsidence and sediment supply, and by problems deriving from the index formula, needing additional corrections for such a proximal environment as that of PRAD1-2.

- About ten intervals, interpreted as the Adriatic equivalent of the sapropel deposition in the Eastern Mediterranean, have been recognised in PRAD1-2 record. A detailed study has been devoted to these paleoceanographic anomalies, paying particular attention to their description, characterisation and expression in a proximal, peripheral context of the Eastern Mediterranean, as the Central Adriatic. The particularly expanded sapropel equivalent Se5 of PRAD1-2 borehole have been compared with other Eastern Mediterranean records, and an overall correspondence of the main foraminiferal events have been demonstrated; few discrepancies have been explained as local paleoceanographic distinctive features of the Adriatic basin. The paleoceanographic inferences allowed clustering of the sapropel-equivalents in three distinct groups: during the deposition of Se10, Se' and Se9 equivalents, all independent proxies suggest climate conditions not so extreme to hamper life of the benthic microfauna. On the contrary, Se8, Se7, Se6, Se5 and Se4 show a more severe paleoceanographic context with probably exceptionally rainy conditions, that is possibly the consequence of a northward shift of the African monsoon, resulting in a dysoxic to anoxic sea floor environment. Finally, deposition during recent Se3 and Se1 events reflects a markedly different paleoceanographic setting in the Central Adriatic, compared to the other Eastern Mediterranean sites. These latest Central Adriatic sapropels depict the scenario of a more isolated basin, weakly linked to the rest of the Eastern Mediterranean, allowing benthic life even when conditions became critical in the adjacent deeper water basins.

- High resolution climate variability has been pointed out as regards the deposition of the last 6000 years BP both in the Central and Southern Adriatic basins. Peaks of foraminfers' biomarker species *V. complanata* and *G. sacculifer* clearly identify respectively the main phases of the Little Ice Age (LIA) and periods of Climatic Optimum, such as, for instance, the Medieval Warm Period, the Roman Age, and the late Bronze Age, reaching a secular (and in some cases even decadal) degree of resolution. Moreover, the LO of *G. sacculifer*, dated at about 550 years BP, approximates the base of the LIA, and it is an important bioevent in the stratigraphy of the Adriatic basin. These paleoclimate-linked bioevents, especially the planktic ones, can be identified both in proximal environments and in more distal areas, even in different depositional basins, whereas the benthic correlation can be operated in areas located at several hundreds kilometres apart, within the same (clay belt) environment. Whereas traces of human impact, expressed in terms of forest clearance, have already been demonstrated for more proximal locations (Oldfield et al., 2003), cores collected in deeper settings show a purer climatic control, being less affected by inland inputs. Only abrupt and catastrophic events, such as, for instance, river floods, manage to reach and have an effect on distal areas.

- The achievement of a detailed ecobiostratigraphic framework of the last 60000 years BP, mainly relying on planktic and benthic foraminifers' quantitative analyses, and strengthened by stable isotope stratigraphy, ^{14}C datings and tephrochronological data, for both Central and Southern Adriatic deposits, revised and significantly improved the stratigraphic zonation available so far from literature for these basins. Age models, characterised by the highest possible number of reliable control points, allowed the obtainment of 16 ecobiozones, spanning a period of time from MIS4 to the present interglacial. Ecobiozone 5, corresponding to the Pre-Boreal interval (base of the Holocene), has been additionally subdivided in five subzones, consenting an even better resolution of the stratigraphic control.

Acknowledgments

Many people contributed with data, communications, reviews and precious discussions to significantly improve the work done in this 3 years-lasting PhD.

I am grateful to my tutors, Gian Battista Vai, Alessandra Asioli, Fabio Trincardi and Ralph Schneider, who believed in me and patiently helped me watering the promising seeds which produced such fine results. I am particularly thankful to Alessandra and Fabio, who gave me the chance to improve my knowledge and always made me like my job.

I would also like to acknowledge Domenico Ridente, Antonio Cattaneo, Luigi Vigliotti and Leonardo Langone, who significantly helped my research to advance with data, suggestions and talks about science.

Elena Colmenero-Hidalgo, José Abel Flores, Francisco J. Sierro, Joan O. Grimalt, Jaime Frigola, Bernard Dennielou and Serge Bernè are part of PROMESS1 team, as well, and contributed with data and hints to the stratigraphic and paleoceanographic reconstruction of borehole PRAD1-2.

I would like to thank Nils Andersen for providing the isotope data and for the precious hints in their first interpretation, as well as Anna Maria Mercuri, for her indications on pollen data.

I would like to express thanks to Paolo Ferrieri, for his helpfulness and professional competence for SEM pictures.

I acknowledge Simon P. Blockley and John J. Lowe for the interesting talks about ^{14}C ages and tephra layers.

It has been a real pleasure for me to work and discuss with all these people and I hope to have the chance to collaborate again with all of them in the future.

APPENDIX I

Taxonomic list

Benthic foraminifera

Adelosina spp. scattered specimens belonging to the genus *Adelosina* d'Orbigny, 1826
Ammonia beccarii (Linnè) = *Nautilus beccarii* Linnè, 1758
Ammonia papillosa (Brady) = *Rotalia papillosa* Brady, 1884
Ammonia perlucida (Heron-Allen and Earland) = *Rotalia perlucida* Heron-Allen and Earland, 1913
Amphicoryna scalaris (Batsch) = *Nautilus scalaris* Batsch, 1791
Articulina tubulosa (Seguenza) = *Quinqueloculina tubulosa* Seguenza, 1862
Astaculus cfr. *reniformis* (Hausler) = *Cristellaria reniformis* Hausler, 1881
Asterigerinata mamilla (Williamson) = *Rotalina mamilla* Williamson, 1858
Astrononion stelligerum (d'Orbigny) = *Nonionina stelligera* d'Orbigny, 1839
Astrononion sp.1 = cfr. *Astrononion italicum* Cushman and Edwards, 1937
Bigenerina nodosaria d'Orbigny, 1826
Biloculinella globula (Bornemann) = *Biloculina globulus* Bornemann, 1855
Biloculinella labiata (Schlumberger) = *Biloculina labiata* Schlumberger, 1891
Bolivina albatrossi Cushman, 1922
Bolivina ordinaria Phleger and Parker, 1952 (Plate II, 2)
Bolivina pseudoplicata Heron-Allen and Earland, 1930
Bolivina striatula Cushman, 1922 (Plate II, 1)
Bolivina subspinescens Cushman, 1922
Bolivina sp.1. generally tiny in size, hyaline, microperforate, flat, presenting a thick greed (Plate II, 5a-c), similar to Bolivina cf. B. thalmanni Renz, as classified by Murray (Plate 1, fig.4), in the initial reports of DSDP Leg 81, Roberts, Schnitker et al. (eds), 1984, pag. 503-534
Brizalina aenariensis Costa, 1856
Brizalina alata (Seguenza) = *Vulvulina alata* Seguenza, 1862
Brizalina difformis (Williamson) = *Textularia variabilis* Williamson, var. *difformis* Williamson, 1858
Brizalina dilatata (Reuss) = *Bolivina dilatata* Reuss, 1850
Brizalina spathulata (Williamson) = *Textularia variabilis* Williamson, var. *spathulata* Williamson, 1858
Buccella granulata (Di Napoli Alliata) = *Eponides frigidus* (Cushman) var. *granulata* Di Napoli Alliata, 1952
Bulimina costata d'Orbigny, 1852
Bulimina elongata d'Orbigny, 1846
Bulimina marginata d'Orbigny, 1826 morphotypes *marginata* and *aculeata*
Bulimina spp. scattered specimens belonging to other species of the genus *Bulimina* d'Orbigny, 1826, or not determinable at specific level
Buliminella elegantissima (d'Orbigny) = *Bulimina elegantissima* d'Orbigny, 1839
Cancris auriculus (Fichtel and Moll) = *Nautilus auricula* Fichte land Moll, 1798
Cancris oblongus (d'Orbigny) = *Valvulina oblonga* d'Orbigny, 1839
Cassidulina laevigata d'Orbigny var. *carinata* Silvestri, 1896
Cassidulina crassa d'Orbigny, 1839
Cassidulinoides bradyi (Norman) = *Cassidulina bradyi* Norman, 1881
Chilostomella oolina Schwager, 1878
Chilostomella ovoidea Reuss, 1850
Cibicides lobatulus (Walker and Jacob) = *Nautilus lobatulus* Walker and Jacob, 1798
Cibicidinella foliorum Saidova, 1975
Cibicidoides floridanus (Cushman) = *Truncatulina floridana* Cushman, 1918
Cibicidoides pachyderma (Rzehak) = *Truncatulina pachyderma* Rzehak, 1886
Cornuspira carinata (Costa) = *Operculina carinata* Costa, 1856
Cornuspira foliacea (Philippi) = *Orbis foliaceus* Philippi, 1884
Cornuspira involvens (Reuss) = *Operculina involvens* Reuss, 1850

Cruciloculina staurostoma (Schlumberger) = *Triloculina staurostoma* Schlumberger, 1883
Cycloforina tenuicollis (Wiesner) = *Miliolina tenuicollis* Wiesner, 1923
Dentalina leguminiformis (Batsch) = *Nautilus (Orthoceras) leguminiformis* Batsch, 1791
Dentalina mucronata Neugeboren, 1856
Discorbia valvulinerioides Sellier de Civrieux, 1977
Discorbis spp. scattered specimens belonging to the genus *Discorbis* Lamarck, 1804
Ehrembergina bradyi Cushman, 1922
Elphidium albiumbilicatum (Weiss) = *Nonion pauciloculum* Cushman, susp. *albiumbilicatum* Weiss, 1954 (Plate III, 1a-c)
Elphidium advenum (Cushman) = *Polystomella advena* Cushman, 1922
Elphidium articulatum (d'Orbigny) = *Polystomella articolata* d'Orbigny, 1839, cfr. *Elphidium advenum* (Cushman) var. *margaritaceum* Cushman, 1930 (Plate III, 2a-c)
Elphidium clavatum (Cushman) = *Elphidium incertum* (Williamson) var. *clavatum* Cushman, 1930 (Plate III, 3a-c, 4a-c)
Elphidium crispum (Linnè) = *Nautilus crispus* Linnè, 1758
Elphidium decipiens (Costa) = *Polystomella decipiens* Costa, 1856
Elphidium excavatum (Terquem) = *Polystomella excavata* Terquem, 1875
Elphidium granosum (d'Orbigny) = *Nonionina granosa* d'Orbigny, 1826
Elphidium poeyanum (d'Orbigny) = *Polystomella poeyana* d'Orbigny, 1839
Elphidium spp. scattered specimens belonging to other species of the genus *Elphidium* Montfort, 1808, or not determinable at specific level
Epistominella exigua (Brady) = *Pulvinulina exigua* Brady, 1884
Eponides pusillus Parr, 1950
Eponides tumidulus (Brady) = *Truncatulina tumidula* Brady, 1884
Fissurina castanea (Flint) = *Lagena castanea* Flint, 1899
Fissurina marginata (Montagu) = *Vermiculum marginatum* Montagu, 1803
Fissurina pseudoorbignyana (Buchner) = *Lagena pseudoorbignyana* Buchner, 1940
Fissurina staphyllearia Schwager, 1866
Fissurina spp. scattered specimens belonging to other species of the genus *Fissurina* Reuss, 1850, or not determinable at specific level
Florilus spp. scattered specimens belonging to the genus *Florilus* Montfort, 1808
Fursenkoina tenuis (Seguenza) = *Virgulina tenuis* Seguenza, 1862
Gavelinopsis praegeri (Heron-Allen and Earland) = *Discorbina praeger*i Heron-Allen and Earland, 1913
Glabratella spp. scattered specimens belonging to the genus *Glabratella* Doreen, 1948
Glandulina laevigata (d'Orbigny) = *Nodosaria (Glanduline) laevigata* d'Orbigny, 1826 (Plate II, 3a-b)
Globobulimina affinis (d'Orbigny) = *Bulimina affinis* d'Orbigny, 1839
Globobulimina psudospinescens (Emiliani) = *Bulimina pyrula* d'Orbigny var. *pseudospinescens* Emiliani, 1949
Globocassidulina oblonga (Reuss) = *Cassidulina oblonga* Reuss, 1850
Globocassidulina subglobosa (Brady) = *Cassidulina subglobosa* Brady, 1881
Guttulina communis (d'Orbigny) = *Polymorphina (Guttuline) communis* d'Orbigny, 1826
Gyroidinoides altiformis (R. E. and K. C. Stewart) = *Gyroidina soldanii* d'Orbigny var. *altiformis* R. E. and K. C. Stewart, 1930
Gyroidinoides neosoldanii (Brotzen) = *Gyroidina neosoldani* Brotzen, 1936
Gyroidinoides umbonatus (Silvestri) = *Rotalia soldanii* (d'Orbigny) var. *umbonata* Silvestri, 1898
Hanzawaia boueana (d'Orbigny) = *Truncatulina boueana* d'Orbigny, 1846
Hoeglundina elegans (d'Orbigny) = *Rotalia elegans* d'Orbigny, 1826
Hyalinea balthica (Schroeter) = *Nautilus balthicus* Schroeter, 1783

Islandiella islandica (Nörvang) = *Cassidulina islandica* (Nörvang), 1945 (Plate II, 6a-c)
Laevidentalina inflexa (Reuss) = *Nodosaria inflexa* Reuss, 1866
Lagena apiopleura Loeblich and Tappan, 1953
Lagena striata (d'Orbigny) = *Oolina striata* d'Orbigny, 1839
Lagena spp. scattered specimens belonging to other species of the genus *Lagena* Walker and Boys, 1784, or not determinable at specific level
Lenticulina calcar (Linnè) = *Nautilus calcar* Linnè, 1758
Lenticulina cultrata (de Monfort) = *Robulus cultratus* de Monfort, 1808
Lenticulina gibba (d'Orbigny) = *Cristellaria gibba* d'Orbigny, 1839
Lenticulina orbicularis (d'Orbigny) = *Robulina orbicularis* d'Orbigny, 1826
Lenticulina peregrina (Schwager) = *Cristellaria peregrina* Schwager, 1866
Lenticulina stellata (Seguenza) = *Robulina stellata* Seguenza 1880
Lenticulina spp. scattered specimens belonging to other species of the genus *Lenticulina* Lamarck, 1804, or not determinable at specific level
Melonis barleeanum (Williamson) = *Nonionina barleeana* Williamson, 1858, cfr. *Nonion padanum* Perconig, 1952
Miliolinella subrotunda (Montagu) = *Vermiculum subrotundum* Montagu, 1803
Neoconorbina terquemi (Rzehak) = *Discorbina terquemi* Rzehak, 1888, cfr. *Rosalina orbicularis* (non d'Orbigny) Terquem, 1876
Nodosaria ovicula d'Orbigny, 1826
Nodosaria radicula (Linnè) = *Nautilus radicula* Linnè, 1758
Nodosaria raphanistrum (Linnè) = *Nautilus raphanistrum* Linnè, 1758
Nonion depressulus (Walker and Jacob) emend. Murray, 1965, cfr. *Nautilus depressulus* Walker and Jacob, 1798 (initial plate)
Nonion pauciloculum Cushman, 1944 (Plate III, 5a-c)
Nonion spp. scattered specimens belonging to other species of the genus *Nonion* Montfort, 1808, or not determinable at specific level
Nonionella turgida (Williamson) = *Rotalina turgida* Williamson, 1858
Nonionella spp. scattered specimens belonging to other species of the genus *Nonionella* Cushman, 1926, or not determinable at specific level
Oolina hexagona (Williamson) = *Entosolenia squamosa* (Montagu) var. *hexagona* Williamson, 1848
Ophthalmidium margaritiferum Heron-Allen and Earland, 1922
Ophthalmidium spp. scattered specimens belonging to other species of the genus *Ophthalmidium* Kübler and Zwingli, 1870, or not determinable at specific level
Patellina corrugata Williamson, 1858
Planularia spp. scattered specimens belonging to the genus *Planularia* Defrance, 1826
Planulina ariminensis d'Orbigny, 1826
Planorbulina mediterranensis d'Orbigny, 1826
Polymorphina spp. scattered specimens belonging to the genus *Polymorphina* d'Orbigny, 1826
Protoelphidium anglicum Murray, 1965, cfr. *Hayesina germanica* (Ehremberg), emend. Banner and Culver, 1978
Pseudoclavulina crustata Cushman, 1936
Pullenia bulloides (d'Orbigny) = *Nonionina bulloides* d'Orbigny, 1846
Pullenia compressicula Reuss var. *quadriloba* Reuss, 1867
Pullenia quinqueloba (Reuss) = *Nonionina quinqueloba* Reuss, 1851
Pyrgo bulloides (d'Orbigny) = *Biloculina bulloides* d'Orbigny, 1826
Pyrgo depressa (d'Orbigny) = *Biloculina depressa* d'Orbigny, 1826
Pyrgo murrhina (Schwager) = *Biloculina murrhina* Schwager, 1866
Pyrgo spp. scattered specimens belonging to other species of the genus *Pyrgo* Defrance, 1824, or not determinable at specific level

Pyrgoella sphaera (d'Orbigny) = *Biloculina sphaera* d'Orbigny, 1839
Quadrimorphina spp. scattered specimens belonging to the genus *Quadrimorphina* Finlay, 1939
Quinqueloculina bosciana d'Orbigny, 1839
Quinqueloculina padana Perconig, 1954
Quinqueloculina seminulum (Linnè) = *Serpula seminulum* Linnè, 1758
Quinqueloculina spp. scattered specimens belonging to other species of the genus *Quinqueloculina* d'Orbigny, 1826 , or not determinable at specific level
Reussella spinulosa (Reuss) = *Verneuilina spinulosa* Reuss, 1850
Robertina translucens Cushman and Parker, 1936
Robertinoides bradyi (Cushman and Parker) = *Robertina bradyi* Cushman and Parker, 1936, cfr. *Bulimina subteres* Brady, 1884
Rosalina globularis d'Orbigny, 1826
Rosalina spp. scattered specimens belonging to other species of the genus *Rosalina* d'Orbigny, 1826 , or not determinable at specific level
Sigmoilina distorta Phleger and Parker, 1951
Sigmoilina sellii D'Onofrio, 1959
Sigmoilina sigmoidea (Brady) = *Planispirina sigmoidea* Brady, 1884
Sigmoilinita tenuis (Czjzek) = *Quinqueoculina tenuis* Czjzek, 1848
Sigmoilopsis schlumbergeri (Silvestri) = *Sigmoilina schlumbergeri* Silvestri, 1904
Siphotextularia concava (Karrer) = *Plecanium concavum* Karrer, 1868
Sphaeroidina bulloides, d'Orbigny, 1826
Spirillina vivipara Ehremberg, 1843
Spiroloculina canaliculata d'Orbigny, 1846
Spiroloculina depressa d'Orbigny, 1826
Spiroloculina excavata d'Orbigny, 1846
Spirophtalmidium acutimargo (Brady) var. *concava* (Wiesner) = *Spiroloculina acutimargo* Brady var. *concava* Wiesner, 1913
Spiroplectammina wrightii (Silvestri) = *Spiropecta wrightii* Silvestri, 1903
Stainforthia complanata (Egger) = *Virgulina schreibersiana* Czjzek var. *complanata* Egger, 1893
Textularia aciculata d'Orbigny, 1826
Textularia conica d'Orbigny, 1839
Textularia sagittula Defrance, 1824
Trifarina angulosa (Williamson) = *Uvigerina angulosa* Williamson, 1858
Trifarina sp.1. species generally smaller in size compared to *T. angulosa*, presenting more rounded chambers (Plate II, 4a-b)
Triloculina tricarinata d'Orbigny, 1826
Triloculina trigonula (Lamarck) = *Miliolites trigonula* Lamarck, 1804
Uvigerina mediterranea Hofker, 1932
Uvigerina peregrina Cushman, 1923
Uvigerina peregrina Cushman var. *dirupta* Todd, 1948
Uvigerina proboscidea Schwager, 1866
Valvulineria bradyana (Fornasini) = *Discorbina bradyana* Fornasini, 1900, cfr. *Rosalina complanata* Brady, 1846
Valvulineria rugosa (d'Orbigny) *var. minuta* (Schubert) = *Discorbina rugosa* (d'Orbigny) –Brady, 1884 (part, non *Rosalina rugosa* d'Orbigny, 1839c, var. *minuta* Schubert, 1904
Valvulineria spp. scattered specimens belonging to other species of the genus *Valvulineria* Cushman, 1926 , or not determinable at specific level
Virgulina mexicana Cushman, 1922

Planktic foraminifera

Globigerina bulloides d'Orbigny, 1826 (Plate I, 4a-c)
Globigerina praedigitata Parker, 1967
Globigerina quinqueloba Natland, 1938
Globigerinella aequilateralis Brady, 1879, cfr. *Globigerina siphonifera* d'Orbigny, 1839
Globigerinella praecalida (Blow) = *Globigerina calida* Parker subsp. *pracealida* Blow, 1969
Globigerinita glutinata (Egger) = *Globigerina glutinata* Egger, 1893
Globigerinita uvula (Ehremberg) = *Pylodexia uvula* Ehremberg, 1861
Globigerinoides ruber (d'Orbigny) = *Globigerina rubra* d'Orbigny, 1939 (var. rosea, initial plate and Plate I, 1a-c)
Globigerinoides quadrilobatus (d'Orbigny) = *Globigerina quadriloba* d'Orbigny, 1846
Globigerinoides sacculifer (Brady) = *Globigerina sacculifera* Brady, 1877 (Plate I, 3a-c)
Globigerinoides tenellus Parker, 1958
Globigerinoides trilobus (Reuss) = *Globigerina triloba* Reuss, 1850
Globorotalia inflata (d'Orbigny) = *Globigerina inflata* d'Orbigny, 1939
Globorotalia scitula (Brady) = *Pulvinulina scitula* Brady, 1882
Globorotalia truncatulinoides (d'Orbigny) = *Rotalina truncatulinoides* d'Orbigny, 1939
Neoacarinina blowi Thompson, 1973
Neogloboquadrina dutertrei (d'Orbigny) = *Globigerina dutertrei* d'Orbigny, 1939 (Plate I, 5a-b)
Neogloboquadrina pachyderma (Ehremberg) = *Aristerospira pachyderma* Ehremberg, 1861
Orbulina bilobata (d'Orbigny) = *Globigerina bilobata* d'Orbigny, 1846
Orbulina suturalis Bronniman, 1951
Orbulina universa d'Orbigny, 1839 (Plate I, 2a-c)
Turborotalia humilis (Brady) = *Truncatulina humilis* Brady, 1884
Zeaglobigerina rubescens (Hofker) = *Globigerina rubescens* Hofker, 1936

APPENDIX II

Plates

Plate I

Planktic foraminifera of Sapropel 5 and 6 in PRAD1-2.

Scale bar=100µm where not specified.

Fig. 1a *Globigerina bulloides*, apertural side, S39 cm 20-22A (30.6 mbfs)

Figg. 1b and 1c details of the wall structure

Fig. 2a *Neogloboquadrina dutertrei*, apertural side, S45, cm 30-32 (35.5 mbsf)

Fig. 2b spiral side

Fig. 3a *Globigerinoides ruber* var. *rosea*, spiral side, S39 cm 20-22A (30.6 mbfs)

Fig. 3b apertural side

Fig. 3c detail of the honeycomb structure

Fig. 3d detail, base of the spine

Fig. 4a *Orbulina universa*, S38 cm 60-62A (30.2 mbsf)

Figg. 4b and 4c details of the wall structure

Fig. 5a *Globigerinoides sacculifer*, apertural side, S39 cm 20-22A (30.6 mbfs)

Fig. 5b spiral side

Fig. 5c detail of the honeycomb structure

Plate 1

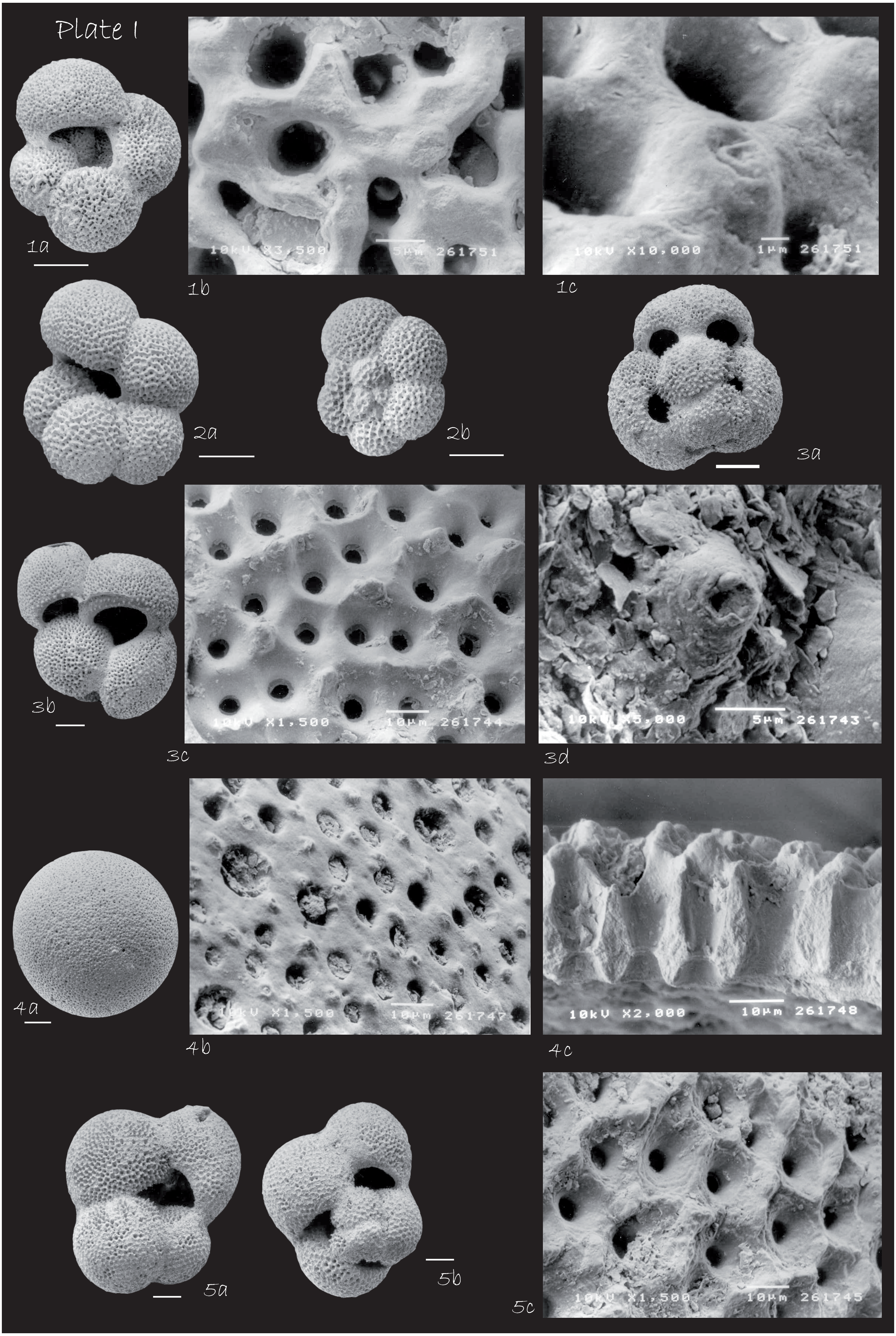
1a
10kV X3,500 5µm 261751
1b
10kV X10,000 1µm 261751
1c
2a
2b
3a
3b
10kV X1,500 10µm 261744
3c
10kV X5,000 5µm 261743
3d
4a
10kV X1,500 10µm 261747
4b
10kV X2,000 10µm 261748
4c
5a
5b
10kV X1,500 10µm 261745
5c

Plate II

Benthic foraminifera typical of sapropel layers and/or of glacial periods in PRAD1-2.

Scale bar=100μm where not specified.

Fig. 1 *Bolivina striatula*, side view, S38 cm 60-62A (30.2 mbsf)

Fig. 2 *Bolivina ordinaria*, side view, S38 cm 60-62A (30.2 mbsf)

Figg. 3a and 3b *Glandulina laevigata*, side view, S8 cm 30-32 (5.882 mbsf)

Fig. 4a *Trifarina* sp.1, side view, S42 cm 30-32 (33.101 mbsf)

Fig. 4b detail of the microperforate test

Fig. 5 *Nonion depressulus*, side view

Fig. 6a *Bolivina* sp.1, side view

Fig. 6b detail of the microperforate test

Fig. 6c detail of the aperture

Fig. 7a *Islandiella islandica*, apertural view, S42 cm 30-32 (33.101 mbsf)

Figg. 7b and 7c details of the aperture

Plate II

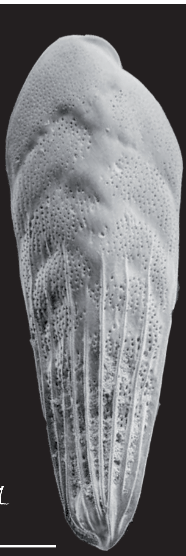
1


2

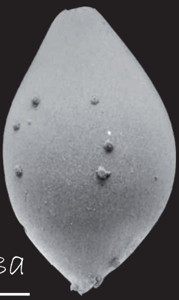
3a

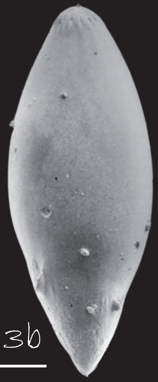
3b


4a

4b
10µm

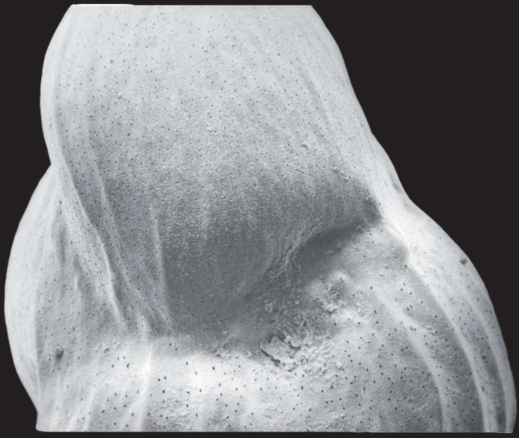


5

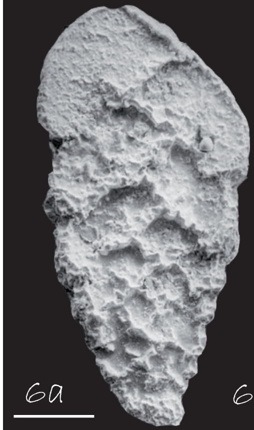
6a
50µm

6b

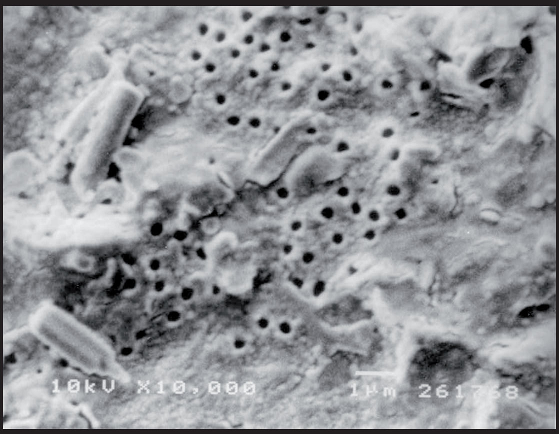

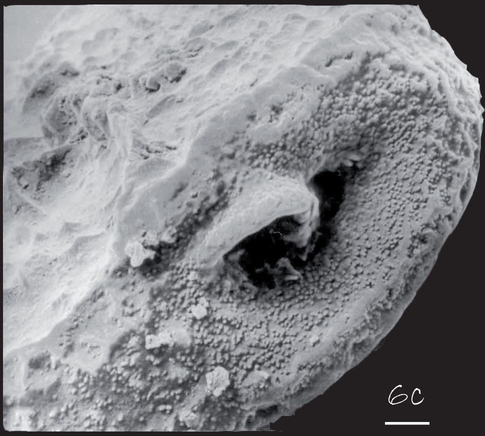
6c
10µm

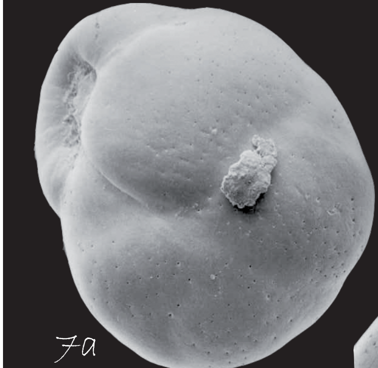
7a

7b

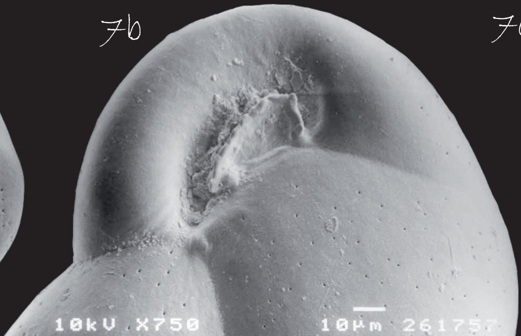

7c

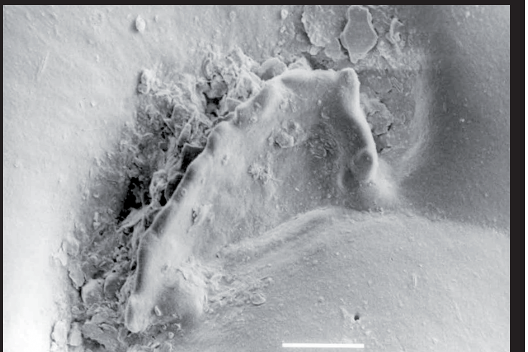

Plate III

Benthic foraminifera typical of glacial periods in PRAD1-2.

Scale bar=100µm where not specified.

Fig. 1a *Elphidium albiumbilicatum*, side view

Fig. 1b detail of the umbilical area

Fig. 1c detail of the microperforate test.

Fig. 2a *Elphidium articulatum*, side view, S42, cm 30-32 (33.101 mbsf)

Fig. 2b detail of the umbilical area

Fig. 2c detail of the aperture

Figg. 3a and 4a *Elphidium clavatum*, side view, S45, cm 30-32 (35.5 mbsf)

Figg. 3b and 4b details of the umbilical area

Figg. 3c and 4c apertural side and detail of the aperture

Fig. 5a *Nonion pauciloculum*, side view

Fig. 5b detail of the umbilical area

Fig. 5c detail of the aperture

Plate III

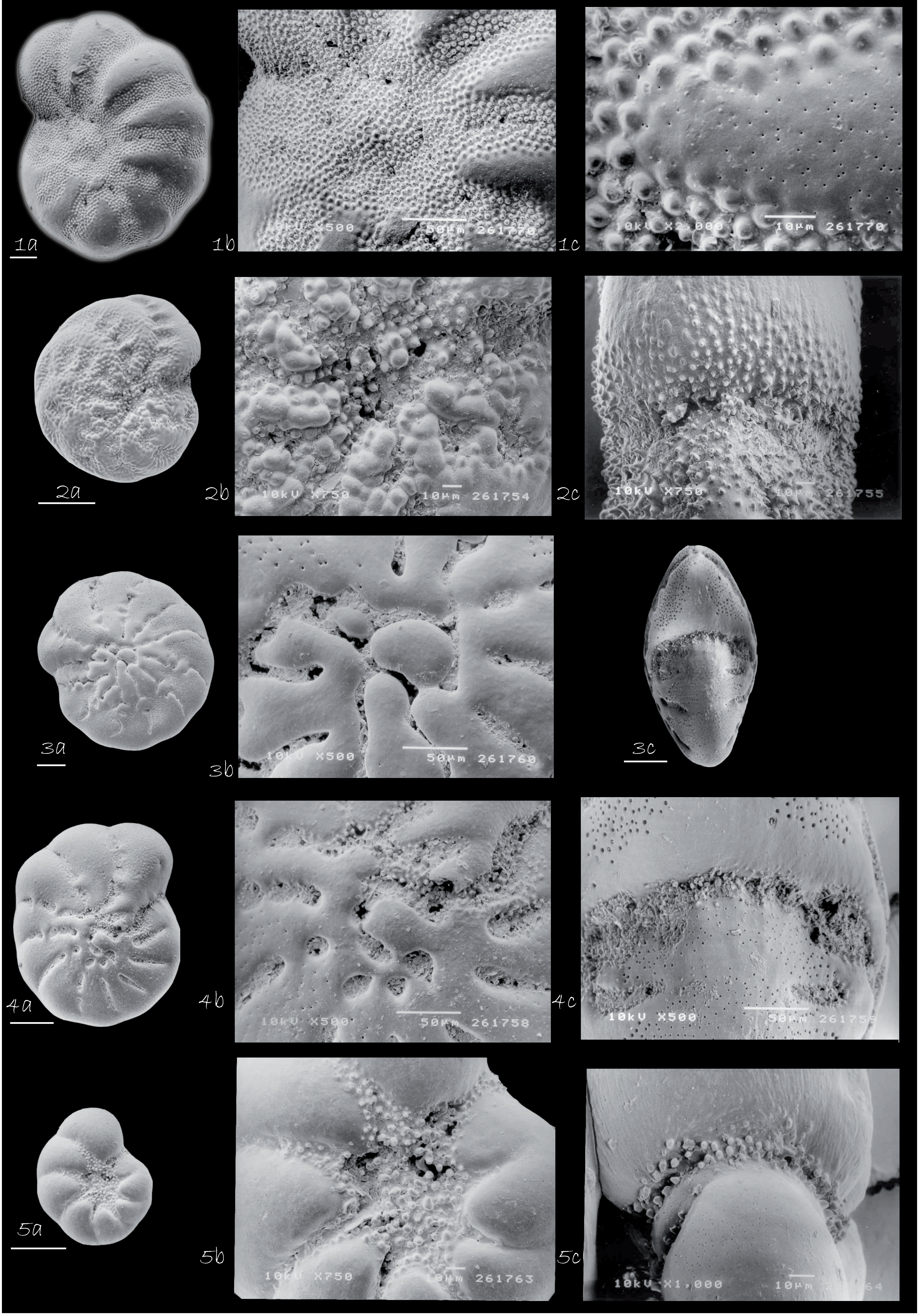
1a
1b
10kV X500 50µm 261770
1c
10kV X2,000 10µm 261770
2a
2b
10kV X750 10µm 261754
2c
10kV X750 10µm 261755
3a
3b
10kV X500 50µm 261760
3c
4a
4b
10kV X500 50µm 261758
4c
10kV X500 50µm 26175
5a
5b
10kV X750 0µm 261763
5c
10kV X1,000 10µm 2 64

Plate IV (a, b)

Lithologic synthesis (m 1-36; 36-72) of borehole PRAD1-2.

Pictures of the most characteristic intervals (sapropel equivalents, tephra layers) are reported aside the lithologic log.

Each section is 80 cm long (including core shoes where available). Consequently, each interval between two ticks in the vertical axis corresponds to 80 cm lenght.

The position of sapropel equivalent intervals is reported aside the log.

⚌ homogenuos mud
⁝ silty mud
▤ silty laminae
▨ sand
▼ tephra layer
∼ erosional surface
☰ laminated sediment
S diffused bioturbation
∫ burrow
⟋ organic matter
◎ biosome
△ bioclast

Plate IVa

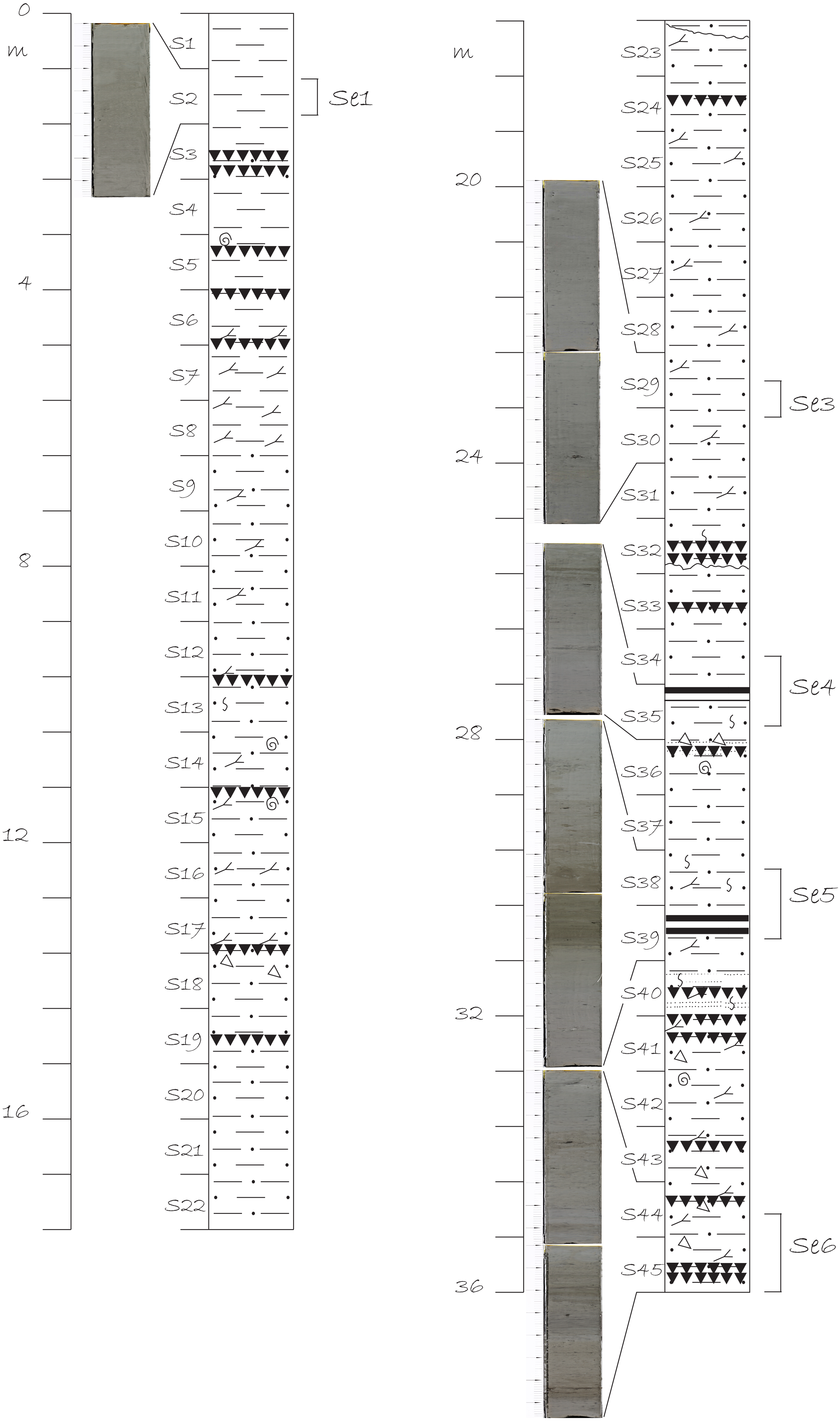
0
m
4
8
12
16
S1
S2
Se1
S3
S4
S5
S6
S7
S8
S9
S10
S11
S12
S13
S14
S15
S16
S17
S18
S19
S20
S21
S22
m
20
24
28
32
36
S23
S24
S25
S26
S27
S28
S29
Se3
S30
S31
S32
S33
S34
Se4
S35
S36
S37
S38
Se5
S39
S40
S41
S42
S43
S44
Se6
S45

Plate IVb

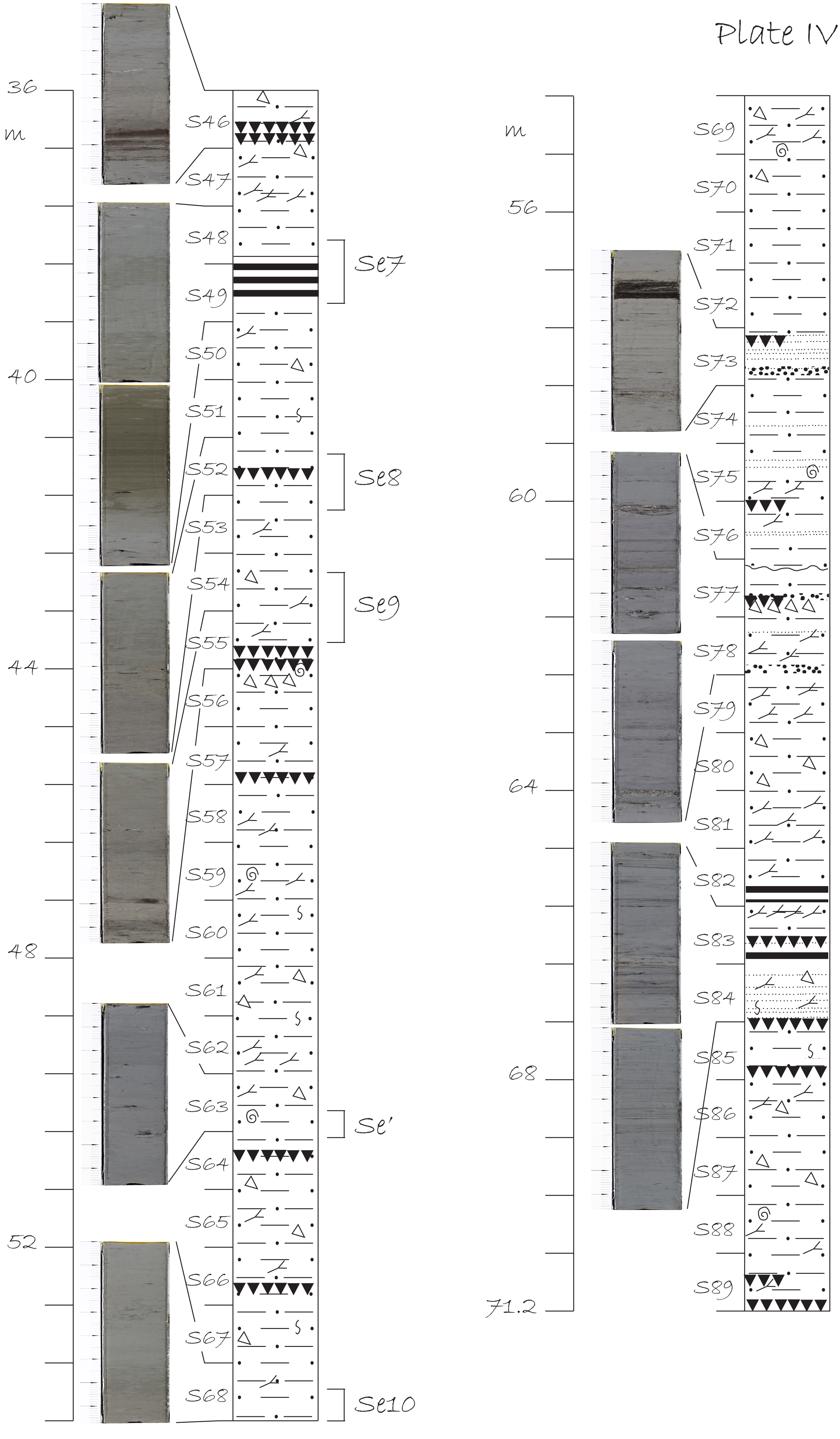
36
m
40
44
48
52
S46
S47
S48
S49
S50
S51
S52
S53
S54
S55
S56
S57
S58
S59
S60
S61
S62
S63
S64
S65
S66
S67
S68
Se7
Se8
Se9
Se'
Se10
m
56
60
64
68
71.2
S69
S70
S71
S72
S73
S74
S75
S76
S77
S78
S79
S80
S81
S82
S83
S84
S85
S86
S87
S88
S89

The impact of cascading currents on the Bari Canyon System, SW-Adriatic Margin (Central Mediterranean).

Trincardi, F.[1], Foglini, F.[1], Verdicchio, G.[1-2], Asioli, A.[3], Correggiari A.[1], Minisini, D.[1-2], Piva, A.[1-2], Remia, A., Ridente, D.[1], Taviani, M.[1]

1 - ISMAR-CNR, Via Gobetti, 101, 40129 Bologna, Italy

2 - DSTGA, Università di Bologna, Via Zamboni 67, 40126 Bologna, Italy

3 - IGG-CNR, Corso Garibaldi 37, 35137 Padova, Italy

ABSTRACT

The Bari Canyon System (BCS) is a peculiar erosional-depositional feature characterised by two main, almost parallel, conduits emanating from a broad crescent-shaped upper slope region. When viewed in cross sections parallel to the margin, BCS appears markedly asymmetric with a right hand (southern) flank that is higher and steeper (about 800 m in relief and more than 30° steep). The left-hand side of the canyon is instead much smoother. As a consequence, bottom currents flowing along the slope from the north enter the canyon and interact with its complex topography leading to preferential deposition on the up-current side of pre-existing morphological relief. Where mass-failure deposits generate morphologic relief, outside the canyon, sediment is preferentially deposited up current (N-ward). BCS includes three main EW-oriented sediment conduits: canyon C, to the south, channel B, in the central area, and moat A in the north. Channel B shows a well developed levee deposit on its right-hand side and appears markedly straight and erosional on the upper slope. The deepest portion of channel B is substantially abandoned and draped but still shows a subdued thickening of the draped unit north (and up current) of pre-existing morphologic relief, confirming the impact of along-slope flowing currents. Canyon C is flanked by erosional walls all the way to the basin floor where deep-sea furrows develop with a NW-SE orientation.

Today, dense water formation in the Adriatic is seasonally modulated and displays a significant variability on inter-decadal scales. Dense water formation during glacial intervals was likely different from the modern because most of the North Adriatic shelf was subaerially exposed and the deep water mixing in the south was likely reduced, as suggested by paleoceanographic reconstructions. The growth patterns of

BCS since the LGM are characterised by concurrent erosion of the upper portion of channel B and of the lower portion of canyon C. It is possible that flows through the straight, narrow and steep upper segment of channel B spill over its right hand levee in ca. 600 m water depth, where the relief of levee B on the channel floor is minimal, and enter canyon C, where substantial erosion takes place. In this view, the upper portion of canyon C, where hard grounds and coral colonies are encountered, is flushed by currents characterised by reduced turbidity, while the lower part of canyon C collects additional flows from upper channel B.

1. INTRODUCTION

Active submarine canyons are extensively described worldwide along oceanic margins (e.g., Shepard et al., 1933; 1981; Daly, 1936, Shepard and Dill, 1966, McAdoo et al., 1997) and along continental margins of confined basins, such as the Mediterranean Sea. Mediterranean active canyons are documented along the Gulf of Lion slope (e.g., Droz and Bellaiche, 1985; Batzan et al., 2005), in the Catalan Margin (e.g., Field and Gardner, 1990; Palanques et al., 1994), and in the Tyrrhenian Margin (e.g., Gallignani, 1982; Gamberi and Marani, this vol.). These sediment conduits occur in a broad range of physiographic and geological contexts, presenting an extreme variability in dimensions, morphology and seafloor sediment. The processes that feed canyon heads and transport sediment along their axes are also greatly diversified, depending primarily on the type and amount of sediment that reach the canyon, and on the oceanographic regime impacting the canyon area (Normark, 1970; Farre, 1983; Normark and Piper, 1991). All these factors are commonly considered as strictly related to the presence of a sediment source close to the canyon head, either a delta or a littoral cell carrying sediment into the canyon (Cutshall et al., 1986). Variations of relative sea level are important in controlling the distance of the canyon head from a river source and the water depth in the outer shelf, in turn controlling its current and wave regime.

Where a canyon head is located on a shallow inner shelf, sediment can be supplied directly from river deltas or long-shore drift; where, instead, the canyon head is more seaward, close to the shelf edge, sediment is fed by shelf currents and/or episodic density currents triggered by the instability of the canyon shoulders. Several Authors have linked the onset of canyons and their activity to sea-level falls and lowstands, when shelves become narrow and fluvial sediment sources may reach directly into the canyon heads, which commonly are situated close to the shelf edge (e.g., Twichell and Roberts, 1982; Carlson and Karl, 1988; Galloway, 1991). Under these conditions, large amounts of sediment are available for remobilization and large-scale slump and turbidity currents may be generated (Mutti, 1985). However, documentation from a great number of canyons described worldwide, indicates that sea-level fall and lowstand are not mandatory requirements for canyon activity. Indeed some canyons have been documented as active during rising and the highstand of sea-level (e.g., Kolla and Perlumutter, 1993; Trincardi et al., 1995).

We focused our attention on the Bari Canyon System (BCS), located along the SW Adriatic Margin, Central Mediterranean. The BCS dissect a relatively steep continental slope far away from river mouths, impacted, at least since the end of the last glacial interval, by very strong bottom currents resulting by the combined flow of the long-lasting contour-parallel slope currents, Levantine Intermediate Water (LIW), and of the episodic slope-transverse cascading currents, North Adriatic Dense Water

(NAdDW) (Verdicchio et al., in press). The peculiar oceanographic context in which BCS developed strongly influences the present day activity and the sedimentary processes inside the canyon. The main interest in studying the recent evolution of the BCS is understanding how cascading and contour currents can be captured within the canyon system defining areas of erosion and increased sediment deposition during periods of sea-level rise and modern sea-level highstand.

2. SETTING

2.1. Geologic setting of the SW Adriatic Margin

The western margin of the Adriatic basin belongs to the Apennine forleand domain (Ricci Lucchi, 1986; Ori et al., 1986, Royden et al., 1987; Doglioni et al., 1996), where the emerged sectors of the Gargano Peninsula and the Apulia region correspond to the flexural bulge (Doglioni et al., 1994; de Alteriis, 1995; Bertotti et al., 1999). Post-Mesozoic tectonic deformation led to the definition of the W-E-trending “Gondola deformation belt” (Fig. 1). The main structural feature of the SW Adriatic Margin, with a clear morphologic expression in the Dauno Seamount (Colantoni et al., 1990; de Alteris and Aiello, 1993; Tramontana et al., 1995). On the Adriatic shelf and upper slope four stacked depositional sequences (termed Sequence 1-4, top down) are separated by shelf-wide unconformities (ES1-ES4) and their correlative conformities; these sequences accumulated during the last ca. 450 kyr (Trincardi and Correggiari, 2000; Ridente and Trincardi, 2002). Each sequence is composed of progradational units (low angle clinoforms passing distally into plane-parallel mud drapes) among which forced regression deposits record phases of sea level fall (Ridente and Trincardi, 2005). These sequences extend along strike over distances up to 300 km from the Central to the South Adriatic and form a composite shelf wedge with an overall backstepping architecture in the central Adriatic and forestepping stacking pattern north and south of Gargano Peninsula, respectively (Ridente and Trincardi, 2002), where Bari Canyon is located. The distribution and thickness variability of the four sequences suggests how tectonic activity controls sediment preservation. In particular, regressive sequence 2 (ca. 230-140 kyr) appears confined more seaward, along the Adriatic margin, compared to the sequences above and below, possibly reflecting a phase of tectonic deformation of the entire region (Ridente and Trincardi, 2006). Sequence 1 (ca. 140-25 kyr) shows variable thickness along the South Adriatic shelf, reaching a maximum in the shelf-edge region that rims the Northern head of BCS.

2.2. Oceanographic setting

Two main bottom-flowing water masses impact today the SW Adriatic Margin (Cushman-Roisin et al., 2001): the Levantine Intermediate Water (LIW) and the North Adriatic Deep Water (NAdDW; Fig. 1). The LIW forms in the Rhodes permanent cyclonic gyre in the Levantine Basin through evaporation during the summer and cooling during winter (Lascarotos et al. 1999). This salty water mass (29,0 kg/m^3) enters the South Adriatic on the eastern side and flows out southward along the SAM slope in intermediate depths (200-600 m; Orlic et al., 1992, Wust, 1961; Manca et al., 2002; Fig. 1). The NAdDW forms in the North Adriatic shelf and densifies through winter cooling and evaporation associated with local wind forcing (Bora events). This cold and dense water mass (29,8 kg/m^3) moves southward along the Italian cost passing around the Gargano promontory (Cushman-Roisin et al.

2001), and cascading obliquely across the SW-Adriatic slope, where strongly interacts with its topography (Vilibic and Orlic, 2002).

The long-lasting contour parallel LIW and the off-shelf cascading NAdDW have a similar southward flow component, and their dynamical interaction leads formation of several type of bottom-current sedimentary feature along the SW-Adratic Margin (Verdicchio et al., in press, Verdicchio and Trincardi, in press). The rate of formation and the physical properties of both water masses show strong seasonality (Roussenov et al., 1995), as indicated by oceanographic time series over the last few decades. Mooring data in the study area confirm that strong seasonally modulated S-flowing bottom currents, have a down-slope component and reach velocities greater than 60 cm sec^{-1} (Turchetto et al., this vol.). The modern current regime through the canyon, and on the open slope to the north, is discussed by Turchetto et al. (this vol.) and by Verdicchio et al. (in press).

Within the South Adriatic Basin, the South Adriatic Dense Water (ADW) reflects an open ocean formation process preconditioned by the permanent cyclonic South Adriatic Gyre (Pinardi and Masetti, 2000). The ADW flows out the Otranto Strait contributing to the formation of the Eastern Mediterranean Deep Water (Artegiani et al., 1989; Bignami et al., 1990).

2.3. Past Changes in the Adriatic oceanographic regime

The Adriatic physiography and oceanography underwent dramatic rearrangements during Quaternary climatic oscillations and particularly since the last glacial lowstand (Cattaneo and Trincardi, 1999). The north Adriatic shelf, where the NAdDW forms today, was subaereally exposed during the Last Glacial Maximum, when sea level was about 125 m below the modern level (Fairbanks, 1989). At that time, stabilized stratification of the water column allowed only weak and shallow temperature-driven winter convection, in the deepest parts of the basin (Myers et al., 1998). Likely, therefore, the last-glacial Adriatic was characterized by a low energy bottom current circulation.

Short-lived but important changes of the Adriatic circulation occurred also during intervals of decreased surface water salinity that impacted the whole Mediterranean leading to the deposition of sapropel layers (Vergnaud-Grazzini, 1977; Rohling and Hilgen, 1991; Ariztegui et al., 2000). The formation of a low-salinity surface water layer acted to hinder the potential overturning and deep-water formation limiting the open ocean convection to the upper 300 – 400 m, and resulting in a cold and relatively fresh outflow from the Otranto Strait and a more sluggish deep-water circulation (Rohling, 1994; Myers et al., 1998).

3. METHODS

A new bathymetric map of the BCS (Fig. 1) was acquired using a RESON 8160 multibeam echo sounder with nominal sonar frequency of 30 kHz and angular coverage sector of 135 beams per ping at 1^{o}. Chirp-sonar profiles were gathered using a hull-mounted 16-transducer source with a sweep modulated 2-7-kHz outgoing signal equivalent to a 3.5 kHz profiler. Chirp-sonar profiles allow vertical resolution of 0.5 m or better. A 30 kHz TOBI side scan sonar mosaic was acquired and processed following Le Bas et al. (1995). All data has been collected with differential GPS ship positioning every 5 seconds. Two current-meter moring were located along the main canyon branches and one on the open slope north of it, and are discussed in Turchetto et al. (this vol.). Long piston cores provide basic stratigraphic information on the evolution of BCS and are complemented by information from dredges on the upper reaches of canyon branches and short cores collected in the mooring sites.

4. RESULTS

4.1. Morphology and backscatter of the Bari Canyon System

A recently acquired multibeam bathymetry on the BCS allows recognize three E-W oriented sub-parallel conduits: the mid slope sinuous moat A, in the northernmost part of the BCS; 2) the channel levee complex B, in the middle part; and 3) the broad and deeply incised Canyon C, to the south (Fig.2).

Moat A is between 500 and 700 m and shows an overall lunate pattern and a substantial downslope broadening. Along the axis of moat A the sea floor displays a prevailing erosional character, as documented by patches of high backscatter on TOBI mosaics (Fig. 2b). The left (Northern) flank of the moat has a relief up to 100m and displays stripes of high and low backscatter sub-parallel to the moat axis, suggesting the presence of erosional steps into units of variable lithology. The right (southern) flank of moat A is characterised by low and more uniform backscatter that suggests the presence of muddy deposits.

Channel B is divided in 3 main parts: 1) down to 620 m the NNW-SSE channel is markedly erosional, narrow, straight and confined by steep walls up to 60-80 m high; 2) further seaward and down to 750 m water depth, the channel (labelled B^{I}) becomes narrower, slightly sinuous and veers along an E-W path; this channel appears somewhat subdued on swath bathymetry but is better recognised on the slope map (Fig. 2c); 3) in greater water depths the system evolves into a well defined channel (called B^{II}) that shows moderate sinuosity, has clear-cut edges and is accompanied by a levee wedge on its right-hand side, to the south (Fig. 2a). The channel disappears in water depths greater than 1100 m, where a subtle basin-ward bulge of the bathymetric contour is observed (Fig. 2c). The axial gradient of channel B decreases from several degrees in the head region to about 3.5° in 620 m water depth. At the exit of this deeply incised segment the sea floor becomes sub-horizontal before defining an area that dips landward (see bathymetric profile in Fig. 2c). In greater water depths channels B^{I} and B^{II} have axial dips of less than 1° but display well developed inner walls up to 6° steep.

Canyon C is broad (about 4 km) and characterised by a 600 m high southern wall that appears extremely steep (up to 31°). Along its straight axis, canyon C shows a terraced floor with repeated gradient changes accompanied by deep scours located in the flat areas downslope of major morphological steps. Multiple scars have high backscatter on TOBI mosaics in water depths of less than 300 m. Low backscatter is encountered in water depths of about 550 to 600 m in the area where channel B approaches the transition between the upper and lower portion of canyon C. The lower portion of canyon C has a more regular axial gradient, compared to the upper portion, and is characterised by dominantly high backscatter, particularly along the southern wall where abyssal furrows develop and multibeam bathymetry suggests the presence of slide blocks. In this area the left hand flank of canyon C is characterised by discontinuous stripes of high and low backscatter elongated parallel to the canyon axis. These features resemble the stripes observed on the erosional flank of moat A and define possible erosional steps.

4.2. Seismic stratigraphy of the Bari Canyon System

High-resolution seismic profiles document sedimentary bodies that thicken northward both within and outside the Bari Canyon System (Fig. 3) suggesting an active migration to the north (with a variable upslope component) that is consistent with the impact of the slope parallel current regime of the entire margin (Verdicchio et al., in press). Locally, bottom-current deposits accumulate on the irregular northward-dipping side of mass-transport deposits (Minisini et al., 2006) and on the southern flanks of the canyons, particularly in their upper reaches (Fig. 3, III-V).

4.2.1. Upper slope stratigraphy (ca. 200-600 m)

The head region of BCS is in of about 200 m water depths, seaward of a narrow outer shelf area that remained likely under marine conditions also during the LGM lowstand. North and south of the head region the regressive sequences exposed on the seafloor have different ages: in the south, deposits of Sequence 2 (Marine Isotopic Stage 7 and 6, Ridente and Trincardi, 2002) are truncated at their top by the steep walls of canyon C; in the north progradational deposits toward channel B belong to Sequence 1 and are therefore younger than MIS 6. This observation suggests that the last major phase of canyon down-cut took place during or at the end of the sea level fall that culminated with MIS 6. During the most recent cycle of sea level fluctuation, shelf margin progradation took place mostly north of BCS, impacted on the area of channel B and culminated in a phase of outer shelf and upper slope canyon down cut during the MIS 2 lowstand.

Seismic profiles define areas of dominant sea floor erosion both in canyon C and channel B and on the northern side of moat A (Figs. 2 and 4). The upper straight segment of channel B is characterised by sharp erosional flanks and a narrow relatively flat floor. The uppermost reaches of channel B are sediment barren and show sharply truncated parallel reflectors that belong to gently dipping regressive sequences. Proceeding downslope, the channel floor shows patches of acoustically transparent deposits with hummocky top. The age and facies of these deposits is poorly constrained but seismic profiles indicate repeated depositional phases (Fig. 4). Channel B is flanked by asymmetric levee wedges with the right-hand wedge higher and more developed in extent (Fig. 4). In particular, the right-hand levee of channel B advances onto the floor of the adjacent canyon C and pinches out with a low angle downlap onto older acoustically transparent deposits that provide an irregular substrate (Figs. 4, I-III). The southern flank of canyon C is characterised by very low acoustic-signal penetration, likely caused by the steep slope and the presence of cemented materials. Locally, truncated seaward dipping reflectors can be discerned (Fig. 4, IV).

4.2.2. Lower slope stratigraphy (ca. 600-900 m)

A channel-levee complex, below 600 m w.d., corresponds to the narrow channel detected on swath bathymetry seaward of the markedly erosional channel B (Fig.2). This channel-levee complex appears draped by a uniform plane-parallel unit (up to 20 m tick) with a very subtle wedging on the right-hand (southern) levee (Fig. 3, VI). Basinward, the draping unit decreases in thickness and the edges of the narrow channel beneath appear more evident. Concurrently, the right-hand levee becomes progressively more developed. In this sector of the channel-levee complex the base of the narrow channel reaches 40 m below the levee crest. The levee wedge and the underlying units are sharply truncated by canyon C that down cuts the sea floor to about 150 m deeper than the levee crest (Fig. 5). The lower part of canyon C is therefore surrounded by two markedly asymmetric flanks: the steep and high E-W-trending slope to the right (south) and the sharp but smaller erosional flank down cutting the channel levee complex on the left (north). Seismic profiles in figure 3 indicate that the units truncated by the left flank of canyon C are older than the last glacial interval.

4.2.3. Transitional area

Between the two areas described above (in between 600 and 700 m w.d.) channel B^I is poorly defined on morpho-bathymetric images compared to the deeply erosional channel B, upslope, and the channel-levee complex B^{II}, further downslope. On seismic profiles, the narrow channel B^I is accompanied by a small levee wedge and buried beneath a thick unit characterised by low-angle reflectors converging away from the channel axis. This feature appears down-cut on both sides by moat A, in the north, and Canyon C to the south (Fig. 4).

4.2.4. Mass-transport deposits in the Bari Canyon System

Mass-transport deposits into the BCS reach up to 150 km^2 in extent and 15 m in thickness. Seismic-stratigraphic correlation allows define simultaneous events affecting several sectors of the SW Adriatic Margin. Most mass-wasting deposits within the BCS do not extend to the basin floor and are less thick than elsewhere on the SW Adriatic Margin (Trincardi et al., 2004; Minisini et al., 2006). Within the BCS, mass-wasting deposits are typically buried, have erosional bases, irregular tops and chaotic or acoustically transparent seismic facies (Fig. 6). Seismic stratigraphic correlation indicates that at least one major mass-wasting deposit extends over most of the canyon area and appears coeval to extensive mass-wasting deposits generated along the SAM during the MIS 2 sea level lowstand (Minisini et al., 2006).

4.3. Sediment cores and sea floor samples

4.3.1. Sea floor samples

Surface samples (dredges and box cores) come from the outer shelf just outside the canyon, from the floor and the walls of Canyon C between 300 and 600 m (Tab. 1 and Fig. 7) and from the sites of mooring deployment (Turchetto et al., this volume). Samples recovered from canyon walls include various types of carbonate firm- and hardgrounds, with irregular, somewhat nodular surfaces often patinated by Fe-Mn oxides and affected by bioerosion (Fig. 7a-c). These indurated substrates provide a suitable ecospace to encrusting epifauna, mainly serpulid polychaetes, bryozoans, sponges, solitary corals (*Caryophyllia smithii*) and inarticulated brachiopods (*Neocrania anomala*) some of which still alive when sampled (Fig. 7d). Other lithologies contributing to the canyon stratigraphy include marly sandstones intensely bored by *Pholadidea loscombiana* clams (Fig. 7g), a cold Pleistocene indicator (Colantoni et al., 1975; Malatesta and Zarlenga, 1986) and loose “pipes” resembling fluid escape chimneys (Fig. 7e,f; Kulm and Suess, 1990; Schwartz et al., 2003). Dead but sub-recent (dating in progress) azoxanthellate scleractinian corals (*Desmophyllum dianthus*, *Lophelia pertusa*, *Madrepora oculata*) occur as well in the dredged catch (Fig. 7h). These taxa are known to colonize deep-water firm and hard substrata (Taviani et al., 2005, with references therein), a further indication of communities exploiting the canyon walls since the late Holocene at least. An articulated shell of the sediment-nestling mytilid *Modiolula phaseolina* embedded within a carbonate hardground (Fig. 7i) provided a calibrated AMS- C^{14} age of 50000±3000 years BP (Poznàn Radiocarbon Laboratory). Combined sedimentary and biological data provide evidence of prolonged temporal exposition to seawater under sedimentstarving conditions that promoted submarine lithification and oxide precipitation, and the concurrent and still persistent action of strong currents coupled with trophic regimes capable to sustain sessile filter feeding and micro-carnivore communities.

Samples obtained by coring and dredging from the outer shelf contain shell assemblages dominated by the glacial Pleistocene pectinid *Pseudamussium septemradiatum* associated with other molluscs such as the cold–water faunas *Iothia fulva*, *Buccinum humphreysianum* and *B. undatum*, the bivalves *Venus casina* and *Karnecampia bruei*, large Pleistocene morphotypes of the bryozoan *Turbicellepora coronopus*, the terebratulid brachiopod *Gryphus vitreus*, the solitary scleractinian coral *Caryophyllia smithi* and many other invertebrates (Fig. 7l). These dominantly last glacial assemblages are widely distributed in this area and often still exposed (Colantoni and Gallignani, 1978; Taviani, 1978). Traditional C^{14} dating of *P.septemradiatum* valves provide calibrated ages of 19000±370 and 15350 ±250 years BP (Colantoni et al., 1975), suggesting that post-Last Glacial Maximum communities settled on a silty-muddy middle-outer shelf, characterised by times of sediment starvation as documented by advanced shell bioerosion and epifaunal occupancy (bryozoans, oysters, serpulid polychaetes, corals) of many shells (Fig. 7-l).

4.3.2. Sediment cores and stratigraphic correlations

Figure 8 shows a stratigraphic correlation among core SA03-01, north of the BCS, and two cores collected through the right-hand levee of the upper portion of channel B and outside the left levee of B’. Core correlation is mainly based on foraminifera assemblages and magnetic susceptibility curves whose peaks commonly indicate the presence of tephra layers (Verdicchio et al., in press). Ages are ascribed to biozone boundaries based on published literature (Jorissen et al., 1993; Asioli, 1996; Asioli, et al., 1999; 2001; Capotondi et al., 1999; Ariztegui et al., 2000). The planktonic foraminifera ecozones defined for the Central Adriatic for the last 20 kyr (Asioli, 1996; Asioli et al., 1999, 2001) correlate to the Southern Adriatic ones. Reference cores in the Central Adriatic are also constrained by oxygen stable isotope stratigraphy, ^{14}C AMS datings, tephrochronology, pollen record, planktic and benthic foraminifera assemblages in a well defined seismic stratigraphic context (Trincardi et al., 1996, 1998; Asioli, 1996; Calanchi et al., 1998; Ariztegui et al., 2000).

In the BCS area core stratigraphy shows from top to bottom: 1) a late-Holocene interval above the Last Occurrence of *Globorotalia inflata* (Asioli, 1996); 2) a well defined Sapropel S1 interval characterised by large specimens of *Globigerinoides ruber* (pink) with thin and inflated tests; all cores show evidence of a marked break of Sapropel 1 characterised by the re-appearance of *Globorotalia inflata* (Rohling et al., 1997; Ariztegui et al., 2000). All cores include a tephra layer into the sapropel sediment likely corresponding to the Mercato event (Calanchi et al., 1998; Siani et al., 2001; Lowe et al., in press); 3) the pre-Boreal interval, characterised by repeated and short-term oscillations in abundance of cold- and warm-water species; 4) the GS-1 (Younger Dryas) interval marked by a dominant cold-water association with *Globigerina bulloides*, *Neogloboquadrina pachyderma* and *Globorotalia scitula*, and including a tephra layer, known as C1, that corresponds to the Pomici Principali event (Asioli, 1996; Calanchi et al., 1998; Lowe et al., in press); 5) the GI-1 interval (Bolling/Allerod) marked by a basal peak in the abundance of *Globigerinoides ex gr. ruber* and an oscillatory cooling trend as previously observed in the Central Adriatic (Asioli et al., 1999, 2001); 6) a glacial interval dominated by cold-water species like *Globigerina bulloides*, *Neogloboquadrina pachyderma* and *Globorotalia scitula* (the interval below the Bolling-Allerod interval on Fig. 8).

In contrast to other Adriatic cores a small percentage of *G.inflata* is present throughout the last 6 kyr interval (HST) in cores SA03-09 and SA03-01 (Fig. 8). Several authors (Jorissen et al., 1993; Asioli, 1996; Capotondi et al., 1999; Ariztegui et al., 2000) have demonstrated that the disappearing of *G. inflata* from the Adriatic circa 6 kyr B.P. is a well documented bio-event, which approximates the achievement of the modern sea level highstand and corresponds to the maximum flooding surface defined on seismic profiles on the shelf (Trincardi et al., 1996; Cattaneo and Trincardi, 1999, Cattaneo et al., 2003). The occurrence of *G. inflata* during the last 6 kyr is ascribed to a component of re-sedimentation and deposition by either slope parallel currents or by sediment shedding from shallower waters. Also south of BCS in 716 m w.d. Jorissen et al. (1993) document the occurrence of a very low percentage of *G. inflata* in a core that recoverd a relatively expanded sequence (ca. 1.20 m) of the last 6 kyr B.P.

The last glacial-interglacial transition was an interval of extreme variability in sediment accumulation rates on the SAM slope (Verdicchio et al., in press; Verdicchio and Trincardi, in press): in the northern portion of the margin, after the late glacial period, sedimentation rates are in the order of 25 cm kyr^{-1}, while in the BCS area sediment accumulation rates are up to about 185 cm kyr^{-1}. The post-LGM sediment accumulation rates likely reflect increased off-shelf sediment transport proceeding to the south. Along most of the SAM slope, deposition decreased during the last 6 kyr, when modern sea level highstand was achieved, with sediment accumulation rates varying between 2 and 35 cm kyr^{-1} (Verdicchio et al., in press). Away from the main erosional pathways, sediment accumulation rates in the BCS reached values between 35 and 70 cm kyr^{-1} during this interval.

4.3.3. *Seismic stratigraphic correlation*

The cores collected in the BCS allow assign an age to key reflectors and compare how sediment accumulation rates change in time and space. By projecting core SA03-09 on a seismic profile (Fig. 9) we can ascribe ages to key reflectors as follows: 1) the onset of the channel-levee complex predates the LGM and a down-section age extrapolation suggests that the base of the deposit is within the last 120 kyr; 2) the levee wedge was still growing during at least the first half of the post glacial sea level rise; 3) the draped unit that mantles the channel-levee complex B is Holocene (post GS-1) and shows a subtle reflector convergence toward canyon C; 4) all units are down cut by canyon C. In its upper reaches, channel B is deeply down-cut and the levee on its right shows relatively-low accumulation rates since the Younger Dryas suggesting that sediment bypass the area in flows that are mostly confined within the canyon axis (Fig. 9).

5. DISCUSSION

The BCS develops north of a high (up to 800 m) and steep (> 30°) E-W wall on the continental slope, likely reflecting structural control (Ridente et al., this vol.). This morphological wall not only provides a source for mass wasting but also forms a barrier capable of diverting along-slope bottom currents that flow southward reaching velocities greater than 60 cm sec^{-1} (Turchetto et al., this vol.). BCS has a complex history of erosion and deposition that includes major phases of down cut, well documented on the outer shelf, during MIS 8 and 6 (Ridente et al., this vol.), leading to the formation of a broad canyon partially floored by mass-transport deposits beneath the modern C and B conduits (Fig. 10-1). This large canyon was likely reactivated during falling sea level conditions after MIS 5 and until the LGM. We discuss the stratigraphic evidence that characterises the canyon evolution during and after the LGM.

5.1. Activity of the Bari Canyon System since the LGM lowstand

During the LGM lowstand, the shoreline was located close to the modern 125 m isobath and in the order of 10 km from a rather deep shelf edge (now in ca. 180-200 m; Fig. 10-1). The outer-shelf remained submerged during the LGM and was swept by currents as indicated by the sharp truncation of progradational clinoforms in this area. The direction of progradation of Sequence 1 suggests that circulation was likely southward (Ridente and Trincardi, 2002), as today, and bottom-hugging currents could be captured by the head of BCS located near shore and in very shallow water (40-60 m). During LGM, progradational units were mainly deposited on the NW side of the BCS indicating sustained sediment transport into the canyon. Channel-levee complex B begun to grow during the last sea level cycle and particularly during the LGM lowstand, resulting in a pronounced levee asymmetry (Figs. 9 and 10-2). Seismic profiles (Figs. 5 and 9) show consistently that the right-hand levee of channel B advances onto the floor of canyon C, located just south, that remained sediment starved as documented by the presence of firm- and hard-ground substrates and by a peculiar assemblage of molluscs and corals. This lateral spreading of levee B is consistent with flows that tend to overbank predominantly to the right of the conduit, resulting in a downlap termination or a more gradual pinch out of seismic reflectors in the thalweg of canyon C.

During this phase, channel B evolved down slope into a low-sinuosity submarine channel (B^{I} and B^{II} in Fig. 2) reaching the basin floor but not resulting in significant depositional relief as observed in most examples of turbidity systems (e.g., Normark and Piper, 1991; Weimer, 1991; Galloway, 1998). The transitional area (B^I) is subdued both on multibeam images and on Chirp-sonar profiles reflecting lateral infill and partial burial by contourite deposits. The lack of a depositional lobe at the channel terminus and the evidence of lateral infill of part of the channel, upslope, indicate that the system has been continuously affected by slope transverse currents able to divert down slope flows and/or rework sediment transported through channel-levee complex B.

Several schemes have been proposed that define possible interactions between turbidity-current deposits and along-slope bottom currents (e.g., Faugères et al., 1999; Stow et al., 2002). Most attention has been directed to the reworking of base-of-slope deposits that become progressively re-organised into contour-parallel, typically mounded, deposits (Normark et al., 1993; Ross et al., 1994). In the BCS an additional effect is the lateral infill of a channel feature (channel B^I, in particular) by the flow of slope-parallel currents against the inner side of the right-hand (and most developed) levee wedge (Fig. 4).

5.2. Recent Activity of the Bari Canyon System

Sediment cores also indicate that channel-levee complex B has been growing well after the end of the LGM (Fig. 8), although the wedging of seismic reflectors across the levee became progressively less pronounced. Today, density-driven bottom currents cascade off shelf and flow both across the open slope and through the BCS, reaching velocities greater than 60 cm sec^{-1} (Turchetto et al., this vol.). At core scale, the upslope portion of levee wedge B does not show typical overbank turbidity current deposits, as observed in many examples of deep sea fans (e.g., Piper and

Savoye, 1993; Migeon et al., 2001). Deposition is instead dominated by hemipelagic sediment and results in a reduced thickness of the Late-Holocene unit compared to cores on the open slope north of BCS (Verdicchio et al., in press). During this interval of reduced deposition, density flows had reduced sediment load and/or remained confined within channel B, which was likely waxed by downslope currents, as indicated by the evidence of steep erosional canyon walls and truncated subsurface reflectors. These observations are consistent with the evidence of limited levee aggradation during the mid-late Holocene.

The upper part of Canyon C is sediment starved and swept by intense but relatively clear bottom currents. In contrast, the lower part becomes gradually more erosional, as documented by the occurrence of truncated reflectors and erosional steps on the left canyon wall (Fig. 5). The lower canyon C down-cuts B^{II} levee wedge including its Holocene drape, indicating substantial erosion during modern interglacial conditions (Fig. 10-3). The steep and high southern wall of BCS acts as a hydrological barrier that confines bottom currents flowing either along slope (LIW) or cascading off the shelf oblique to the slope (NAdDW), possibly favouring their acceleration. This view is consistent with the occurrence of erosional furrows further eastward at the exit of canyon C. The main erosional elements of the BCS are the upper, straight and narrow, portion of channel B, down to about 600 m water depth, and the deepest portion of canyon C, beyond 700m water depth. A possible connection between these two elements corresponds to the area where levee wedge B reaches the minimum elevation and presents elongated erosional steps on its outer-bank side dipping toward canyon C. In contrast, the upper part of canyon C is flushed by turbidity bottom currents while the lower segment of channel B is abandoned. We suggest that after the LGM, and probably in very recent times, density currents started to down cut substantially the upper portion of channel B. The gradient inversion at the exit of this straight erosional segment may be instrumental in generating flow detachment and spill over into lower canyon C (Figs. 2c and 10-3). Whether this pathway reflects a single major event or recurrent spill over flows is difficult to ascertain with the available data.

5.3 Sediment sources during LST and HST conditions

During the last glacial lowstand the sediment source for channel B was likely long-shore drift, while during higjstands, when the shoreline is further landward, the canyon is impacted by off-shelf density currents (the NAdDW) that cascade along the entire SAM (Fig. 10). Sediment cores through the upper section of levee wedge suggest that deposition took place through diluted flows resulting in the deposition of mottled and structure-less mud. Also in the area outside the left-hand levee of the upper channel B cores do not show sedimentary structures typical of turbidity current deposits, despite downslope transport is proved by the presence of a small but persistent component of recycled benthonic foraminifera from the shelf (Fig. 7). Direct observation from current-meter moorings and sediment traps North of BCS, within channel B and in canyon C define clear episodes of dense waters cascading off the shelf and resulting in net downslope transport at rates that appear similar within and outside the BCS (Turchetto et al., this vol.).

In summary, the BCS is impacted by down slope currents, both during sea level lowstand and modern conditions. In the first case, the growth of channel-levee complex B suggests an activity of mud-laden turbidity currents. In the latter case, down slope flowing water mass is instead driven by density gradients and impacts the entire margin outside BCS. When this water mass is captured by the narrow conduit of channel B lateral confinement leads to flow acceleration and consequent channel floor erosion. At the exit of this straight conduit, a high momentum down slope flow impacts an area of flat or up-slope dipping sea floor and may result in flow detachment and spill over into the lower canyon C (Fig. 11).

CONCLUSIONS

Bari Canyon System (BCS) is the main active sediment conduit of the SW Adriatic margin since the last glacial interval. During this interval, processes typical of active submarine canyons, such as turbidity currents and mass-transport events, are replaced or overshadowed by intense cascading currents impacting seasonally the entire SW Adriatic margin and accelerating through the canyon. When captured by the BCS, the off-shelf cascading current becomes confined eroding, transporting and depositing fine-grained sediment mimicing a very-dilute turbidity current.

Geomorphological, seismo-stratigraphic, sedimentological and biostratigraphic data support the following conclusions: **1.** BCS is characterised by a marked morphological asymmetry with a high-relief, steep and erosional right hand flank. **2.** The most recent phase of extensive canyon erosion occurred during the lowstand of MIS 6, as part of a long-term history of canyon down-cut over the last ca. 350-400 kyr. **3.** During the last sea level cycle (MIS 5e to present), shelf-margin progradation was particularly active on the Northern side of BCS where the apex of channel B is located. **4.** Channel-levee complex B begun to grow during the last sea level cycle and particularly during the LGM when the levee asymmetry became more pronounced. After the LGM, channel B became abandoned in water depths greater than ca. 700 m but more actively incised in shallower areas. **5.** Today, the cold and dense bottom waters that form on the Adriatic shelf through winter cooling enter the BCS with a reduced sediment load but capable to hug the seafloor and entraining sediment. Since these dense waters can reach velocities greater than 60 cm sec^{-1} it is conceivable that, during modern highstand conditions, they down cut the steep walls and sweep the floor of the upper portion of channel B. In deeper waters, instead, the most actively eroded element is canyon C which down cuts the abandoned levee complex of channel B. **6.** The evidence of active erosion both on the upper portion of channel B and the lower part of canyon C suggests that cascading currents flushing the upper trunk of B tend to overbank towards the right and spill over into canyon C.

Acknowledgments We thank captains and crews of R/V *Urania* for helping during cruises SA03, ST04 and ST05. The TOBI team at NOC, Southampton, is also acknowledged for their invaluable work on cruise SAGA03 and post-cruise processing. This study is supported by the European projects EUROSTRATAFORM (EC contract n. EVK3-CT-2002-00079), the European Access to Seafloor Survey Systems "EASSS III-TOBI side-scan sonar" (HPRICT199900047) , and the HERMES European project (G0CECT200551112341). This is ISMAR (CNR) contribution number 1514.

Figures list

Figure 1. Location of the Adriatic in the Mediterranean Sea with area of formation and main circulation path of the Levantine Intermediate Waters (upper left). Schematic bathymetry and main current path of the Adriatic basin and areas of formation of the North Adriatic Deep Waters (NAdDW) and Adriatic Deep Waters (ADW) (upper right). Bathymetry of the SW Adriatic Margin showing the Bari Canyon System (BCS) and major slump scars affecting the outer shelf and slope. The Dauno Seamount and the trace of Gondola deformation belt are also reported. Triangles represent mooring locations.

Figure 2. a) Detailed bathymetry of the BCS; b) TOBI mosaic on the same area with simplified bathymerty superimposed for reference; c) map of the slope gradient. Note that the upper and lower portions of channel B (called B and B^{II}, respectively) are best detected on bathymetry data while the intermediate portion of this system (B^{I}) is less evident morphologically, possibly in response to lateral infill. The highest backscatter values are in canyon C, particularly along its southern steep and erosive wall. Other areas of high backscatter are the erosional walls of the upper portion of channel B and the Northern flank of moat A.

Figure 3. Seismic profiles across the BCS document the spatial relationship among the three main conduits from shallower to deeper slope areas. The thalweg of channel B is deeply incised than canyon C in the upper slope (I), viceversa in areas deeper than 650 m where canyon C is actively eroding the levee of channel B (IV). Moat A is visible on the right portion of profiles in intermediate slope depths (II) and disappears downslope (VI). Outside the canyon, bottom-current deposits (star symbol) are asymmetrically distributed on the northern flank of pre-existing sea floor reliefs (IV) and sediment waves (V). All profiles have the same vertical exaggeration. Dashed lines are location of dredges that collected samples showed in figure 7.

Figure 4. Detailed N-S profile along the upper slope showing the morphologic and stratigraphic relationship among canyon C, channel levee complex B and moat A. The channel-levee complex of B is filled by stacked acoustically transparent deposits and downlaps into the adjacent canyon C. The floor of the channel levee complex B and

of canyon C consist of acoustically transparent deposits interpreted as mass transport deposits. Location in Fig. 3.

Figure 5. Evidence of canyon C down-cutting the right-hand levee of channel B and producing elongated erosional steps seen on TOBI (arrows) and on a Chirp sonar profile. The Chirp profile also documents the asymmetric deposition of Holocene deposits north of the pre-existing depositional relief of channel-levee complex B. TOBI mosaic also shows furrows in deeper waters (dashed lines). Location in Fig. 3.

Figure 6. Chirp profile oriented downslope (roughly EW) and positioned in figure 3 through the erosional upper portion of channel B (left) and the floor of moat A (right) where acoustically-transparent mass-transport deposits are partly buried and partly exposed at sea floor. The close-up shows marked erosional truncations of older tilted deposits below and younger depositional units pinching out above the mass-transport deposit. Cores SA03-02 and SA03-09 are positioned and will be discussed later in the text.

Figure 7. Seafloor samples recovered from stations indicated in Fig. 3. a) large slab of carbonate hardground; note irregular nodular surface and localised oxide patination; b) carbonate hardground showing intense epifaunal colonisation by serpulid polychaetes, brachiopods and bryozoans; c) carbonate hardground showing a complete stratigraphy from firm mudstone still including pockets of unlithified sediment to micritised upper surface, micro-bioeroded and encrusted by Recent epifauna; the mudstone retains *in situ* shells (arrow) of the nestling mytilid *Modiolula phaseolina* that provided an age > 50 kyr; d) close-up of a living specimen of the inarticulated brachiopod *Neocrania anomala* (arrow) documenting present sediment-starvation at this site; on the lower left side a serpulid polychaete; e) ‘pipe’ encrusted by recent epifauna (serpulid polychaetes, brachiopods and bryozoans); note scalloped external surface; f) section of a hollowed ‘pipe’; g) articulated shell of the boring clam *Pholadidea loscombiana* (late Pleistocene) still *in situ* within fine sandstones; sample hosted in the Zoological Museum of the University of Bologna (catalog n. MZB44056); h) articulated nestling mytilid *Modiolula phaseolina* embedded in a carbonate concretion; i) deep-water scleractinian corals from the southern wall of Bari Canyon: L= *Lophelia pertusa*, M = *Madrepora oculata*, D = *Desmophyllum*

dianthus; C = *Caryophylli*a sp; l) skeletal assemblage from post-LGM Pleistocene silty-muddy units: P = *Pseudamussium septemradiatum,* V = *Venus casina*, N = *Neopycnodonte cochlear*, C = *Caryophyllia smithii*, T = *Turbicellepora coronopus*, S = serpulid polychaetes, E = echinoid spine; note that most valves are often bioeroded and encrusted by epifaunal organisms also inside the shell.

Figure 8. Core correlation between SA03-2 and SA03-9 within the BCS (location in Figs. 4 and 7) and SA03-1 (location in Fig. 1) just north of it. Quantitative micro-paleotological analysis of core SA03-01 allows identify the last occurrence datum of *G. inflata*, that approximates the base of the highstand deposits. The post-glacial record that accompanies the eustatic rise, includes Sapropel S1 and the Pre-Boreal, both within the Holocene, and the GS-1 and GI-1 intervals, below Holocene. Note that core SA03-02 documents a reduced rate of levee aggradation after MIS2 and, in particular, during the HST (above the L.O of *G. inflata*). During the same interval, both cores SA03-01 and SA03-09, respectively outside and within the BCS, show much higher sediment accumulation rates with a continuous shedding of reworked shelf material also during the modern HST.

Figure 9. Seismic stratigraphic correlation based on biostratigraphic information from cores SA03-02 and SA03-09. Chirp profiles ST179 and ST166 report the seismic reflectors that approximate the top of MIS 2 and the base of the HST thereby bracketing the section that deposited during the eustatic rise and the resulting drowning of the Adriatic shelf.

Figure 10. Cartoons portraying three phases in the late-Quaternary evolution of the BCS (left); fixed schematic profiles of the upper and lower slope show three key intervals of the canyon evolution: 1) lowstand of MIS 6 after a broad erosional valley formed; this valley remained active during the following cycle of sea level fluctuation leading to the lowstand of MIS 2. 2) during the lowstand of MIS2, BCS was fed by alongshore drift and channel-levee complex B developed occupying the northern portion of the pre-existing erosional valley. During this phase channel B was connected, upslope, to the area of rapid progradation of Sequence 1. 3) during modern highstand conditions the canyon is impacted by the same bottom currents as the rest of the slope outside. Currents down flowing through channel B may accelerate,

entraining sediment from the canyon walls and floor, and *jump* into the lower part of canyon C, actively eroded at present.

Figure 11. 3D bathymetry of the BCS viewed from the NE. Arrows denote the path of two main water masses in the area: the LIW flowing along the slope and the NAdDW cascading across the slope outside and within the BCS. During modern highstand conditions the canyon head is not fed directly by river born density flows as it may have been during glacial intervals. NAdDW may however focus into the straight upper segment of channel B, accelerate and possibly *jump* into canyon C, bypassing the area where the relief of the right hand levee of B is minimum. Moat A is also impacted by down slope flows and along slope bottom currents (red arrows denoting the LIW). The upper part of canyon C is also swept by down slope currents but the living faunal assemblage encountered here suggests that flows have a reduced turbidity.

Table 1. Position of dredges and box core samples.

References:

Artegiani, A., Azzolini, R., Salusti, E. 1989. On dense water in the Adriatic Sea. Oceanol. Acta, 12, 151-160.

Ariztegui, D., Asioli, A., Lowe, J. J., Trincardi, F., Vigliotti, L., Tamburini, F., Chondrogianni, C., Accorsi, C. A., Bandini Mazzanti, M., Mercuri, A. M., van der Kaars, S., McKenzie, J. A., Oldfield, F., 2000. Palaeoclimate and the formation of sapropel S1; inferences from late Quaternary lacustrine and marine sequences in the central Mediterranean region. Palaeogeography, Palaeoclimatology, Palaeoecology, 158, 215-240.

Asioli, A., 1996. High-resolution foraminifera biostratigraphy in the central Adriatic basin during the last deglaciation: a contribution to the Paliclas Project. In: Guilizzoni, P., Oldfield, F.L. (Eds.), Palaeoenvironmental analysis of Italian crater lake and Adriatic sediments (PALICLAS project). Mem. Istit. It. Idrob., 55, 197-217.

Asioli A., Trincardi F., Lowe J.J., Oldfield F. 1999. Short-term climate change durino the Last Glacial-Holocene transition: comparison between Mediterranean records and Grip event stratigraphy. Journal of Quaternary Science, 14, 373-381.

Asioli A., Trincardi, F., Lowe, J. J., Ariztegui, D., Langone, L., Oldfield, F. 2001. Sub-millennial climatic oscillations in the Central Adriatic during the last deglaciation: paleoceanographic implications. Quaternary Science Reviews, 20, 33-53.

Baztan, J., Berne, S., Olivet, J., Rabineau, M., Aslanian, D., Gaudin, M., Rehault, J. P., Canals, M. 2005. Axial incision; the key to understand submarine canyon evolution (in the western Gulf of Lion). Marine and Petroleum Geology, 22, 805-826

Bertotti, G., Casolari, E., Picotti, V. 1999. The Gargano Promontory; a Neogene contraction belt within the Adriatic Plate. Terra Nova, 11-4168-173.

Bignami, F., Salusti, E., Schiarini, S. 1990. Observations on a bottom vein of dense water in the Southern Adriaticand Ionian Seas. Journal of Geophysical Research, 95, 7249-7259.

Calanchi N., Cattaneo A., Dinelli E., Gasparotto G., Lucchini F. 1998. Tephra layer in Late Quaternary sediments of the Central Adriatic Sea. Marine Geology, 149, 191-209.

Capotondi L., Borsetti A. M., Morigi C. 1999. Foraminiferal ecozone, a high resolution proxy for the late Quaternari biochronology in the central Mediterranean Sea. Marine Geology, 153, 253-274.

Carlson, P. R. and Karl, H.A. 1988. Development of large submarine canyons in the Bering Sea, indicated by morphologic, seismic, and sedimentologic characteristics. GSA Bulletin, 100, 10, 1594-1615.

Cattaneo, A. and Trincardi, F. 1999. The late-Quaternary transgressive record in the Adriatic Epicontinental Sea: basin widening and facies partitioning. In: Bergman K., Snedden J. (Eds.), Isolated shallow marine sand bodies: sequence stratigraphic analysis and sedimentologic interpretation. SEPM, Spec. Publ., 64, 127-146.

Cattaneo, A., Correggiari, A., Langone, L., Trincardi, F. 2003. The late-Holocene Gargano subaqueous delta, Adriatic shelf: Sediment pathways and supply fluctuations. Marine Geology, 193, 61-91.

Colantoni, P. and Gallignani, P. 1978. Quateranry evolution of the continental shelf off the coast of Bari (South Adriatic Sea): shallow seismic, sedimentological and faunal evidences. Geologie Mediterraneenne, V (3), 327-338.

Colantoni P., Noto P., Taviani M. 1975. Prime datazioni assolute di una fauna fossile a *Pseudamussium septemradiatum* dragata nel basso Adriatico. Giornale di Geologia (s. 2a) 40, 133-140.

Colantoni, P., Tramontana, M., Tedeschi, R. 1990. Contributo alla conoscenza dell'avampaese apulo: struttura del Golfo di Manfredonia (Adriatico meridionale): Giornale di Geologia, 52 (1-2), 19-32.

Cushman-Roisin, B., Gacic, M., Poulain, P. M. & Artegiani, A. (eds) 2001. Physical oceanography of the Adriatic Sea: Past, present and future. pp. 304.Artegiani, A., Azzolini, R., Salusti, E. 1989. On dense water in the Adriatic Sea. Oceanologica Acta, 12, 151-160.

Cutshall, N.H., Larsen, I.L., Olsen, C.R., Nittrouer, C.A., DeMaster, D.J. 1986. Columbia River sediment in Quinault Canyon, Washington – Evidence from artificial radionuclides. Marine Geology, 71, 125-136.

Daly, R,A., 1936. Origin of submarine canyons. Am. Jour. Sc., 31, 401-420.

de Alteriis, G. 1995. Different foreland basins in Italy; examples from the central and southern Adriatic Sea. Tectonophysics, 252, 1-4, 349-373.

de Alteriis, G., Aiello, G. 1993. Stratigraphy and tectonics offshore of Puglia (Italy, southern Adriatic Sea). Marine Geology, 113, 3-4, 233-253.

Doglioni, C., Mongelli, F., Pieri, P., 1994. The Puglia uplift (SE Italy): an anomaly in the foreland of the Apennine subduction due to buckling of a thick continental lithosphere. Tectonics, 13, 1309-1321.

Doglioni, C., Harabaglia, P., Martinelli, G., Mongelli, F., Zito, G. 1996. A geodynamic model of the Southern Apennines accretionary prism. Terra Nova, 8, 540-547.

Droz, L., and Bellaiche, G., 1985, Rhone deep-sea fan: morpho-structure and growth pattern: AAPG Bulletin, v. 69, p. 460-479.

Fairbanks, R.G. 1989. A 17,000 year glacio-eustatic sea level record: influence of glacial melting rates on the Younger Dryas event and deep-ocean circulation. Nature, 342, 637–642.

Farre, J.A., MecGregor, B.A., Ryan, W.B.F., Robb, J.M. 1983. Breaching the shelfbreak: passage from youthful to mature phase in submarine canyon evolution. In: Stanley D.J., Moore T.G. (Eds.), The shelfbreak: critical interface on continental margins SEPM, Spec. Publ., 33, 25-39.

Faugères, J. C., Stox, D. A. V., Imbert, P., Viana, A. 1999. Seismic features diagnostic of contourite drifts. Marine Geology, 162, 1-38.

Field, M.E., and Gardner, J.A. 1990. Pliocene-Pleistocene growth of the Rio Ebro margin, northeast Spain: A prograding-slope model: Geological Society of America Bulletin, v. 102, p. 721-733.

Gallignani, P. 1982, Recent sedimentation processes on the Calabrian continental shelf and slope (Tyrrhenian Sea, Italy): Oceanologica Acta, 5, 493-500.

Galloway, W.E. 1998. Siliciclastic slope and base-of-slope depositional systems: Component facies, stratigraphic architecture, and classification. AAPG Bulletin, 82-4, 569-595.

Galloway, W.E., Dingus, W.F., Paige, R.E. 1991. Seismic and depositional facies of Paleocene-Eocene Wilcox Group submarine canyon fills, Northwest Gulf Coast, U.S.A. In: Weimer P., Link M.H. (Eds.), Seismic facies and sedimentary processes of submarine fans and turbidite systems. Springer-Verlag, 247-271.

Kolla, V. and Perlmutter, M.A. 1993. Timing of turbidite sedimentation on the Mississippi fan: American Association of Petroleum Geologists Bullettin, 77, 1129-1141.

Kulm, L.D. and Suess, E. 1990. Relationship between carbonate deposits and fluid venting: Oregon accretionary prism. J. Geophys. Res. 95-B6, 8899–8915.

Jorissen, F.J., Asioli, A., Borsetti, A.M., Capotondi, L., de Visser, J.P., Hilgen, F.J., Rohling, E.J., van der Borg, K., Vergnaud-Grazzini, C., Zachariasse, W.J. 1993. Late Quaternary central Mediterranean biochronology. Marine Micropalaeontology, 21, 169-189.

Lascaratos, A., Roether, W., Nittis, K. & Klein, B. 1999. Recent changes in deep water formation and spreading in the eastern Mediterranean Sea: a review. Progress in Oceanography. 44, 5–36.

Le Bas, T.P. , Mason D.C. & Millard N.W. 1995. TOBI Image Processing - The State of the Art. IEEE Journal of Oceanic Engineering, 20, 85-93.

Lowe, J.J., Blockley, S., Trincardi, F., Asioli, A., Cattaneo, A., Matthews, I.P. Pollard, Wulf, S., in press. Age modelling of late Quaternary marine sequences in the Adriatic: towards improved precision and accuracy using volcanic event stratigraphy. Continental Shelf Research.

Malatesta, A. and Zarlenga, F. 1986. Northern guests in the Pleistocene Mediterranean Sea. Geologica Romana, 25, 91-154.

Manca, B. B., Kovacevic, V., Gacic, M., Viezzoli, D. 2002. Dense water formation in the Southern Adriatic Sea and interaction with the Ionian Sea in the period 1997-1999. Journal of Marine System, 33-34, 133-154.

McAdoo, B.G., Orange, D.L., Screaton, E., Lee, H., Kayen, R. 1997. Slope basins, headless canyons, and submarine palaeoseismology of the Cascadia accretionary complex. Basin Research, 9, 313-324.

Migeon, S., Savoye, B., Zanella, E., Mulder, T., Faugères, J.C., Weber, O. 2001. Detailed seismic-re£ection and sedimentare study of turbidite sediment waves on the Var Sedimentare Ridge (SE France): Significance for sediment transport and deposition and for the mechanisms of sedimentwave construction. Marine and Petroleum Geology, 18, 179-208.

Minisini, D., Trincardi, F., Asioli, A. 2006. Evidences of slope instability in the South Adriatic Margin. Natural Hazards and Earth System Sciences, 6, 1, 1-20.

Mutti, 1985. Turbidite systems and their relations to depositional sequences. In: G.G. Zuffa (Eds.) Provenance of arenites. NATO ASI Series. Reidel Publishing, Holland: 65-93.

Myers, P. G., Haines, K., Rohling E. J. 1998. Modeling the paleocirculation of the Mediterranean: the last glacial maximum and the Holocene with emphasis on the formation of Sapropel S1. Paleoceanography, 13-6, 586-606.

Normark, W.R. 1970. Growth patterns of deep sea fans. AAPG Bulletin, 54, 2170-2195.

Normark, W.R., and Piper, D.J.W. 1991, Initiation processes and flow evolution of turbidity currents: implications for the depositional record, in Osborne, R.H., ed., From Shoreline to Abyss: SEPM Special Publication, 46, 207-230.

Normark, W.R., Posamantier, H.W., Mutti, E. 1993. Turbidite systems: state of the art and future directions. Reviews of Geophysics, 31, 91-116.

Palanques, A., Alonso, B., Farràn, M. 1994. Progradation and retreat of the Valencia fanlobes controlled by sea-level changes during the Plio-Pleistocene (northwestern Mediterranean). Marine Geology, 117, 195-205.

Piper, D.J.W. and Savoye, B. 1993. Processes of late Quaternary turbidity current flow and deposition on the Var deep-sea fan, north-west Mediterranean Sea: Sedimentology, 40, 557-582.

Ori, G.G., Roveri M., Vannoni, F. 1986. Plio-Pleistocene sedimentation in the Apenninic-Adriatic foredeep (Central Adriatic sea, Italy). In: Allen, P.A. & Homewood, P. (Eds.) Foreland Basins. IAS Spec. Publ. 8, 183-198.

Orlic, M., Gicic, M., La Violette, P.E. 1992. The currents and circulation of the Adriatic Sea. Oceanologica Acta, 15, 109-122.

Ortolani, F. and Pagliuca, S. 1987. Tettonica transpressiva nel Gargano e rapporti con le Catene Appenninica e Dinarica. Mem. Soc. Geol. It., 38, 205-224.

Pinardi, N. and Masetti, E. 2000. Variability of the large scale general circulation of the Mediterranean Sea from observations and modelling: a review. Palaeogeography, Palaeoclimatology, Palaeoecology, 158, 153–173.

Ricci Lucchi F. 1986. The Oligocene to Recent foreland basins of the Northen Apennines. In: Allen P., Homewood P. (Eds.), Foreland basins. IAS, Spec. Publ., 8, 105-139.

Ridente, D. and Trincardi, F. 2002. Eustatic and tectonic control on deposition and lateral variability of Quaternary regressive sequences in the Adriatic basin. Marine Geology, 184, 273-293.

Ridente, D. and Trincardi, F. 2005. Pleistocene “muddy” forced-regression deposits on the Adriatic shelf: a comparison with prodelta deposits of the late Holocene highstand mud wedge. Marine Geology, 222-223, 213-233.

Ridente D. and Trincardi F. 2006. Propagation of shallow folds and faults in late Pleistocene and Holocene shelf-slope deposits, central and South Adriatic margin (Italy). Basin Research, 18-2, 171-188.

Rohling, E. J. 1994. Review and new aspects concerning the formation of eastern Mediterranean sapropels. Marine Geology, 122, 1–28.

Rohling, E. J., Jorissen, F. J., de Stigter, H. C. 1997. 200 year interruption of Holocene sapropel formation in the Adriatic Sea. Journal of Micropalaeontology, 16-. 2, 97-108.

Rohling, E. J. and Hilgen F.J. 1991. The eastern Mediterranean climate at times of sapropel formation: A review. GEOL. MIN. 70- 3, 253-264.

Ross, W.C., Halliwell, B.A., May, J.A., Watts, D.E., Syvitski, J.P.M. 1994. Slope readjustment: a new model for the development of submarine fans and aprons: Geology, 22, 511-514.

Roussenov, V., Stanev, E., Artale, V., Pinardi, N. 1995. A seasonal model of the Mediterranean Sea general circulation. Journal of Geophysical Research, 100- C7, 13,515-13,538.

Royden, L.E., Patacca, E., Scandone, P. 1987. Segmentation and configuration of subducted lithosphere in Italy: an important control on thrust-belt and foredeep-basin evolution. Geology, 15, 714-717.

Schwartz, H., J. Sample, K. D. Weberling, D. Minisini, and J. C. Moore 2003. An ancient linked fluid migration system: cold-seep deposits and sandstone intrusions in the Panoche Hills, California, USA. Geo-Marine Letters, 23, 3-4, 340-350.

Shepard, F.P. 1933. Canyons beneath the Seas. Scientific Monthly, 37, 31-39.

Shepard, F.P. 1981. Submarine canyons: multiple causes and long-time persistence. AAPG Bulletin, 65-6, 1062-1077.

Shepard F.P. and Dill, R.F. 1966. Submarine canyons and other sea valleys. Rand McNally & Co., Chicago, 381 pp.

Siani G., Paterne M., Michel E., Sulpizio R., Sbrana A., Arnold M., Haddad G. 2001. Mediterranean Sea surface radiocarbon reservoir age changes since the Last Glacial Maximum. Science, 294, 1917-1920.

Stow, D.A.V., Faugères, J.C., Pudsey, C.J., Viana, A.R. 2002. Bottom currents, contourites and deep-sea sediment drifts; current state-of-the-art. In: Stow, D. A. V., Pudsey C. J., Howe J. A., Faugères J. C. & Viana A. Deep-water contourite systems: modern drifts and ancient series, seismic and sedimentary characteristics. Geological Society, London, Memoirs, 22, 191-208.

Taviani, M. 1978. Associazioni a molluschi pleistoceniche-attuali dragate nel Basso Adriatico. Bollettino di Zoologia, 45, 297-306.

Taviani, M., Freiwald, A., Zibrowius, H. 2005. Deep-coral growth in the Mediterranean Sea: an overview. In Freiwald, A., Roberts, M. (Eds.), Deep-water Corals & Ecosystems Springer-Verlag, 137-156.

Tramontana, M., Morelli, D., Colantoni, P. 1995. Tettonica plio-quaternaria del sistema sud-garganico (settore orientale) nel quadro evolutivo dell'Adriatico centro meridionale. Studi Geologici Camerti, 2, 467-473.

Trincardi, F. and Correggiari, A. 2000. Quaternary forced-regression deposits in the Adriatic basin and the record of composite sea-level cycles. In: Hunt D., Gawthorpe R. (Eds.), Depositional Response to Forced Regression. Geol. Soc., Spec. Publ., 172, 245-269.

Trincardi F., Correggiari A., Field M. E., Normark W. R. 1995. Turbidite deposition from multiple sediment sources: Quaternary Paola Basin (Eastern Tyrrhenian Sea). Journal of Sedimentary Research, 65 B, 469-483.

Trincardi, F., Asioli, A., Cattaneo, A., Correggiari, A., Langone, L. 1996. Stratigraphy of the late-Quaternary deposits in the Central Adriatic basin and the record of short-term climatic events. In: Guilizzoni, P., Oldfield, F.L. (Eds.), Palaeoenvironmental analysis of Italian crater lake and Adriatic sediments (PALICLAS project). Mem. Istit. It. Idrob., 55, 39-64.

Trincardi, F., Cattaneo, A., Correggiari, A., Ridente, D. 2004. Evidence of soft-sediment deformation, fluid escape, sediment failure and regional weak layers within the late-Quaternary mud deposits of the Adriatic Sea. Marine Geology, 213, 91-119.

Twichell, D.C and Roberts, D.G., 1982. Morphology, distribution, and development of submarine canyons on the United States Atlantic continental slope between Husdon and Baltimore Canyons. Geology, 10, 408-412.

Verdicchio, G. and Trincardi, F., in press. Short-distance variability in abyssal bed-forms along the Southwestern Adriatic Margin (Central Mediterranean). Marine Geology.

Verdicchio, G., Trincardi, F., Asioli, A., in press. Mediterranean bottom-current deposits: an example from the Southwestern Adriatic Margin. In Viana, A.R., Rebesco, M. (Eds.) Economic and palaeoceanographic importance of Contourite. Geol. Soc. Spec. Pub.

Vergnaud-Grazzini, C., Ryan, B. F., Cita, M. B. 1977. Stable isotopic fractionation, climatic change and episodic stagnation in the Eastern Mediterranean during the late Quaternary, Marine Micropaleontology, 2, 353-370.

Vilibic, I. and Orlic M. 2002. Adriatic water masses, their rates of formation and transport through the Otranto Strait. Deep-Sea Research I, 49, 1321–1340.

Weimer, P. 1991. Seismic facies, characteristics, and variations in channel evolution, Mississippi fan (Plio-Pleistocene), Gulf of Mexico, in Weimer, P., and Link, M.H., eds., Seismic Facies and Sedimentary Processes of Submarine Fans and Turbidite Systems: New York, Springer-Verlag, p. 323-347.

Wust, G. 1961. On the vertical circulation of the Mediterranean Sea. Journal of Geophysical Research, 66, 321-327.

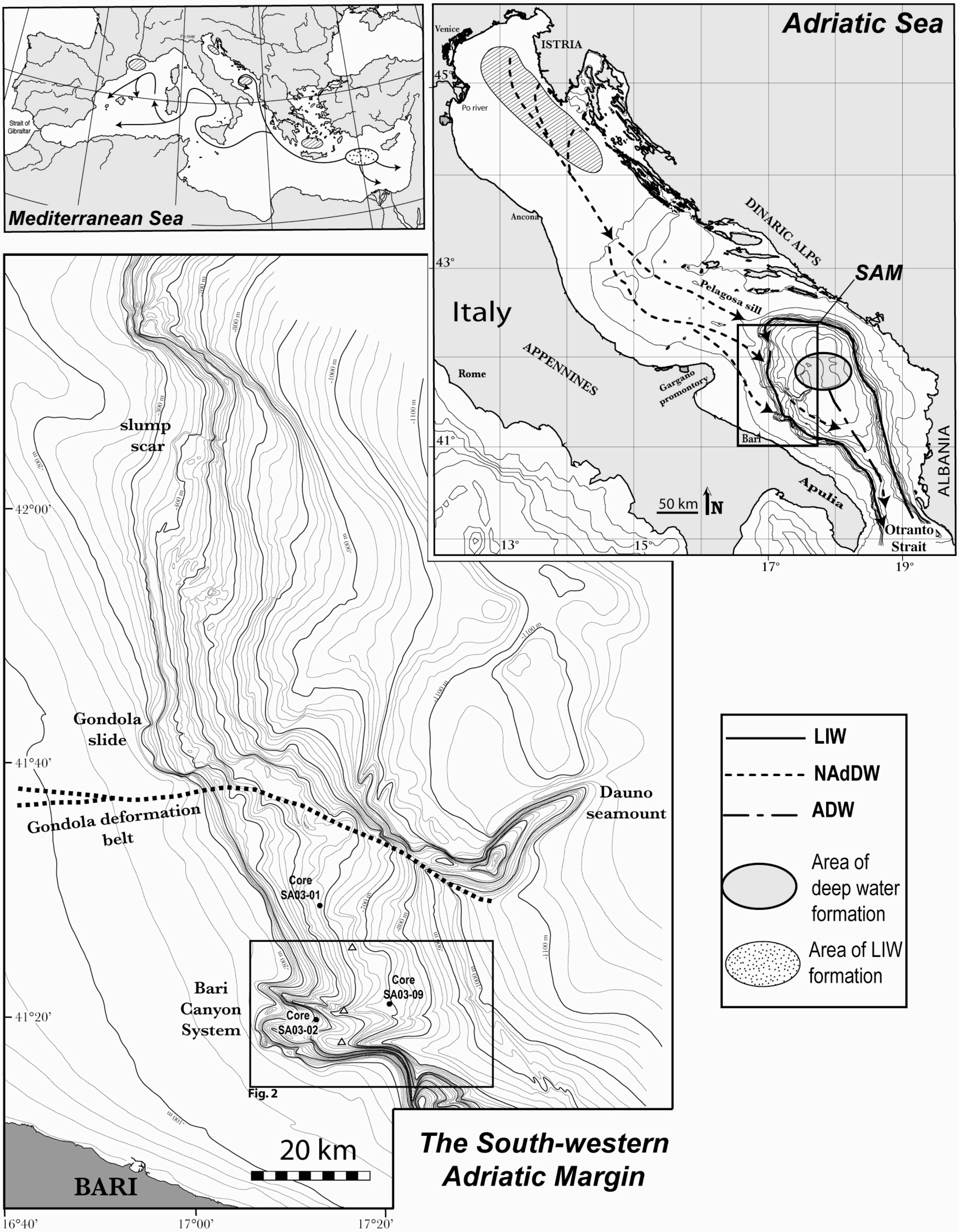
Mediterranean Sea
Strait of Gibraltar
Po river
Adriatic Sea
Venice
ISTRIA
45°
Po river
Ancona
DINARIC ALPS
43°
SAM
Italy
Pelagosa sill
APPENNINES
Rome
Gargano promontory
41°
Bari
Apulia
ALBANIA
50 km
N
Otranto Strait
13°
15°
17°
19°
slump scar
42°00'
Gondola slide
41°40'
Gondola deformation belt
Dauno seamount
Core SA03-01
Bari Canyon System
Core SA03-09
Core SA03-02
41°20'
Fig. 2
BARI
20 km
16°40'
17°00'
17°20'
-200 m
-400 m
-700 m
-800 m
-900 m
-1000 m
-1100 m
-100 m
The South-western Adriatic Margin
LIW
NAdDW
ADW
Area of deep water formation
Area of LIW formation

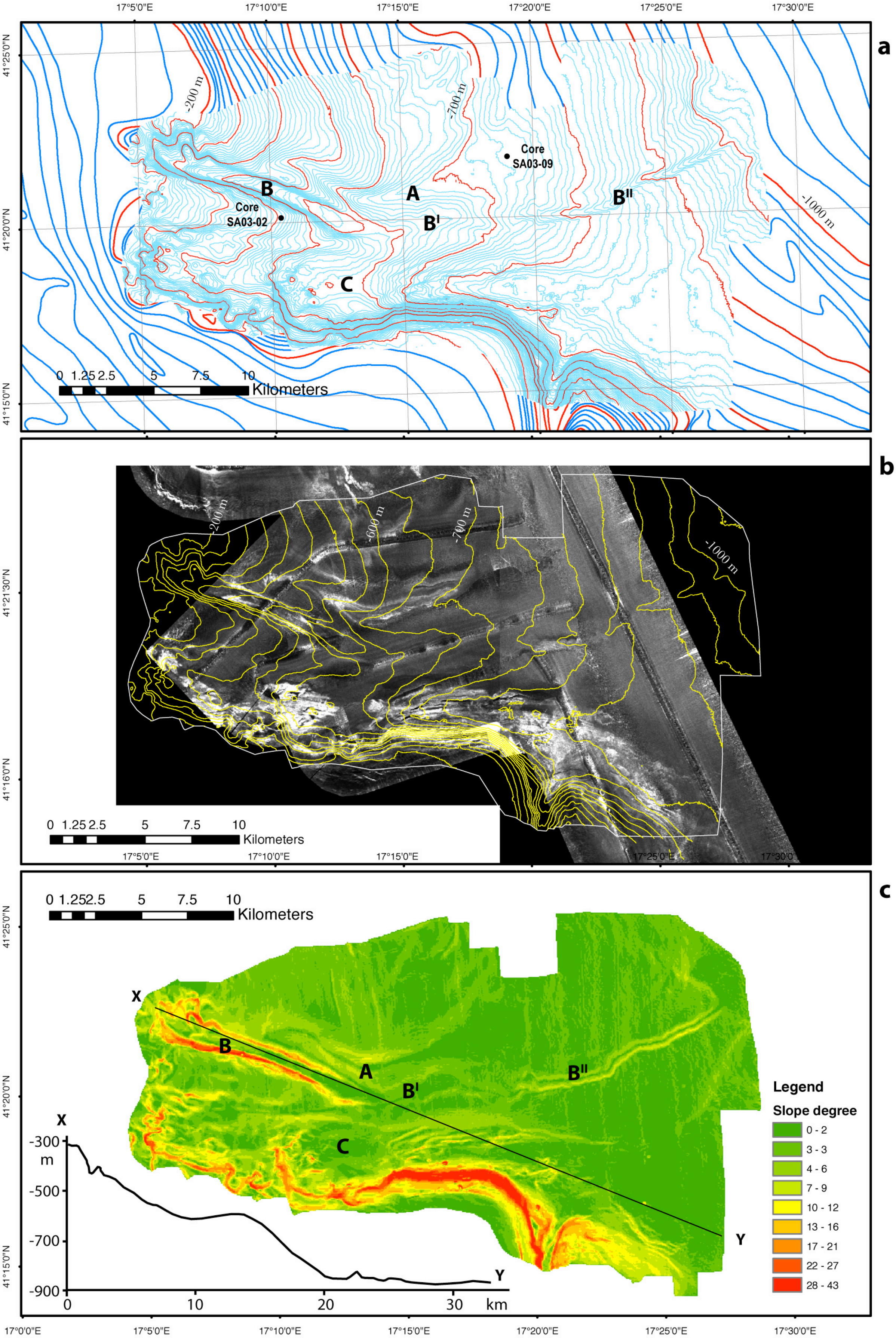
17°5'0"E
17°10'0"E
17°15'0"E
17°20'0"E
17°25'0"E
17°30'0"E
41°25'0"N
41°20'0"N
41°15'0"N
a
-200 m
-700 m
-1000 m
Core SA03-09
Core SA03-02
A
B
B^I
B^II
C
0 1.25 2.5 5 7.5 10
Kilometers
b
-200 m
-600 m
-700 m
-1000 m
41°21'30"N
41°16'0"N
c
X
Y
-300
m
-500
-700
-900
0
10
20
30
km
Legend
Slope degree
0 - 2
3 - 3
4 - 6
7 - 9
10 - 12
13 - 16
17 - 21
22 - 27
28 - 43
17°0'0"E

Figure 2

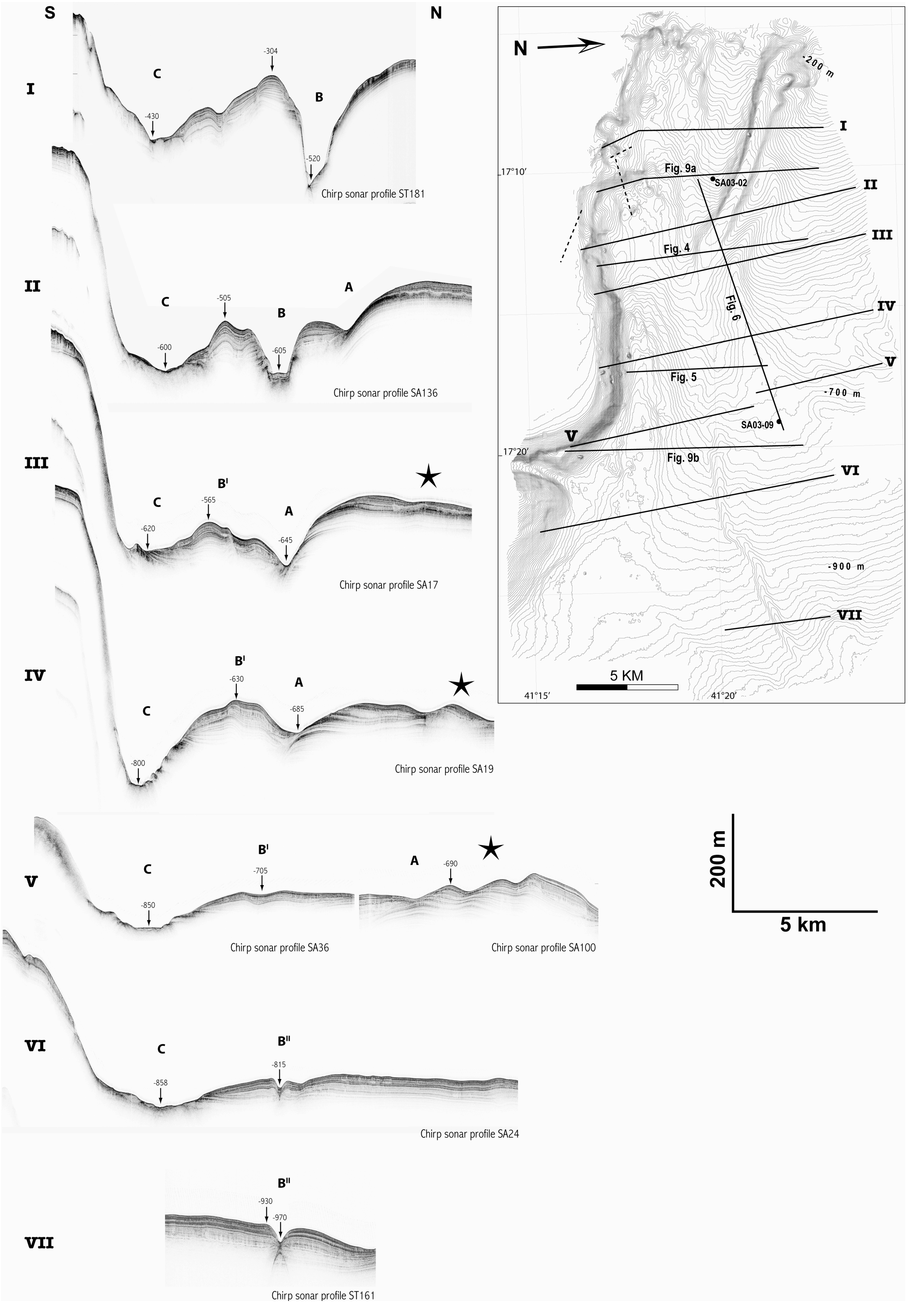
S
N
I
C
-304
B
-430
-520
Chirp sonar profile ST181
II
C
-505
B
A
-600
-605
Chirp sonar profile SA136
III
★
C
B^I
-565
A
-620
-645
Chirp sonar profile SA17
IV
B^I
-630
A
★
C
-685
-800
Chirp sonar profile SA19
V
C
B^I
-705
A
-690
★
-850
Chirp sonar profile SA36
Chirp sonar profile SA100
VI
C
B^II
-815
-858
Chirp sonar profile SA24
VII
B^II
-930
-970
Chirp sonar profile ST161
200 m
5 km
N
-200 m
I
_17°10′
Fig. 9a
SA03-02
II
III
Fig. 4
Fig. 6
IV
V
Fig. 5
-700 m
SA03-09
V
_17°20′
Fig. 9b
VI
-900 m
VII
5 KM
41°15′
41°20′

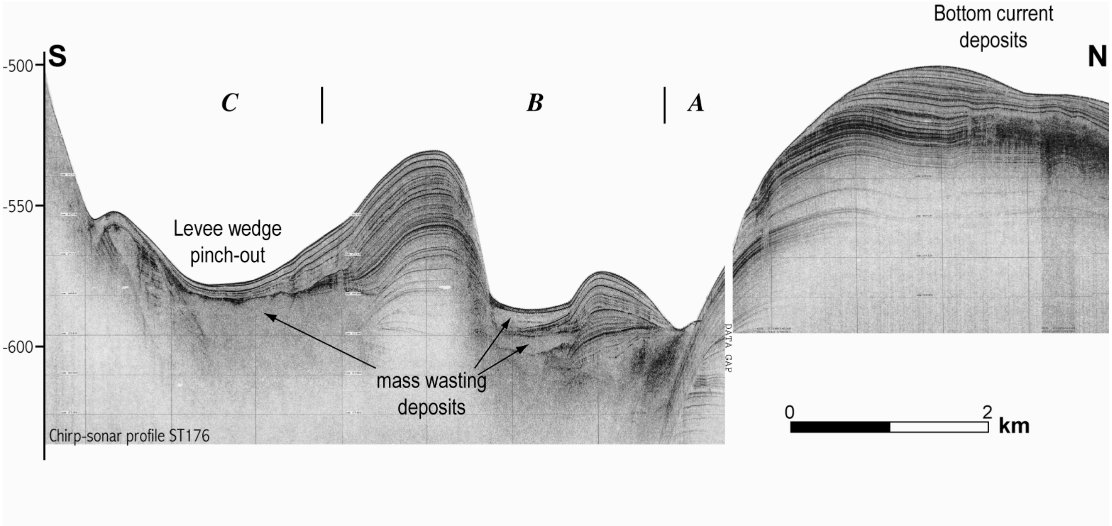
Bottom current deposits
S
N
-500
-550
-600
C
B
A
Levee wedge pinch-out
mass wasting deposits
DATA GAP
0
2
km
Chirp-sonar profile ST176

Figure 4

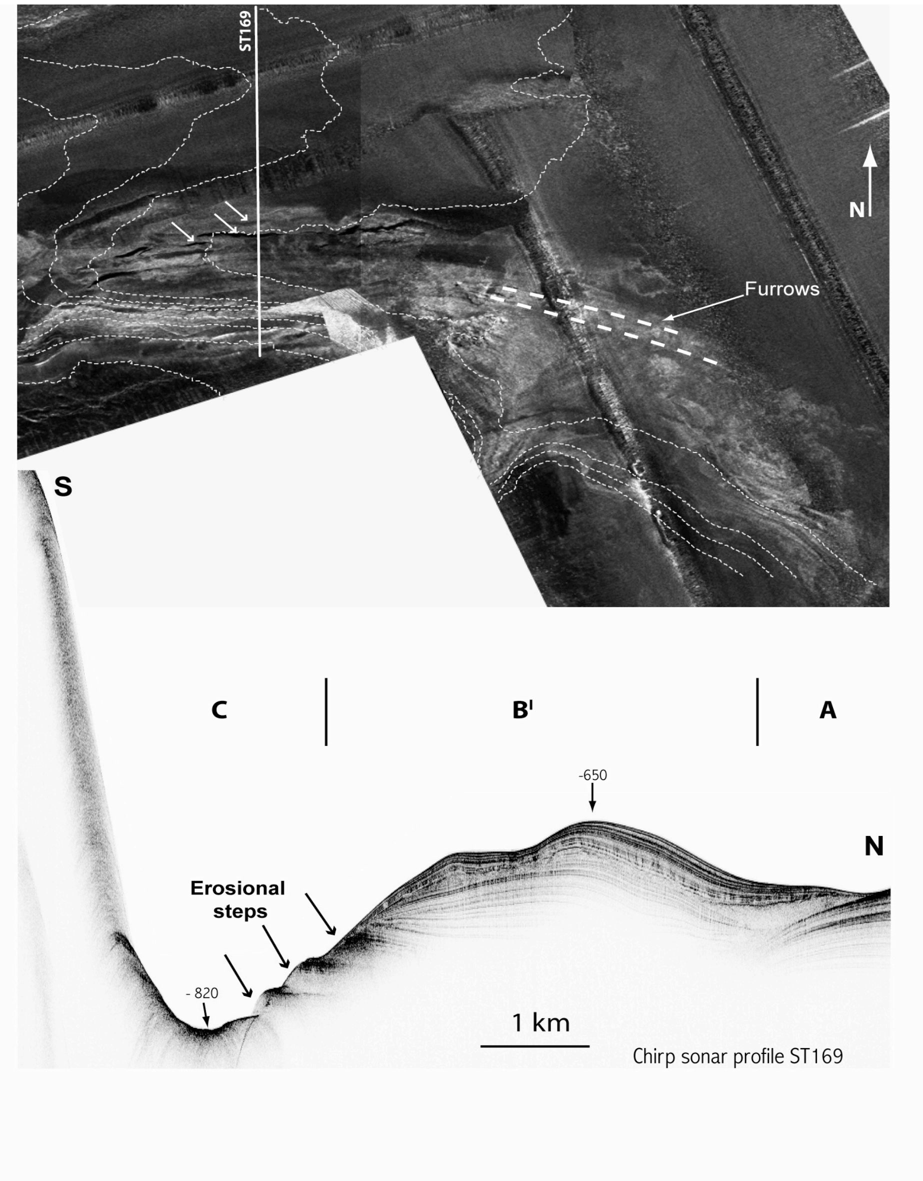
ST169
N
Furrows
S
C
B'
A
-650
N
Erosional steps
- 820
1 km
Chirp sonar profile ST169

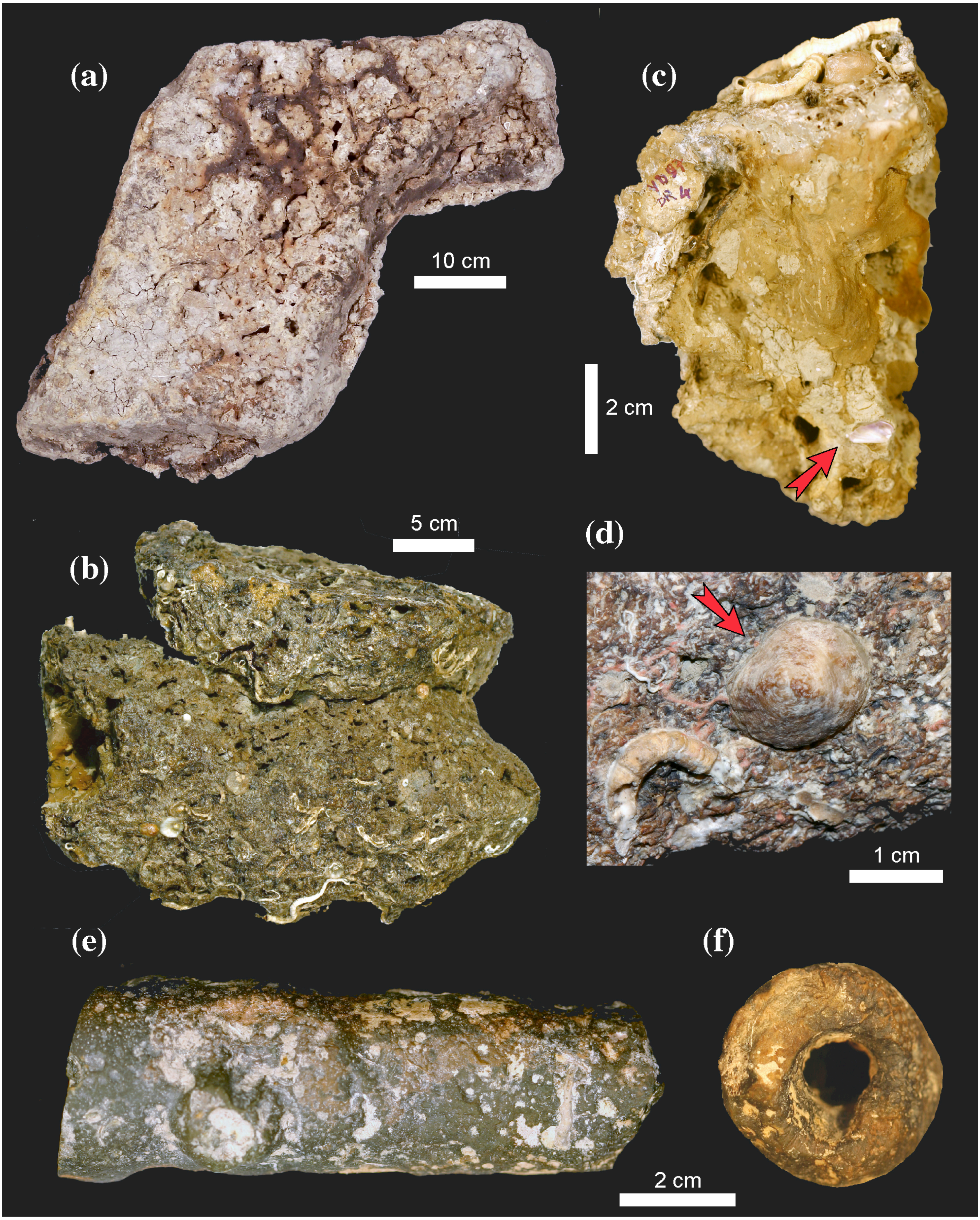

Figure 7/1

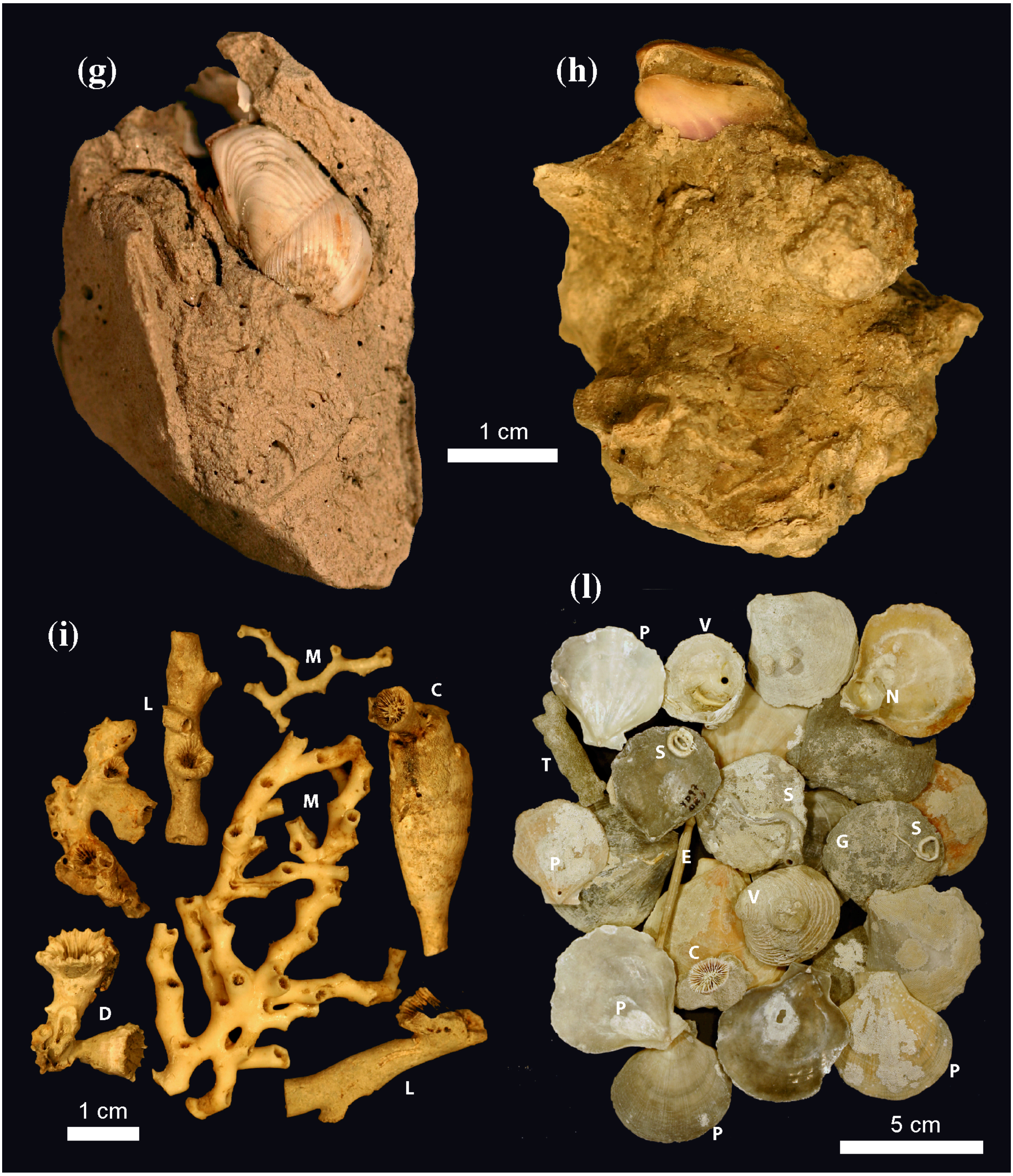

Figure 7/2

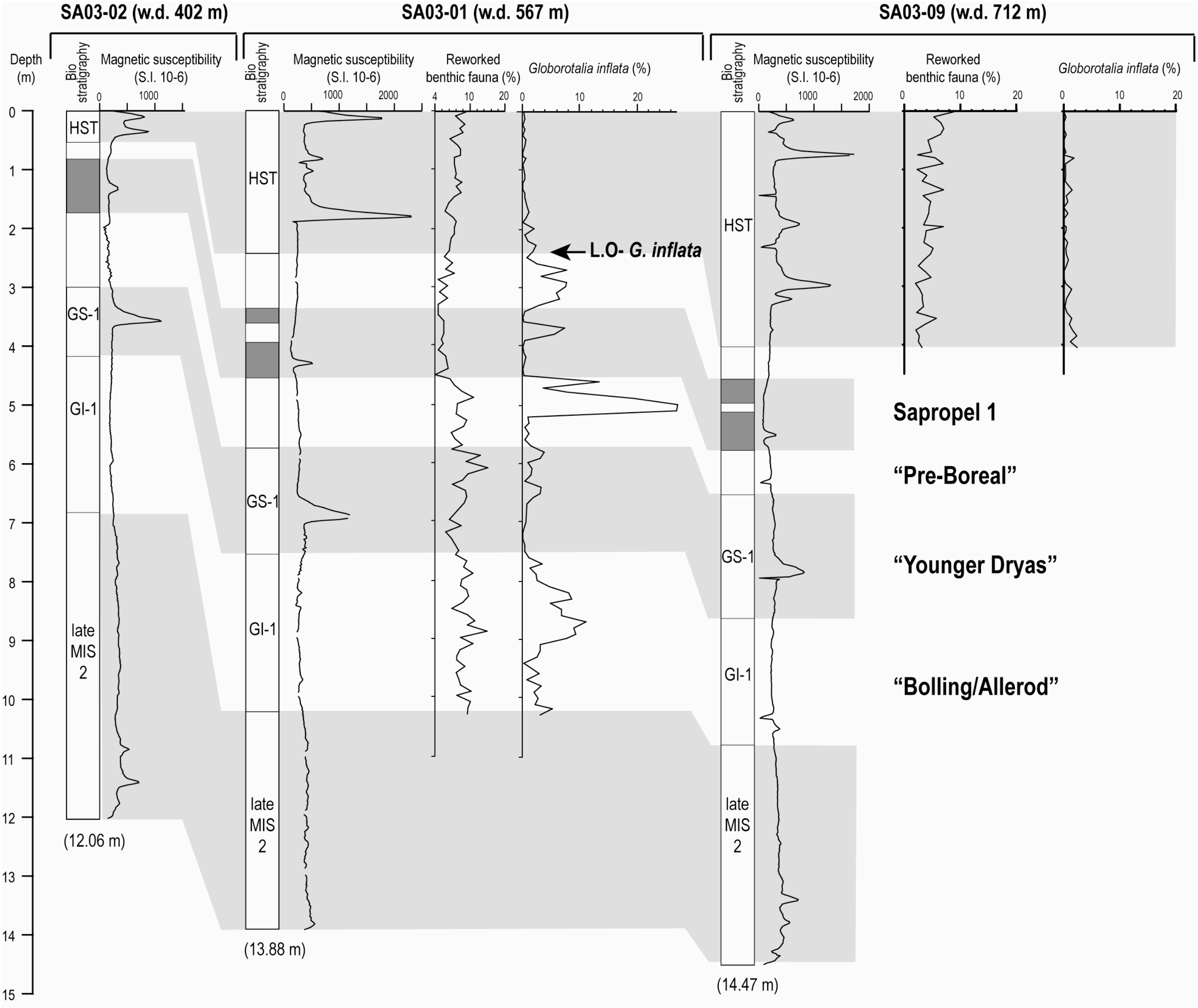
SA03-02 (w.d. 402 m)
SA03-01 (w.d. 567 m)
SA03-09 (w.d. 712 m)
Depth (m)
Bio stratigraphy
Magnetic susceptibility (S.I. 10-6)
Reworked benthic fauna (%)
Globorotalia inflata (%)
0
1000
2000
4
10
20
1
2
3
5
6
7
8
9
11
12
13
14
15
HST
GS-1
GI-1
late MIS 2
(12.06 m)
(13.88 m)
(14.47 m)
L.O- G. inflata
Sapropel 1
“Pre-Boreal”
“Younger Dryas”
“Bolling/Allerod”

Figure 8

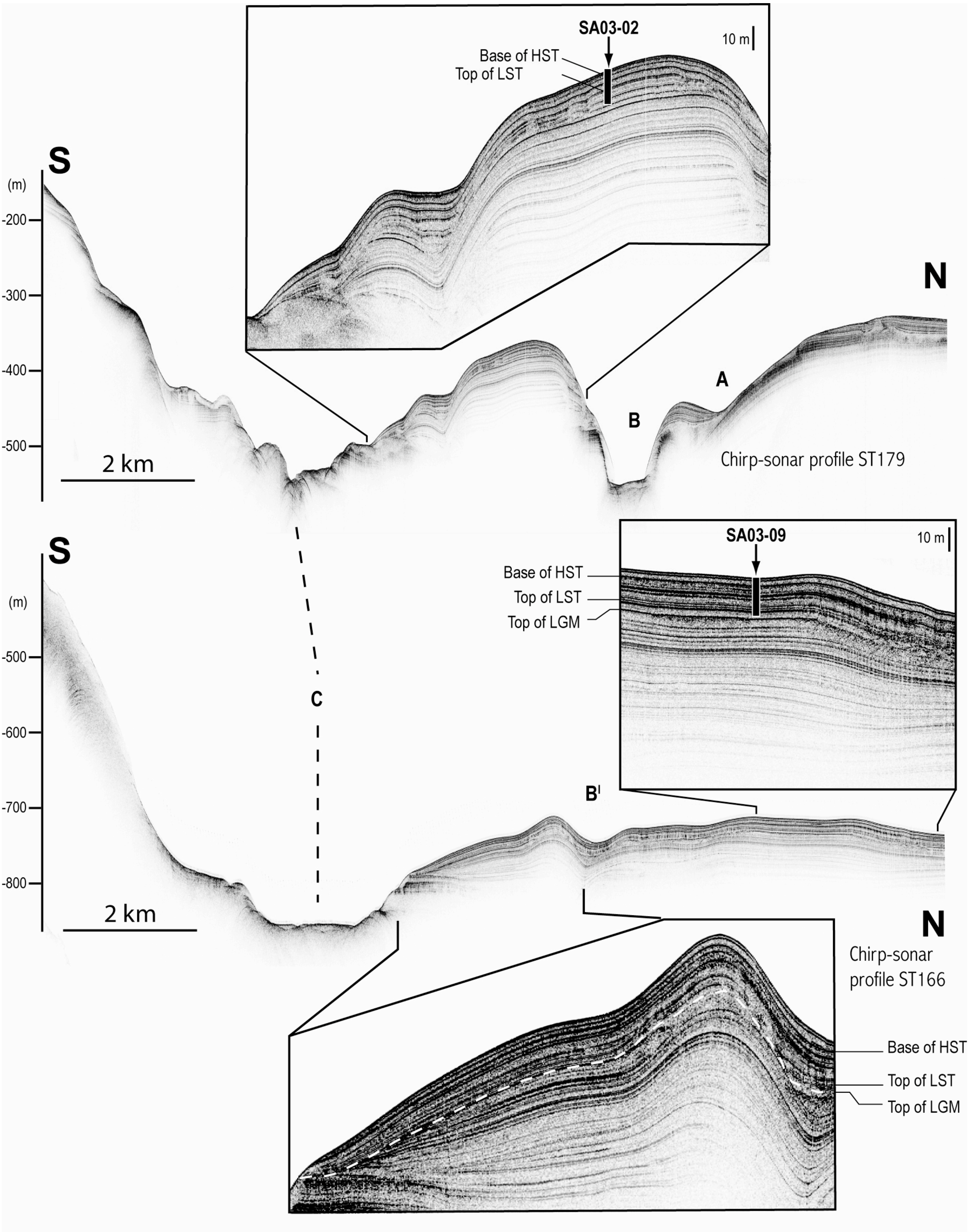
SA03-02
10 m
Base of HST
Top of LST
S
(m)
-200
-300
-400
-500
2 km
N
A
B
Chirp-sonar profile ST179
S
(m)
-500
-600
-700
-800
2 km
C
SA03-09
10 m
Base of HST
Top of LST
Top of LGM
B'
N
Chirp-sonar profile ST166
Base of HST
Top of LST
Top of LGM

Figure 9

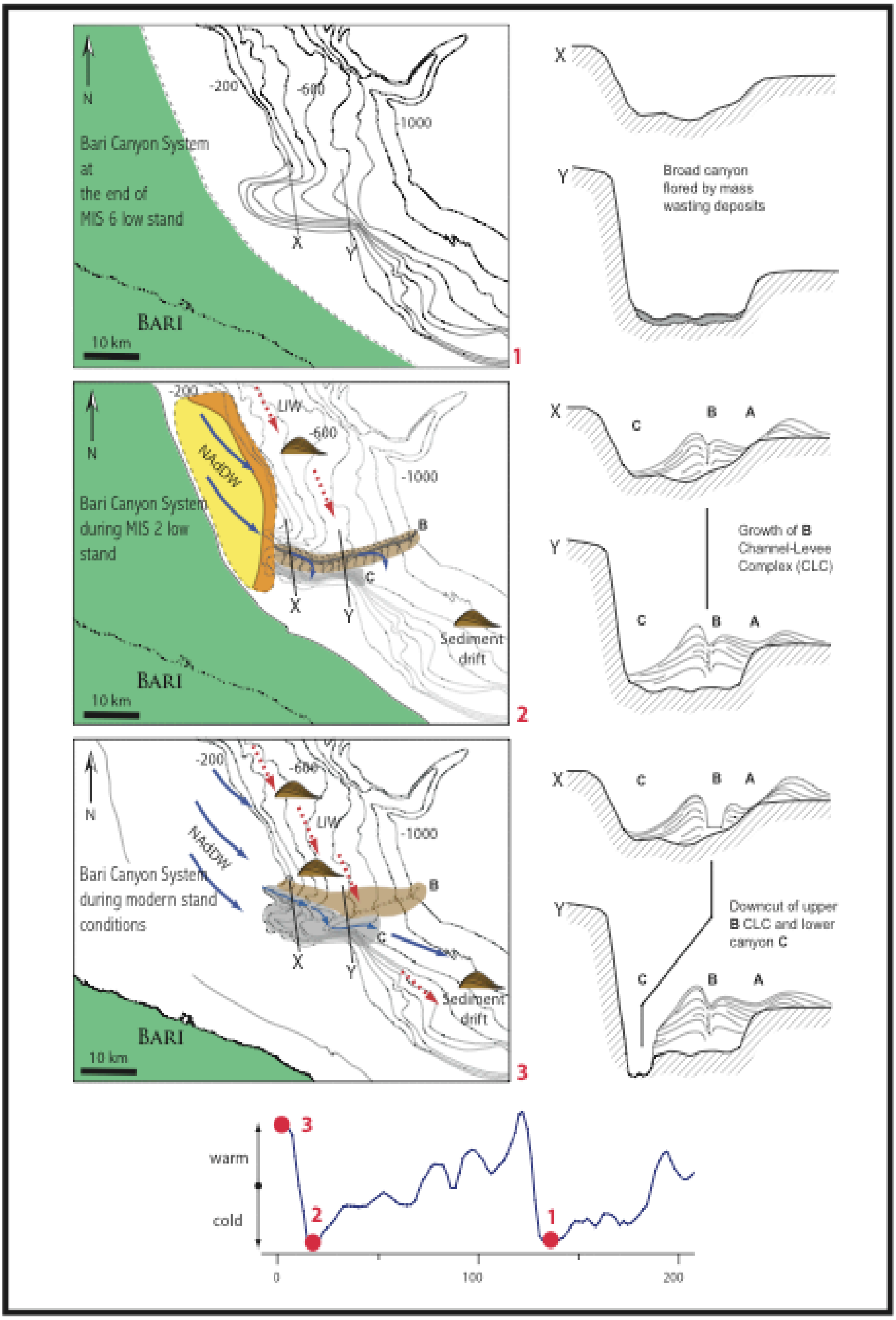
N
-200
-600
-1000
Bari Canyon System at the end of MIS 6 low stand
X
Y
BARI
10 km
1
Broad canyon flored by mass wasting deposits
LIW
NAdDW
Bari Canyon System during MIS 2 low stand
B
C
Sediment drift
2
A
Growth of B Channel-Levee Complex (CLC)
Bari Canyon System during modern stand conditions
3
Downcut of upper B CLC and lower canyon C
warm
cold
0
100
200

Figure 10

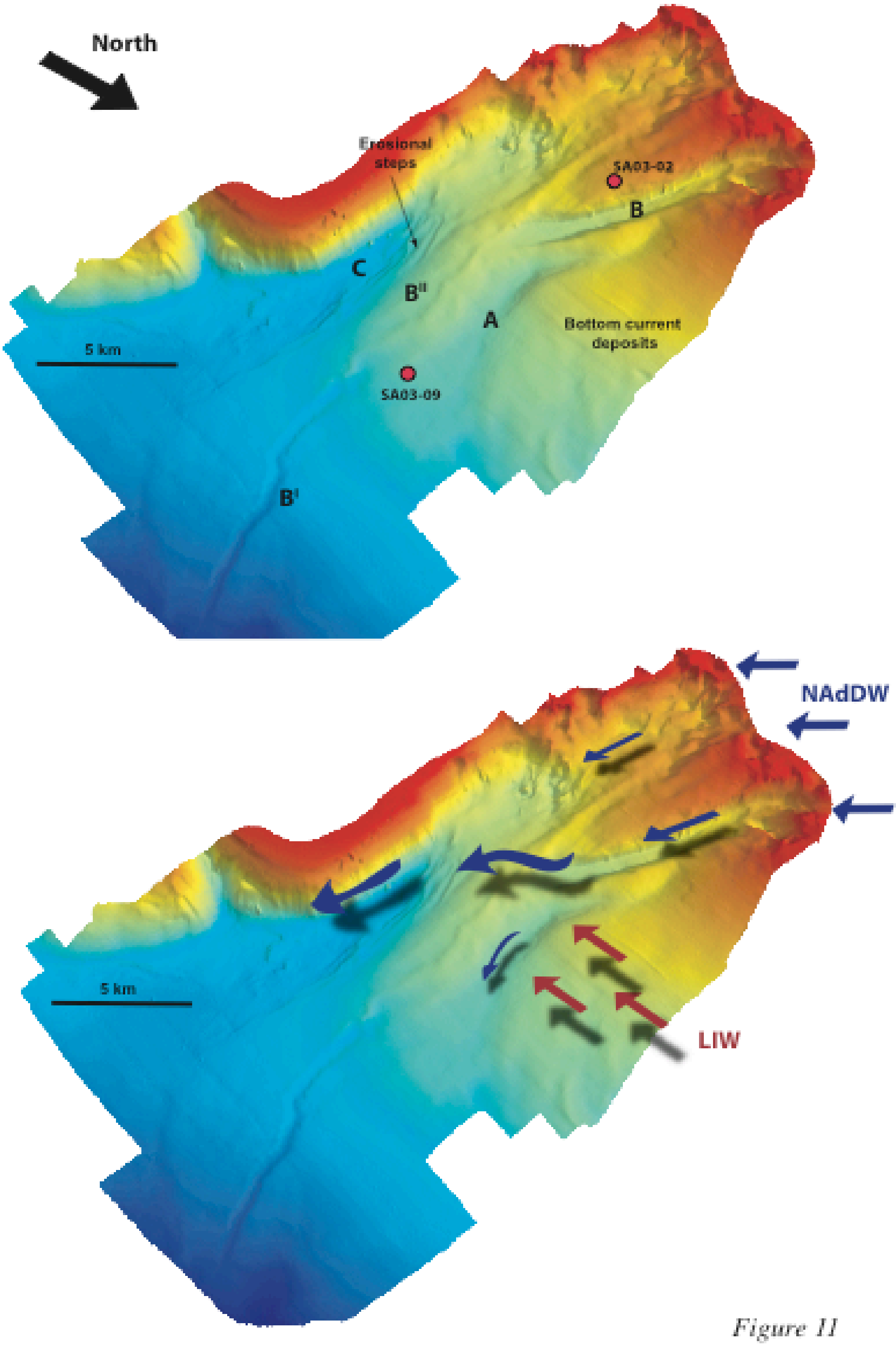
North
Erosional steps
SA03-02
B
C
B^{II}
A
Bottom current deposits
5 km
SA03-09
B^{I}
NAdDW
5 km
LIW

Figure 11

TABLE

Cruise/Station	Lat N (start)	Lat N (end)	Long E (start)	Long E (end)	DEPTH m	GEAR	REMARKS
YD97-DR2	41° 18' 55	41° 19.0'	17° 05' 21	17° 05 '14	334	Dredge	Sub fossil corals
YD97-DR3	41° 18' 51	41° 19' 13	17° 05' 27	17° 04° 47	316/246	Dredge	
YD97-DR4	41° 18' 06	41° 17' 41	17° 11' 43	17° 09' 33	585/348	Dredge	
YD97-DR5	41° 17' 41		17° 09' 32		347	Dredge	
MAI 2-97 St A 4, even 109	41° 19' 02		17° 04' 95		250	Box corer	
Ad 70/14	41° 22.2' N	41° 23.0' N	17° 05.6' E	17° 05.7' E	320/198	Dredge	
Ad 70/29	41° 17.9'	41° 16.0'	17° 10.9'	17° 10.6'	300/180	Dredge	

Inizio del messaggio inoltrato:

> **Da:** Author Gateway <authorsupport@elsevier.com>
> **Data:** 19 febbraio 2007 14:10:27 CET
> **A:** fabio.trincardi@bo.ismar.cnr.it
> **Oggetto: Article tracking [MARGO_3997]**
>
> Article title: The impact of cascading currents on the Bari Canyon System, SW-Adriatic Margin (Central Mediterranean).
> Reference: MARGO3997
> Journal title: Marine Geology
> Corresponding author: Dr. F. Trincardi
> First author: Dr. F. Trincardi
> Received at Editorial Office: 10-JAN-2006
> Article revised: 3-OCT-2006
> Article accepted for publication: 19-JAN-2007
> Expected dispatch of proofs: 12-MAR-2007
>
> Author Gateway article tracking service from Elsevier
>
> The expected dispatch date of your proofs will be 12-MAR-2007. Please note this date is only provided as a guide: it may change due to delays in the production process.
>
> When you receive the proofs please use it to check the typesetting and editing, also the completeness and correctness of the text, tables and figures. Changes to the article as accepted for publication will not be considered. You may also be asked to validate any questions that have arisen during the preparation of your proofs and these are included in a "query form" which is sent along with the proofs.
>
> More detailed information will follow when you receive the proofs.
>
> --
>
> This e-mail has been sent to you from Elsevier Limited, The Boulevard, Langford Lane, Kidlington, Oxford OX5 1GB, United Kingdom. To ensure delivery to your inbox (not bulk or junk folders), please add authorsupport@elsevier.com to your address book or safe senders list.
>
> For all enquiries, problems or suggestions regarding this service, please contact mailto:authorsupport@elsevier.com.
>
>
>
> [T-16-v5.3.1]

Il ruolo dei foraminiferi nelle ricostruzioni paleoceanografiche e paleoclimatiche: esempi dal Mediterraneo Centrale (Adriatico) per il tardo Olocene attraverso un approccio multidisciplinare

ALESSANDRA ASIOLI E ANDREA PIVA

ABSTRACT – *The role of foraminifera in paleoceanographic and paleoclimatic reconstruction: examples of multidisciplinary approach from the Late Quaternary Central Mediterranean* - We present quantitative analysis of the foraminifera assemblages in two cores spanning the last 6000 years the Central Adriatic middle shelf and slope basin (the Middle Adriatic Depression) respectively. The chronological framework is based on several independent evidences. The results are compared to the reference core RF93-30, already published and investigated with a strongly multidisciplinary approach. This study allowed to obtain a significative improvement of the foraminifera ecobiostratigraphy for the Central Adriatic, and in particular: 1) the last occurrence of the planktonic foraminifer *Globigerinoides sacculifer* represents a bio-event recognisable over the entire basin and correlatable between differentiated depositional environments, such as the clay belt on the shelf and the Middle Adriatic Depression, and marking approximately the base of the Little Ice Age, 2) before its last occurrence, the relative abundance of *G. sacculifer* shows three major positive peaks, marking intervals characterised by relative climatic optimum conditions. This feature has a significant impact on the limitations in the applicability of the ecobiostratigraphy generally adopted in the literature for this time interval and suggests how it needs to be revised, 3) the variations of the benthic foraminifera assemblages in the middle shelf (e.g. *Valvulineria complanata*) are quite similar between cores located at considerable distance along the clay belt (e.g. 300km) providing an additional ecobiostratigraphic tool, 4) conversely, the variations of the benthic foraminifera assemblages observed in the middle shelf during the last 6000 years do not have an obvious equivalent in the deepest basin (MAD). This evidence is here tentatively ascribed to the short duration of the climatic oscillations detected by the planktic assemblages, duration probably not sufficient to impact also deep environments such as the MAD, and/or to the evidence that the most sensitive environment to these kind of climatic oscillations (the clay belt) is confined to relatively shallow depths (middle shelf), by the general circulation pattern of the Adriatic.

Key words: planktic and benthic foraminifera, ecobiostratigraphy, paleoenvironment, Late Holocene, Adriatic

INTRODUZIONE

La ricerca paleoceanografica e paleoclimatica ha fatto notevoli progressi negli ultimi decenni. Ricostruire l'evoluzione della paleocircolazione oceanica, delle oscillazioni climatiche, delle interazioni tra oceano, atmosfera e biosfera, è di radicale importanza nell'interpretazione del passato, nello studio del presente e nella previsione dei mutamenti climatico-ambientali futuri. Il clima globale, infatti, è strettamente legato al funzionamento della circolazione termoalina oceanica ed alla produttività degli oceani. I numerosi studi sui sedimenti del passato hanno evidenziato come il clima (sistema oceano/atmosfera) abbia fluttuato notevolmente nel passato, e, più recentemente, negli ultimi 2.6 Ma, ossia dall'inizio delle glaciazioni nell'emisfero nord. Queste fluttuazioni, ossia cicli glaciali-interglaciali, risultano marcatamente prolungati ed intensificati (aumento del contrasto tra intervalli freddi e caldi) dal Pleistocene medio (ca. 800 ka) e ben visibili nella curva degli isotopi stabili dell'Ossigeno con il caratteristico aspetto a dente di sega (raffreddamenti lenti e prolungati alternati a riscaldamenti rapidi e di grande ampiezza) e con frequenza intorno a 100 ka. Il Quaternario, inoltre, mostra rapide variazioni climatiche anche alla scala millenaria, secolare o decadale (ossia a scala sub-Milankoviana), specialmente per gli ultimi 90-100 ka (per esempio, eventi Dansgaard-Oeschger, Heinrich events, Piccola Età del Ghiaccio) (DANSGAARD ET AL., 1993; BOND ET AL., 1993; MASLIN ET AL., 2001 e referenze in esso). Questa variabilità comporta salti di stato da un regime di circolazione ad un altro, che avvengono in alcuni casi nell'arco di pochi anni o decenni, ossia alla stessa scala della vita umana (Alley e Clark, 1999), con conseguente possibilericaduta sulla società umana stessa.

La miglior risoluzione degli eventi paleoclimatici è stata finora ottenuta nelle carote di ghiaccio, sulla base esclusiva di parametri fisico-chimici, data l'assenza di indicatori biologici all'interno del ghiaccio. Gli studi paleoclimatici in depositi marini o continentali, invece, si basano anche, ed estesamente, sulle variazioni degli indicatori biologici.

Per quanto riguarda il record marino uno dei bioindicatori più studiati ed utilizzati nelle ricostruzioni paleoceanografiche e paleoclimatiche è costituito dai foraminiferi. Questi microrganismi, planctonici e bentonici, oltre alla loro ben nota utilità in campo biostratigrafico, rivestono da tempo un ruolo importante della data la loro sensibilità alle variazioni dei fattori biotici e abiotici che si verificano nell'ambiente in cui vivono, oltre ad avere il vantaggio di un ottimo potenziale di conservazione e alla loro abbondanza in piccole quantità di sedimento. Lo studio non solo qualitativo ma anche quantitativo delle associazioni a foraminiferi planctonici e bentonici fornisce infatti un quadro paleoceanografico, nonché una definizione precisa della ciclicità climatica, ossia dell'avvicendarsi di condizioni climatiche calde, fredde o temperate (per una sintesi si veda: Hemleben et al., 1989; Murray, 1991 e Sen Gupta, 1999).

Tuttavia, contemporaneamente, si è fatta sempre più forte l'esigenza di combinare le informazioni ottenute tramite i microfossili (in questo caso foraminiferi) con quelle ottenute con altri indicatori (*proxy*) biologici, di ambiente marino (nannoplancton calcareo, diatomee, radiolari, ostracodi, molluschi), e/o continentale (vertebrati, pollini, resti di piante, insetti, ostracodi e molluschi), e con dati geochimici (isotopi stabili dell'ossigeno e del carbonio, alchenoni, contenuto in Ba, Cd), mineralogici, sedimentologici, geofisici, nonché con metodi statistici (esempio funzioni transfer, Modern Analogue Technique) che convalidino e permettano ricostruzioni paleoambientali più raffinate e sensibili attraverso controlli incrociati e studi multi-disciplinari.

In questo articolo sarà illustrato un esempio di ricostruzione integrata paleoclimatica e paleoceanografica da carote provenienti dal Mediterraneo centrale (Adriatico) relativamente agli ultimi 6 ka. Nella prima parte sarà trattato in breve l'habitat dei foraminiferi, con particolare attenzione al tipo di ambiente in cui si inserisce l'esempio di ricostruzione paleoclimatica, trattata successivamente.

I FORAMINIFERI

I foraminiferi costituiscono il gruppo vivente di micro-organismi provvisto di conchiglia più diversificato negli oceani attuali. Essi vivono nella colonna d'acqua (quelli planctonici) oppure nei sedimenti del fondo marino (quelli bentonici) e sono molto abbondanti sia nel record fossile sia negli ambienti attuali. Tutto ciò indica una loro notevole sensibilità ai fattori biotici e abiotici che caratterizzano l'ambiente che li ospita.

I più diffusi modelli di habitat suggeriti per i foraminiferi planctonici prevedono, in via generale, una distribuzione latitudinale in province in relazione alla temperatura delle masse d'acqua (provincia polare, subpolare, transizionale, subtropicale e tropicale), nonché una distribuzione verticale all'interno della colonna d'acqua (forme di acque superficiali, intermedie e profonde), in responso a variazioni di parametri quali temperatura, ossigeno disciolto, disponibilità di cibo, presenza di mescolamento delle acque durante l'inverno, e livello trofico (Hemleben et al., 1989).

I foraminiferi bentonici sono presenti in tutti gli ambienti marini, da quello supratidale a quello abissale, e possono vivere sia all'interfaccia acqua-sedimento (epifauna), o all'interno del sedimento fino ad alcuni centimetri di profondità (infauna superficiale, intermedia e profonda), dove i valori di parametri quali contenuto in ossigeno quantità e qualità di cibo possono essere notevolmente differenti rispetto a quelli all'interfaccia acqua-sedimento. La distribuzione verticale nel sedimento di una particolare specie non è necessariamente la stessa sempre e ovunque, ma può variare in risposta a variazioni dell'ambiente in un determinato sito. E' stato quindi sviluppato il concetto di "microhabitat", ossia un microambiente caratterizzato da precise condizioni fisiche, chimiche e biologiche, e che può essere considerato come il risultato dell'adattamento dinamico per l'acquisizione del cibo. Studi recenti hanno indicato, tra i fattori più determinanti per la distribuzione dei foraminiferi bentonici nel sedimento, il contenuto in ossigeno e l'ammontare di sostanza organica nelle acque di fondo e nel sedimento (si veda il modello TROX che combina il microhabitat dei foraminiferi – infaunale profondo, infaunale intermedio, infaunale superficiale, epifaunale – con questi principali parametri) (Fig. 1).

Fig. 1

Modello TROX che mostra la profondità di microhabitat dei foraminiferi bentonici in funzione della disponibilità di cibo e/o di ossigeno nel sedimento per tre ecositemi (oligotrofico, mesotrofico ed eutrofico) (da Jorissen et al, 1995).

TROX model showing the relationship between the depth of the benthic foraminifera microhabitat and the food availability and/or oxygen content into the sediment in the oligotrophic, mesotrophic and eutrophic ecosystems (from Jorissen, et al., 1995)

Negli ambienti attuali di piattaforma siliciclastica sono presenti diversi tipi associazioni a foraminiferi bentonici: da quelle caratteristiche di palude alta (=marsh), importanti come indicatrici delle variazioni del livello marino (Scott e Medioli, 1978, 1980) e dominate da specie agglutinanti e ialine, a quelle di laguna, di piattaforma interna e piattaforma esterna-scarpata alta. In quest'ultima area i foraminiferi planctonici sono presenti, mentre in piattaforma interna, nonché in laguna e palude, sono assenti o estremamente rari.

Sulla base di questi modelli di distribuzione vengono quindi interpretate dal punto di vista del paleoambiente le sequenze sedimentarie del passato, con vari tipi di applicazione, tra cui quello paleoclimatico (per esempio distinzione di intervalli glaciali ed interglaciali), paleoceanografico (caratteristiche delle masse d'acqua), o paleobatimetrico.

E' importante per lo scopo di questo articolo soffermare l'attenzione su un tipo di ambiente presente tra la piattaforma interna e quella esterna in piattaforme di tipo siliciclastico e caratterizzate da apporti fluviali. In questo ambiente l'azione combinata dell'apporto fluviale e delle correnti si traduce nella deposizione di sedimenti molto fini e ricchi in sostanza organica. Questi sedimenti fini (che costituiscono la cosiddetta "fascia dei limi") sono generalmente disposti più o meno parallelamente alla costa. E' importante notare che l'apporto fluviale può indurre a condizioni disossiche o anossiche anche a distanze notevoli dalla sorgente di acqua dolce. Questo particolare tipo di ambiente influenza notevolmente il tipo di associazioni a foraminiferi bentonici promuovendo lo sviluppo di specie opportunistiche. Van der Zwaan and Jorissen (1991) hanno condotto uno studio micropaleontologico su questo ambiente peculiare in tre aree di piattaforma tra loro molto distanti e dominate da sistemi deltaici, ossia Mare Adriatico, Golfo del Messico e Golfo dell'Orinoco. In tutte e tre le aree le associazioni a foraminiferi, presenti nella fascia dei limi, non solo confermano l'incidenza regolare (stagionale) e arealmente diffusa di condizioni anossiche o disossiche all'interfaccia acqua sedimento, ma anche mostrano una marcata zonazione trasversalmente alla fascia dei limi stessa (Fig. 2). Van der Zwaan e Jorissen (1991) hanno sviluppato un modello che spiega le variazioni stagionali osservate nel microhabitat dei foraminiferi bentonici sulla base dei due seguenti assunti: 1) la profondità nel sedimento del livello critico di ossigeno controlla sia la presenza sia il tipo di associazione e 2) alcune specie bentoniche sono esclusivamente epifaunali, mentre altre conducono vita infaunale durante i periodi con buona ossigenazione dell'acqua di fondo (per esempio in inverno) e si spostano in posizione epifaunale durante i periodi di bassa ossigenazione nelle acque di fondo (in particolare fine estate ed autunno). (Fig. 2).

Fig. 2

Modello di microhabitat durante diversi stadi di carenza di ossigeno nel sedimento per un transetto ideale dalle sabbie costiere passanti alla fascia dei limi e alle successive sabbie relitte distali (da Van der Zwaan e Jorissen, 1991). L'associazione *Ammonia-Elphidium* domina la parte costiera, mentre *Cassidulina laevigata* e *Melonis barleeanum* quella più esterna, meno influenzata dallo scarico fluviale. Nella parte centrale la fascia dei limi è composta dall'epifauna *Nonionella turgida* e, nella parte più profonda, *Valvulineria complanata*, mentre l'infauna è data da *Textularia* e *Bulimina marginata* forma aculeata e *Bulimina marginata* forma denudata. Quando il livello critico di ossigeno comincia a salire verso la superficie durante l'estate, l'infauna è costretta a migrare verso l'interfaccia acqua-sedimento, mentre durante la fine estate, autunno in cui la concentrazione di ossigeno scende a valori minimi, il centro della fascia dei limi può risultare privo di fauna bentonica provocando una compressione dei microhabitat verso le aree più esterne della fascia dei limi stessa.

Microhabitat model for benthic foraminifera during different stages of oxygen deficiency (from Van der Zwaan and Jorissen, 1991) from a nearshore sandy zone passing to muddy middle and again to offshore relict sands). The *Ammonia-Elphidium* assemblage inhabits the nearshore zone, while *Cassidulina laevigata* and *Melonis barleeanum* dominate the most distal zone, less directly influenced by river outflow. In the mud belt during winter, the vertical succession is composed by epifauna *(Nonionella turgida* and *Valvulineria complanata* in somewhat deeper water) and infauna (*Textularia* and *Bulimina marginata* forma aculeata and *Bulimina marginata* forma denudata). When the critical oxygen level starts to rise in summer, the infauna is forced to migrate to the epifaunal microhabitat, while during the late summer/autumn, when oxygen concentration falls to minimum values, the centre of the "mud belt" may be devoid of benthic life, resulting in a succession of microhabitats that is more compressed towards its outer edges (Van der Zwaan and Jorissen, 1991).

Come già sottolineato, sulla base dei vari modelli di distribuzione dei foraminiferi vengono interpretate le sequenze sedimentarie del passato, anche se è comunque da sottolineare che in studi moderni le informazioni paleoambientali ottenute dai foraminiferi debbano essere integrate con altri indicatori indipendenti di paleotemperatura e paleoproduttività (tra cui records pollinici, alchenoni, isotopi stabili dell'ossigeno e del carbonio), e con stratigrafia sequenziale e sedimentologia.

ESEMPIO DI RICOSTRUZIONE INTEGRATA PALEOCLIMATICA E PALEOCEANOGRAFICA NEL MEDITERRANEO CENTRALE (ADRIATICO) DURANTE GLI ULTIMI 6000 ANNI

L'esempio di ricostruzione paleoclimatica di seguito discusso considera il record di tre carote (RF93-30, AN97-15 e AMC99-1) prelevate, le prime due, sul fianco occidentale dell'Adriatico Centrale e la terza nel punto più profondo della Depressione Meso Adriatica a profondità rispettivamente di 77m, 55m e 256m.

In via generale, l'Adriatico Centrale può essere considerato un bacino ideale per ricostruzioni paleoclimatiche ad alta risoluzione per diversi motivi, tra cui la presenza di sequenze sedimentarie ben espanse e continue, caratterizzate da sedimenti fini per il tardo Quaternario, e l'ubicazione prossima alle terre emerse, che consente per esempio una buona comparazione tra record pollinici continentali e marini. Dal punto di vista invece del contesto oceanografico, l'Adriatico Centrale è connesso con il bacino meridionale attraverso la soglia di Pelagosa, profonda attualmente 160m. La circolazione è di tipo ciclonico ed è caratterizzata dalla presenza di acque atlantiche modificate (MAW) e dalle sottostanti acque intermedie levantine (LIW). Infine durante l'inverno, in conseguenza della presenza di venti freddi e secchi, quelli la Bora, si ha la formazione di acque fredde, dense e profonde che, dopo aver passato la soglia di Pelagosa, ventilano il bacino del Mediterraneo Orientale.

Fig. 3
Mappa dell'Adriatico Centrale con riportate le ubicazioni delle carote discusse nel testo. In toni di grigio sono riportati anche gli spessori del cuneo di stazionamento alto olocenico in millisecondi (10ms=7.5m per una velocità di 1500m/s in acqua e sedimento superficiale).
Location map of the cores discussed in this paper. In grey is shown the Late Holocene mud wedge (thickness Two Way Travel Time in millisecond, 10ms=7.5m for a sound speed in water and superficial sediment of 1500m/s).

La carota RF93-30 (Fig. 3), che costituisce il riferimento di letteratura, attraversa il cuneo sedimentario formatosi durante il tardo Olocene o, meglio, durante lo stazionamento alto ("high stand system tract") (TRINCARDI ET AL., 1996; CORREGGIARI ET AL., 2001). Questi depositi sono costituiti dai sedimenti portati dal Po e dai corsi d'acqua appenninici, formano un corpo spesso fino a 35m posizionato parallelamente alla costa occidentale adriatica, ed infine giacciono, in termini di stratigrafia sequenziale, su un riflettore sismico di importanza regionale ("maximum flooding surface") che individua il tempo di massima ingressione marina al culmine dell'innalzamento del livello del mare, avvenuto circa 5.5 ka ed approssimabile dal punto di vista ecobiostratigrafico alla scomparsa del foraminifero planctonico *Globorotalia inflata*, bioevento riconoscibile per tutto il bacino Adriatico. La carota RF93-30 attraversa questa superficie notevole, sopra la quale bisogna attendersi tuttavia un intervallo di deposizione condensata a causa dello spostamento verso terra della linea di riva e del conseguente intrappolamento dei sedimenti a minori profondità. Pertanto, la sequenza sedimentaria recuperata da questa carota ha permesso uno studio ad alta risoluzione (potenzialmente fino a scala decadale) per un intervallo di tempo in cui si sovrappongono cambiamenti ambientali per cause naturali e per cause antropiche (OLDFIELD ET AL., 2003).

La carota AN97-15 (Fig. 3) è stata prelevata al largo di Ancona sempre nel cuneo di stazionamento alto (HST) e la sua base non raggiunge la "maximum flooding surface" (CORREGGIARI ET AL., 2001). Di questa carota sono state studiate le associazioni a foraminiferi planctonici e bentonici. I risultati ottenuti con i foraminiferi bentonici verranno confrontati con quelli della carota RF93-30 per verificare se le due carote, ubicate all'interno dello stesso tipo di facies (fascia dei limi) ma tra loro distanti oltre 300km, presentano una sequenza di associazioni confrontabile e quindi con un potenziale stratigrafico per almeno l'Adriatico centrale.

La terza carota (AMC99-1) (Fig. 3) attraversa invece sedimenti che comprendono gli ultimi 14 ka circa ed in questa sede saranno mostrati quelli relativi agli ultimi 6 ka, per comparazione con il record della carota RF93-30, in particolare per quanto riguarda le faune a foraminiferi, per verificare se il segnale microfaunistico presente nella carota più prossimale è riconoscibile anche in ambiente più profondo, sia dal punto di vista ecobiostratigrafico che paleoambientale.

I risultati micropaleontologici delle carote AN97-15 e AMC99-1 sono presentati qui per la prima volta.

Prima di passare alla lettura dei risultati delle due carote, si precisa che il campionamento per lo studio delle microfaune a foraminiferi è consistito nel prelievo di una fetta di sedimento di 1cm circa di spessore (per un volume di circa 30cc). Il sedimento è stato poi seccato in forno a 50°C circa, disgregato in acqua e lavato con un setaccio di maglia 0.063mm. Lo studio quantitativo delle associazioni a foraminiferi è stato fatto sulla frazione>0.063mm. La frazione>0.063mm è stata suddivisa in aliquote con un microsplitter tipo Jones e sono state conteggiate per intero tante aliquote quante necessarie per raggiungere almeno 300 individui per i foraminiferi planctonici e 300 per quelli bentonici.

Per quanto riguarda invece i metodi di preparazione per gli altri proxies qui considerati per la carota RF93-30, si rimanda a GUILIZZONI E OLDFIELD (1996) e OLDFIELD ET AL. (2003).

CAROTA RF93-30

La cronologia di questa carota è stata affrontata e discussa in OLDFIELD ET AL. (2003). In sintesi, essa è basata su datazioni ^{14}C AMS fatte su foraminiferi planctonici o bentonici, riconoscimento di livelli vulcanoclastici, bioeventi pollinici e a foraminiferi planctonici, variazione secolare del campo magnetico terrestre (Fig. 4).

Come accennato, per questa carota sono disponibili i dati per diversi indicatori, tra cui quelli biologici (foraminiferi, pollini), geochimici (isotopi stabili del

C sulla sostanza organica, alchenoni, Total Organic Carbon) e fisici (proprietà magnetiche dei sedimenti), nonché naturalmente quelli sedimentologici e geofisici (OLDFIELD ET AL., 2003).

Le associazioni a foraminiferi planctonici sono risultate abbastanza scarse dal punto di vista quantitativo (ossia basso numero di individui), a differenza delle associazioni a foraminiferi bentonici. L'associazione planctonica è dominata da forme che vivono preferenzialmente in acque superficiali calde e oligotrofiche (*Globigerinoides ex gr. ruber*, *Globigerinoides sacculifer*, *Orbulina*), mentre l'unica forma di acque più profonde è *G. inflata*, presente solo nella parte più bassa della carota (pre-mfs) ed indicativa di acque omogenee, fredde e con buon mescolamento verticale durante l'inverno. E' da notare l'andamento della forma tropicale portatrice di simbionti *G. sacculifer*, che mostra due notevoli picchi in corrispondenza dell'Età del Bronzo e dell'età romana.

Fig. 4

Sintesi dei principali indicatori per la carota di riferimento RF93-30. Gli eventi principali sono dati da due episodi di deforestazione e di impatto antropico intorno a 3600 anni fa (tarda Età del Bronzo) e 700 anni fa (Medievale). Ciascuno di questi eventi ha prodotto un'accelerazione nella sedimentazione, a sua volta causata dalla risposta dei processi superficiali (quali erosione dei suoli) alla diffusa deforestazione e coltivazione (OLDFIELD ET AL., 2003).

Summary of the proxy record of sediment core RF93-30 plotted against the chronology. The most striking events are the episodes of deforestation and expanding human impact around 3600 yr BP (Late Bronze Age) and 700 yr BP (Medieval), each leading to an acceleration in sedimentation, reflecting the response of surface processes (e.g., soil erosion) to widespread forest clearance and cultivation (OLDFIELD ET AL., 2003).

Per quanto riguarda i foraminiferi bentonici si può notare come la parte inferiore, in corrispondenza della presenza di *G. inflata*, sia caratterizzata da forme più comuni in ambiente di piattaforma medio-esterna, sostituite verso l'alto prima da associazioni dominate da *Cassidulina laevigata carinata* ed indicatrici di ambiente esterno alla fascia dei limi, poi da associazioni tipiche di ambiente della fascia dei limi (per esempio *Valvulineria complanata*, *Nonionella turgida*, *Bulimina marginata*), che suggeriscono, specialmente dalla fine dell'età romana, un forte aumento dell'influenza fluviale in quest'area, raggiungendo la massima frequenza in corrispondenza delle due fasi riferibili alla Piccola Età del Ghiaccio. Si noti inoltre come in corrispondenza dei valori minimi di forme quali *V. complanata* corrisponda un massimo della forma planctonica *G. sacculifer*, che sulla base delle sue caratteristiche di habitat, richiede acque fortemente oligotrofiche con conseguente bassa torbidità dell'acqua. Secondo la cronologia di questa carota la scomparsa definitiva di *G. sacculifer* (ca. 1200AD) anticipa l'inizio della Piccola Età del Ghiaccio, e, per il momento, può considerarsi come il miglior bioevento a foraminiferi planctonici che approssima questo limite.

Il record pollinico mostra in particolare due intervalli di deforestazione e di aumento della coltivazione di cereali e ulivo: il primo tra 3600-3000 anni BP in corrispondenza dell'Età del Bronzo, il secondo tra 1100 e 600 anni BP. In questi due intervalli, in particolare il più antico, la presenza di chiari segnali di attività umana (coltivazione cereali) sono stati interpretati come possibile indicazione di impatto antropico sia sulla vegetazione sia sui processi superficiali quali accelerazione nell'erosione dei suoli, maggior apporto di terrigeno nei sedimenti marini. Quest'ultimo aumento è confermato non solo dalle associazioni a foraminiferi, ma anche dalla variazione delle proprietà magnetiche dei sedimenti. Tuttavia, data la notevole complessità dei vari parametri indagati, non è comunque stato escluso che cambiamenti climatici abbiano giocato un ruolo nelle variazioni dei parametri osservati. Va comunque riportato che anche in sequenze lacustri dell'Italia Centrale altri studiosi (RAMRATH ET AL. 2000, SADORI ET AL. 2004) sono giunti a conclusioni simili a quelle riportate da OLDFIELD ET AL. (2003).

CAROTA AN97-15

Per questa carota è disponibile una datazione ^{14}C AMS a profondità di circa 190cm effettuata su foraminiferi bentonici (1070 ± 50 anni BP; età calibrata 1380-1450AD) e che indicherebbe approssimativamente l'inizio della Piccola Età del Ghiaccio geofisico (CORREGGIARI ET AL., 2001). Questa profondità, cui è associata una superficie di annegamento minore, marca anche un cambiamento dei sedimenti dal punto di vista sedimentologico e geofisico (CORREGGIARI ET AL., 2001): infatti, si assiste ad una variazione, comunque graduale ed iniziata quasi un metro prima, di alcune parametri, quali la diminuzione dei valori della suscettività magnetica, della densità, dei carbonati totali, della sostanza organica ed un aumento del tasso di sedimentazione rispetto alla parte più bassa della carota (CORREGGIARI ET AL., 2001) (Fig. 5).

Fig. 5

Principali curve di foraminiferi planctonici e bentonici della carota AN97-15. In puntinato è marcato l'intervallo riferibile alla Piccola Età del Ghiaccio.

Most significant curves for planktic and benthic foraminifera of the core AN97-15. Total carbonates, TOC and magnetic susceptibility are also reported (from

CORREGGIARI ET AL., 2001). The stippled area corresponds to the Little Ice Age.

La scarsa profondità a cui è stata prelevata questa carota nonché il tasso di sedimentazione relativamente alto giustificano la bassa concentrazione di foraminiferi planctonici e l'attesa dominanza di forme superficiali. Sebbene quindi il record debba essere considerato con alcune cautele, va notata la scomparsa definifiva di *G. sacculifer* a circa 290cm. Secondo i risultati della carota RF93-30 questo bioevento avverrebbe intorno al 1200 AD, e quindi la datazione disponibile a cm 190 sembra coerente. Questa datazione marca il primo picco maggiore di *V. complanata* a cm 190ca., picco che in carota RF93-30 avrebbe un'età leggermente più giovane, ossia ca. 1600AD. Non si può escludere che i due picchi non siano tra loro coevi, tuttavia è bene considerare che le datazioni su foraminiferi bentonici, per esempio quelle effettuate sulla carota RF93-30 con età inferiore ai 3000 anni (comunque le stesse forme utilizzate per la datazione in AN97-15), hanno fornito tutte età sistematicamente più vecchie di quanto altre linee di evidenza dimostravano (OLDFIELD ET AL. 2003); pertanto non può escludere a priori che la datazione disponibile per la carota AN97-15 fornisca un'età invecchiata. Un altro possibile supporto alla cronologia proviene dalle stime del tasso di sedimentazione per gli ultimi 100 anni dei profili del ^{210}Pb (FRIGNANI ET AL., 2003) ottenuti su una carota prelevata nello stesso sito di AN97-15 con un carotiere acqua-sedimento. Queste stime indicherebbero un tasso di sedimentazione di circa 2.7 mmanno^{-1}, e quindi di un'età approssimativa di circa 100 anni a 27 cm di profondità, a cui corrisponde il forte declino di *V. complanata* (Figg. 5 e 6).

Fig. 6
Sintesi della cronologia proposta per le due carote AN97-15 e AMC99-1 in rapporto alla carota di riferimento RF93-30. In puntinato è marcata la Piccola Età del Ghiaccio, mentre le bande grigie correlano gli eventi di relativo ottimo climatico. In carota AN97-15 non si hanno elementi sufficienti per correlare con sicurezza l'intervallo con *G. sacculifer* con il picco più alto di *G. sacculifer* in RF93-30. Sono riportati anche le posizioni del tephra Avellino (AV) (ca. 3.6ka B.P.) per la carota RF93-30, nonché quella del tephra presente in AMC99-1. La correlazione con una carota prelevata nello stesso sito (CM92-43, ARIZTEGUI ET AL., 2000) non esclude che tale tephra possa essere Agnano Monte Spina (4.4ka B.P.). La linea continua di base marca la scomparsa di *G. inflata*, non raggiunta in AN97-15, mentre quella più alta marca approssimativamente la fine della piccola Età del Ghiaccio.
Summary of the chronology for cores AN97-15 and AMC99-1 correlated to the reference core RF93-30. The stippled area marks the Little Ice Age, while the three grey areas correlates events of relative climatic optimum. In core AN97-15 there are no evidences supporting the correlation between the interval with *G. sacculifer* and the most recent major peak of *G. sacculifer* in core RF93-30. Moreovere, are reported the depths of the Avellino tephra (ca. 3.6 kyr B.P.) in core RF93-30 and the tephra found in core AMC99-1. Comparison with another reference cor (CM92-43, ARIZTEGUI ET AL., 2000), collected at the same site of core AMC99-1, does not rule out that this tephra may be the Agnano Monte Spina tephra (4.4kyr B.P.). The bottom continuous line marks the LO of *G. inflata*, not reached in core AN97-15, while the uppermost line marks approximatively the end of the Little Ice Age.

Questa stima, seppur indicativa, non sembra in contrasto con quanto è possibile dedurre dall'andamento piuttosto simile di *V. complanata* in carota RF93-30, in cui sono visibili due picchi principali positivi all'interno della Piccola Età del Ghiaccio. La diminuzione di questa specie è visibile al tetto della carota RF93-30, cui si può assegnare un'età di circa 106 anni, ed è correlabile a quella sopra descritta al tetto della carota AN97-15 (Fig. 6). Oltre alle variazioni della specie *V. complanata*, si assiste anche alla progressiva diminuzione delle forme epifite (*Asterigerinata mamilla*, *Buccella granulata frigida*, *Cibicides lobatulus*, *Gavelinopsis laevigatus* e *Rosalina globularis*) durante l'intervallo corrispondente alla Piccola Età del Ghiaccio e questo potrebbe suggerire una maggiore torbidità delle acque. Successivamente, si assiste, come al top della carota RF93-30 (OLDFIELD ET AL., 2003), ossia successivamente alla fine della Piccola Età del Ghiaccio, ad un aumento delle forme *Brizalina*, *Bolivina*, *B. marginata* ed *Epistominella. vitrea* che, secondo BARMAWIDJAJA ET AL. (1992) rappresentano forme potenzialmente infaunali, ossia forme apparentemente piuttosto mobili che spostano il loro microhabitat da infaunale ad epifaunale, riflettendo in qualche modo la variabilità stagionale. Pertanto, un loro aumento potrebbe significare una maggiore frequenza in episodi disossici o un maggior contrasto delle condizioni di ossigenazione del fondo a livello stagionale.

CAROTA AMC99-1

In questa carota, che presenta la sequenza più espansa per i sedimenti di stazionamento alto relativamente alla Depressione Meso Adriatica, i campioni conteggiati sono tra loro spaziati di circa 6 cm, ed in alcuni casi anche ogni 3cm, consentendo quindi una risoluzione più alta di quanto al momento disponibile in letteratura per intervalli di tempo equivalenti in quest'area. La litologia di questa porzione di carota è argilla omogenea, con la presenza di materiale vulcanoclastico tra cm 246 e cm 268. Per quanto riguarda la cronologia, l'associazione a foraminiferi planctonici permette di limitare ai primi 320cm di carota l'intervallo di tempo tra 0 e 6 ka (LO *G. inflata* a cm 330).

Fig. 7
Principali curve di foraminiferi planctonici e bentonici della carota AMC99-1. Le bande grigie rappresentano gli eventi di relativo ottimo climatico. Per evidenziare meglio l'andamento generale, alla curva di *G. sacculifer* è stata sovrimposta una curva (spessore maggiore) ottenuta dalla media mobile ogni 5 punti.
Most significant planktic and benthic foraminifera curves for core AMC99-1. The grey areas represent intervals of relative climatic optimum. A smoothing line (5 points moving average) has been calculated and reported for *G. sacculifer* (bold line).

Inoltre, l'andamento di *G. sacculifer* presenta tre intervalli di relativa alta frequenza (cm280-230; cm 210-130; cm 100-15) separati tra loro da minimi (Figg. 6 e 7). Nella carota RF93-30 la LO di *G. sacculifer* approssima la base della Piccola Età del Ghiaccio, pertanto in carota AMC99-1 si potrebbe considerare che la base della Piccola Età del Ghiaccio sia intorno a cm 10. Questa ipotesi non è in contrasto con le stime di tasso di sedimentazione ottenute per la Depressione Meso Adriatica tramite radionuclidi a vita breve (^{210}Pb, FRIGNANI ET AL., in stampa). Infine, studi ancora in corso sulla variazione secolare del campo magnetico terrestre su questa carota suggeriscono, in via preliminare, che cm180-200 corrispondano ad un'età di circa 3500 anni BP e cm 100 a circa 2000 anni BP (LUIGI VIGLIOTTI, comunicazione personale orale 2004). Se la cronologia proposta è corretta, si può concludere che: 1) l'aumento relativo di *G. sacculifer* corrisponde a condizioni di relativo ottimo climatico, con forte oligotrofia e minore torbidità delle acque superficiali, 2) tale segnale è leggibile anche in records pelagici, non soltanto di piattaforma media (carote RF93-30 e AN97-15), 3) nel bacino adriatico centrale esiste più di un picco di frequenza di tale forma. Quest'ultima considerazione comporta implicazioni eco-biostratigrafiche: infatti in letteratura (CAPOTONDI ET AL., 1999, SBAFFI ET AL., 2001, SPROVIERI ET AL., 2003) è stata finora sempre considerata, per gli ultimi 6 ka nel Mediterraneo Centrale, l'esistenza di un solo aumento di frequenza di questa forma, corrispondente ad un'ecozona variamente datata, ma comunque compresa tra 2500 e 6000 anni BP. Non si può pertanto escludere che in realtà, con studi a più alta risoluzione, quell'unico aumento di frequenza considerato in letteratura non comprenda, almeno per quanto riguarda il bacino adriatico, più eventi tra loro simili, e che quindi la correlazione tra picchi di frequenza di tale forma presenti in siti diversi debba essere operata con molta cautela.

L'associazione a foraminiferi planctonici è sostanzialmente di tipo temperato caldo simile a quella riportata in carote prelevate nell'area (ASIOLI, 1996, ARIZTEGUI ET AL., 2001) per gli ultimi 6 ka con forme quali *G. ex gr. ruber*, *G. sacculifer*, *Orbulina* spp, *Zeaglobigerina rubescens* e *Globigerinella* spp. L'associazione bentonica è composta per oltre il 40% da forme infaunali (*Brizalina spathulata*, *Uvigerina mediterranea*, *Uvigerina peregrina* e *Bulimina gr. marginata*) che richiedono un contenuto di sostanza organica relativamente alto e basso contenuto in ossigeno nel sedimento. Tuttavia la contemporanea presenza di forme epifaunali, che invece richiedono condizioni di buona ossigenazione delle acque di fondo (esempio *Cibicidoides pachyderma*), fanno ritenere che l'ecosistema possa essere considerato, per tutto l'intervallo, di tipo mesotrofico, in accordo con il modello TROX. Le principali forme bentoniche presentano in generale valori abbastanza costanti, eccettuate minori oscillazioni; le due forme che presentano un trend generale di diminuzione e di aumento dal basso verso l'alto sono, rispettivamente, *B. spathulata* e *C. laevigata carinata.* Questa variazione a lungo termine potrebbe essere interpretata come un miglioramento relativo delle condizioni di ossigenazione del fondo e, per *C. laevigata carinata*, ad un aumento della salinità delle acque di fondo (VERHALLEN, 1991). Dall'andamento delle varie forme, tuttavia, non traspare una chiara variazione dell'ambiente di fondo in corrispondenza dei massimi (e minimi) relativi della curva di frequenza di *G. sacculifer.* Questa evidenza potrebbe essere dovuta al fatto che le variazioni registrate in acque superficiali non siano state di entità/durata sufficiente a produrre variazioni significative sul fondo oppure, considerando le carote RF93-30 e AN97-15, che tali variazioni abbiano avuto un maggior impatto a profondità minori dove si registra il maggior accumulo di sedimenti e dove l'influenza fluviale è senz'altro maggiore, considerato anche l'andamento della circolazione generale del bacino adriatico.

CONCLUSIONI

L'analisi di due nuove carote prelevate sulla piattaforma continentale e al centro della Depressione Meso Adriatica consente di ricostruire le variazioni microfaunistiche a foraminiferi planctonici e bentonici avvenute durante gli ultimi 6000 anni. I risultati e le implicazioni paleoambientali di queste ricostruzioni sono stati confrontati con la carota di riferimento RF93-30 (Oldfield et al., 2003) da cui è emerso che:

1. la scomparsa della specie planctonica *G. sacculifer* costituisce il bioevento a foraminiferi planctonici che meglio approssima, nell'Adriatico Centrale, l'inizio della Piccola Età del Ghiaccio
2. la comparazione tra il record più prossimale (carote AN97-15 e RF93-30) e quello più distale (AMC99-1) indica la presenza nell'Adriatico Centrale durante gli ultimi 6000 anni di almeno tre oscillazioni positive maggiori di *G. sacculifer*, ciascuna delle quali è riferibile ad intervalli di relativo ottimo climatico. La possibilità che questo andamento non sia locale ma estendibile ad almeno tutto l'Adriatico, non è remota, perchè: a) *G. sacculifer* è una forma superficiale (la soglia poco profonda di Pelagosa non

dovrebbe quindi aver costituito un ostacolo nell'intervallo in esame), b) per quanto riguarda l'ecobiostratigrafia sviluppata negli ultimi anni per l'Adriatico per gli ultimi 16000 anni esiste una notevole corrispondenza nella composizione microfaunistica delle ecozone tra il bacino centrale e quello meridionale. Questo invita alla cautela nell'utilizzazione della eco-biostratigrafia disponibile in letteratura.

3. esiste una buona similitudine tra la microfauna bentonica delle carote prelevate nel cuneo di stazionamento alto. Un esempio è l'andamento di *V. complanata*, che presenta in due carote (AN97-15 e RF93-30) distanti tra loro almeno 300km due picchi positivi di frequenza all'interno della Piccola Età del Ghiaccio, indicativi di relativamente maggiore influenza fluviale. Questo indica che tale andamento può essere utilizzato con valore ecostratigrafico per carote prelevate nel cuneo di stazionamento alto in corrispondenza della piattaforma intermedia almeno per l'Adriatico Centrale.
4. non è stata riscontrata una similitudine della microfauna bentonica tra le carote prese a minore profondità e quella distale. Questa evidenza può'essere attribuita alla breve durata delle oscillazioni climatiche, forse non sufficienti a generare un impatto esteso alle acque profonde e/o al confinamento dell'influenza fluviale a minori profondità con il conseguente accumulo di sedimenti sotto costa a causa della circolazione.
5. le considerazioni sopra riportate confermano non solo la notevole sensibilità dei foraminiferi (planctonici e bentonici) alle variazioni paleoambientali ma anche la necessità di un approccio interdisciplinare (vedi in particolare la costituzione della carota di riferimento RF93-30, senza la quale la maggior parte delle considerazioni fatte sulle altre due carote qui studiate non sarebbe stata possibile)

Ringraziamenti – Si ringraziano Antonio Cattaneo, Anna Correggiari, Leonardo Langone, Luigi Vigliotti per le discussioni sui dati delle carote AMC99-1 e AN97-15 ed in particolare Carla Alberta Accorsi, Marta Bandini e Anna Maria Mercuri per avere offerto a A.Asioli l'opportunità di partecipare al Convegno (Modena, Novembre 2003). Grazie infine a Fabio Trincardi per la lettura critica della prima versione del manoscritto e per le discussioni sui dati. Questa ricerca è stata finanziata dal progetto EC-Eurodelta (European Co-ordination on Mediterranean and Black Sea Prodeltas; EC contratto n. EVK3-CT-2001-20001; coord. Fabio Trincardi). Contributo n. 1443 per ISMAR-Bologna (CNR).

LETTERATURA CITATA

Allen J.R.M., Brandt U., Brauer A., Hübberten H.W., Huntley B., Keller J., Kraml M., Mackensen A., Mingram J., Negendank J.F.W., Novaczyk N.R., Oberhänsli H., Watts W.A., Wulf S., Zolitschka B., 1999. *Rapid environmental changes in southern Europe during the last glacial period.* Nature, 400, p.740-743.

Alley, R.B., Clark, P.U., 1999 - *The deglaciation of the northern hemisphere: a global perspective.* Ann. Rev. Earth Planet. Sci. 27, 149–182.

Ariztegui, D., Asioli, A., Lowe, J. J., Trincardi, F. , Vigliotti, L., Tamburini, F., Chondrogianni, C., Accorsi, C.A., Bandini Mazzanti, M., Mercuri, A.M., Van der Kaars, S., McKenzie, J.A Oldfield, F., 2000 - *Palaeoclimatic reconstructions and formation of sapropel S1: inferences from Late Quaternary lacustrine and marine sequences in the Central Mediterranean region.* Palaeoclimatology, Paleoecology, Paleogeography, vol. 158 (3-4), pp. 215-240

Asioli, A., 1996 - *High resolution Foraminifera biostratigraphy in the Central Adriatic basin during the Last Deglaciation: a contribution to the PALICLAS project.* In Guilizzoni, P. and Oldfield, F. (eds). *Palaeoenvironmental Analysis of Italian Crater lake and Adriatic Sediments (PALICLAS).* Memorie del'Istituto Italiano di Idrobiologia, 55,197 – 218

Barmawidjaja D.M., Jorissen, F.J., Puskaric, S., Van der Zwaan, G.J., 1992 - Microhabitats selection by benthic foraminifera in the northern Adriatic Sea. Jour. For. Res. 22, 4: 297-317.

Bond G., Broecker W., Johnsen S., McManus J., Labeyrie L., Jouzel J., Bonani G., 1993 – *Correlations between climate records from North Atlantic sediments and Greenland ice.* Nature, 365, 143-147.

Capotondi L. Borsetti A.M., Morigi C., 1999 - *Foraminiferal ecozones, a high resolution proxy for the late Quaternary biochronology in the central Mediterranean Sea*, Marine Geology, 153, 253-274.

Correggiari, A., Trincardi, F., Langone, L., Roveri, M., 2001 - *Styles of failure in heavily sedimented highstand prodelta wedges on the Adriatic shelf.* Journal of Sedimentary Research 71/2, 218–236.

Dansgaard, W., Johnsen, S., Clausen, H.B., Dahl-Jensen, D., Gundestrup, N.S., Hammer, C.U., Hvidberg, C.S., Steffensen, J.P., Sveinbjornsdottir, A.E., Jouzel, J. and Bond., G., 1993 - *Evidence for general instability of past climate from a 250-kyr ice core record*, Nature, 364, 128-220.

Frignani, M., L. Langone, M. Ravaioli, D. Sorgente, F. Alvisi, S. Albertazzi. *Fine sediment mass balance in the western Adriatic continental shelf over a century time scale.* Marine Geology (in stampa).

Guilizzoni P., Oldfield F., (eds.) 1996 - *Palaeoenvironmental Analysis of Italian Crater Lake and Adriatic Sediment*,Mem. Ist. ital. Idrobiol., 55.

Hemleben C., Spindler M., Anderson O.R., (eds.) 1989 - *Modern planktic foraminifera*, Springer-Verlag, New York.

Maslin M., Seidov D., Lowe, J., 2001. – Synthesis of the Nature and Causes of Rapid Climate Transitions During the Quaternary. In: Seidov, HAUPT E MASLIN (ed.), The Oceans and Rapid Climate Change: Past, Present and Future, Geophysical Monograph 126, p. 9-52.

MURRAY J.W., 1991 - *Ecology and paleoecology of benthic foraminifera.* Longman Scientific e Technical Ed.

OLDFIELD, F., A. ASIOLI, C.A. ACCORSI, A.M. MERCURI, S. JUGGINS, L. LANGONE, T. ROLPH, F. TRINCARDI, G. WOLFF, Z. GIBBS, L. VIGLIOTTI, M. FRIGNANI, K. VAN DER POST, N. BRANCH, 2003 - *A high resolution late Holocene palaeoenvironmental record from the central Adriatic Sea.* Quaternary Science Reviews, 22, 319 –342.

RAMRATH, ANTJE, SADORI, LAURA, NEGENDANK, JÖRG F.W., 2000 - *Sediments from Lago di Mezzano, central Italy: a record of Lateglacial/Holocene climatic variations and anthropogenic impact.* The Holocene *10*, pp. 87 – 95..

SADORI, L., GIRAUDI, C., PETITTI, P., RAMRATH, A.. 2004 - *Human impact at Lago di Mezzano (central Italy) during the Bronze Age: a multidisciplinary approach.* Quaternary International, 113: 5–17

SBAFFI L., WEZEL F.C., KALLEL N., PATERNE M., CACHO I., ZIVERI P., SHACKLETON N., 2001 - *Response of the pelagic environment to palaeoclimatic changes in the central Mediterranean Sea during the Late Quaternary.* Marine Geology 178, p. 39-62.

SCOTT DB, MEDIOLI FS., 1978 - *Vertical zonations of marsh foraminifera as accurate indicators of former sea-levels.* Nature 272: 528–531.

SCOTT, D.B., SCHAFER, C.T., MEDIOLI, F.S., 1980 - *Eastern Canadian estuarine Foraminifera: a framework for comparison*: Journal of Foraminiferal Research, 10: 205-234.

SEN GUPTA B.K., 1999 - *Modern foraminifera.* Kluwer Academic Publishers, 371 pp.

SPROVIERI R., DI STEFANO E., INCARBONA A., GARGANO M.E., 2003 - *A high-resolution record of the last deglaciation in the Sicily Channel based on foraminifera and calcareous nannofossil quantitative distribution.* Palaeogeography, Palaeoclimatology, Palaeoecology 202, 119-142.

TRINCARDI F., CATTANEO, A., ASIOLI, A., CORREGGIARI, A., LANGONE L., 1996 - *Stratigraphy of the late-Quaternary deposits in the central Adriatic basin and the record of short-term climatic events*, In *Palaeoenvironmental Analysis of Italian Crater Lake and Adriatic Sediments*, edited by F. Oldfield and P. Guilizzoni, Memorie dell'Istituto Italiano di Idrobiologia, 55, 39-70.

VAN DER ZWAAN, G.J. F.J. JORISSEN, 1991 - *Biofacial patterns in river-induced shelf anoxia.* In: *Modern and Ancient Continental Shelf Anoxia*, R.V. Tyson and T.H. Pearson, eds., Geol. Soc. Spec. Publ., 58, 65-82.

VERHALLEN, P.J.J.M. 1991 - *Late Pliocene to Early Pleistocene Mediterranean mud-dwelling foraminifera; influence of changing environment on community structure and evolution.* Utrecht Micropal. Bull., v. 40, 187 pp.

RIASSUNTO – Vengono qui presentati i risultati delle analisi quantitative delle associazioni a foraminiferi palnctonici e bentonici di due carote prelevate nell'Adriatico Centrale in piattaforma media ed in bacino per gli ultimi 6000 anni. La cronologia delle due carote è basata su diverse ed indipendenti linee di evidenza. I risultati sono stati confrontati con la carota di riferimento RF93-30 studiata con un approccio fortemente multidisciplinare. Questo studio ha permesso di ottenere un significativo avanzamento della ecobiostratigrafia a foraminiferi dell'Adriatico Centrale, ed in particolare: 1) la scomparsa del foraminifero planctonico *G. sacculifer* è un bioevento presente in tutto il bacino e correlabile anche tra ambienti piuttosto diversi tra loro (fascia dei limi e Depressione Meso Adriatica) e marca approssimativamente l'inizio della Piccola Età del Ghiaccio, 2) prima della sua scomparsa *G. sacculifer* presenta almeno tre picchi positivi di frequenza, riferibili ad intervalli di relativo ottimo climatico. Questo si ripercuote sulla ecobiostratigrafia a foraminiferi esistente in letteratura per l'Adriatico che necessita quindi di revisione e di cautela nella sua applicazione. 3) il segnale bentonico in piattaforma media (*V. complanata*) produce risultati simili anche tra carote tra loro distanti centinaia di chilometri, fornendo un ulteriore strumento ecobiostratigrafico, 4) diversamente, le variazioni delle associazioni a foraminiferi bentonici osservate in piattaforma media, durante l'intervallo di tempo considerato, non producono variazioni equivalenti in bacino, forse per la durata relativamente breve delle oscillazioni climatiche, individuate dalla associazione planctonica, che non hanno influenzato le acque più profonde del bacino e/o perché l'ambiente probabilmente più sensibile a tali variazioni climatiche (quello della fascia dei limi) è circoscritto a profondità relativamente basse, anche in funzione del regime di circolazione generale dell'Adriatico.

ALESSANDRA ASIOLI, ANDREA PIVA

Alessandra Asioli, Istituto di Geoscienze e Georisorse del C.N.R.- Sezione di Padova, c/o Dip. Geologia, Paleontologia e Geofisica dell'università di Padova, via Giotto, 1, 35137 Padova
Andrea Piva, Istituto di Scienze del Mare del C.N.R.- Sezione di Geologia Marina di Bologna, via P. Gobetti, 101, 40129 Bologna

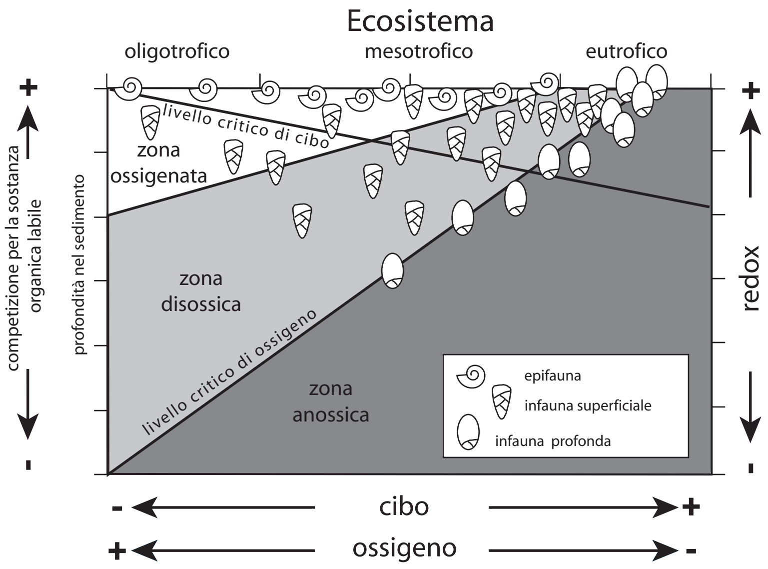

Asioli e Piva Fig. 1

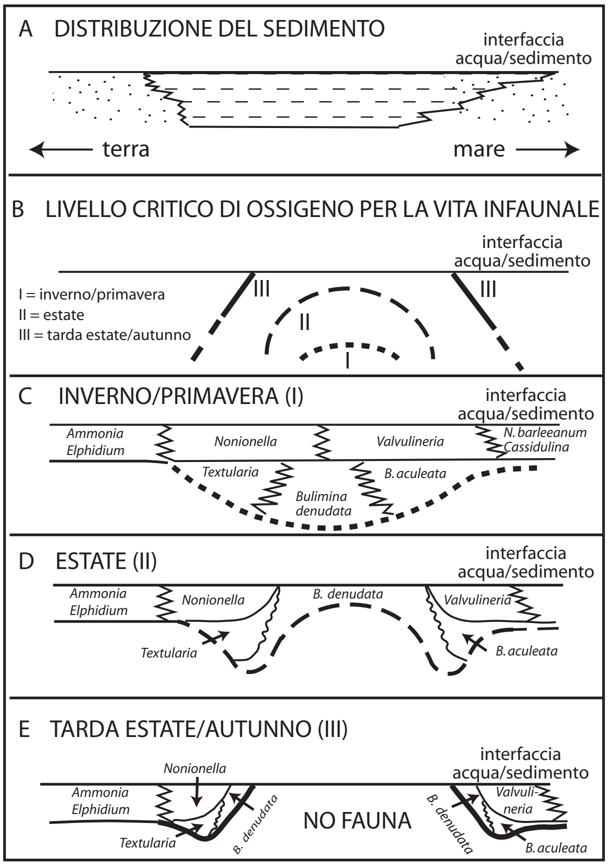

Asioli e Piva Fig. 2

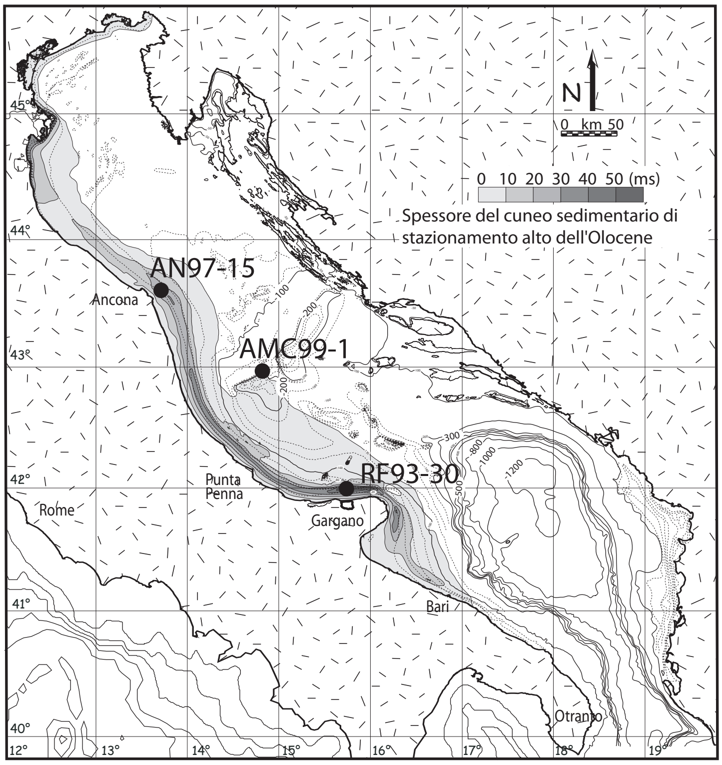

Asioli e Piva Fig. 3

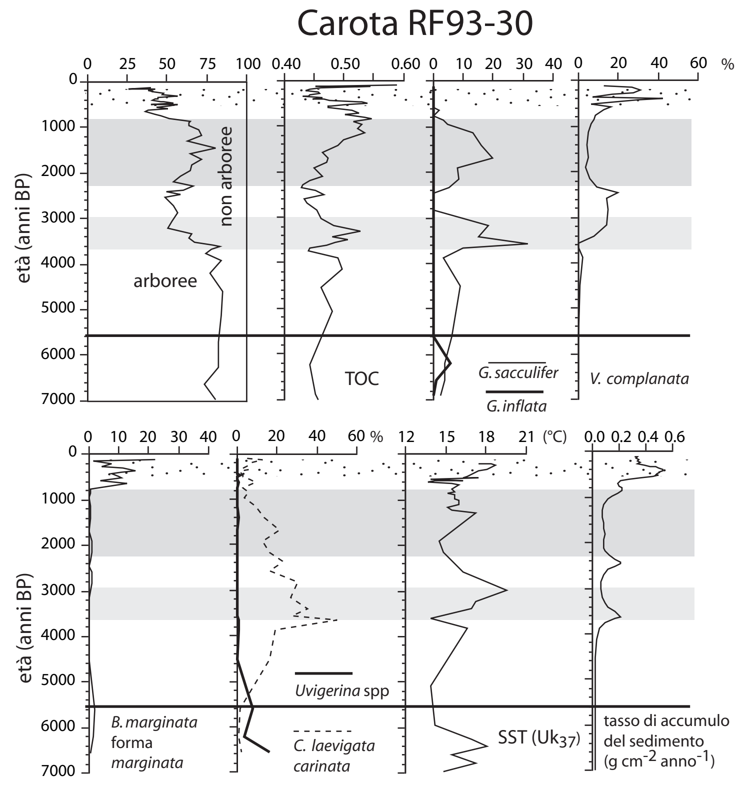

Carota RF93-30

Asioli e Piva FIg. 4

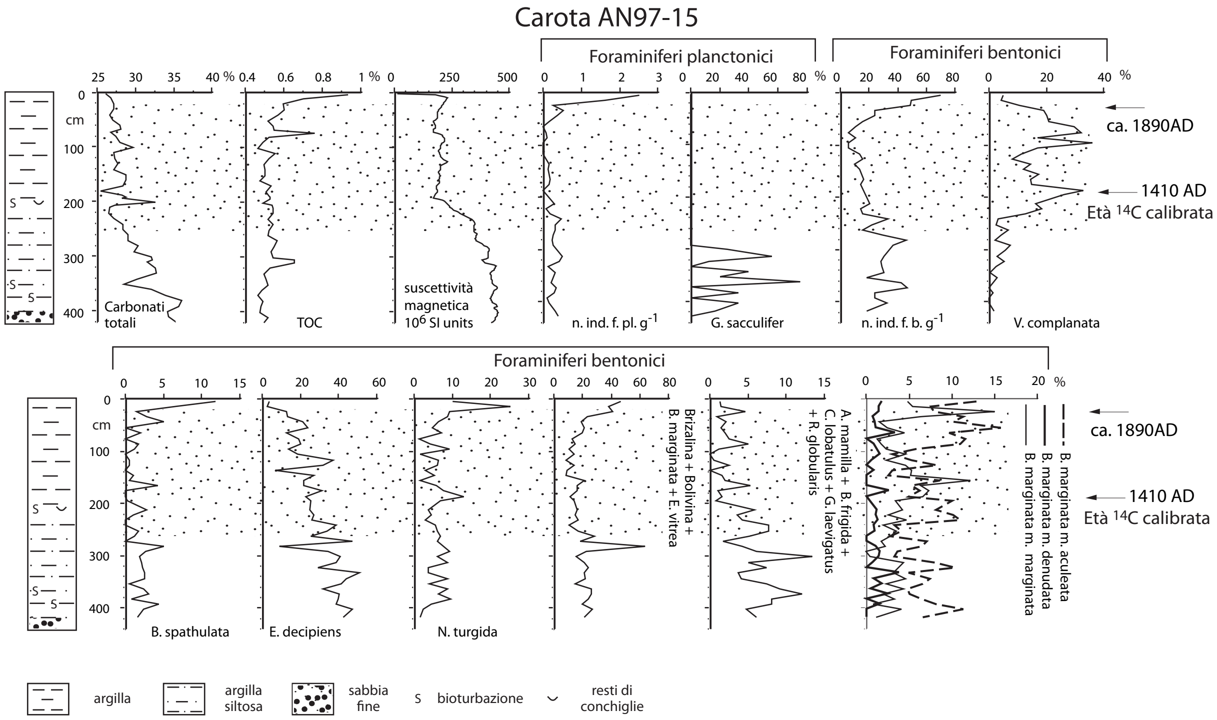

Asioli e Piva Fig. 5

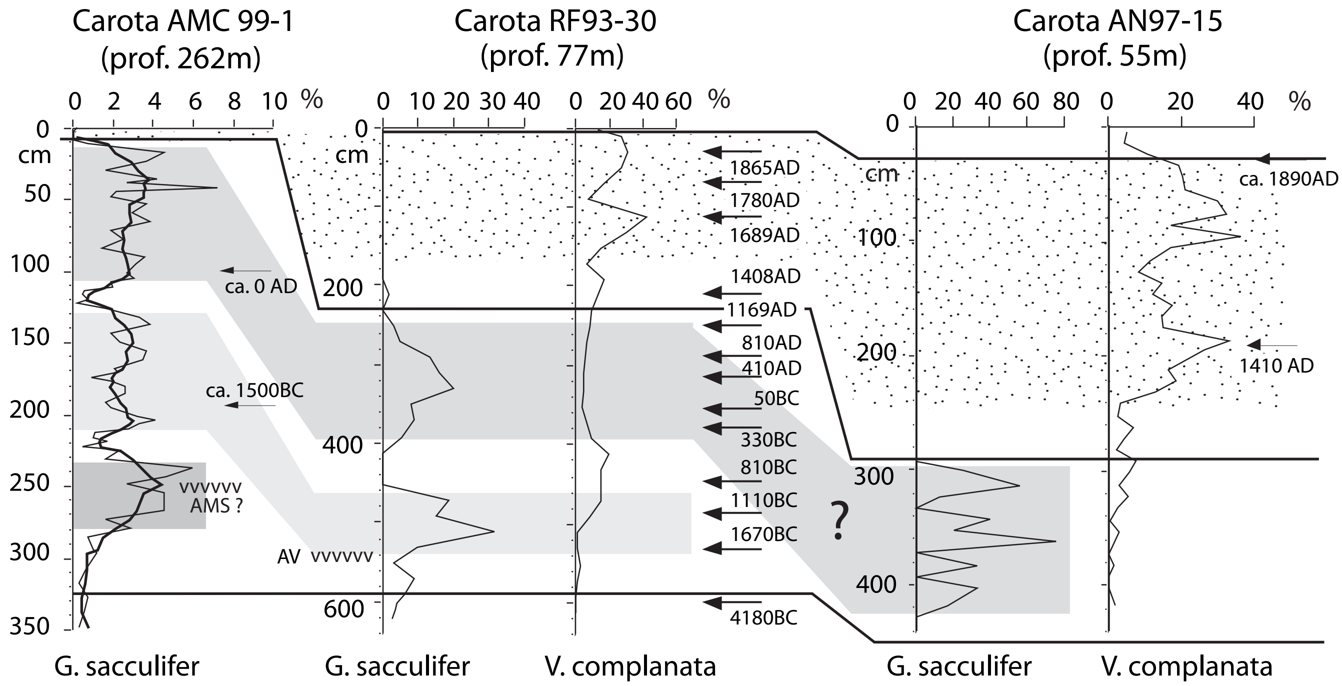

Asioli e Piva Fig. 6

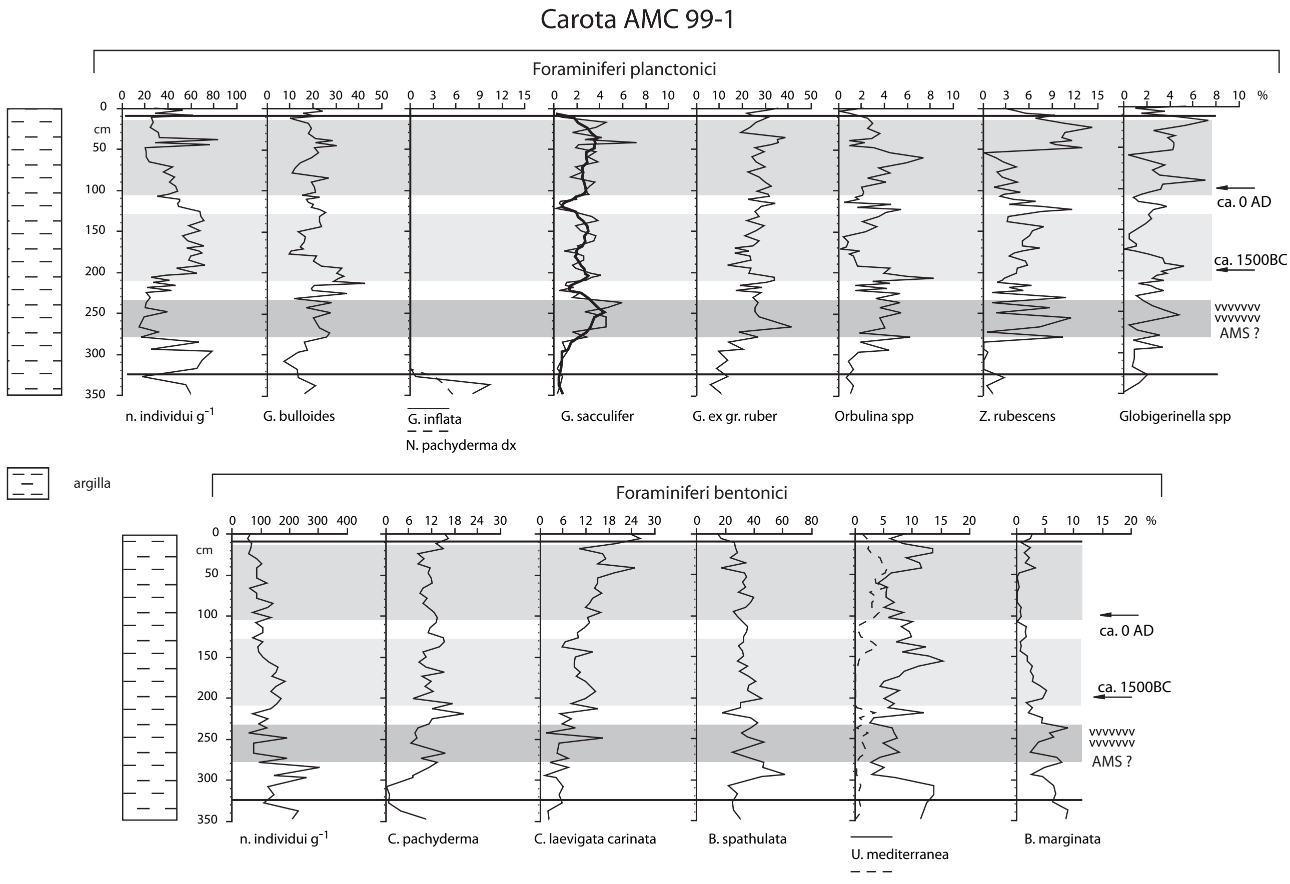

Asioli e Piva Fig. 7